UNIVERSITY OF BIRMINGHAM

Development of Local Drug Delivery Device for the Treatment of Pancreatic Cancer Resection Margin

By

Manna Amin

A thesis submitted to the University of Birmingham for the degree of

DOCTOR OF PHILOSOPHY

School of Pharmacy

College of Medical and Dental Sciences

University of Birmingham

May 2023

Abstract

Pancreatic cancer is a significant cause of cancer-related deaths worldwide, characterised by a 5-year survival rate that is notably low, typically ranging from 7-8%. Currently, the accepted norm for medical treatment is the surgical removal of the affected tissue, followed by administration of chemotherapy, particularly the highly potent one, FOLFIRINOX regimen. Due to the high toxicity associated with systemic delivery of FOLFIRINOX, and the intricate nature of the microenvironment of pancreatic cancer within the pancreas, there is a need for a more safer drug delivery method such as local delivery to treat the resection margin and prevent tumour recurrence. The study aimed at developing a local drug delivery device (Chemo Patch) composed of 3-dimensional printed catheter import part, a gelatine sponge and an ethylene vinyl acetate releasing membrane.

Various sponges manufactured utilizing freeze-drying technique were prepared and characterized to ascertain the effects of gelatine concentration, blending with sodium alginate, and crosslinking with glutaraldehyde on the physical and mechanical properties of the sponges. The selection of the best sponge was based on its desirability, primarily determined by its mechanical properties. These properties are influenced by the characteristics of the control sponge, Gelfoam®. The results demonstrated that the dry Gelfoam® sponge had hardness value of 2.703Kg/mm^2 ±35, whereas the hydrated sponge had 8.698 Kg/mm^2 ±117.7. The dry Gelfoam® sponges had an elasticity ratio (the ratio between the force of retraction and the maximum force) of 78.71%±1.9, whereas hydrated sponges had 12.14%±1.7. The results showed that increasing gelatine content increases sponge hardness, with 1% and 2% lower than Gelfoam® sponge and 4% and 10% higher. Oppositely, an increase in gelatine concentration resulted in a decrease in the elasticity of the prepared sponges. This study examined how gelatine concentration and blending with sodium alginate affect precursor hydrogel rheology. The results revealed that as gelatine concentration increased, both viscoelastic moduli

increased and that the storage modulus G′ dominated the loss modulus G″, indicating more robust hydrogel behaviour. Similarly, as sodium alginate concentration increases, storage modulus G' surpasses loss modulus G", indicating a stronger hydrogel behaviour. The results demonstrated that for both dry and hydrated sponges, gelatine concentration increases hardness and decreases elasticity. Porosity and swelling ratio decrease as gelatine content increases. Similarly, with increasing the polymer blends concentration, the hardness increases, elasticity decreases, swelling ratio and porosity decrease. Also, for dry and hydrated sponges, glutaraldehyde concentration increases hardness and elasticity. Additionally, increased glutaraldehyde content decreases the porosity and swelling ratio.

The optimum sponge was (4% gelatine, 4% sodium alginate, 0.5% glutaraldehyde), which was further characterised in comparison to Gelfoam®. The results revealed that a diverse pore structure in scanning electron microscopy for both sponges with an average pore size of 100µm. Raman mapping revealed non homogenous distribution for ironitican in both sponges. Fourier transform infrared spectroscopy analysis confirmed successful crosslinking with an Amide I shift peak associated with crosslinking. Differential scanning calorimetry showed a glass transition temperature of 125.24°C for the optimum sponge which was greater than Gelfoam® one (110°C). The hydrolysis degradation was more than 6 weeks for the optimum sponge, and the drug release exhibited a biphasic profile over 7 days. Linearity, range, accuracy, limit of detection, and limit of quantification validated the high liquid chromatography irinotican method.

Ethylene vinyl acetate melt rheology was used to determine processing temperature for fused deposition three-dimensional printing chemo patch device. Melt rheology predicted a printing temperature of 84°C to 132°C, later confirmed by the greatest printed quality achieved at 120°C. A feasibility study tested two designs—square and oblong. The square-shaped device was 4 cm by 4 cm, while the elongated device was 15mm by 30mm and fits the cadaver pig's

surgical margin. After characterisation of different membranes in thickness, infill percentage, number and size of pores, the best one chosen was 1mm thickness and 75% infill based on drug release ,which was included as part of the Chemo Patch device. The three-dimensional printing parameters were, print speed 15 mm/s, print temperature 110 °C, build plate 55 °C, zig zag infill pattern, 120mm/sec travel speed, 35% flow rate, and 0.15mm layer height. Furthermore, the mechanical testing results indicated that the catheter attachment to Chemo Patch was satisfactory, and there was no evidence of any leakage from the walls of the device. Additionally, the *in vitro* FOLFIRINOX release was sustained over one week.

The study's *in vivo* testing demonstrated that the Chemo Patch did not exhibit any significant incompatibility issues in the pig model. However, it was observed to elicit some immune response and fibrosis, which is a typical occurrence in implantable drug delivery devices. Furthermore, the study proved the effectiveness of the Chemo Patch device in delivering FOLFIRINOX locally in murine model, hence suppressing tumour growth.

Acknowledgment

This work was contemporaneous with numerous world-changing events, such as the Covid pandemic and several wars. Therefore, I am grateful to Allah for bringing this project to completion and to those who assisted in the achievement of it.

To my late father (Afal) and my late sibling (Muhammed), who passed away from leukaemia and Glioblastoma, your suffering has been always inspiring me to help in fighting all cancers. I will never forget your support, even though I lost you before this journey.

I am speechless when it comes to Dr Christopher McConville; I cannot thank him enough for all his support and insightful comments throughout this PhD journey. Dr McConville has inspired me to become an independent, passionate researcher.

My deepest gratitude goes to all my family members. I would like to thank my mother (Khadeja), sister (Amna), and husband (Ali) for their emotional, financial, and babysitting support.

My children Haitham (son), Layal (daughter), and Leen (daughter) deserve special thanks. I appreciate having you in my life, as you have been my greatest inspiration. Haitham, thank you for always being responsible; Layal, thank you for being the family's troublemaker; and Leen, thank you for tolerating my anxiety while pregnant with you. I will never forget our Saturdays spent in Birmingham city centre; you were the climax of this journey.

I'd want to thank my lab mate friends, Ghadeer, Dina, Shahreen, Ali Al Kolaib, Tariq, Tahani, Ibrahim, Becky, Ilay, and John, for their companionship; I'll never forget our days and nights in the lab and in Birmingham. I also want to thank my friends in Birmingham, Sophia, Hameeda, Maha, Radwa, and Pashmin for being like family and always being there for me. A very special thank you to our incredible lab manager, Deborah Croom-Carter; I will never forget your support when I was pregnant during the pandemic and working in the lab, as well as after the birth of my daughter; you were always there to listen to me and reassure me that I would survive.

I am grateful to Umm Al-Qura University for funding me, the Saudi Cultural Bureau, and the Saudi Royal Embassy in London for their financial and logistical support.

Table of content

List of tables

List of figures

Figure 5. 9: Histology slides from the tumour tissue for the (from right to left) device plus 15% FOLFIRINOX, 100% systemic FOLFIRINOX and 15% systemic groups.**Error! Bookmark not defined.**

List of abbreviations

AM: Additive manufacturing

ADM: Acinar to ductal metaplasia

AUC: Area under the curve

ANOVA: A one way analysis of variance

BDM: Bile duct margin

CRM: Circumferential resection margin

CAD: Computer aided design

DSC: Differential scanning calorimetry

EVA: Ethylene vinyl acetate

ECM: Extracellular matrix

FOLFIRINOX: Folinic acid, fluorouracil, ironitican and oxaliplatin

FDA: Food and Drug Administration

FTIR: Fourier transform infrared spectroscopy

H&E: Haematoxylin/Eosin

HPLC: High performance liquid chromatography

HME: Hot melt extrusion

IPMNs: Intraductal papillary mucinous neoplasms

ILP: intraluminal pressure

IRN: Ironitican

Kg: Kilograms

LOD: Limit of detection

LOQ: Limit of quantification

LVER: Linear Viscoelastic region

MHRA: Medicines and healthcare product regulatory agency

MI: Melting index

MCNs: Mucinous cystic neoplasms

NICE: National institute of health and care excellence

NBF: Neutral buffered formalin

NSG: NOD scid gamma mouse

BT: Pancreatic body and tail

PC: Pancreatic cancer

PH: Pancreatic head

PDAC: Pancreatic ductal adenocarcinoma

PD: Pancreaticoduodenectomy

PanINs: Pancreatic intraepithelial neoplasms

PSCs: Pancreatic stellate cells

PTM: Pancreatic transection margin

VP: Percutaneous vertebroplasty

PBS: Phosphate buffered saline

PDS: Polydioxanone suture

PECs: Polyelectrolyte complexes

SEM: Scanning electron microscopy

SOP: standard operating procedure

STL: stereolithography

SMA: Superior mesenteric artery

SMV: Superior mesenteric vein

3D: Three dimensional

TACE: Transcatheter Arterial Chemoembolization

TME: Tumour microenvironment

TNM: Tumour, nodes, and metastasis

Chapter 1: Introduction

1.1 Overview of pancreatic cancer

Pancreatic cancer (PC) has a very high mortality rate that is directly proportional to its prevalence (Siegel, Miller and Jemal, 2015; Kamisawa *et al.*, 2016; Khdhir, Belghith and Othmen, 2023). PC is the fourteenth most common cancer and the seventh leading cause of cancer death worldwide (McGuigan *et al.*, 2018). According to the American Cancer Society's projections for 2021, approximately 60,430 individuals are expected to receive a diagnosis of PC, while some 48,220 persons are expected to die due to the disease (Siegel *et al.*, 2021; Takikawa *et al.*, 2022). Moreover, PC is one of the most common malignant neoplasms of the digestive system. It is commonly acknowledged as' the king of cancer' due to its rapid progression, early metastasis, elevated mortality rates, and unfavourable prognosis (Aslan *et al.*, 2018; Siegel, Miller and Jemal, 2018; Liu *et al.*, 2019). Most PC originate from small non-invasive epithelial proliferations within the pancreas. Therefore, pancreatic intraepithelial neoplasia has an impact on the ducts of the pancreas (Kamisawa *et al.*, 2016). PC arises from genetic mutations inherited through the germline or acquired somatically. These mutations affect genes associated with cancer and can contribute to the progression and metastasis of the disease (Goral, 2015). Moreover, PC is attributed to the influence of four primary genes: KRAS, CDKN2A, TP53, and SMAD4 (Kamisawa *et al.*, 2016; Pelosi, Castelli and Testa, 2017). The presence of a KRAS mutation in 90% of PC patients indicates its role as a driver gene in the progression of this disease. Additionally, inactivating mutations in TP53, CDKN2A, and SMAD4 are observed in 50 to 80% of PC patients (Jones *et al.*, 2008; Ren *et al.*, 2018).

The pancreas is a vital organ in the human body that performs both endocrine and exocrine secretions and is vulnerable to various pathological conditions, as reported by Liu et al. and Khdhir, Belghith, and Othmen (Goral, 2015; Liu *et al.*, 2019; Khdhir, Belghith and Othmen,

2023). Furthermore, the pancreas is an endocrine gland located on the dorsal aspect of the abdominal cavity. Physically, the pancreas is described as an elongated, soft, flat, lobulated organ, and has yellowish appearance with a transverse orientation. Moreover, according to Mahadevan, the pancreas shows a transverse curvature as it traverses from the right to the left side of the body, approximately at the level of the first lumbar vertebra in the transpyloric plane. Additionally, this anatomical structure of the pancreas is situated anteriorly to the aorta and vertebral column (Mahadevan, 2019). Consequently, the retroperitoneal location of the pancreas renders any clinical examination for PC impractical for diagnostic purposes (Mahadevan and Von Hoff, 2007; Gheorghe *et al.*, 2020) . In addition, unlike a breast lesion, the pancreas lacks palpable external lumps or observable skin changes during a routine physical examination (Badger *et al.*, 2010; Kim and Ahuja, 2015) . Therefore, the potential impact of the anatomic location of pancreatic tumours on survival has been proposed (Brennan, Moccia and Klimstra, 1996). According to research, around 65% of PCs are in the head of the pancreas (HD), while 15% are found in the body and tail (BT) (figure 1.1). Also, the remaining tumours affect the gland diffusely (Greenlee *et al.*, 2000). The observed survival discrepancy between HD and BT tumours has been ascribed to the comparatively delayed clinical manifestation of individuals with BT tumours (Clinic *et al.*, 1984; Artinyan *et al.*, 2008).

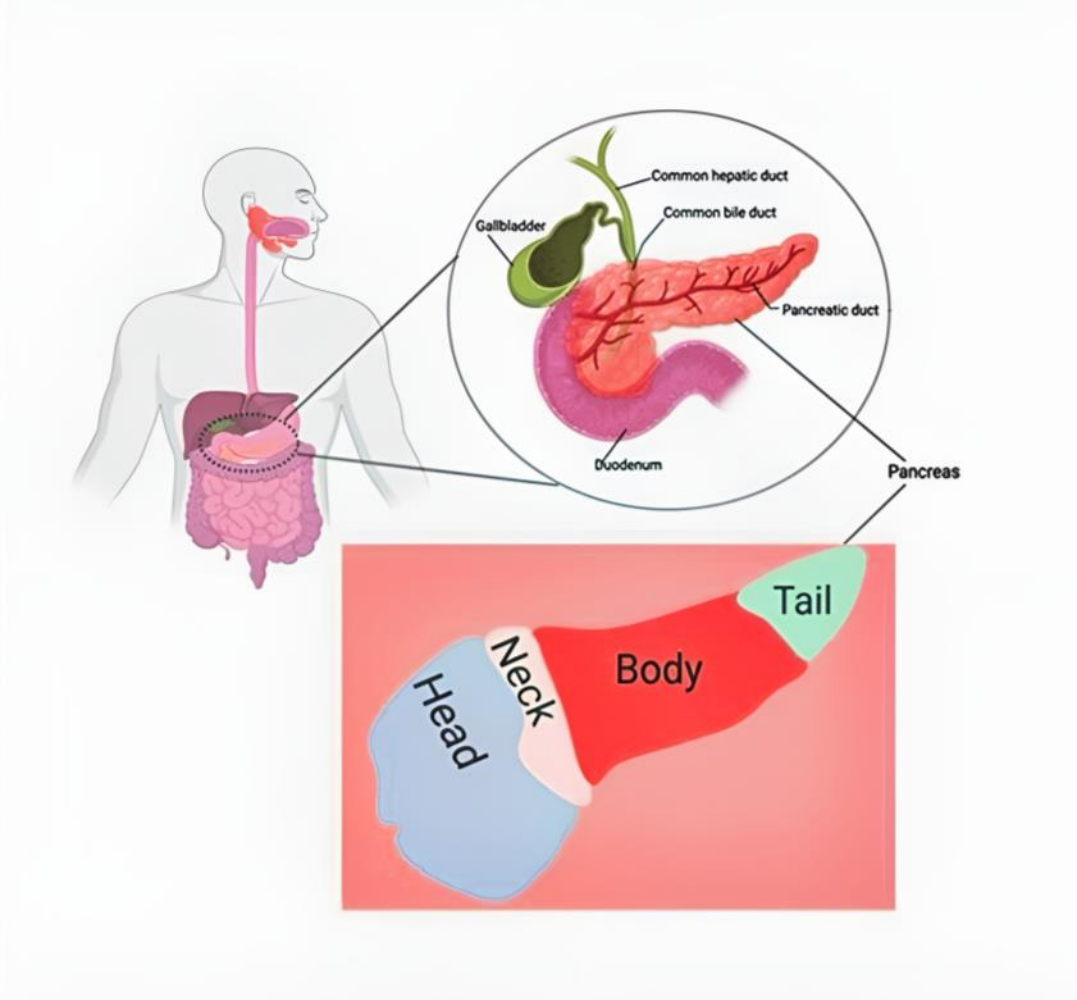

Figure 1. 1: The anatomical structure of the pancreas and its various regions where cancerous growths may arise adopted from (Olajubutu et al., 2023).

PC remains asymptomatic until it progresses to an advanced stage, which strongly correlated with a diminished survival rate (Zhao and Liu, 2020; Badowska-kozakiewicz *et al.*, 2023). Furthermore, the unfavourable prognosis of PC can be attributed to two main factors. Firstly, the insidious growth and non-specific symptoms are often only detected in advanced stages. Secondly, the need for more sensitive and specific techniques for early detection (Gheorghe *et al.*, 2020). While the precise aetiology of PC remains inadequately understood, various risk factors have been identified, including but not limited to cigarette smoking, positive family history and genetics, diabetes mellitus, obesity, dietary factors, alcohol consumption, and sedentary lifestyle (Ilic and Ilic, 2016; Eissa *et al.*, 2019; Badowska-kozakiewicz *et al.*, 2023).

According to a study, the proportion of patients diagnosed with PC in a localized stage of the disease is approximately 7% (Kim and Ahuja, 2015). This percentage is notably lower than that of other types of cancer, such as breast cancer (61%), colon cancer (40%), lung cancer (16%), ovarian cancer (19%), and prostate cancer (91%) (Jemal *et al.*, 2009; Gheorghe *et al.*, 2020).

1.2 Classification of PC

The pancreas can present a range of primary and secondary malignant neoplasms with distinct clinicopathologic features and biological behaviour (Mostafa *et al.*, 2017). Generally, pancreatic neoplasms are categorized into two major groups based on their cellular histology: benign and malignant. Pancreatic tumours that impact the epithelial tissue are classified into two distinct categories: endocrine and exocrine (Hidalgo *et al.*, 2015; Hani *et al.*, 2021). Additionally, pancreatic endocrine neoplasms, tumours originating from the endocrine component of the gland, are frequently observed. In contrast, acinar cell carcinomas, which develop from the pancreatic cells responsible for enzyme production, are infrequent (Alexakis *et al.*, 2004; Badger *et al.*, 2010).

These neoplasms include solid pseudopapillary neoplasms and neuroendocrine tumours, which exhibit relatively benign and indolent behaviour. Conversely, acinar-type cancers are reasonably aggressive and differ significantly from pancreatic ductal adenocarcinoma (PDAC) (Mostafa *et al.*, 2017).

1.2.1 PDAC

PDAC is the most prevalent forms of PC, accounting for more than 85% of all cases with the majority being invasive ductal adenocarcinoma (Alexakis *et al.*, 2004; Klimstra and Adsay, 2009; Ying *et al.*, 2016; Ren *et al.*, 2018), also there is a less prevalent type known as a pancreatic neuroendocrine tumour, which accounts for approximately 5% of total pancreatic malignancies (Hidalgo *et al.*, 2015; Hani *et al.*, 2021) . As a result, the term PC is synonymous

with PDAC and usually used interchangeably (Klimstra and Adsay, 2009). PDAC is a relatively infrequent occurrence among individuals younger than 30, with the average age of presentation being 63 years (Becker *et al.*, 2014; Mostafa *et al.*, 2017). Additionally, as PDAC is the predominant primary malignant neoplasm affecting the pancreas. Therefore, most characteristics associated with "PC" are attributed to this tumour. Hence, PDAC is commonly denoted as "ordinary" or "conventional" pancreatic adenocarcinoma (Mostafa *et al.*, 2017).

PDAC has an aggressive growth pattern, with an early start that spreads into the surrounding tissue primarily along neural sheets, early metastasis, and resistance to radiation and most systemic therapies, resulting in a poor prognosis. Therefore, the overall 5-year survival rate for those with the disease is less than 5 % (Loos *et al.*, 2008). Genetic research has proposed that PDAC originates from one of three established precursor lesions, namely pancreatic intraepithelial neoplasias (PanINs), intraductal papillary mucinous neoplasms, and mucinous cystic neoplasms. However, the preponderance of evidence suggests that most PDAC cases arise from PanINs, which evolve from PanIN-1A and -1B stages to the more advanced PanIN-3 stage (Real, 2003; Real, Cibrián-Uhalte and Martinelli, 2008; Hidalgo *et al.*, 2015) .

PDAC is derived from the exocrine component of the pancreas, which accounts for 90% of the organ and comprises acinar cells and a ductal system (figure 1.2). The plasticity of acinar cells enables them to maintain pancreatic exocrine tissue homeostasis and regeneration. Acinar cells have been observed to transform into a more epithelial phenotype in response to environmental stimuli such as tissue damage, inflammation, and stress. This phenomenon is called acinar to ductal metaplasia (ADM) (Orth *et al.*, 2019; Min *et al.*, 2023). The susceptibility of acinar cells to mutational hits during ADM can result in accumulating such hits, ultimately leading to the development of precursor neoplasms and invasive adenocarcinoma, as illustrated in Figure 1.2. In addition, PanINs represent the predominant type of precursor lesions affecting the pancreas. The progression of PanIN is characterized by three grades, namely PanIN-1A (flat)

and PanIN-1B (papillary), PanIN-2 and PanIN-3, which exhibit a gradual increase in cellular atypia as presented in figure 1.2 (Distler *et al.*, 2014). Furthermore, it should be noted that intraductal papillary mucinous neoplasms (IPMNs) and mucinous cystic neoplasms (MCNs) are types of cystic pancreatic lesions that have the potential to progress to invasive PDAC (Distler *et al.*, 2014; Orth *et al.*, 2019). The invasive PDAC arises due to the accumulation of genetic alterations in various oncogenic and tumour suppressor genes within the cells. Furthermore, diagnosis of PDAC is one of the most difficult tasks for surgical pathologists due to the overlapping features with chronic pancreatitis. Additionally, the anatomical position of the pancreas makes it difficult to access and diagnose (Klimstra and Adsay, 2009).

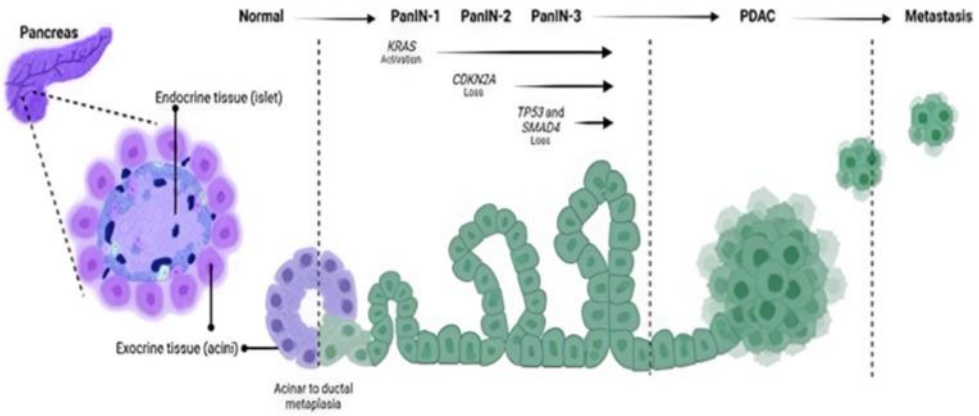

Figure 1. 1: The development and cellular differentiation of PDAC adopted from(Distler et al 2014).

5.1.1.1 Classification of PDAC

PDAC is categorized into four stages: resectable, borderline resectable, locally advanced (non-metastatic), or metastatic, depending on the scope of the ailment. According to Seo and Katz, the assessment of resectability is contingent upon anatomical criteria, precisely the extent to which they seem to approximate the central mesenteric vasculature on high-definition cross-sectional imaging studies (Seo and Katz, 2022). Furthermore, according to Katz et al. and Seo and Katz, implementing anatomic staging systems have demonstrated advantageous outcomes in defining the technical protocols required for removing tumours and the surgeon's adeptness

in achieving radical resection during pancreatectomy (Katz *et al.*, 2017; Seo and Katz, 2022). As per the American Hepato-Pancreato-Billiary Association (Roth and Berlin, 2018; Lambert et al., 2019), the resectable disease was identified by the absence of distant metastases, distinct fat planes surrounding the celiac axis, and the lack of any indication of the hepatic artery, superior mesenteric artery, superior mesenteric vein, or portal vein involvement (Roth and Berlin, 2018; Lambert *et al.*, 2019). In addition, the determination of resectability status is not only contingent upon the absence of distant metastases but also the positioning of the tumour relative to the portal vein, superior mesenteric vein, and superior mesenteric artery. In general, neoadjuvant chemotherapy is recommended as the initial treatment for tumours that envelop over 180 degrees of one of these vessels (Bachmann *et al.*, 2006; Muñoz *et al.*, 2017).

Furthermore, PDAC is categorized based on the tumour, nodes, and metastasis (TNM) staging system, a widely employed system for various tumours. As noted by Tomlinson et al. and Kamisawa et al., the precise determination of the T stage necessitates an evaluation of the size of cancer and its infiltration into adjacent structures, such as the bile duct and duodenum (Tomlinson *et al.*, 2007; Kamisawa *et al.*, 2016).

1.3 Treatment of PC

Radiotherapy, chemotherapy, surgery, and palliative care are all components of traditional PC treatment. Targeted therapy, immunotherapy, and microbial therapy have all undergone extensive research in recent years and may one day be used with conventional PC treatment strategies (Zhao and Liu, 2020).

1.3.1 Surgery

Surgery is the only curative procedure for PDAC. However, only about 20% of PDAC patients are clearly anatomically resectable at the time of diagnosis, with 10% surviving for 5 years. As a result, PDAC is regarded as a cancer with an interminably poor prognosis (Kamisawa *et al.*, 2016; Gray *et al.*, 2022). The remaining cohort of patients, comprising 80% of the total, are

diagnosed with either locally advanced or metastatic disease, rendering them ineligible for surgical intervention (Miller, Garcia and Yoon, 2020).

Pancreaticoduodenectomy (PD) is considered the conventional approach in pancreatic surgery, as most PDACs originate in the pancreatic head. The classical PD, initially outlined by Kausch and Whipple, was the preferred procedure for numerous years (Whipple, Parsons and Mullins, 1935; Loos *et al.*, 2008). Moreover, the conventional approach for addressing tumours located in the head of the pancreas is through the implementation of a PD, commonly referred to as the Whipple procedure, which is pylorus-preserving. Conversely, tumours situated in the body or tail of the pancreas can be effectively treated through a distal pancreatectomy (Neoptolemos *et al.*, 2004; Bachmann *et al.*, 2006). Furthermore, it is recommended that patients diagnosed with adenocarcinoma situated in the left pancreas, specifically in the body or tail, undergo distal pancreatectomy with splenectomy. To achieve an R0 surgical margin status that is histologically complete, Strasberg and colleagues have proposed a modified technique that involves an anterograde approach, complete dissection of N1 lymph node stations, and enlargement to the left prerenal fascia of the posterior dissection plane. This technique, known as radical anterograde modular pancreatosplenectomy, has improved the retroperitoneal resection margin (Strasberg, Linehan and Hawkins, 2007; Lambert *et al.*, 2019). Moreover, the Whipple procedure is a surgical technique that involves the removal of the pancreatic head, the duodenal curve, the gallbladder, and the common bile duct. Additionally, the standard of care involves the skeletonization of the superior mesenteric artery (SMA) down to the adventitia on its anterior, lateral, and posterior borders (Tempero *et al.*, 2017; Lambert *et al.*, 2019). Additionally, this approach is commonly employed for the treatment of neoplasms that affect the head and neck of the pancreas (Penumadu *et al.*, 2015; Qiubo Zhang *et al.*, 2016).

5.1.1.2 Resection margin status

According to Hinni et al., the resection margin or surgical margin is any tissue plane where the surgeon's blade contacts the patient (Hinni et al., 2013; Shah, 2018). Furthermore, during surgical removal, a margin of normal tissue is removed around the palpable or visible tumour to guarantee its total removal. This mostly depends on the clinical opinion of the surgeon, the interpretation of imaging studies, and the preoperative planning of the size of the resection(Kurita et al., 2006; Shah, 2018). Furthermore, the pathologist must determine whether the surgeon has successfully attained a negative (R0) resection margin. On the other hand, the R1 margin is characterized by a positive status at the microscopic level, while the R2 resection is identified by grossly visible cancer at the resection margin. However, the absence of standardized protocols for the pathological determination of margin status has led to inconsistencies in the evaluation of margin status (Wanebo and Vezeridis, 1995). The presence of perineural invasion and microscopic tumour spread towards the arteries during a resection for PC almost always results in an R1 situation at the medial/posterior margin (18-85% of the time). These R1 resections, along with para-regional lymph node metastases, are responsible for a significant proportion of local recurrences following initially curative procedures (Hishinuma et al., 2006; Verbeke and Gladhaug, 2012; Strobel et al., 2013). Furthermore, the superiority of potentially curative (R0) surgery over palliative (R1/R2) surgery has been demonstrated by various studies (Trede, Richter and Wendl, 2001; Wagner et al., 2004; Bachmann et al., 2006). Also, the efficacy of tumour debulking or R2 resection as a potential treatment for patients with PDAC in the palliative context was examined more than twenty years ago. The findings indicated that this approach offers limited advantages, as it only slightly extends survival rates while increasing morbidity when compared to palliative chemotherapy or bypass procedures (Gouma et al., 1999; Klose, Ronellenfitsch and Kleeff, 2021). Moreover, many clinicopathologic characteristics have been suggested as potential postoperative prognostic variables, among which the involvement of the resection margin is thought to be

crucial for longer survival rate. Indeed, careful preoperative planning and surgical methods can prevent macroscopic margin involvement, but microscopic margin involvement is frequently detected unexpectedly (Jamiyan et al., 2020). In general, the objective of surgical intervention is to attain a state of complete resection of the neoplasm with negative margins under microscopic examination, commonly referred to as R0. As per the latest publications, after PD, R0 resection should be characterized by eliminating a margin of healthy tissue surrounding the resected tumour that measures greater than 1mm (Delpero *et al.*, 2017; Lambert *et al.*, 2019). In situations where R1 margin status is present, it is imperative to provide additional details to differentiate between cases where the margin is tumour-free but less than 1mm in the distance (R1 (<1mm)) and instances where tumour cells are in direct contact with the margin (R1 (direct)). The latter scenario, characterized by direct invasion, is associated with a less favourable prognosis (Strobel *et al.*, 2017; Lambert *et al.*, 2019). Furthermore, PC surgical margins is classified into two categories: transaction margins and circumferential resection margins (CRMs) (Verbeke, 2013). The transection margins of PC encompass several margins, including the pancreatic duct margin (also known as the pancreatic neck margin), the bile duct margin, the proximal margin of the duodenum or stomach, and the distal margin of the duodenum. The CRMs encompass various anatomical structures: the posterior pancreatic surface, the medial margin, the groove along the superior mesenteric vein/portal vein, and the anterior surface. Moreover, the anterior surface is unique as it does not qualify as an authentic surgical margin but rather as a dissection area distinct from the adjacent surfaces as presented in figure 1.3 (Schlitter et al., 2010). Additionally, the nomenclature pertaining to resection margin is straightforward and predicated on anatomical localization or proximity with respect to the superior mesenteric vessels. Therefore, various terms have been used to refer to the surfaces that are in proximity to the superior mesenteric artery (SMA) or vein (SMV), such as retroperitoneal, uncinate, mesenteric, medial, and posterior (Verbeke, 2013).

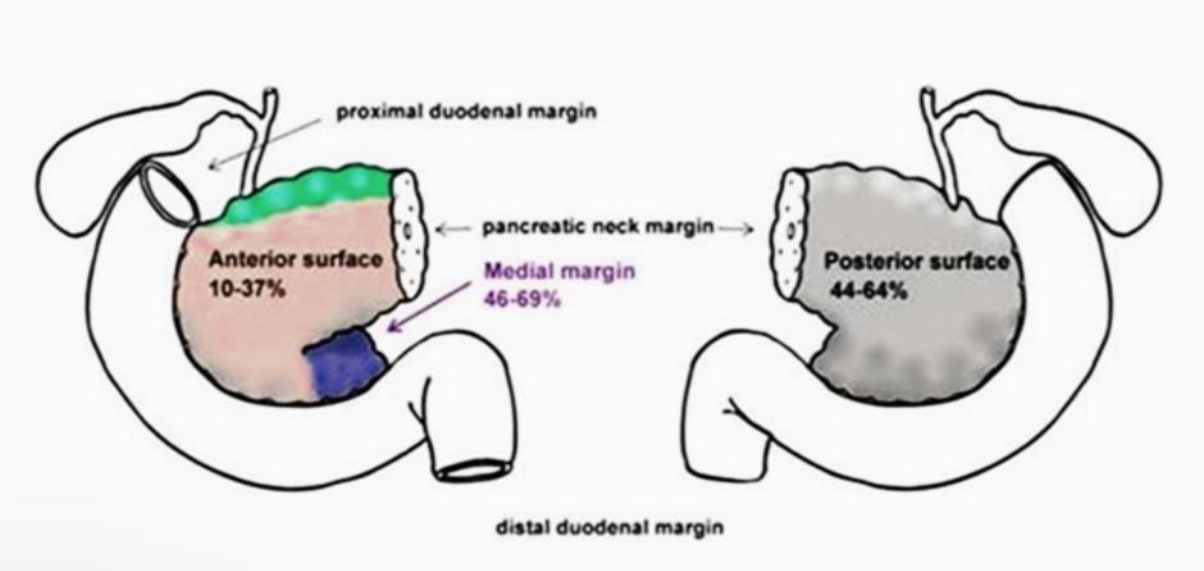

Figure 1. 2: The surgical resection margins of PC adopted from (Schlitter et al., 2010).

1.3.2 Chemotherapy

Chemotherapy constitutes a crucial component of the all-encompassing therapeutic approach to PC. Research has demonstrated that implementing adjuvant chemotherapy following radical resection can notably enhance the disease-free survival and overall survival rates of individuals diagnosed with PC (Zhao and Liu, 2020). The administration of chemotherapy in PC is typically performed before the surgical procedure (known as neo-adjuvant chemotherapy) or after the surgical procedure (known as adjuvant chemotherapy) (Ghosn *et al.*, 2016; Hani *et al.*, 2021).

Following surgery, adjuvant chemotherapy with gemcitabine or S-1, an oral fluoropyrimidine derivative, is administered. For patients who are not surgical candidates but have a satisfactory performance status, FOLFIRINOX and gemcitabine plus nanoparticle albumin-bound paclitaxel (nab-paclitaxel) are the treatments of choice (Kamisawa *et al.*, 2016) .The implementation of conventional cytotoxic chemotherapeutics as the standard of care for PDAC patients occurred in the 1980s. During this time, it was discovered that including a

fluoropyrimidine, specifically 5-fluorouracil, in conjunction with radiation therapy improved 1-year survival rates (Klaassen *et al.*, 1985; Miller, Garcia and Yoon, 2020).

5.1.1.3 Gemcitabine

Gemcitabine is a fluorinated nucleoside analogue (2',2'-difluorodeoxycytidine, dFdC) (Burris *et al.*, 1997; Jacobetz *et al.*, 2013), which exhibits efficacy against diverse solid tumours, including but not limited to pancreatic, non-small cell lung, breast, and ovarian malignancies (Ozols, 2005; Moysan, Bastiat and Benoit, 2013). Since its approval in 1996, gemcitabine has served as the reference regimen for PC. The compound is classified as a prodrug, necessitating cellular absorption and phosphorylation to generate active metabolites. Consequently, these metabolites impede the elongation of DNA chains, ultimately resulting in DNA fragmentation and subsequent cellular mortality (Noble and Goa, 1997; Pliarchopoulou and Pectasides, 2009). The administration of gemcitabine has demonstrated a modest survival advantage of slightly over five weeks. However, the utilization of gemcitabine-based combination regimens has exhibited restricted advancements in enhancing overall survival (Burris *et al.*, 1997; Sultana *et al.*, 2007; Jacobetz *et al.*, 2013). Gemcitabine is the predominant treatment option for patients diagnosed with PC (Kamisawa *et al.*, 2016; Muñoz *et al.*, 2017). However, over the past half-decade, there has been a notable increase in the availability of novel chemotherapeutic alternatives. Nevertheless, many of these novel therapies comprise gemcitabine in conjunction with inhibitors or other chemotherapeutic agents, along with a blend of various chemotherapeutic agents. FOLFIRINOX represents a chemotherapeutic blend regimen for instance (Conroy *et al.*, 2011; Muñoz *et al.*, 2017).

5.1.1.4 FOLFIRINOX

The FOLFIRINOX regimen includes three chemotherapy drugs (5-fluorouracil, irinotecan, and oxaliplatin) and folinic acid. (a vitamin B derivative reducing the side effect of 5-fluorouracil)

(Li *et al.*, 2015; Liu *et al.*, 2020). Research reported in the past suggests that combination therapy may be more effective than gemcitabine alone (Marsh *et al.*, 2015) . This is especially true after the confirmation of the promising phase II findings of FOLFIRINOX (oxaliplatin 85 mg/m2, leucovorin 400 mg/m2, irinotecan 180 mg/m2, bolus 5-fluorouracil 5FU) in a sentinel phase III investigation (PRODIGE 4/ ACCORD 11) (Conroy *et al.*, 2011; Marsh *et al.*, 2015). Furthermore, FOLFIRINOX was launched into clinical practice in 2010, and in this randomised study, individuals with metastatic PC less than 75 years of age received either gemcitabine or FOLFIRINOX With a median follow-up of 26.6 months and 171 patients in each group, median survival with FOLFIRINOX was 11.1 months compared to 6.8 months with gemcitabine (P 0.001, HR = 0.57, 95% CI = 0.45–0.73). Moreover, survival at one year was 48.4% against 20.6%, and this disparity was maintained after 18 months, 18.8% versus 6%. Similarly, quality of life measures greatly favoured the FOLFIORINOX group (Gourgou-Bourgade *et al.*, 2013; Marsh *et al.*, 2015). While FOLFIORINOX is more clinically beneficial than gemcitabine, it is significantly more toxic and is consequently limited to advanced-stage PDAC patients with good health condition (Conroy *et al.*, 2011; Liu *et al.*, 2020). In addition, the effect on bone marrow was discovered to be primarily attributable to irinotecan, accounting for 70% of neutropenia. Also, ironitican contributed to the gastrointestinal effects, such as 70% of patients suffering vomiting, diarrhoea, nausea, and anorexia (Shitara *et al.*, 2008; Conroy *et al.*, 2011; Liu *et al.*, 2020).

1.4 Local drug delivery to PC

The use of systemic chemotherapy following resection has been the gold standard for dealing with recurrence and subsequent metastasis. However, because of the lower concentrations reaching the PC site, systemic chemotherapy efficacy is not always good. As a result, local drug delivery is a promising strategy for overcoming the limitations of systemic drug delivery in chemotherapy(Yi *et al.*, 2016). Nonetheless, systemic chemotherapy causes toxicity because

of off-target effects. Hence, local delivery of chemotherapy reduces systemic toxicity while increasing drug concentration at the tumour site (Ramot *et al.*, 2016). There are several drug delivery barriers to PDAC treatment, including cellular chemo resistance, fibrous tissue formed because of tumour growth, and hypo vascularity. Furthermore, the difficulty in treating PC stems from the disease's poor prognosis (Indolfi, Ligorio, David T. Ting, *et al.*, 2016). Additionally, the profuse and compact stroma, a distinguishing feature of PDAC, leads to a rise in interstitial fluid pressure. The hindrance of chemotherapeutic drug delivery and the facilitation of tumour advancement are consequences of the compression caused by intra-tumoral vasculature, which creates a low-oxygen environment (Erkan *et al.*, 2012; Jiang *et al.*, 2020).

Moreover, it is widely accepted that the tumour microenvironment (TME) plays a crucial role in nurturing or inhibiting tumour development (Maman and Witz, 2018; Laplane *et al.*, 2019). In PDAC, the TME actively contributes to tumour progression, immune evasion, and drug response (Martinez-bosch, 2018; Bishehsari, 2021). Furthermore, the TME consists of the spatially located elements close to the tumour (Laplane *et al.*, 2019). Further, cancer cells, stromal cells, and extracellular are the elements that comprise the PC TME. It is primarily pancreatic stellate cells (PSCs), regulatory T cells (Tregs), myeloid-derived suppressor cells (MDSCs), and tumour-associated macrophages (TAMs) that contribute to the progression of PC (Chronopoulos *et al.*, 2016; Ren *et al.*, 2018). Upon activation due to pancreatic injury, PSCs undergo a series of cellular changes, including the loss of lipid droplets, upregulation of α-smooth muscle actin, proliferation, migration, and overproduction of extracellular matrix (ECM) proteins. Consequently, this dysregulation of ECM production and degradation ultimately culminates in the development of fibrosis (Tahara, Shimizu and Shiratori, 2008; Wilson, Pirola and Apte, 2014). Additionally, early interactions of transforming neoplastic ductal cells with PSCs, fibroblasts, and macrophages initiate a fibroinflammatory process and

the subsequent recruitment of T regs as part of an adaptive immune response (figure 1.4). As the tumour advances, cancer cells invade the blood vessels and inhibit the vessel's lumen, a process known as endothelial ablation. In conjunction with a suppressive immune milieu, endothelial ablation and a desmoplastic stroma reduce drug delivery and chemoresistance at the site (Bishehsari, 2021).

Zhan et al. have reported that the localized delivery of low-dose FOLFIRINOX from a drug-eluting scaffold in an orthotopic murine model have shown efficacy (Zhan *et al.*, 2013). Furthermore, Studies of Yi et al shows the importance of local drug delivery to PC, by hypothesizing that using three-dimensional printing technology to create a local drug delivery patch loaded with high drug concentrations to deliver chemotherapy locally to PC patients would be a promising approach (Yi *et al.*, 2016; Bazeed, Day and Garg, 2022). A few researchers such as Indolfi also aimed to create a local delivery device that would deliver high drug concentrations directly to the tumour site. The developed device was an implantable stainless steel disc containing paclitaxel and poly (lactic-co-glycolic) acid capable of linearly releasing high doses of chemotherapeutic drugs(paclitaxel) for up to two months. They discovered that local therapy suppressed tumour growth up to a 12-fold more than systemic administration and reduced retention into off-target organs. As a result, they concluded that developing a locally implantable drug delivery device is critical for treating PC (Indolfi, Ligorio, David T Ting, *et al.*, 2016). Additionally, Byrne et al. have devised an implantable iontophoretic drug delivery system that can administer FOLFIRINOX locally, resulting in superior tumour response and tolerability compared to the systemic delivery (Byrne *et al.*, 2016).

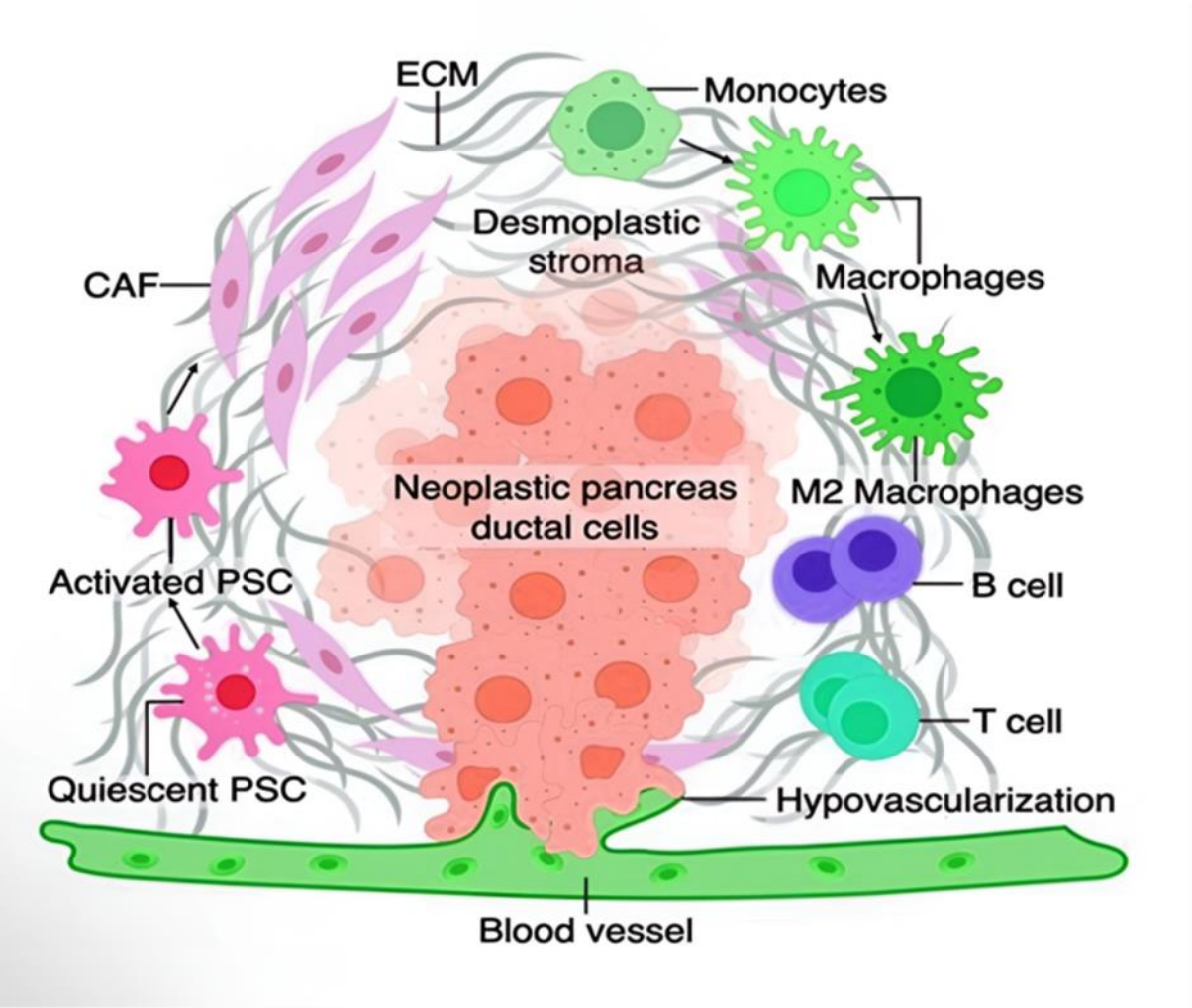

Figure 1. 4: The TME of PC is composed an overview of the interplay between PSCs and PC cells, as well as the interactions between PSCs and other stromal cells that may facilitate the progression and metastasis of cancer (Bishehsari, 2021).

1.5 Sponges (aerogels) in drug delivery systems: overview, preparation, and polymers

1.5.1 Overview

In recent years, there has been a growing concern regarding the administration of drugs to patients and its impact on their efficacy (Friess, 1998; Teodora Tihan *et al.*, 2015). Therefore, Studies have been conducted for instance on systems wherein the rate of osmotic pumping of

medicine from a reservoir regulates the degree of drug delivery. Furthermore, drug release through a membrane or sponge can result in prolonged drug availability and sustained action. This phenomenon depends on the amount of cross-linking agent or the drug and polymer concentration (Teodora Tihan *et al.*, 2015) . Indeed, sponges have recently attracted more attention in the pharmaceutical sciences (Veres *et al.*, 2015; Stergar and Maver, 2016). Porous materials possessing a three-dimensional structure, commonly called sponges, have many applications within the biomedical domain. Drug delivery, tissue engineering, and wound healing are among the instances that can be cited as presented in figure 1.5. Furthermore, the superior properties of sponges, such as their large porosity, elastic deformation, and three-dimensional reaction environment, have been attributed to the applications mentioned in the literature (Leffler and Mü, 2000; Garg *et al.*, 2012; Zhang *et al.*, 2021).

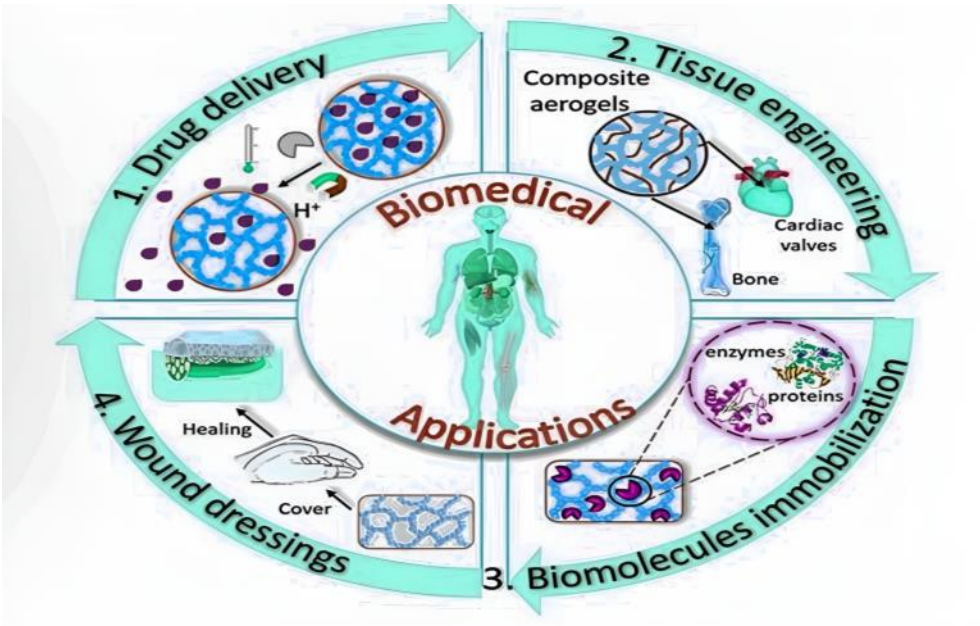

Figure 1. 3: The vast majority applications of sponges in biomedical field adopted from (Nita et al., 2020).

The quick formation of an occlusive clot is essential during surgery, and topical hemostatic sponges are frequently used to aid in this process. Additionally, they are used for various purposes, including microcoil embolization for upper and lower gastrointestinal haemorrhage

(Tamargo et al., 1989; Ledermann et al., 1998), urological surgery, intestinal surgery, orthopaedic surgery, middle ear surgery, and dental extractions (Tamargo et al., 1989; Liening et al., 1997). Moreover, related to their ability to resorb are transcatheter artery embolization in malignant disorders (Tamargo et al., 1989; Nagata et al., 1998), transcatheter chemoembolization (Tamargo et al., 1989; Chung et al., 1998), and drug delivery directly into organs that are difficult to reach by systemic administration, such as the brain (Tamargo et al., 1989; Cenni et al., 2000). As hemostatic sponges, numerous materials are employed, including vitamin A-soaked (Haws et al., 1994; Kabiri et al., 2010) poly-2-hydroxyethylmethacrylate (poly-HEMA) (Santin et al., 1996; Kabiri et al., 2010), microfibrillar collagen resorbable and non-resorbable gelatine (Colon et al., 1996; Kabiri et al., 2010). Moreover, absorbable gelatine sponges are utilised to stop bleeding and demonstrate a haemostatic function in some surgical procedures (Chanu *et al.*, 2022). Freeze-dried gelatine sponges offer several benefits, including their capability to expand and occupy empty spaces, their capacity to be tailored to fit any injury or defect site, and their controlled degradation at varying rates to ensure mechanical stability and drug release (Rodriguez *et al.*, 2013).

Further, several scholars have documented the utilization of gelatine sponges as a means of implantable drug delivery. For instance, Jiang et al. devised a hybrid delivery system that consisted of a gelatine sponge combined with poly-lactide-co-glycoside–paclitaxel (PLGA–PTX) or PLGA–rhodamine microspheres, which was employed for trans lymphatic delivery of chemotherapy. This system possesses the advantage of being self-sustaining and having a localized delivery mechanism. Consequently, utilizing microspheres conferred a sustainable attribute, while the structural benefit of gelatine sponge facilitated localized delivery to the system. Also, the findings of Liu et al. suggested that this system exhibits a favourable mode of transportation to the lymphatic system (Liu *et al.*, 2007, 2009).

Furthermore, Shukla and colleagues reported the utilization of a multilayer film that releases vancomycin on a gelatine sponge that is commercially available, highly absorbent, and porous, with significant therapeutic implications. Furthermore, the utilization of layer-by-layer constructed vancomycin-containing films on a significantly porous substrate increased drug loading by approximately 880% compared to a flat substrate. As a result, the duration of vancomycin's release was extended to six days, in contrast to the two-day release period observed for film-coated flat substrates. Moreover, Shukla et al. concluded that using spray layer-by-layer assembly incorporating a gelatine sponge considerably improves vancomycin's loading and prolongs its release duration in contrast to a previously utilized planar substrate (Shukla *et al.*, 2012). Additionally, a gelatine sponge was used in drug delivery to treat burn wounds, as evidenced by a separate research investigation (Kaur *et al.*, 2016). Also, the integration of a curcumin-b-cyclodextrin molecular inclusion complex into a gelatine sponge was demonstrated by Kaur et al. Furthermore, applying a curcumin-b-cyclodextrin-infused sponge resulted in wound healing rates like those of commercially available formulations, and no adverse effects were observed. Thus, the study conducted by Kaur et al. provides robust evidence supporting the therapeutic benefits of curcumin-cyclodextrin-loaded sponge in speeding up wound healing (Kaur *et al.*, 2016). Again, the development of gelatine-konjac glucomannan hybrid sponges loaded with gold (Au) nanoparticles and gentamicin sulfate has been documented by Zou et al. Also, the utilization of sponges as a possible remedy for bacterial wounds has been suggested in recent studies conducted by Zou et al. and Ndlovu et al. (Zou *et al.*, 2020; Ndlovu *et al.*, 2021). Furthermore, Ye et al. generated gelatine-gelatine sponges crosslinked with tannic acid and incorporated silver nanoparticles for wound healing, as Ndlovu et al. reported. Additionally, Ye et al. developed a novel composite sponge by integrating gelatine and bacterial cellulose in a structure resembling a honeycomb. The hybrid composite sponges demonstrated noteworthy characteristics such as a considerable surface

area, even distribution of pores, high porosity, and remarkable swelling capacity. The findings from the *in vitro* drug release experiments suggested that ampicillin was consistently sustained over 48 hours, and the release mode adhered to a non-Fickian diffusion pattern. As reported by Ye et al. and Ndlovu et al. the gelatine-based hybrid sponges exhibited significant antibacterial characteristics and favourable biocompatibility, making them appropriate for diverse antibacterial applications (Ye *et al.*, 2019; Ndlovu *et al.*, 2021).

Commercially available gelatine sponges include Lyostypt (Baumann *et al.*, 2009), Surgifoam (Skovrlj *et al.*, 2014) , Spongostan (Vordemvenne *et al.*, 2020) , and Gelfoam® (Wee *et al.*, 2012).

5.1.1.5 Gelfoam® sponge

The utilization of Gelfoam®, a gelatine sponge variant manufactured by Pfizer Inc., has been acknowledged as a significant hemostatic agent in neurosurgery. Furthermore, the gelatinous sponges derived from purified porcine skin exhibit properties of inertness and insolubility in water. Additionally, there have been reports indicating that they possess the ability to undergo multiple assimilations of their mass while in a liquid state (JENKINS and JANDA, 1946; Holste *et al.*, 2022). As per the report provided by the manufacturer, the duration required for the complete dissolution of Gelfoam® ranges from 4 to 6 weeks. However, the time of the procedure may be impacted by several factors, such as the size of the sponge, the surgical site, and the amount of fluid intake, as documented by Treves and Holste et al. (Treves, 1952; Holste *et al.*, 2022). In addition, the Gelfoam® sponge is a sterile and absorbable haemostatic agent (Wong *et al.*, 2013; Ashour *et al.*, 2018). Also, the sponge Gelfoam® exhibits a significant increase in size, approximately twice its original dimensions, and can absorb a substantial amount of blood, up to 40 times its weight (Vyas and Saha, 2013; Ashour *et al.*, 2018). Furthermore, the advantage of employing gelatine instead of collagen matrix lies in its straightforward preparation and extraction procedures, leading to a higher yield and more

economical production of the gelatine matrix. Additionally, as per Rohanizadeh, Swain, and Mason and Ashour et al., it can be observed that, unlike collagen, gelatine does not demonstrate any antigenicity when subjected to physiological conditions (Rohanizadeh, Swain and Mason, 2008; Ashour *et al.*, 2018). Moreover, Gelfoam® has been employed in distal target embolization, followed by proximal embolization using coils for many years. Consequently, Kumar et al. have suggested a new technique that involves using a Gelfoam® "slurry" to fill the sac of the pseudo-aneurysm, resulting in the accumulation of particles and the formation of an aggregate (Abada and Golzarian, 2007; Kumar *et al.*, 2013).

In addition, percutaneous vertebroplasty (VP), a medical procedure, is linked with several complications, such as infection, new fractures of the adjacent vertebral body, and cardiopulmonary complications. For instance, Cement leakage following VP is a significant complication, with reported rates ranging from 38% to 75%. Further, Kim et al. reported that Ahn and Oh had documented the utilization of the Gelfoam® technique in Percutaneous VP as a prophylactic measure for the cement leakage following VP (Kim *et al.*, 2014; Ahn and Oh, 2020). Similarly, Geng et al. have established a rabbit model for spinal tuberculosis by implementing an appropriate implantation technique to introduce the bacterium. As per the findings of Geng et al., introducing *M. tuberculosis* suspension into a Gelfoam® sponge exhibited a significant potential in managing or averting bacterial overflow in the event of bleeding (Geng *et al.*, 2015). Furthermore, the employment of Transcatheter Arterial Chemoembolization (TACE) represents an important therapeutic modality in treating Hepatocellular Carcinoma. Consequently, the Gelfoam® sponge is a frequently utilized material for this purpose and is commonly employed as an embolic agent in clinical settings (Xu, Wang and Li, 2021).

Research findings have demonstrated that several forms of cancer have the capability to proliferate on Gelfoam sponge and then disperse within the gel matrix. Additionally, it has

been demonstrated that Gelfoam histoculture exhibits true three-dimensional characteristics as compared to Matrigel, which can be considered at most two-and-a-half-dimensional (Yano *et al.*, 2015; Yamamoto *et al.*, 2020).

For the treatment of stage III non-small cell lung cancer, the Gelfoam plaque was utilized as a carrier for the implantation of either radioactive l-125 or Pd-103 seeds. After the surgical resection was performed, the radioactive Gelfoam plaque was securely attached to the tumor bed using either clips or sutures. The observed rate of local control during the latest follow-up period was 82%. The data indicated that the overall survival rate after a two-year period was 45%, however the cause-specific survival rate during the same timeframe was 56.46%. Hence, the application of the intraoperative Gelfoam I-125 or Pd-103 planar implant technique has been identified as a reliable and effective approach for the management of stage III non-small cell lung cancer instances characterized by a positive surgical margin (Nori, Li and Pugkhem, 1995).

Antineoplastic medications are administered via direct arterial injection, facilitating the achievement of elevated concentrations of pharmaceuticals within the tumor site. Consequently, this approach serves to mitigate the occurrence of systemic side effects. The coadministration of chemotherapeutic drugs with Gelfoam® leads to an extended duration of retention for anticancer medicines within tumor tissues. Additionally, the tumor undergoes ischemia damage as a result of the subsequent mechanical embolization of the artery that supplies it (Ikeda *et al.*, 2005).

1.5.2 Preparation techniques for sponges

Generally, in the formation of aerogels or sponges, the liquid component of the gel is replaced with gas without causing the gel to collapse, resulting in a lightweight, extremely porous material (Nita *et al.*, 2020; Azum *et al.*, 2021). In 1931, Samuel Stephens Kistler at the

University of the Pacific in Stockton, California, USA, used pressure and heat to extract fluid from a wet gel, resulting in extraordinarily lightweight materials with high porosities (about 98 %) (Azum *et al.*, 2021). Furthermore, the most crucial stage in bio-based aerogels is removing the pore-filling solvents from the wet gels without significantly decreasing the volume or compacting the network, which is accomplished by mixing the precursors, followed by a gelling process. Then, the pore-filling solvent is typically transformed into a supercritical fluid before being gently expelled as a gas. Therefore, this method ensures that aerogels maintain the same structural integrity as their wet gel starting materials (Figure 1.6) (Nita *et al.*, 2020).

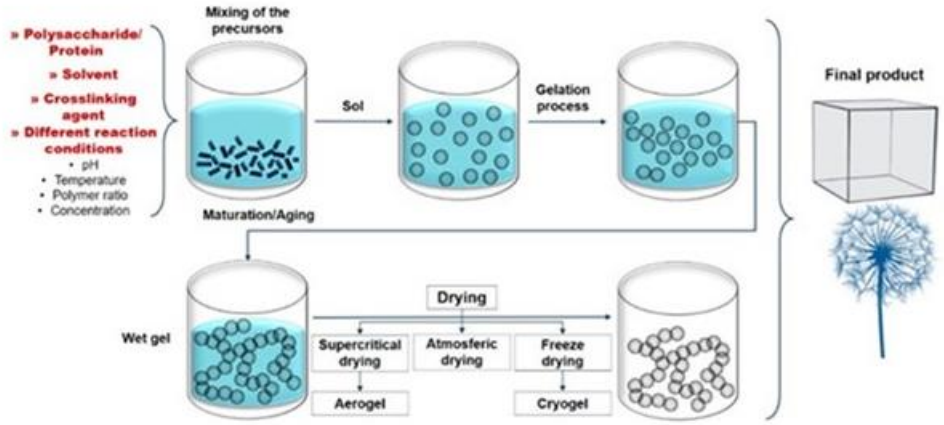

Figure 1. 4: The common techniques for sponge preparation (Nita et al., 2020).

The drying process is crucial to generating an aerogel since it determines the final structures' shape, porosity, and structural integrity. Capillary pressure causes the gel's pore structure to collapse and break when using traditional drying procedures. This prompted the development of novel techniques such as supercritical drying (with alcohol, acetone, or CO2), ambient pressure drying, freeze drying, microwave drying, and vacuum drying (Zuo *et al.*, 2015; Nita *et al.*, 2020)

5.1.1.6 Freeze drying technique

The freeze-drying technology can be traced back to prehistoric eras and was employed by the Aztec and Eskimo communities to preserve food items. In the late 1880s, the process was implemented at a laboratory scale, and the fundamental principles were comprehended during that era (Crowe, Crowe and Chapman, 1984; Wolkers and Oldenhof, 2021). The freeze/sublimation-drying principle is founded on a physical phenomenon. This phenomenon was built on the assumption that if the partial pressure of the ambient water vapour is less than that of the ice at its corresponding temperature. Subsequently, the ice present in the product undergoes direct conversion into water vapour, bypassing the intermediate fluid state (Kumar, 2012). The process of water sublimation can occur at pressures and temperatures lower than the triple point, precisely at 4.579 mm of Hg and 0.0099°C (Kumar, 2012; Shinde, 2022). Additionally, Whang et al. were the first to use the freeze-drying process to create PLGA scaffolds (Whang *et al.*, 1995; Loh and Choong, 2013).

Lyophilization, also known as freeze-drying, is a prevalent drying technique that extensively applies in the pharmaceutical sector. Furthermore, the products offered by freeze drying exhibit enhanced stability and desirable physicochemical properties, including improved dissolution rates and bioavailability. In contemporary times, biotechnology has led to a surge in the production and creation of biopharmaceutical commodities, specifically proteins and peptides. Though, many proteins and peptides exhibit limited stability, necessitating freeze-drying to achieve strength for extended storage periods (Liu, 2006).

In general, the freeze-drying method consists of three key stages: freezing, primary drying and secondary drying (Abdelwahed *et al.*, 2006; Jakubowska and Lulek, 2021) . In the primary drying process, water is frozen out of an aqueous solution before evaporating away because of sublimation. In secondary drying, the non-frozen water is removed through diffusion and desorption (Geidobler and Winter, 2013).

There are multiple fabrication techniques for building three-dimensional biomimetic scaffolds, aside from freeze drying. These alternative approaches encompass electrospinning (Chung *et al.*, 2010; Soliman *et al.*, 2010), phase separation (Blaker, Knowles and Day, 2008; Budyanto, Goh and Ooi, 2009), and self-assembly (Nagahama, Ouchi and Ohya, 2008; Peck *et al.*, 2011; Lu, Li and Chen, 2013).

1.5.3 Polymers utilized in sponge preparation

Polymeric materials have been increasingly utilized as drug-delivery platforms within the pharmaceutical industry, as reported by Alam et al. and Abdul Khalil et al. (Alam *et al.*, 2018; Abdul Khalil *et al.*, 2023). Furthermore, various biopolymers, such as cellulose (Abeer, Mohd Amin and Martin, 2014; Abdul Khalil *et al.*, 2023) , starch (Mallakpour and khodadadzadeh, 2018; Abdul Khalil *et al.*, 2023), chitosan (Shariatinia and Mazloom-Jalali, 2019; Abdul Khalil *et al.*, 2023), have been employed in the field of drug delivery. Moreover, it has been reported by Yao et al. and Mania et al. that materials possessing a porous texture can be classified into three distinct groups depending on the source of their constituent raw materials, namely, synthetic, natural, and ceramic (Yao *et al.*, 2018; Mania *et al.*, 2019).

5.1.1.7 Gelatine

Gelatine is a biopolymer that is created by hydrolysing collagen to denature it. Further, collagen is derived from numerous animal and human organs, including the skin and connective tissues (Gomez-Guillen *et al.*, 2011; Qiang Zhang *et al.*, 2016). Additionally, the biomedical industry has made extensive use of gelatine as a controlled drug-delivery vehicle (Ooi, Ahmad and Amin, 2016; Kirdponpattara, Phisalaphong and Kongruang, 2017)and bone scaffold (Wang *et al.*, 2016; Kirdponpattara, Phisalaphong and Kongruang, 2017). Besides, gelatine's biological origin and biocompatibility have led to its use in a wide variety of pharmaceutical and medical applications, such as vascular prosthesis sealants (Guidoin *et al.*, 1994), bone-repairing

matrices, controlled drug release systems (Cortesi, Nastruzzi and Davis, 1998), wound dressing materials (Ulubayram *et al.*, 2001), and tissue engineering scaffolds (Ulubayram *et al.*, 2002).

The use of gelatine in pharmaceutical and biomedical applications is especially interesting due to its biocompatibility and biodegradability, as well as the complete absence of toxicity or allergic reactions typically associated with synthetic polymers. Moreover, gelatine is typically derived from collagenous tissues and is more practical than collagen itself since it lacks antigenicity, whereas collagen exhibits some antigenicity under physiological settings (Ulubayram *et al.*, 2002). Other than being biodegradable and non-immunogenic, gelatine is also inexpensive, and it was developed as a cell-matrix imitation. However, gelatine needs to be augmented with other compounds to get rid of its limitations or add new effective characteristics. Gelatine, for instance, is rigid and inflexible when it's completely dry (Xing *et al.*, 2010; Kirdponpattara, Phisalaphong and Kongruang, 2017).

5.1.1.8 Sodium alginate

Sodium alginate is an anionic polysaccharide made up of the sugars b-D-mannuronic acid and a-L-guluronic acid, both of which are found in seaweed. Furthermore, alginate hydrogels are utilised in numerous industries including food, tissue engineering, pharmaceutical, and more because of their high-water solubility, biocompatibility, biodegradability, and diversity in natural sources (Pawar and Edgar, 2012; Barros *et al.*, 2016).

The limited mechanical strength of natural polymers often poses challenges in handling and processing. Therefore, employing derivatives or blends with diverse polymers is often necessary to achieve suitable mechanical characteristics for their intended application (Aldana *et al.*, 2021; Puertas-Bartolomé, Mora-Boza and García-Fernández, 2021).

5.1.1.9 Approaches of enhancing mechanical properties of sponges

1.5.3.1.1 Blending approach

Due to the combining of many functionalities in one entity, composite materials are always appealing (Ulker and Erkey, 2014). Moreover, biodegradable polymers are a type of polymer that has applications ranging from tissue engineering, wound management, drug delivery, and orthopaedic devices to packaging and film. Furthermore, to broaden their potential applications, biodegradable polymers are modified using various methods such as blending and composites forming, resulting in new materials with unique characteristics such as high effectiveness, low cost, and good processability (Hamad *et al.*, 2014) . Additionally, polymer blends and composites are of great scientific and commercial interest for changing the properties of polymers. However, chemical modification or novel polymer architecture can improve the properties of a polymer system, but blends and composites are one of the most effective and cost-effective techniques with superior technological properties. Furthermore, there is a specific interaction between polymer/polymer, polymer/filler, or polymer/polymer/additives in polymer blends and composites, resulting in properties that differ from those of basic polymers. As a result, they have been proposed as a method of providing materials with new properties (Logothetidis, 2018). Therefore, recently, there has been an increasing interest in the development of new material blends. The blending of two or more polymers is expected to improve the mechanical properties of the resulting material. Nonetheless, blends can be made from synthetic and natural polymers, as well as two (or more) biopolymers (Sionkowska, 2021) . Implants, temporary prostheses, tissue engineering scaffolds, biosensors, and controlled release systems are all examples of biodegradable polymeric blends in biomedical applications. Furthermore, blending is an efficient method for creating a novel material with desired properties that cannot be achieved with a single polymer component (Pawar and Srivastava, 2019). However, to avoid degradation concerns in

mammalian tissues, it is helpful to blend biocompatible and non-immunogenic polymers (Veres *et al.*, 2015).

In principle, a key aspect of developing a novel blend or composite of two or more polymers is to improve the performance of the newly blended material rather than to radically change the properties of the components (Yu, Dean and Li, 2006; Toh *et al.*, 2021). In the last two decades, there has been a surge of interest in self-assembling structures formed in aqueous solutions, such as polyelectrolyte complexes (PECs). Furthermore, PECs can be created by combining biopolymers with opposing charges, such as proteins and polysaccharides (Kizilay, Kayitmazer and Dubin, 2011; Derkach *et al.*, 2020).

1.5.3.1.2 Crosslinking

The inherent brittleness and solubility in water of pure gelatine material pose a challenge to its utilization in tissue engineering. Furthermore, the existing literature suggested that crosslinking gelatine molecules can enhance gelatine material's mechanical and thermal characteristics (Haiyan *et al.*, 2017). Moreover, the attainment of desired stability necessitates the implementation of cross-linking treatments through physical or chemical means. The physical cross-linking techniques commonly employed include de hydrothermal treatment and exposure to ultraviolet radiation. The principal benefit of utilizing physical techniques lies in their ability to preserve the scaffold's chemical composition while exhibiting minimal toxicity to cells, as evidenced by the limited number of reported cases. Nonetheless, it should be noted that these techniques have a drawback in that they exhibit reduced efficacy in achieving the intended level of cross-linking (Wang *et al.*, 2015; Arif *et al.*, 2020). Numerous chemical agents, including formaldehyde, glutaraldehyde, poly epoxy compounds, tannic acid, dimethyl suberimidate, carbodiimide, and acyl azide, have been employed to alter gelatine for biomedical purposes chemically. Furthermore, chemical crosslinkers are known to offer enhanced hydrolysis resistance and thermal stability. However, it is essential to note that these

synthetic crosslinking agents are toxic to the cell, which suggests that they may not be the most efficient option regarding biocompatibility (Oryan *et al.*, 2018a; Arif *et al.*, 2020). Generally, the cross-linking process involves the chemical or physical reaction between the active functional groups of polymer chains and crosslinking agents, forming a three-dimensional network (O'Brien, 2011; Oryan *et al.*, 2018a). The formation of a network structure by cross-linking polymer chains can be covalent or ionic. Dialdehydes, such as glutaraldehyde, are the most common covalent cross-linkers, and the slow hydrolysis of covalent bonds can control drug release (Jin *et al.*, 2021). Despite reports of cytotoxicity, the success of thousands of bioprosthetic implants over the last ten years indicates that glutaraldehyde crosslinking is clinically acceptable and has many benefits (Jayakrishnan and Jameela, 1996; Imani, Rafienia and Emami, 2013). Glutaraldehyde has been widely employed as a protein crosslinker, an activator of supports, and a crosslinker for enzymes and supports in many applications (Barbosa *et al.*, 2014). Furthermore, it is widely employed as a cross-linking agent in the fabrication of bioprostheses, including heart valves, vascular grafts, elastic cartilage, and artificial skin. It is also utilized for cell and enzyme immobilization, as well as protein and polysaccharide stabilization. The process of glutaraldehyde cross-linking in collagenous tissues has been found to have a significant impact on reducing biodegradation. This effect enhances the biocompatibility and non-thrombogenic properties of the tissues, while also keeping their anatomical integrity, strength, and flexibility. Among the several aldehydes utilized to cross-link a protein matrix, glutaraldehyde has several advantages. Firstly, glutaraldehydeexhibits a rapid reaction rate, facilitating efficient cross-linking processes. Additionally, glutaraldehyde proves to be a cost-effective option compared to other alternatives. Moreover, glutaraldehyde is easily accessible and possesses high solubility in aqueous solutions. Furthermore, glutaraldehyde demonstrates compatibility with a wide range of amino groups that are abundantly found in proteins (Ulubayram *et al.*, 2002).

1.6 Implantable drug delivery device: manufacturing and polymers

Implantable drug delivery devices refer to medical devices that release drugs at a predetermined rate and duration upon being implanted within the human body (Rajgor, Patel and Bhaskar, 2011; Stewart *et al.*, 2020). Furthermore, implantable systems present numerous benefits compared to traditional delivery methods such as oral and parenteral administration (Kaurav and Kapoor, 2017; Kutlehria *et al.*, 2022). In addition, implantable delivery systems have been utilised in various clinical contexts, primarily for contraceptive purposes (e.g., Nexplanon® and NuvaRing®) and cancer therapy (e.g., Vantas®) (Dash and Cudworth, 1998; Stewart *et al.*, 2020).

1.6.1 Manufacturing techniques

Various techniques can be employed to produce implantable systems, such as compression, solvent casting, hot melt extrusion, injection moulding, and, more recently, three-dimensional (3D) printing (Fialho and Da Silva Cunha, 2005; Stewart *et al.*, 2018).

5.1.1.10 3D printing technology

Additive manufacturing (AM) is a critical component of the rapid product development process, which includes but not limited to, rapid nanotechnology, rapid prototyping, and rapid manufacturing. Moreover, there are numerous AM technologies available in the world. Stereolithography, selective laser 3D printing, laminated object manufacturing, sintering, polymer jetting, selective laser melting, direct metal laser sintering, laser engineered net shaping, direct metal deposition, electron beam melting, and fused deposition modelling (FDM) are the most widely used AM technologies worldwide (Udroiu and Nedelcu, 2011). Furthermore, based on the status of the materials used, the AM process is broadly divided into three categories: liquid-based, solid-based, powder-based, and hybrid-based productions (Yuxuan Wang *et al.*, 2020).

3D printing with FDM process, invented by Stratasys, is widely used in the production of drug delivery systems and scaffolds for biomedical use(biomanufacturing) and medical devices, alloy production, and biological tissue replacement (Genina *et al.,* 2016; Huang and Bártolo, 2018; Deshmane *et al.*, 2021). Furthermore, FDM raw feedstock materials could be filaments or pellets (Singamneni *et al.,* 2018). FDM, on the other hand, enables the creation of personalised medications or drug delivery systems based on patient needs or disease complexity. However, the lack of large-scale production as well as a lack of regulatory guidelines remain significant barriers for this disruptive technology (de Carvalho Rodrigues *et al.*, 2022).

By the end of 2005, 3D printing had accounted for 44.3% of all AM manufacturing processes. The three main categories of 3D printing technologies (inkjet printing) are Laser based writing systems, printing based inkjet systems, and nozzle-based deposition systems. A laser is used to photosensitize a liquid resin to form a solid layer in laser-based printing, and this process is repeated layer by layer to form the 3D object. Inkjet printing, on the other hand, works by jetting the liquid containing the medicine and additives onto a predetermined area to form a layer, and by repeating the process, successive layers that build the 3D shape are formed. The nozzle-based system is based on the extrusion of pharmaceutical substances from a narrow nozzle, either by pressure, known as Pressure Assisted Micro-syringe or by melting the material filaments, known as FDM (Mohammed *et al.*, 2021).

In 1980, the initial 3D printed item was produced utilising rapid prototyping, which entailed using computer-aided design (CAD) to fabricate the intended object. The US Food and Drug Administration (FDA) granted marketing approval for Aprecia Pharmaceutical Co.'s Spritam® (levetiracetam) fast-dissolving tablets on August 5, 2015. The product was subsequently introduced to the market in 2016. Additionally, the achievement of 3D printing technology in fabricating human organs has opened up new avenues for the development of precision-

targeted pharmaceuticals in the future, as evidenced by recent studies (Tian *et al.*, 2019; Mohammed *et al.*, 2021). Furthermore, according to Yuxuan Wang et al., the utilisation of 3D printing technology has yielded a more dependable manufacturing process compared to conventional methods that employ techniques like machining (Yuxuan Wang *et al.*, 2020).

In essence, the 3D printing technology is based on a manufacturing principle that involves layering and deposition, as discussed in previous studies (Udroiu and Nedelcu, 2011; Fuenmayor *et al.*, 2018; Gebhardt, Kessler and Thurn, 2018) . After scaling, 3D physical objects can be produced through the direct utilisation of 3D CAD data, as stated by Kumar et al. (Kumar *et al.*, 2018) . Generally, the AM process chain can be categorised into two primary stages, the initial of which is a virtual phase wherein CAD software generates a virtual model referred to as a stereolithography (STL) file. Furthermore, STL also known as Standard Triangulation Language, is widely accepted as the prevailing exchange format within the AM industry. Moreover, the STL file replaces the original surface of a solid, texture, or scanned model, utilising a triangulated surface segment mesh. Furthermore, according to Udroiu and Nedelcu, most contemporary CAD systems can produce an STL file by utilising the File, Save As, and STL options (Udroiu and Nedelcu, 2011). Additionally, Mohammed et al. reported that there is a range of computer software applications, including but not limited to auto CAD, 3D Slash, SketchUp, Fusion 360, and Solid Works, that can be utilised to design 3D objects (Mohammed *et al.*, 2021). In addition, the subsequent phase involves the physical aspect, precisely the engineering stage, wherein a 3D model is generated through the process of slicing the virtual design(CAD) into layers and shaping them into the desired form using specialised slicing software (Fuenmayor *et al.*, 2018; Gebhardt, Kessler and Thurn, 2018). Further, there are several software programs capable of slicing include KISSlicer, Slic3r, OctoPrint, Simplify3D, and Cura. Moreover, the 3D slicer application is designed to transform a 3D design file, specifically an STL file, into G-code, which is a machine-readable language utilised

by 3D printers. Besides, the slicer software establishes the printing parameters for the sliced object, encompassing the number of layers, the proportion of infill, the initial offset height between the printer head and the printer stage/platform, the interlayer spacing, the printing velocity, and the overall printing duration. Upon generation, the G-code is subsequently transferred to the 3D printer, which executes the print command to produce an object of the intended dimensions and configuration (Mohammed *et al.*, 2021).

In contemporary times, there has been a notable upsurge in the attention given to 3D printing, which is regarded as a promising form of AM that facilitates the production of 3D objects. Furthermore, its versatility makes it suitable for medical implant applications. Indeed, the use of implants in pharmaceutical applications has been found to offer benefits over alternative drug delivery methods, explicitly enhancing patient compliance and adherence, as evidenced by studies conducted by Wallis et al. and Yonghui Wang et al. (Wallis *et al.*, 2020; Yonghui Wang *et al.*, 2020). Additionally, the utilisation of 3D printing to produce pharmaceutical devices presents several benefits, such as cost-effectiveness, the removal of organic solvents, the capacity to combine drugs and polymers through hot melt extrusion (HME), the capability to create multi-drug devices, and the potential to modify drug release profiles by altering shape and density. These advantages of 3D printing have been highlighted in previous studies (Beck *et al.*, 2017; Wallis *et al.*, 2020).

The existing body of research pertaining to the utilization of additive manufacturing techniques in medical applications can be broadly categorized into five distinct areas of focus. These areas include the development of disease models, the creation of inert implants, the fabrication of tissue-engineered scaffolds, the production of functional tissues and organs in controlled laboratory environments, and the generation of organ models for preoperative planning and educational purposes (Yan *et al.*, 2018; Perspectives, 2019).

1.6.2 Polymers used for implantable drug delivery devices

The classification of polymers utilised in producing implantable drug delivery devices can be divided into two groups: biodegradable and non-biodegradable (Dash and Cudworth, 1998; Stewart *et al.*, 2018). Moreover, polymers, such as silicones, poly(urethanes), poly(acrylates), or copolymers, such as poly (ethylene vinyl acetate), are frequently utilized in the production of non-biodegradable implants (Zur *et al.*, 2011; Colaris *et al.*, 2017; Stewart *et al.*, 2018). Furthermore, devices constructed from non-biodegradable polymers exhibit structural durability and resilience throughout their lifespan. However, the primary limitation associated with non-biodegradable implants is their requirement for removal once their drug payload has been finished. In addition, the utilized materials for the fabrication of implantable devices exhibit favourable biocompatibility over extended periods, occasionally resulting in infections, tissue impairment, or aesthetic deformities (Stewart *et al.*, 2018).

5.1.1.11 Ethylene vinyl acetate (EVA)

EVA is a non-biodegradable thermoplastic copolymer of ethylene (E) and vinyl acetate (VA). Furthermore, VA values typically range from 0 to 50% and have an impact on several important properties such as transition temperatures, crystallinity, hardness, and polarity. Because of its biocompatibility and formulation versatility, EVA is widely used in transdermal systems with functional applications (de Carvalho Rodrigues *et al.*, 2022). Previous studies have reported EVA-based drug delivery systems, including intravaginal rings, oral sustained tablets, and 3D printed devices. Nuvaring®, an intravaginal ring made by HME, is one of them (de Carvalho Rodrigues *et al.*, 2022). Additionally, EVA has FDA approval and is widely used in implantable controlled release applications. Correspondingly, IUS Progestasert® was one of the first EVA-based products to hit the market. Further, the EVA T-shaped body (Progestasert®) housed a reservoir of microcrystalline progesterone dispersed in silicone fluid.

However, Progestasert® was withdrawn from the market in 2001 (Genina *et al.*, 2016). Also, another commercially available EVA-based device is the contraceptive IVR Nuvaring®, in which the active pharmaceutical ingredients (etonogestrel and ethinylestradiol) are homogeneously distributed within the core polymer, which is then covered by the rate-limiting drug-free EVA sheet. Furthermore, EVA was used in the production of the contraceptive implantable SR Implanon®, which has a delivery profile that releases etonogestrel for a period of three years (Genina *et al.*, 2016).

1.7 Application of 3D printing in PC

In general cancer is a leading cause of global mortality. Despite the implementation of various treatment strategies, several challenges are associated with current cancer management approaches, including but not limited to surgery, drug development, in vitro and in vivo models, and diagnosis methods (Serrano, Terres and Lalatsa, 2018; Safhi, 2022).

Given the constraints mentioned above, 3D printing methodologies present a promising avenue for improving cancer treatment. Furthermore, the utilization of this technology enhances the efficacy of cancer surgery through its facilitation of pre-surgical planning. It also serves as a valuable educational resource for patients and trainees. Additionally, it contributes to the advancement of personalized cancer therapy (Haleem, Javaid and Vaishya, 2020; Safhi, 2022). For instance, based on preoperative CT data, it is feasible to produce a 3D model with high accuracy that can be utilized to customize the morphology of implant material to suit the unique anatomical features of an individual (Lindegaard *et al.*, 2016; Huang *et al.*, 2017, 2018; Park *et al.*, 2017).

Moreover, drug-eluting stents have effectively treated various illnesses, including cancer, by enabling targeted drug delivery to the affected area (Wolinsky, Colson and Grinstaff, 2012; Indolfi, Ligorio, David T Ting, *et al.*, 2016; Pan *et al.*, 2023). Consequently, a substantial amount of drug is administered to the affected area. Additionally, the utilization of topical

medications can mitigate the occurrence of systemic adverse effects that are frequently associated with the administration of systemic drugs (Brem *et al.*, 1995) (Pan *et al.*, 2023).

The utilization of 3D printing technology in the context of PC is currently in its infancy as evidenced from the few examples in the literature. Specifically, the primary use of applications focuses on managing treatment and surgical resection procedures. Furthermore, there is a few of examples of the utilization of local drug-delivery implants for treating PC.

Pan et al. utilized 3D printing technology to create a dual-layer drug-coated pancreaticojejunostomy device to address the elevated incidence of local recurrence in PC patients. The device can potentially impede the occurrence of local recurrence of PC after surgery and facilitate the healing of pancreatic intestinal anastomosis (Pan *et al.*, 2023).

Nonetheless, Pancreatic tumour resections are intricate surgical procedures that carry a significant risk of morbidity, as reported in the literature (Dindo, Demartines and Clavien, 2004; Ali *et al.*, 2020). Therefore, to achieve successful objective, using 3D-printed anatomical models to outline tumour anatomy is beneficial. Such models have been documented in case series about the application of PC (Marconi *et al.*, 2016, 2017).

Moreover, the authors Roeth et al. extended the utilization of 3D printing technology to PDAC to enhance the efficacy of magnetic hyperthermia treatment using magnetic nanoparticles (Roeth *et al.*, 2021). Additionally, the authors Huang et al. developed a coplanar template using 3D printing technology. This template was found to be a reliable and secure tool for guiding iodine-125 seed implantation, leading to enhanced implantation accuracy and optimised dosimetry distribution for PC treatment (Huang *et al.*, 2018). Similarly, Wang et al. conducted a study to examine the clinical effectiveness and safety of utilising 3D printing coplanar templates to assist with iodine-125 (125I) seed implantation as a palliative treatment option for patients with inoperable PC. The findings indicated that the application of 3D

printing technology in producing coplanar devices proved to be a viable and secure method of palliative intervention for patients with PC who are not eligible for surgical procedures, yielding positive clinical results (Wang *et al.*, 2022).

The researchers Yi et al. utilized 3D printing in developing a biodegradable patch that incorporates a potent dose of an anti-cancer agent, enabling targeted delivery of the drug to the precise location of PC. Further, the utilization of 3D printing technology in fabricating porous patches with varied shapes has exhibited the capacity to modulate drug release by manipulating surface area (Yi *et al.*, 2016).

1.8 Hypothesis and objectives

This study aims to develop an implantable device that can be implanted during surgery and deliver chemotherapy locally over at least 7 days at a time after surgery when the patient is suitably recovered.

The first objective is to create and evaluate diverse gelatine sponge compositions by integrating sodium alginate (blending method) and the cross-linking of glutaraldehyde (crosslinking method). Subsequently, an evaluation will determine the impact of varying concentrations of gelatine, composite blend, and crosslinker on precursor hydrogels' mechanical and rheological characteristics, as well as the mechanical properties of the corresponding sponges compared to a commercially available sponge utilised as a reference control.

The second objective of this study is to provide additional characterization of the optimum sponge regarding its microstructural, thermal, spectral analysis, hydrolytic properties and drug distribution pattern. Furthermore, the influence of the optimum sponge qualities on the *in vitro* drug release of one drug from the FOLFIRINOX regimen will be assessed.

The third objective of this study is to produce a drug-delivery device that can be implanted and is appropriate for the anatomical characteristics of PC resection margin through 3D printing technology. The device will subsequently be evaluated and analysed based on its mechanical properties and *in vitro* drug release characteristics.

The fourth objective of the study is to evaluate the *in vivo* safety and efficacy of the final device, which comprises a 3D-printed component and a gelatine sponge. The biocompatibility and implantability of the device will be assessed in pigs. In contrast, the device's efficacy in suppressing tumour growth through the release of the FOLFIRINOX regimen will be evaluated in mice.

Chapter 2: Preparation and mechanical characterisation of hydrogel-based sponges for local drug delivery

2.1 Introduction

PC is widely recognised as a highly lethal solid tumour due to its clinically diagnosed late and aggressive nature, resulting in a 5-year survival rate of less than 5% (Bengtsson, Andersson and Ansari, 2020; Bazeed, Day and Garg, 2022). A key obstacle in the treatment of PC is the predominance of older patients, whose poor general health, due to their advanced age reduces their treatment options and response to treatment (Aquib *et al.*, 2020; Bazeed, Day and Garg, 2022). Inadequate drug delivery to the cancer, due to the desmoplastic stroma and poor vascularization characteristic of PC is another significant obstacle. The gold standard is surgery; however, it is rarely curative. Further, it has been demonstrated that adjuvant chemotherapy improves survival, and surgery followed by adjuvant therapy is currently the standard of care for all patients with resectable PC (Lambert *et al.*, 2021). FOLFIRINOX, a recently identified first-line treatment for PC, is a promising combination of cytotoxic drugs; nevertheless, it is not suited for all patients due to its systemic toxicity (Byrne *et al.*, 2018). As a result, numerous local drug delivery systems have been developed to address the deficiencies of conventional chemotherapy (Yi *et al.*, 2016).

To successfully transition a local delivery system from the laboratory to the clinic, clinicians must have access to a versatile drug-eluting platform tailored to PC patients (Indolfi, Ligorio, David T. Ting, *et al.*, 2016). Moreover, due to the unevenness of surgical wounds, a soft-malleable-like substance would be ideal as an implanted system (Aquib *et al.*, 2020). Sponges are distinguished by their 3D porous structures, which have potential applications in medicine and other disciplines such as scaffolding in bone regeneration, chemo catalysis, resin exchange and energy storage (Reddy, Reddy and Jiang, 2015; Zhang *et al.*, 2021). Scaffolds or sponges

are also used as implants to deliver cells, genes, and, more importantly, drugs into the body (Garg *et al.*, 2012). Because of their low density, large porosity, and high surface area, porous materials have become popular in drug delivery (Duan *et al.*, 2017). They can achieve optimal drug loadings with high efficiency drug delivery to specific sites. Natural polymers (alginate, proteins, collagens, gelatine, fibrins, and albumin) and synthetic polymers (polyvinyl alcohol and polyglycolide) have all been used in the preparation of scaffolds (Garg *et al.*, 2012; Nagarajan *et al.*, 2019). Collagen-based films and sponges are among the most commonly used biomaterials (Rault *et al.*, 1996).

Gelatine is a biocompatible and biodegradable polymer utilised in the pharmaceutical and medical industries, primarily in creating wound dressings and drug delivery systems. In aqueous conditions, gelatine granules, films, and sponges rapidly hydrate and disintegrate *in vivo* (Cortesi, Nastruzzi and Davis, 1998; Ulubayram *et al.*, 2002). Therefore, gelatine's poor mechanical and adhesive properties limit its end-use applications despite its biodegradability, biocompatibility, and unique biological properties. To improve gelatine's bio adhesivity, chemical modifications and blending with other biomaterials have been proposed (Ahmady and Abu Samah, 2021). Additionally, crosslinking is a crucial method for overcoming sponges' poor mechanical properties and instability in aqueous environments (Rault *et al.*, 1996; Reddy, Reddy and Jiang, 2015). Furthermore, crosslinking can improve the structure's mechanical qualities, increase stability, and lengthen its endurance. There are several crosslinking techniques, such as heat treatment (Esposito, Cortesi and Nastruzzi, 1996) , UV or gamma irradiation (Weadock *et al.*, 1995) , and chemical agent addition (Cortesi, Nastruzzi and Davis, 1998). These chemical agents include, but are not restricted to, sugar (Cortesi, Nastruzzi and Davis, 1998) , genipin (Sung *et al.*, 1999) , carbodiimides (Guidoin *et al.*, 1994) , and glutaraldehyde (Lin *et al.*, 1998; Ulubayram *et al.*, 2002). However, the toxicity of the

crosslinking agent must be carefully considered while designing biomaterials (Kabiri *et al.*, 2010).

This chapter investigates how the mechanical properties of gelatine sponges can be improved through blending and crosslinking techniques. The goal is to produce a stable gelatine sponge that can provide sustained drug release over several weeks. This will be achieved by assessing how blending and crosslinking increase the sponges' hardness and elasticity and learning more about the rheological behaviour of the precursor hydrogels. Moreover, the influence of crosslinking and blending on the sponges' swelling ratio and porosity percent. Consequently, Gelatine concentration (1%, 4%, 7%, and 10%), sodium alginate concentration (1% and 4%) in combination with gelatine concentration (4%, 7%, and 10%), and crosslinking the composite (4% sodium alginate and 4% gelatine) with (0.1%, 0.5% and 1%) glutaraldehyde, were investigated. Comparison studies between these methods should shed light on the mechanical properties of sponges and precursor hydrogels and their physical differences. Furthermore, the sponges that have been prepared will undergo an evaluation process in comparison to a commercially available sponge, namely Gelfoam®, which will serve as the control in this study.

2.2 Materials and methods

2.2.1 Materials

A high bloom strength (250 G) gelatine was obtained from Sigma-Aldrich (Dorset, United Kingdom). Glutaraldehyde (GTA) solution, 50% in the water was purchased from Sigma-Aldrich (Dorset, United Kingdom). Sodium alginate was obtained from Scientific Laboratory Supplies (Nottingham, United Kingdom). Ethanol HPLC grade was purchased from the university store (Fisher chemical). Gelfoam® sponge was purchased from AEGIS

LIFESCIENCES PVT. LTD, Gujarat, India. Irinotecan Hydrochloride was purchased from LGM Pharma (Georgia, USA).

2.2.2 Preparation of the sponges

The gelatine and sodium alginate solutions were made individually by dissolving each substance in 20 ml water at a temperature of 80 °C using a hot plate. Subsequently, the temperature reduced to 50 °C, following which the two solutions were combined. The mixture was subsequently agitated on a heated plate at a temperature of 37 °C, and the intended concentration of glutaraldehyde, serving as a crosslinking agent, was introduced. The agitation process was sustained for one hour. Subsequently, the gel obtained was transferred into moulds with a rectangular shape and subsequently subjected to freezing at a temperature of -80 °C for 24 hours and then lyophilized for 48 hours at 0.01mbar, -85°C temperature using a freeze dryer instrument (Labconco Corporation, Missouri, USA). The gel sample was utilized to conduct rheological characterization prior to freezing and freeze drying.

The formulation compositions are provided in table 2.1.

Table 2. 1: The different types of sponges and their ingredients

Formulation code	Gelatine % w/v	Sodium alginate % w/v	Glutaraldehyde % w/v
F1	1	0	0
F2	4	0	0
F3	7	0	0
F4	10	0	0
F5	4	1	0
F6	4	4	0
F7	7	1	0
F8	7	4	0
F9	10	1	0
F10	10	4	0
F11	4	4	0.1
F12	4	4	0.5
F13	4	4	1

2.2.3 Rheological measurements

The hydrogels were rheologically characterised to investigate the effect of varying gelatine concentration and blending approach on their viscoelastic behaviour. The rheological analysis was conducted using a discovery HR10 TA rotational rheometer fitted with a Peltier heating system. A plate-plate geometry with a 40 mm (PP40) diameter was utilised, and an average force of 0.15 N was applied to prevent the sample from slipping. The gap between the plates was around 1mm, depending on the hydrogel sample height. Amplitude sweep tests were performed on each hydrogel to determine the linear viscoelastic region (LVER) at a frequency of 1 Hz and a strain between 0.005 and 1%. Storage (G′) and loss (G″) moduli of the hydrogels were monitored as a function of strain % in the range of viscoelastic region (LVER).

2.2.4 Mechanical evaluation of the sponges

The hardness and elasticity of the sponges were assessed using a TA-XT2 Texture Analyzer (Stable Micro Systems, Haslemere, UK) equipped with a 5 kg load cell and Texture Exponent-32® software program. A 6-mm cylindrical stainless-steel probe (P6 probe) was used in compression mode. The test chosen was Make up sponges for firmness and springiness determination. The mode was Measure Force in Compression, the pre-test speed was 1.0 mm/s, the test–speed was 1.0 mm/s, the post–test speed was 10.0 mm/s, the target mode was distance, the hold time was the 30s, and the strain was 50%. The resulting plot depicts a Force-Time curve displaying the characteristics of a sponge firmness and springiness test. The probe compressed the sample until it reaches 50% of the product height and held it for 30 seconds before withdrawing from the sample and returning to its original position. Firmness is defined as the force (in grammes, kilogrammes, or Newtons) required to compress a product by a predetermined distance, such as 50%. To calculate the springiness property, the force after 25 seconds was taken, divided by the maximum force, and multiplied by 100 per cent. F25

multiplied by 100 equals Fmax. The product is more like a 'spring' the closer the resulting value is to 100%.

2.2.5 Porosity of the sponges

Sponge porosity was assessed by the liquid displacement method. Absolute ethanol was used because it permeates through the sponge but does not cause any swelling or shrinkage. The dry sponge was weighed, then subsequently immersed in 10 ml ethanol (V1) and degassed for 5 min with a vacuum pump. The total volume of ethanol and sponge was recorded as V2. The soaked sponge was removed, and the remaining volume of ethanol was recorded as V3. The porosity was calculated using the equation:

$\varepsilon 1\ (\%) = (V1 - V3)/\ (V2 - V3) \times 100$ (Yang *et al.*, 2018).

2.2.6 Swelling ratio of the sponges

The swelling ability of the sponges was measured by immersing the pre-weighed sponge (W0) in deionized water for 1 hour at room temperature. The soaked sponge was removed and re-weighed (W1) after gently removing the excess water with filter paper. The swelling ratio was calculated using the equation:

$\varepsilon 2\ (\%) = (W1 - W0)/W0 \times 100$ (Yang *et al.*, 2018).

2.2.7 Statistical analysis

A t-test was used for the statistical analysis (GraphPad Prism version 9.4.1 for Windows, GraphPad Software, San Diego, CA), to compare between each group and the control group Gelfoam® to answer the question if there is a significance difference between each group and the control group. In every instance, a significance threshold of $p<0.05$ was accepted to signify importance.

2.3 Results

2.3.1 Rheological evaluation

2.3.1.1 Influence of gelatine concentration on the viscoelastic moduli of the hydrogels

The rheological behaviour of the hydrogels with different gelatine concentrations is presented in figure 2.1. The effect of gelatine concentration on the viscoelastic moduli (storage or elastic modulus G′ and loss or viscous modulus G″) was studied. The region in which the moduli are strain-independent and parallel corresponds to the LVER. As demonstrated, a higher gelatine concentration corresponds to higher moduli, a reduction of the LVER and a decrease of the yield strain (critical strain value at which the moduli crossover occurs), and the capability of holding during lower stress before being subjected to deconstruction behaviour at higher stresses. It demonstrated a predominance of the storage modulus G′ above the loss modulus G″ with increasing gelatine content, indicating more assertive hydrogel behaviour.

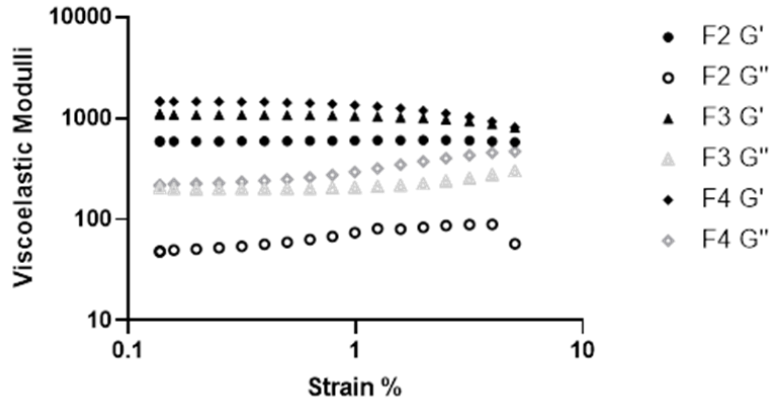

Figure 2. 1: Amplitude sweep for various concentrations of gelatine hydrogels. Solid and empty points represent, respectively, the storage (elastic) modulus G′ and the loss (viscous) modulus G".

2.3.1.2 Influence of blending on the viscoelastic moduli of the hydrogels

The rheological behaviour (storage or elastic modulus G′ and loss or viscous modulus G″) of the hydrogels with various gelatine and sodium alginate concentrations is presented in figures 2.2A and 2.2B. An increase in the sodium alginate concentration corresponds to higher moduli,

as well as to an increase of the LVER indicating a predominance of the storage modulus G′ above the loss modulus G″ with increasing sodium alginate concentration, thereby indicating more robust hydrogel behaviour.

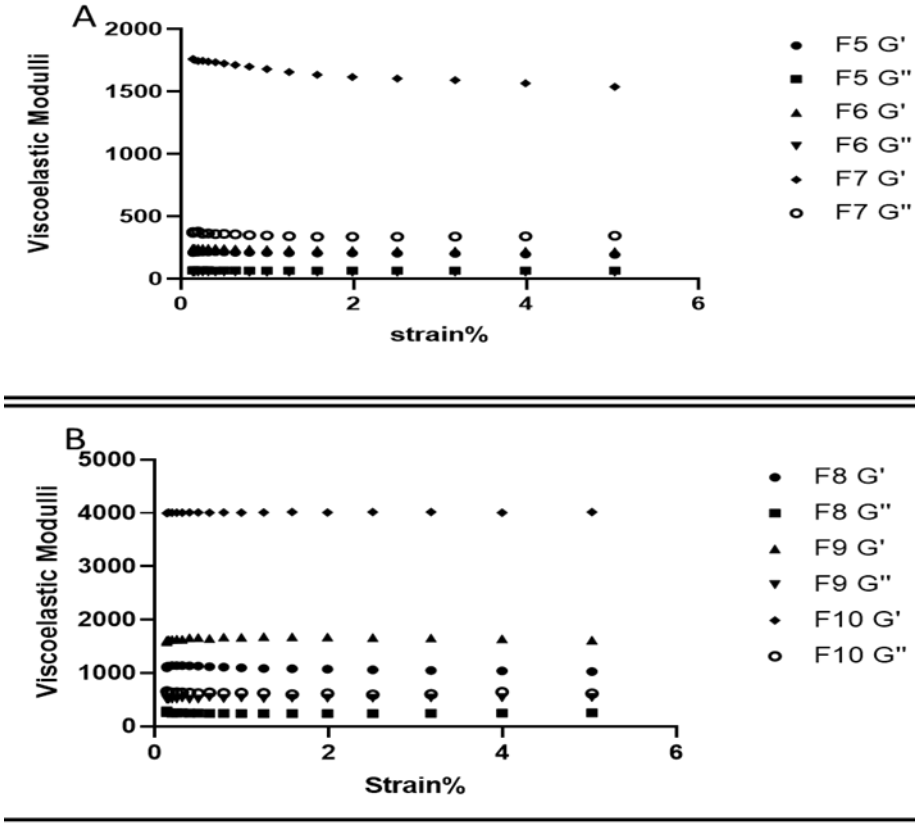

Figure 2. 2: Amplitude sweep for various blends of gelatine and sodium alginate hydrogels. (A) for formulations F5, F6 and F7, while (B) is for F8, F9, and F10. Solid and empty points represent, respectively, the storage (elastic) modulus G′ and the loss (viscous) modulus G″.

2.3.2 Mechanical testing

The hardness of the dry Gelfoam® sponge was 2.70Kg/mm^2 ±35.0, while hydrated it was 8.69Kg/mm^2 ±117.7. The dry Gelfoam® sponge had an elasticity ratio of 78.71 %±1.9, and the hydrated had a ratio of 12.14%±1.7. Gelatine sponges with a hardness similar to that of the Gelfoam® (e.g., hardness of 2.70± 270.3 Kg/mm^2 and elasticity of 78.71 %± 7.87), sponge will be easily handled without any damage.

2.3.2.1 Influence of gelatine concentration on the hardness and elasticity of dry and hydrated sponges

Figure 2.3 depicts the hardness of dry sponges (A) and hydrated sponges (B), with different gelatine concentrations (1%,4%,7%, and 10%) (w/v) and compared to the Gelfoam® sponge. Firstly, the hardness value of the dry sponges recorded was significantly different from the Gelfoam® sponge (2.70Kg/mm^2 ± 35.0). The hardness value for F1 (1% gelatine) and F2 (4% gelatine) were reduced to 4.69 Kg/mm^2 ±13.2. and 1.50 Kg/mm^2 ±24.6, respectively. However, the F3 (7% gelatine) and F4 (10% gelatine) hardness values, were increased to 5.42 Kg/mm^2 ± 40.4 and 5.41 Kg/mm^2 ± 37.1, respectively.

The hardness values of the same hydrated sponges are shown in Figure 2.3 (B). The hardness values for F1 (3.18 Kg/mm^2 ± 76.08) and F2 (1.42 Kg/mm^2 ± 32.79) in which there is a significant difference as per the statistical analysis from the Gelfoam® sponge 8.69 Kg/mm^2 ±117.7. The hardness values for F3 (1.74 Kg/mm^2 ± 790) and F4 (5.40 Kg/mm^2 ± 36.5) were greater than the Gelfoam® sponge. Additionally, figure 2.4 depicts the elasticity ratios of sponges with varying gelatine concentrations compared to Gelfoam® sponges both dry and hydrated. F1 and F2 have respective elasticity ratios of 84.7%±1.0 and 81%±1.7 for dry sponges. In contrast, the elasticity ratios of hydrated sponges for F1 and F2 were 10%±5.9 and 45.7%±2.0, respectively. F3 and F4 had a ratio of 0 and were inelastic. F1 elasticity was significantly greater than that of Gelfoam® sponge, which was 78.7%±1.9. However, F2 elasticity was smaller than that of Gelfoam®, although the difference was not statistically significant. Hydrated, the F1 elasticity was not significantly different than the Gelfoam® hydrated elasticity of 12%±1.7. Nevertheless, the F2 elasticity was much more significant than Gelfoam®.

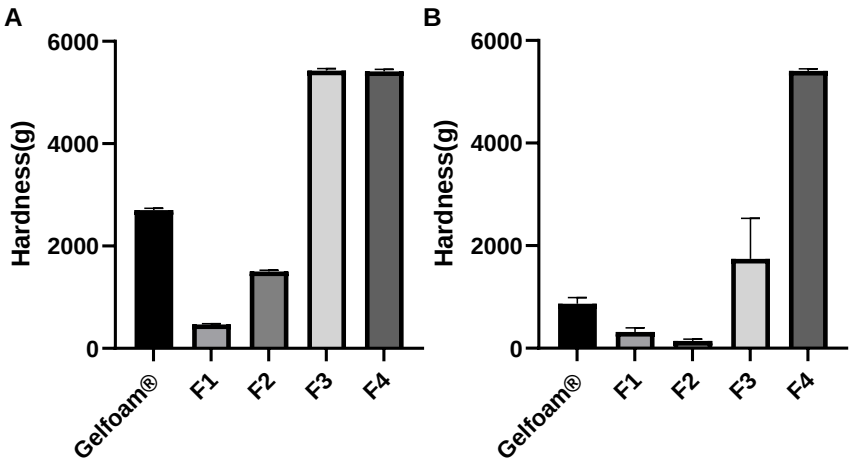

*Figure 2.3: Effect of different gelatine concentration (1%, 4%, 7%, and 10%) on hardness of dry(A) and hydrated(B) sponges. Results shown as mean ± SD, n= 3, significance found using a t-test between each group and the Gelfoam® sponge, * = P<0.05, ** = P<0.01, ***<0.001, ****P<0.0001.*

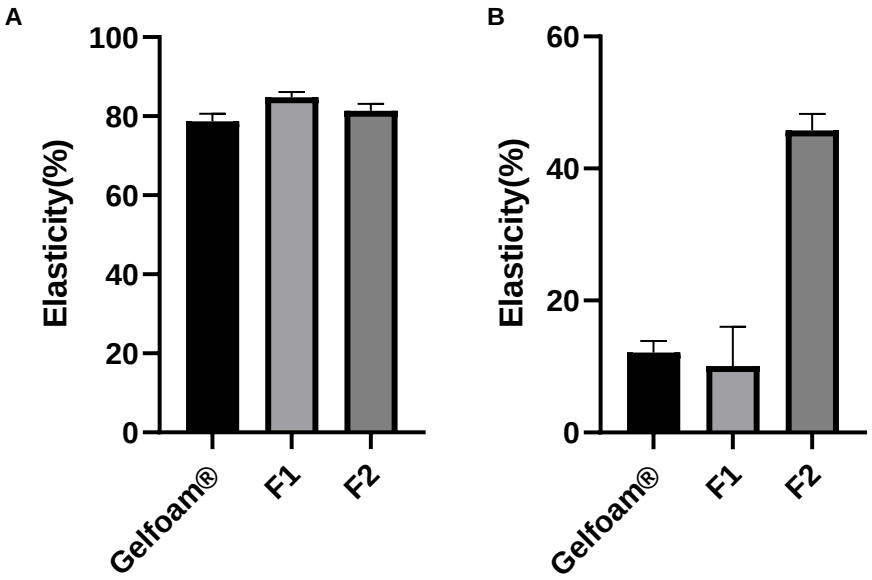

*Figure 2.4: Influence of gelatine concentration on the elasticity of dry (A) and hydrated (B) sponges. Results shown as mean ± SD, n= 3, significance found using a t- test, * = P<0.05 ** = P<0.01, *** = P<0.001, ****P<0.0001.*

2.3.2.2 Influence of blending on the hardness and elasticity of dry and hydrated sponges

The impact of blending different polymers has on the mechanical properties of dry and hydrated sponges with 4%, 7%, and 10% (w/v) gelatine and either 1% and 4% (w/v) sodium

alginate was investigated, and the results presented in Figure 2.5. The hardness of the dry F5 (4.65 Kg/mm^2 ± 26.2) and F6 (3.71 Kg/mm^2 ± 26.6) sponges was significantly lower than the Gelfoam® sponge 2.70 Kg/mm^2 ±35.0. In contrast, the hardness values for F7 (5.44 Kg/mm^2 ± 17.9), F8 (5.45 Kg/mm^2 ± 28.7), F9 (5.41 Kg/mm^2 ± 68.8), and F10 (5.40 Kg/mm^2 ± 34.1) were significantly higher than the Gelfoam®. Hardness values for the hydrated F5 (1.71 Kg/mm^2 ± 49.8), F6 (2.13 Kg/mm^2 ± 32.4), F7 (4.31 Kg/mm^2 ± 7.2), and F8 (5.59 Kg/mm^2 ± 55.2), sponges were significantly lower than those of Gelfoam®, while hardness values for hydrated F9 (4.52 Kg/mm^2 ± 203.4), and F10 (5.49 Kg/mm^2 ± 57.2) sponges were significantly higher than those of Gelfoam®. The elasticity of sodium alginate and gelatine composite sponges, relative to Gelfoam® sponges under dry and hydrated conditions, is shown in Figure 2.6A and B, respectively. F5 had an elasticity of 76.1% ± 1.6, F6 82.2% ± 0.9, F7 68.7% ± 2.0, F8 59.2% ± 6.0, F9 51.53% ± 10.2, and F10 was 38 %± 2.0. Compared to Gelfoam®, the elasticity values of dry composite sponges were lower, except for F6, which was higher significantly. In contrast to Gelfoam®, however, variants F7, F8, F9, and F10 showed notable variation. F5 was 6.63% ± 3.1, F6 was 1.25 % ± 0, F7 was 0.19 % ± 0, F8 was 1.50 % ± 0.40, F9 was 1.46 % ± 0.25, and F10 was 0.7 % ± 0.25 for the elasticity of hydrated sponges. All the composite hydrated sponges were far less elastic than Gelfoam®.

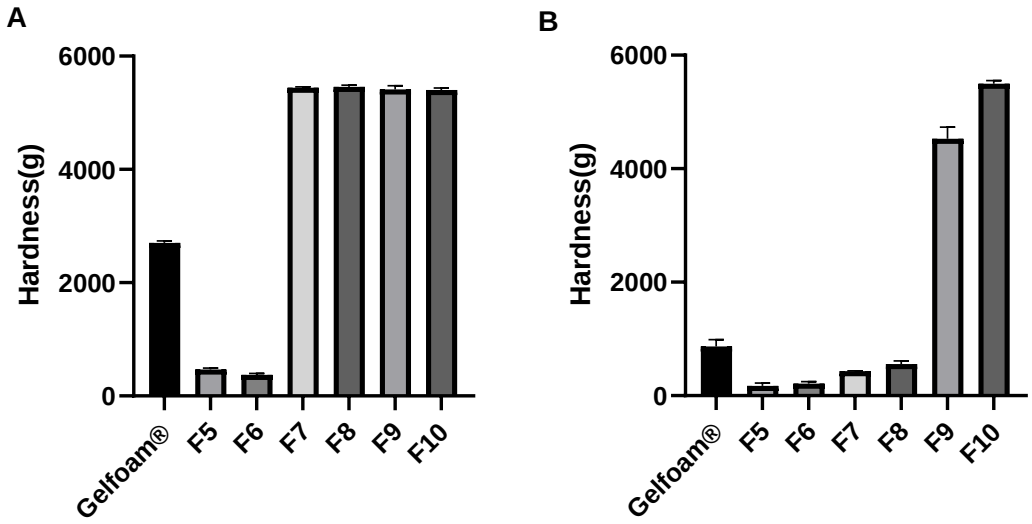

*Figure 2. 5:: Effect of blending sodium alginate (1%, 4%) with gelatine concentration (1%, 4%, 7%, and 10%) on hardness of dry(A) and hydrated(B) sponges. Results shown as mean ± SD, n= 3, significance found using a t-test, * = P<0.05 ** = P<0.01, *** = P<0.001, ****=P<0.0001.*

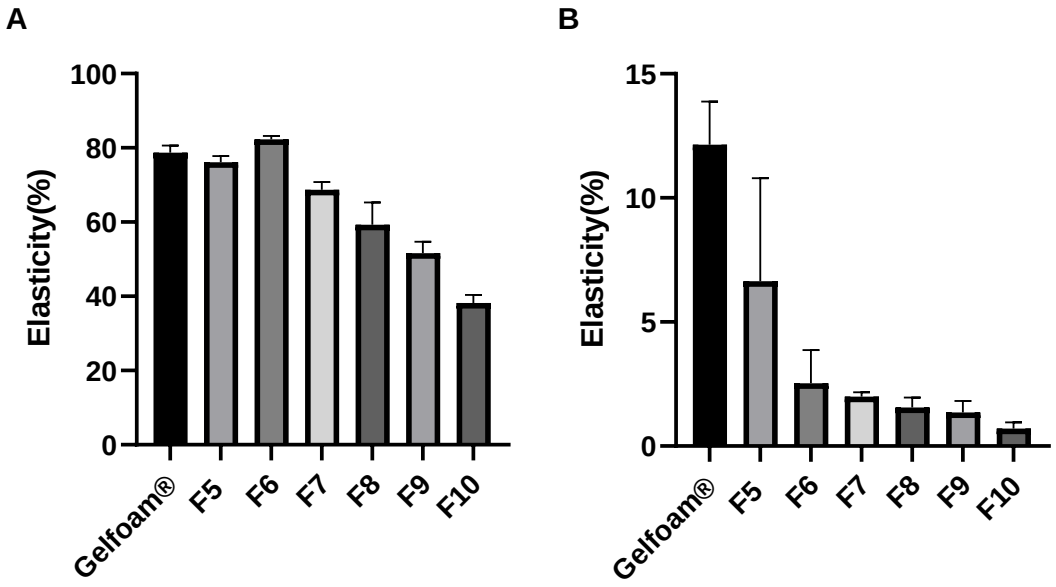

*Figure 2. 6: Effect of blending sodium alginate (1%, 4%) with gelatine concentration (1%, 4%, 7%, and 10%) on elasticity of dry(A) and hydrated (B) sponges. Results shown as mean ± SD, n= 3, significance found using a t-test, * = P<0.05 ** = P<0.01, *** = P<0.001, ****=P<0.0001.*

2.3.2.3 Influence of crosslinking on hardness and elasticity of dry and hydrated sponges

Dry and hydrated sponges were quantified for the impact of crosslinking on their hardness. A blend of gelatine (4%) and sodium alginate (4%) was chosen for further investigation. The composite was crosslinked with glutaraldehyde 0.1%, 0.5% and 1% (v/v), and the resulting formulations are F11, F12, and F13. Dry sponges (Figure 2.7A) ranged in hardness from F11

at 1.23 Kg/mm^2 ±160.0 to F12 at 2.32 Kg/mm^2 ±307.1 with F11 being significantly different, while F12 was non-significantly softer than the Gelfoam® sponge) to F13 at 3.52 Kg/mm^2 ±104.2 (non-significantly harder than Gelfoam®). The hydrated sponges (Figure 2.7 B) were much softer than the hydrated Gelfoam®, with hardness of 0.194 Kg/mm^2 ± 114.2, 7.26 Kg/mm^2 ± 340.0, and 3.22 Kg/mm^2 ± 13.72 respectively.

The elasticity of dry sponges depicted in figure 2.8 A, ranged from F11 at 75% ±0.24, which was not lower than Gelfoam®, to F12 at 85.8% ±0.76 and F13 at 90% ±1.5, which were significantly greater than Gelfoam®. Hydrated sponges (Figure 2.8 B) were significantly more elastic than hydrated Gelfoam®, with elasticity values of 26 ± 4.8, 33.6 ± 12.9, and 68 ± 5.8, respectively.

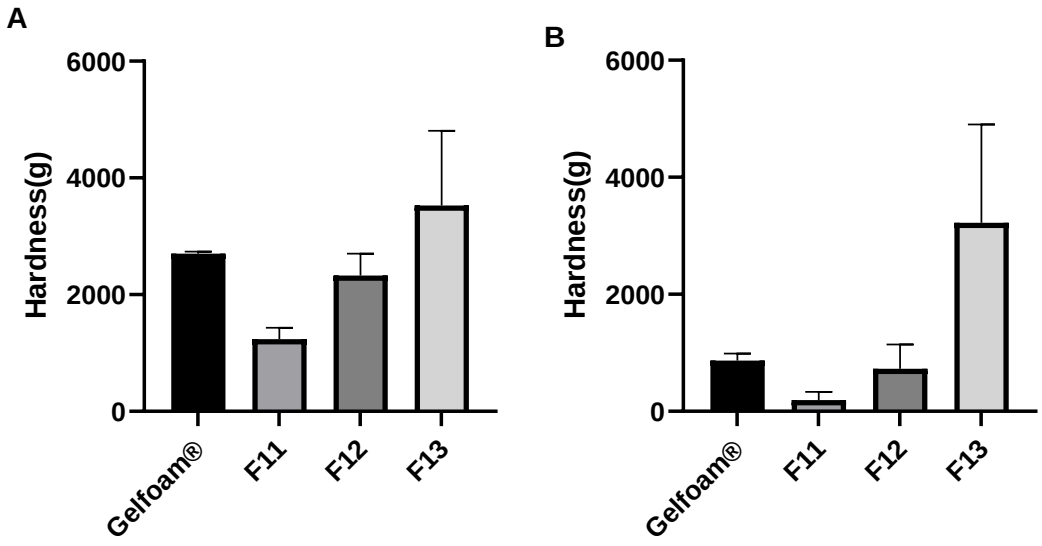

*Figure 2. 7: Effect of crosslinking the composite of sodium alginate (4%) and gelatine (4%) with (0.1%, 0.5% and 1%) glutaraldehyde on the hardness of dry(A) and hydrated(B) sponges. Results shown as mean ± SD, n= 3, significance found using a t- test, * = P<0.05 ** = P<0.01, *** = P<0.001, ****=P<0.0001.*

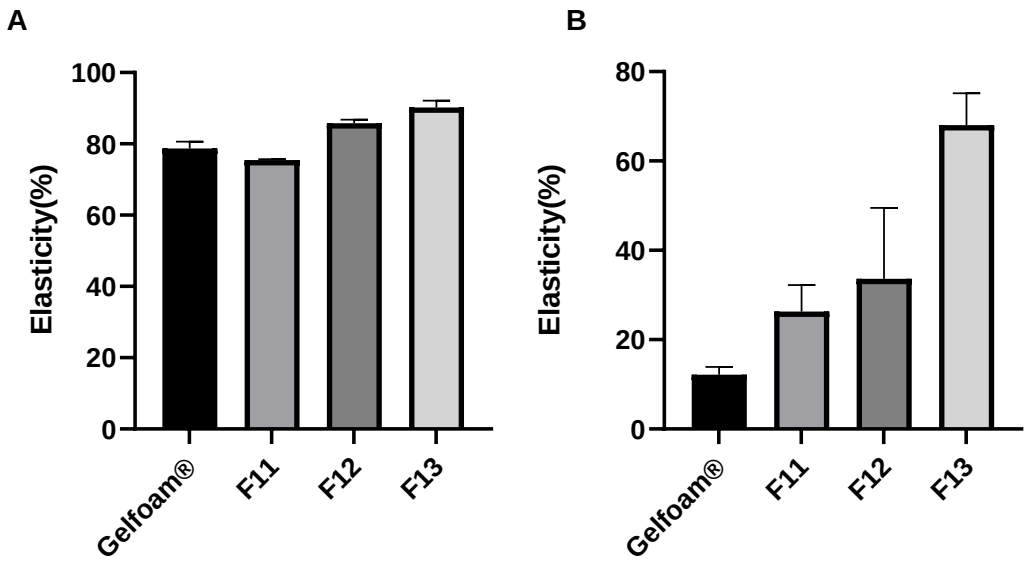

*Figure 2. 8: Effect of crosslinking the composite of sodium alginate (4%) and gelatine (4%) with (0.1%, 0.5% and 1%) glutaraldehyde on the elasticity of dry(A) and hydrated(B) sponges. Results shown as mean ± SD, n= 3, significance found using a t- test, * = P<0.05 ** = P<0.01, *** = P<0.001, ****=P<0.0001.*

2.3.3 Porosity and swelling ratio of the sponges

2.3.3.1 Influence of gelatine concentration on the porosity and swelling ratio of the sponges

The average percentage porosity of gelatine sponges with increasing gelatine concentration is shown in figure 2.9A. The percentage porosity of the gelatine sponges was non significantly lower except for F4 which was significantly lower (88.5% ± 2.7; 94% ± 2.6; 87.9% ± 3.9; and 27.7% ± 9.4, F1-F4 respectively) than that of the Gelfoam® sponge (91%± 8.0). Figure 2.9 B demonstrated that the swelling ratio of different gelatine sponges varied with varying gelatine concentrations, with F1's value (1056 % ±1.4) being much lower than Gelfoam® (1296 % ± 5.8), with F2's value (4663 % ± 7.0) being much higher, while F3 (415.8 % ± 3.6) and F4's (215 % ± 3.5) reduce to below that of both F1 and Gelfoam®.

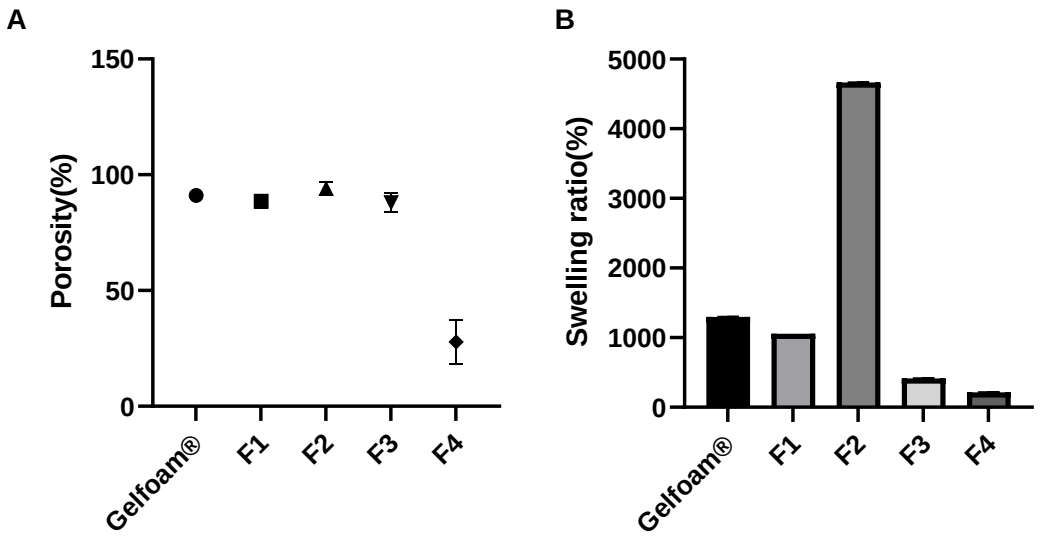

*Figure 2. 9:: Influence of gelatine concentration on the porosity (A) and swelling ratio (B) of sponges. Results shown as mean ± SD, n= 3, significance found using a t-test, * = P<0.05 ** = P<0.01, *** = P<0.001, ****=P<0.0001.*

2.3.3.2 Influence of blending approach on the porosity and swelling ratio of the sponges

The average porosity percentage of gelatine sponges combined with sodium alginate is displayed in figure 2.10A. The values obtained for porosity were 95% ±3.8; 97% ± 3; 98% ± 2.6; 90.6% ± 0.5; 65.7% ± 9.7; 54.8% ± 5, F5 to F9, respectively. Compared to Gelfoam®, the porosity values for the composite sponges indicated a significant decrease, with porosity decreasing with an increase in sodium alginate concentration. The swelling ratios of the sponges containing sodium alginate are shown in Figure 2.10 B. The swelling ratios decreased from 6557.8% ± 8.6 (F5) to 243.6% ± 15.9 (F10), with increasing sodium alginate concentration, with only the swelling ratio of F9 and F10 being lower than the Gelfoam® sponge.

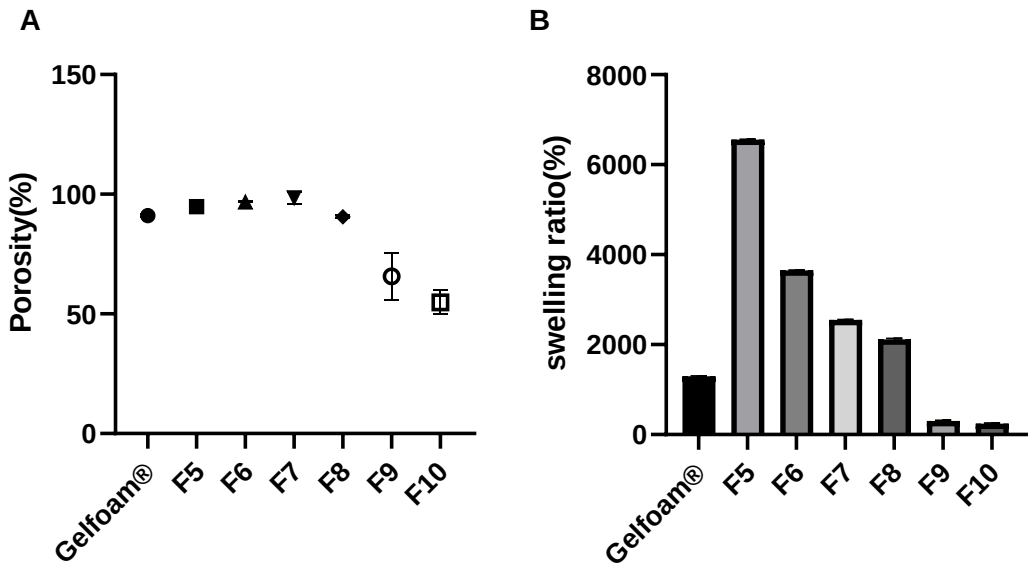

*Figure 2. 10: Effect of blending sodium alginate (1%, 4%) with gelatine concentration (1%, 4%, 7%, and 10%) on porosity (A) and swelling ratio (B) sponges. Results shown as mean ± SD, n= 3, significance found using a t-test, * = P<0.05 ** = P<0.01, *** = P<0.001, ****P<0.0001.*

2.3.3.3 Influence of crosslinking approach on porosity and swelling ratio of sponges

Figure 2.11A presents the porosity of crosslinked sponges compared to the Gelfoam® sponge. The average porosity values ranged from 96.6 ± %5.0 (F11) down to 93.8 ± % 2.0 (F13) and were significantly higher than those of Gelfoam® (91% ± 8.0). Figure 2.11B showed the swelling ratios of the crosslinked sponges in comparison to the Gelfoam® sponge. The swelling ratios decreased with an increase in crosslinking, ranging from 1065.6% ± 67.0 (F11) to 898% ± 22.5 (F13) and were all lower than those of the Gelfoam® sponge.

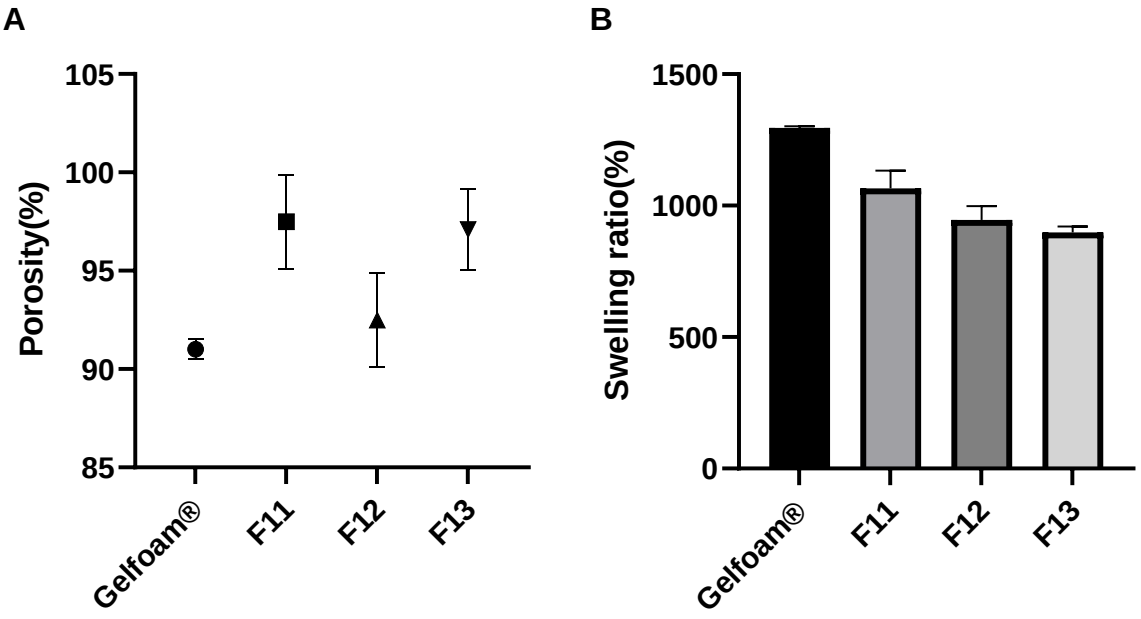

*Figure 2. 11: Effect of crosslinking the composite of sodium alginate (4%) and gelatine (4%) with (0.1%, 0.5% and 1%) glutaraldehyde on porosity (A) and swelling ratio (B) sponges. Results shown as mean ± SD, n= 3, significance found using a t- test, * = P<0.05 ** = P<0.01, *** = P<0.001, ****=P<0.0001.*

2.4 Discussion

This study investigated gelatine sponges prepared using blending and crosslinking techniques as a potential implantable drug delivery system for the localised treatment of PC. The sponges were manufactured by freeze-drying after freezing the precursor gels. The mechanical properties of the sponges were investigated in relation to three primary factors: concentration (1%, 4%, 7%, and 10%) of gelatine, the blending of sodium alginate (1% and 4%) and gelatine (4%, 7%, and 10%), and the crosslinker (glutaraldehyde) concentration (0.1%, 0.5%, and 1%). Texture analysis was used to determine the hardness and elasticity of both dry and hydrated sponges to learn more about the mechanical properties. The optimum sponge was then examined for its morphology, in vitro drug release, and drug distribution in the following chapter. In addition, the rheological characteristics of the precursor hydrogels were studied to determine the link between their mechanical strength and that of the related sponges.

Surgical gelatine sponges must be strong and stable enough to meet their biomedical purposes (Kabiri *et al.*, 2010). Generally, for sponges to be used in vivo, a balance between mechanical strength and flexibility is essential (Freag, Saleh and Abdallah, 2018). In the case of periodontal therapy, for instance, the sponges used in the therapeutic device should have specific mechanical properties that account for their sensitivity to handling during the manufacturing process (Catanzano *et al.*, 2018). Furthermore, the crucial aspect of structural integrity lies in its capacity to endure diverse mechanical impacts that may arise throughout a patient's lifespan either if the sponge is applied externally or implanted internally (Chashchin *et al.*, 2021). So, solid, and elastic sponges are preferred for easy application inside the device to avoid changes to the sponge structure for quick drug solution uptake and release (Bertram and Bodmeier, 2012). Therefore, studying the sponge's hardness or resistance to deformation is essential. Additionally, the sponge must also be resilient enough to withstand deformation and movement (Baghani and Kadkhodazadeh, 2013; Catanzano *et al.*, 2018). A crucial attribute of a sponge is its resistance to collapsing when hydrated. The dry sponge can be compressed to between 15 to 39% of its original thickness, however upon contact with water, it will return to its normal size and shape. If it must expand in a restricted space, it will push against the wall and fill the space. Furthermore, the degree of crosslinking is also responsible for the sponge's resilience and rebound (the amount by which it expands when the compressive force is released) (Chvapil, 1977).

This study used a commercially available sponge called Gelfoam® as a positive control. Gelfoam® is a gelatine sponge created from purified type A pork skin gelatine that has traditionally been used for hemostasis and wound dressing by surgeons during and after surgery (Rohanizadeh, Swain and Mason, 2008). The physical properties of Gelfoam® sponges were investigated to determine the optimal mechanical properties needed for our formulations. The

hardness and elasticity of the sponges, which are the two most important mechanical properties, were studied using the TA. XT plus Texture analyser.

Only a few investigations, such as that published by Sun et al. (2018), have established a link between the hydrogel's rheological properties and the matching aerogel's mechanical characteristics. In particular, how the physical hydrogel's elastic and viscous features influence the aerogel's final properties (Tabernero *et al.*, 2020). Moreover, an amplitude sweep analyses a critical aspect of the hydrogel samples' viscoelastic behaviour. The corresponding dynamic storage modulus, represented by G′, and the loss modulus, denoted by G″, in response to amplitude (or shear strain) (Sun *et al.*, 2018). In this study, hydrogel matrices with different gelatine concentrations were evaluated, providing the typical profiles depicted in Figure 2.1, which is a characteristic profile of a hydrogel matrix and G′ > G″, consistent with a matrix that acts like an elastic solid (Dörr, Kuhn and Altstädt, 2020). For hydrogel samples with a higher gelatine concentration, it was shown that G′ values were consistently greater than G″ values, indicating the formation of a stable network structure. Because of this, the produced physical gels can be thought of as "permanent gels," providing a network that lasts indefinitely; consequently, the gel's elasticity character (solid-like) always predominates over the gel's viscous nature (Tabernero *et al.*, 2020).

It was discovered that increasing sodium alginate concentration increases the storage modulus of hydrogels. This result was additionally reported by Mondal et al. (Mondal *et al.*, 2019). The modulus values increased with increasing sodium alginate content, indicating that the hydrogel exhibited gelling behaviour as shown in figure 2.2. In addition, the increase in storage and loss modulus with increasing concentration of its ingredients is indicative of the hydrogel's strength (Mondal *et al.*, 2019). Nonetheless, both sodium alginate and gelatine, as seen in the figure 2.2, increase storage modulus as their concentrations rise.

The gelatine concentration drastically altered the sponge's mechanical properties. The results from tests on sponge hardness presented in figure 2.3 showed a causative link between gelatine concentration and enhanced hardness. Therefore, sponges made with a low gelatine concentration (1%) resulted in sponges with lower hardness, and sponges made with a higher gelatine concentration (10%) were linked to greater hardness. On this basis, it is discovered that the applied gelatine (more specifically, its molar mass) significantly impacts the hardness of the obtained sponges. The dry sponge hardness increased due to changes in polymer solution viscosity. Generally, the extent of polymer chain molecule entanglement within a solution relates to solution viscosity. Consequently, an increase in polymer chain entanglement as the number of polymer molecules increases results in an increase in viscosity. This conclusion agrees with the literature's observation that the sponges softened and became more flexible as gelatine concentration was reduced (Kabiri *et al.*, 2010). On the other hand, when sponges are hydrated, the hardness of the sponges decreases dramatically. This result can be explained by a gradual dilution of polymeric chains, which results in a lack of consistency of the polymeric solution formed during hydration (Rossi *et al.*, 2012). For F3(7% gelatine) and F4(10% gelatine), the decrease in hardness upon hydration is less pronounced. This result is most likely due to reduce s dilution of the polymeric chains, which results from increasing gelatine concentration. Like with hydrogel's storage modulus, increasing the gelatine concentration in sponges increased sponge hardness, which is consistent with previous research (Gupta et al., 2021).

Elasticity is an essential parameter for evaluating the strength of a material (Haiyan *et al.*, 2017) and is correlated with hardness. In this research, increasing gelatine concentration was found to affect the elasticity of the sponges as shown in figure 2-4. Results demonstrated that as the gelatine concentration increased, the elasticity of dry sponges decreased. Additionally, the elasticity of hydrated sponges decreased as well with increasing the gelatine concentration. The

decrease in elasticity with increasing gelatine concentration is likely due to the hardness (Catanzano *et al.*, 2018). It was also noticeable that the elasticity decreased more when the sponge was hydrated. This result reflects those of Haiyan et al. (2017), who also found that the gelatine sponge dry elasticity is relatively higher than when the sponge absorbs water; its elasticity decreases (Haiyan et al., 2017).

As depicted in Figure 2.5A, as gelatine and sodium alginate concentration were increased during blending, the hardness of the dry sponges increased significantly ($p<0.05$) compared to that of Gelfoam®. F5 and F6 were substantially softer than the Gelfoam® sponge. In contrast, the hydrated sponges F5, F6, and F7, F8 had much lower hardness values than the hydrated Gelfoam® sponge (figure 5-4 B). While F7, F8, F9 and F10 were much higher than Gelfoam® in the dry state, as well as F9 and F10 were significantly higher in their hydrated state. It has been observed that sodium alginate and gelatine can combine to generate a product with increased mechanical characteristics, which is consistent with our findings. The interaction between sodium alginate and gelatine results in intermolecular hydrogen bonds (Xiao et al., 2001). As illustrated in figure 2.6 A, the elasticity values of dry composite sponges decrease as the percentage of blend increases, with the exception of F6, which exhibited a marginally higher value. The findings of this study provide further evidence that hardness is linked to elasticity. This conclusion was also reported by Catanzano et al. (2018), who combined two polymers and discovered that as the concentration of the mix increased, the hardness of the sponges increased while the flexibility decreased (Catanzano et al., 2018).

The concentration of crosslinking affects the mechanical properties of sponges, particularly their hardness and elasticity. As the glutaraldehyde content increases, the dry sponge becomes tougher. F11 and F12 were softer than dry Gelfoam®, and F13 was harder than Gelfoam (no statistically significant difference, $P > 0.05$) as depicted in figure 2.7 A. This result is best explained by the fact that crosslinking affects mechanical strength due to newly created

crosslinks resulting from the interaction of crosslinker and polymer. It is widely known that glutaraldehyde is a non-zero-length crosslinker that can generate more flexible crosslinking linkages than zero-length crosslinking bonds (e.g., EDC) (Imani, Rafienia and Emami, 2013). Therefore, the addition of glutaraldehyde would affect the sponges' mechanical properties, which is consistent with the results of this study. Similarly, the crosslinking of the sponges has an influence on the elasticity of sponges as shown in figure 2.8. Consequently, as the concentration of glutaraldehyde increases, the elasticity of the sponges increases in both the dry and hydrated states compared to Gelfoam®. It has been found that the greater the crosslinking achieved with glutaraldehyde, the greater the elasticity (Ukhrowiyah *et al.*, 2017).

The physical strength of the gelatine sponges was studied by analysing their porosity and swelling ratios to determine the impact of increasing gelatine concentration, blending with sodium alginate, and crosslinking with glutaraldehyde. The macroscopic properties of sponges can be explained by their microscopic features. Essential macroscopic qualities, such as high specific surface area, low thermal conductivity, low density, and high compressive strength, are controlled by these characteristics, which include the high strength of their backbones, high porosities, and open porous designs. Given these characteristics, biopolymer-based sponges are primarily being studied for their potential application in drug delivery systems and scaffolds for tissue engineering and regenerative medicine (Vasvári *et al.*, 2018; Lázár *et al.*, 2020). Additionally, Porous materials, such as porous scaffolds used in tissue engineering or wound healing, must meet certain characteristics, including a certain porosity and swelling ratio. Cell division and tissue expansion are promoted by the free flow of nutrients and oxygen through the porous structure. Furthermore, the nutrition that cells need will depend entirely on tissue fluids surrounding the lesion in the early stage of wound healing. Therefore, the biological activity of a dermal counterpart is largely dependent on the scaffold's capacity to absorb water (Bhattarai *et al.*, 2004; Muthukumar *et al.*, 2014; Dai, 2019). Porosity was shown to decrease

significantly ($p<0.05$) in comparison to Gelfoam® as gelatine concentration was increased. Similarly, increasing the gelatine concentration decreased the swelling ratios. Nonetheless, the swelling ratio of 4% gelatine concentration was higher than that of Gelfoam®. Swelling ratios in sponges decreased significantly ($p<0.05$) with increasing gelatine concentrations (from 1% to 7% to 10%). This occurs because sponges have faster crosslinking rates when more gelatine is used. Additionally, changes in pore size caused by varying amounts of gelatine explains this pattern. The gelatine sponge's structure is more ductile, and its pores are more prominent when the gelatine concentration is lower. The tightening of the sponge structure and the shrinking of the pore size as the gelatine concentration rose led to a reduction in the sponge's porosity. The bulk density of the sponge rises in direct proportion to the gelatine concentration, as the gelatine aqueous solution contains more gelatine and less water at higher concentrations, the swelling ratio is likewise reduced with increasing gelatine concentration. The observed phenomenon can be attributed to the direct relationship between gelatine concentration and viscosity, whereby an increase in the former leads to a rise in viscosity. This results in a more uniform and impermeable structure, promoting a higher nucleation rate and, consequently, more significant restrictions due to crystal growth (Van Vlierberghe *et al.*, 2007; Conoscenti, Carrubba and Brucato, 2017; Torrejon *et al.*, 2022). Since swelling is positively correlated with porosity, this finding follows rationally (Jang and Um, 2017). The findings from the swelling ratio and the porosity study agree with one another.

The swelling ratio decreased significantly ($p<0.05$) compared to Gelfoam® as the composite of gelatine and sodium alginate concentration was increased during blending. Similarly, increasing the blend concentration decreased the porosity of the composite sponges significantly ($p<0.05$). Generally, the swelling of a gel is affected by solvent mobility, solvent-polymer interaction, polymer relaxation time, the structure of the monomer employed, and the chain length of the crosslinker. As a result, increasing the monomer content in the hydrogel

causes a decrease in swelling. Additionally, the native gelatine sample's supramolecular structure is generated by colliding collagen-like fibrils that form a spatial network. Moreover, the concentration of gelatine determines the size of the fibrils. Also, the hydrogel's structure includes distinct zones (cells) scattered along the fibrils of the 3D network. These elements could be uncoiled macromolecule portions. Afterwards, the addition of sodium alginate alters the supramolecular structure of gelatine significantly. The addition of sodium alginate causes considerable alterations in the supramolecular structure of gelatine. Ideally, the polysaccharide causes the production of spherical structures that can be interpreted as sodium alginate-gelatine PECs. These complexes have the potential to function as new links in the hydrogel's structural network (Derkach et al., 2020). As a result, as more PECs are generated, the swelling ratio decreases. Nonetheless, it was reported that increasing the concentration causes the nucleation rate to rise, which in turn causes the chains to pack more closely together, resulting in a smaller pore size (Farokhi *et al.*, 2006). Hence, a smaller pore size explains the reduction in the porosity ratio. Additionally, Since the highly crosslinked structure is unable to hold much water inside its network structure, highly crosslinked sponges often exhibit poor water uptake capabilities (Choi et al., 1999).

As was shown in the figure 2.10, the degree of swelling gradually decreases as the concentration of glutaraldehyde increases. The creation of a thicker gel or cross-linking densities was the reason for the reduction in swelling due to increased glutaraldehyde concentrations. Moreover, when the glutaraldehyde concentration was increased, the gel network became denser, which reduced swelling. This reduction was because the aldehyde groups covalently linked to the -amino groups of lysine in gelatine molecules exerted greater force (Saarai *et al.*, 2013; Guo *et al.*, 2019). This finding is consistent with that of Liu et al., which reported that highly crosslinked sponges could not hold as much water inside their network structure as non-crosslinked or lowly crosslinked sponges. Consequently, the gelatine

sponge swelled less as the degree of crosslinking increased. In like manner, porosity decreases as crosslinker concentration increases (Liu *et al.*, 2007).

2.5 Conclusion:

The primary treatment for PC is tumour resection surgery; unfortunately, this procedure often leaves behind tumour cell residue. PC is treated well with the highly toxic drug FOLFIRINOX. Therefore, FOLFORINOX must be delivered locally at the tumour margin for effective treatment and less systemic toxicity. The exceptional qualities of sponges as drug delivery devices and the efficacy of 3D printing technology justify the concept of integrating these two approaches into a single device to treat the margin of PC. This research has addressed a wide range of gelatine sponge methodologies and proven that it is possible to create a stable gelatine sponge through the use of blending and crosslinking. Viscoelastic studies utilising amplitude sweep validated the improved structural integrity and dynamic stability of the precursor hydrogels. By the end of the optimization process, we had created a sponge (F12) with mechanical properties similar to the Gelfoam® control sponge. The influence of altering gelatine concentration on the rheological, mechanical, porosity and swelling ratio of the sponges was significant. Furthermore, blending gelatine with sodium alginate offers an additional strength to the sponges. Consequently, the introduction of blending has led to a reduction in the required concentration of crosslinker, so reducing the toxicity and increasing the mechanical strength of sponges more safely. We argue that our optimised cross-linked composite sponge should be integrated into an implantable drug delivery device for the local delivery of FOLFIRINOX therapy of PC.

Chapter 3: Characterisation of the optimum gelatine sponge in comparison to the Gelfoam® control

3.1 Introduction

Local delivery along soft tissue surgical resection margins presents a unique administration challenge: achieving adequate surface coverage, fixation, and drug diffusion into the tissue with the highest risk of local recurrence. In most instances, the irregular shape of soft tissues following surgery precludes the use of rigid polymers, necessitating alternative strategies to provide a flexible, drug-eluting material. Methods such as coating the tissue surface with a polymerizable hydrogel or applying a layer of microparticles via aerosol or adhesion may result in acceptable coverage; however, other factors, such as the absence of controlled release or mechanical stability, frequently undermine these approaches. The number of successful studies examining local delivery to resection margins for recurrence control is consequently limited (Wolinsky, Colson and Grinstaff, 2012). It is believed that microscopic disease remaining at the surgical resection margin is the primary cause of recurrence (Zhang *et al.*, 2018). However, there is mounting evidence that intraoperative bleeding from patients' damaged tissues and vasculature during tumour resection can release tumour cells into the blood and increase the level of circulating tumour cells, which in turn raises the risk of local recurrence and distant metastasis (Kaifi *et al.*, 2015; Zhang *et al.*, 2018). Therefore, bleeding is thought to be a crucial factor in the early recurrence and tumour metastasis frequently seen after resection of tumours, particularly large bulky tumours (Wolinsky, Colson and Grinstaff, 2012; Zhang *et al.*, 2018). The effectiveness of chemotherapy while reducing its systemic side effects has prompted research into drug delivery systems, particularly local drug delivery implants like drug-loaded fibres, films, particles, and gels (Wolinsky, Colson and Grinstaff, 2012; Zhang *et al.*, 2018).

Despite the impressive results, studies into intraoperative bleeding-induced tumour recurrence and metastasis have not yet recognised the full potential of these strategies. To minimise

intraoperative blood loss, clinicians typically resort to mechanical and thermal techniques, but these methods are ineffective when applied to bleeding coming from inaccessible areas (Kawasaki *et al.*, 2017). Hemostatic topical implants could be helpful in these circumstances. For this reason, novel local cancer chemotherapy implants that also provide a hemostasis function have proven to be highly effective in the treatment of cancer after surgery (Zhang *et al.*, 2018). Biomedical sponges, for instance, have wide applications in the pharmaceutical industry, where they are used not only as a wound dressing (Chen *et al.*, 2013; Abd El-Aziz *et al.*, 2020) but also in ocular delivery (Refai and Tag, 2011; Abd El-Aziz *et al.*, 2020) , buccal administration (Kassem, ElMeshad and Fares, 2015; Abd El-Aziz *et al.*, 2020), and implanted drug delivery systems (Foda, El-Laithy and Tadros, 2004; Abd El-Aziz *et al.*, 2020).

In this chapter, the optimised gelatine sponge from chapter two was selected as part of an implantable device (Chemo Patch) to treat the resection margin of PC. Further in-depth characterisation including morphological, spatial drug distribution, spectral analysis, and thermal and hydrolysis properties were determined for the optimum sponge and compared to Gelfoam®. Additionally, the *in vitro* drug release was studied for the optimised gelatine sponge.

3.2 Material and methods

3.2.1 Materials

Gelfoam® sponge was purchased from AEGIS LIFESCIENCES PVT. LTD, Gujarat, India. Irinotecan Hydrochloride (IRN) was purchased from LGM Pharma (Georgia, USA). Potassium dihydrogen orthophosphate and methanol 99% were purchased from VWR (Leicestershire, UK). Acetonitrile was purchased from Fisher Scientific (Leicestershire, UK). A high bloom strength (250 G) gelatine was obtained from Sigma-Aldrich (Dorset, United Kingdom). Glutaraldehyde (GTA) solution, CA. 50% in the water was purchased from Sigma-Aldrich (Dorset, United Kingdom). Sodium alginate was obtained from Scientific Laboratory Supplies

(Nottingham, United Kingdom). Phosphate buffer saline tablets (PBS) was purchased from Sigma-Aldrich (Dorset, United Kingdom).

3.2.2 Gelatine sponge preparation

The sponge was prepared using the same method that was described in chapter 2, but in a summary, two solutions of 4% gelatine and 4% sodium alginate were separately prepared and then mixed together in a ratio of 1:1 and a solution of 0.5% (v/v) glutaraldehyde subsequently added to the mixture while it was being continuously stirred. The subsequent hydrogel was frozen over 24 hours before being freeze-dried for another 48 hours.

3.2.3 Scanning electron microscopy

Microstructure analysis was determined by looking at both surface and cross-section micrographs of the sponges using scanning electron microscopy (SEM) (Jeol 6060, Oxford Inca EDS). After fixing a small sponge sample (0.5 mm thick) to an SEM sample holder with double-sided adhesive carbon tape, a sputter coater was used to apply a layer of gold for 3 minutes then imaged via SEM.

3.2.4 Raman mapping

Before examination, the sponges were first saturated with the IRN solution and then freeze-dried for 48 hours. Cross-sections were obtained by cutting the sponges orthogonal to the sponge surface with a razor blade. The Raman mapping data was collected using a DXR Raman microscope (Thermo Fisher Scientific, Stafford House, Hemel Hempstead, UK). A laser with an excitation wavelength of 780 nm and a power of 20 mW was used. The sample was focused using an integrated microscope with a 10X objective, and the spot size of the laser was estimated to be 3.1 m. The exposure time was 5 seconds, and the spectra were collected with a step size of 106 m in both the x- and y directions. Using Omnic software, raw spectra were processed to remove noise by performing baseline correction, smoothing, and normalisation. All spectra were obtained in the spectral range of 200 - 3413 cm^{-1} with a resolution range 2.4 - 4.4 cm^{-1} provided by a grating monochromator of 400 lines/mm.

3.2.5 Fourier transform infrared spectroscopy (FTIR)

The FTIR spectra analysis of the sponge's sample was performed using Frontier FTIR spectrophotometer (Model: UATR, PerkinElmer (UK) Ltd). A small quantity of sponge flake was mixed with KBr and placed on the crystal and was measured in attenuated total reflection (ATR) mode.

3.2.6 Thermal analysis

Thermal analysis was conducted using differential scanning calorimetry (DSC) technique. DSC curves were obtained by use of a DSC 25 instrument (TA Instruments, NewCastle, DE) at a heating rate of 10°C/min and nitrogen gas flow rate of 50 mL/min. The samples of approximately 7mg were put in aluminium pan and heated to 300°C against an empty aluminium pan as a reference.

3.2.7 Hydrolysis degradation testing

The investigation of in vitro hydrolytic degradation was performed in PBS. A balance was used to determine the initial dry weight, denoted by the value W0, of each sample and the samples placed in a container that was tightly sealed before being placed in an agitated water bath that was maintained at 37 °C. A sample was taken at regular intervals for 6 weeks, washed with deionized water, and dried until they had the same mass throughout. The dry weight of each sample at time t (Wt) was determined. Using the following formula, the percentage of the mass remaining was calculated.

Remaining weight (%) = Wt /W0 × 100.

3.2.8 High performance liquid chromatography analysis (HPLC)

3.2.8.1 HPLC chromatographic condition

The DIONEX Ultimate 3000 Autosampler (Thermo Scientific) with a quaternary gradient pump and Chromeleon Chromatography Data System (CDS) software was used to analyse the samples. The separation was performed using a C18 column (150mm × 4.6 cm), particle size 5 µm (ThermoFisher Scientific, Loughborough, UK), at 25 ◦C. The injection volume was 20

µL, with a run time of 10min and a flow rate of 1 mL/min. The mobile phase contains a mixture of 0.02 M potassium di-hydrogen orthophosphate (pH adjusted to 3.5 with ortho-phosphoric acid) ethanol and acetonitrile (60:20:20 respectively). The detector UV wavelength was set at 220 nm. The standard calibration curve was established over a 10-60 µg/ml range.

3.2.8.2 Validation of HPLC method

Limit of quantification (LOQ), limit of detection (LOD), and linearity tests were used to validate the HPLC method. The LOD and LOQ were calculated using the lowest concentration in the standard curve as the LOQ and a slightly lower concentration as the LOD. seven replicates of each test were injected with the calculated RSD% value for the peak area. Single measurements at multiple analyte concentrations were utilised to assess linearity. The data were then analysed using least-squares regression. The slope, intercept, and correlation coefficient of the resulting plot provide the desired information on linearity. The accuracy was determined by analysing three replicates of three different concentrations and calculating the recovery percentage, mean, SD, and %RSD.

3.2.9 *In vitro* drug release of IRN from the gelatine sponge

A solution of IRN was prepared at a concentration of 100µg/ml, and 1 ml was loaded to the gelatine sponge and placed in a glass bottle containing 0.5 ml of deionized water (pH 6.5) to ensure that the release media only touched one side of the sponge and that the sponge was not completely immersed inside the release media, then the sponge was placed in an orbital shaking incubator at 37°C and 60 rpm. A 0.5 ml sample was collected at 0, 1, 3, 5 and 7-hour intervals and replaced with 0.5 ml of fresh deionized water and analysed by HPLC. The release study was carried out in triplicate, and the percentage of cumulative released IRN relative to the maximum loaded IRN was calculated.

3.3 Results

3.3.1 Morphological analysis

SEM micrographs of the surface and cross-section of the Gelfoam® and gelatine sponges are shown in figures 3.1 and 3.2, respectively. In contrast to the white and soft Gelfoam® sponge, the gelatine sponge appeared yellow and more robust. The SEM micrographs of both sponges showed a structure that is both uniformly porous, has many closely connected pores with an average pore size of 100µm for both sponges.

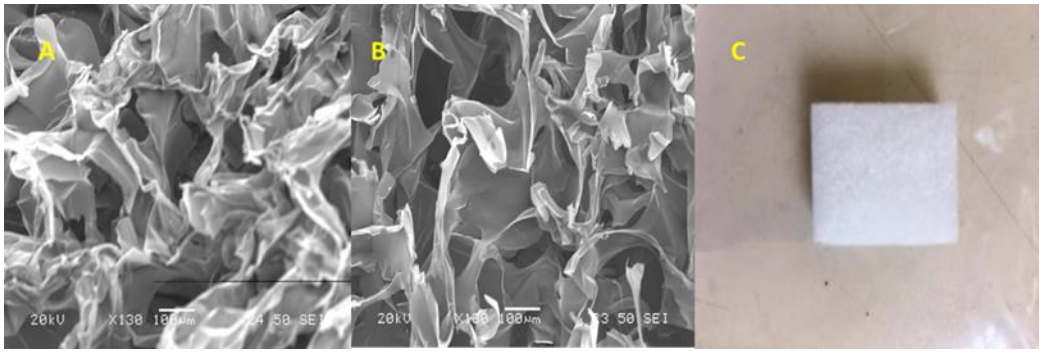

Figure 3. 1: Gelfoam® sponge microstructure (A: surface and B: cross section) and physical appearance (C)

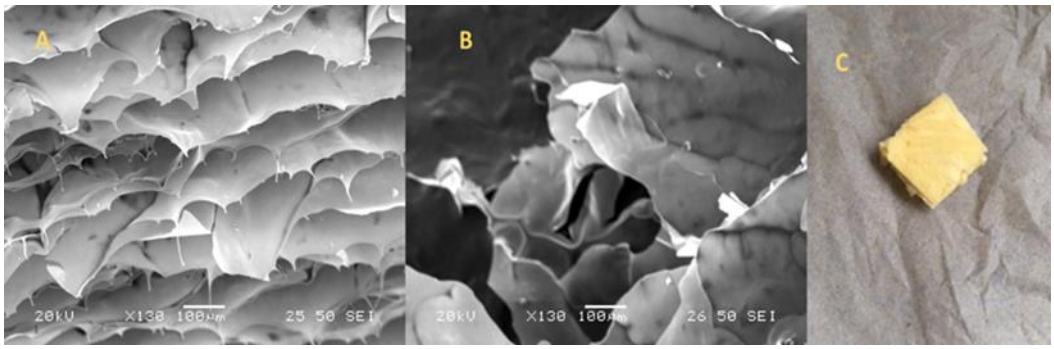

Figure 3. 2: The optimum sponge microstructure (A: surface and B: cross section) and physical appearance (C)

3.3.2 Raman mapping

The distribution of IRN was studies using Raman mapping for both sponges. Figures 3.3A (gelatine sponge) and B (Gelfoam®) showed the distribution of a 5% (w/v) IRN solution in the sponges. The results demonstrated that IRN was found to have to some extent a homogenous distribution in both sponges. A particular region of the sponge as shown in figure 3.3 was subjected to mapping, and the spectra were obtained for the IRN(red) as well as for

each sponge (green). The analysis of the blended spectra revealed that the distribution of IRN within the sponge was not uniform, with certain sections exhibiting homogeneity while others did not.

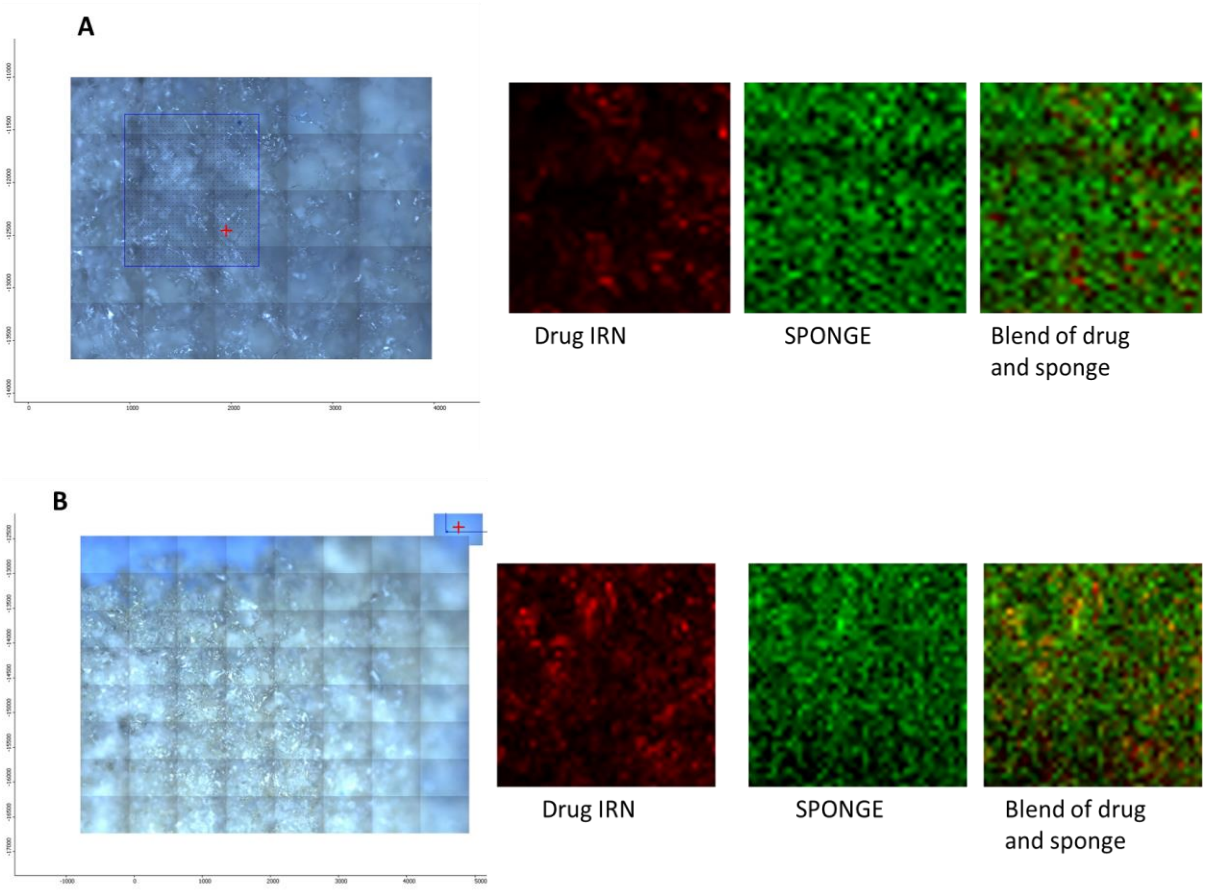

Figure 3. 3: Raman mapping for IRN spatial distribution within the gelatine sponge (A); and Gelfoam® sponge (B). screen shots of the spectra of sponge(green), IRN drug(red) and the blend of both to show the distribution of the drug within the sponge.

3.3.3 FTIR analysis

FTIR measurements were performed on the crosslinked gelatine sponge, which is the optimum sponge for evaluating the crosslinking reaction with glutaraldehyde, figure 3.4. Gelfoam® was also used as a control and for comparison. Figure 3.5 showed a shift of the absorbance band of gelatin amides at 1648.44 cm-1 (Strong) into 1655.68 cm^{-1} (Wide) indicating the formation of imine functional groups, although partial. The absorption band of a Schiff base is expected to be between 1640-1690 cm^{-1}, too close to the amide bond absorption. Hence, a weak absorption

shift is expected for the crosslinked sponge. Furthermore, this shift was absent in the Gelfoam® sponge as there was no chemical crosslinking involved.

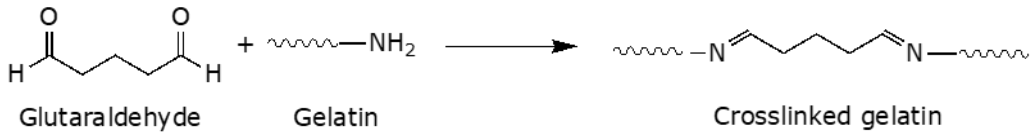

Figure 3. 4: chemical crosslinking of gelatine with glutaraldehyde

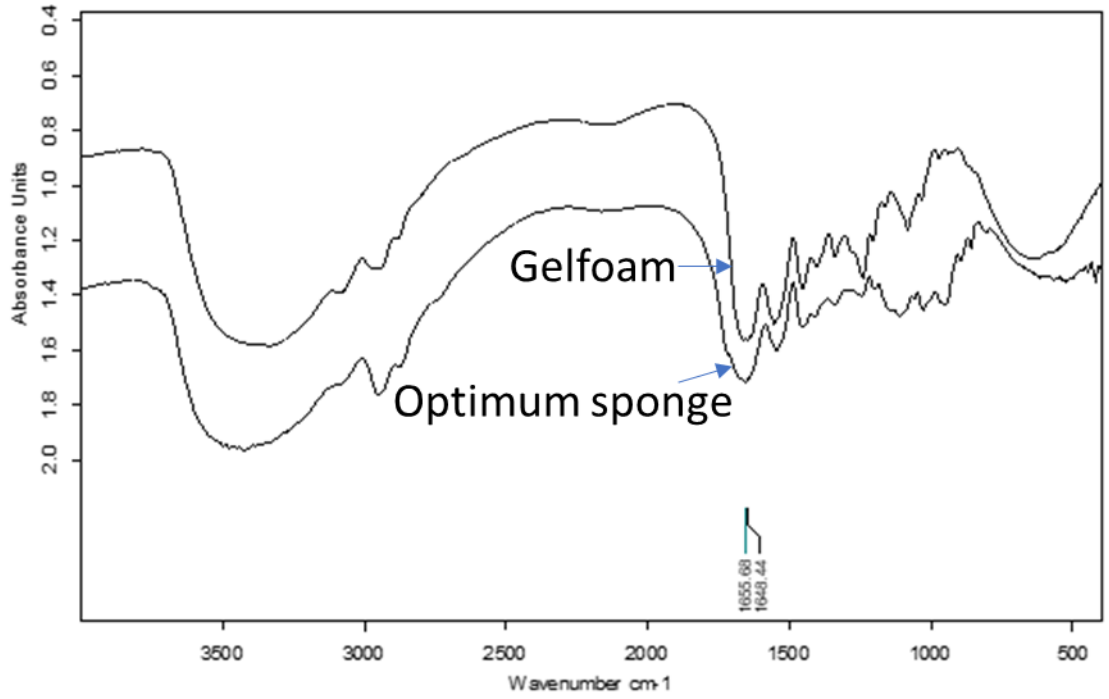

Figure 3. 5: FTIR spectra of optimum sponge and Gelfoam® control sponge.

3.3.4 Thermal analysis

The DSC thermograms of both gelatine (A) and Gelfoam® (B) sponges are presented in figure 3.6, with both sponges having similar thermogram profiles. The peaks observed around 100°C for both sponges are the glass transition temperature of the amorphous region. The second peak observed at 220°C for both sponges was for the melting temperature of the crystalline region. At temperatures between 280 and 380°C, endothermal peaks related to thermal degradation were also detected for both sponges.

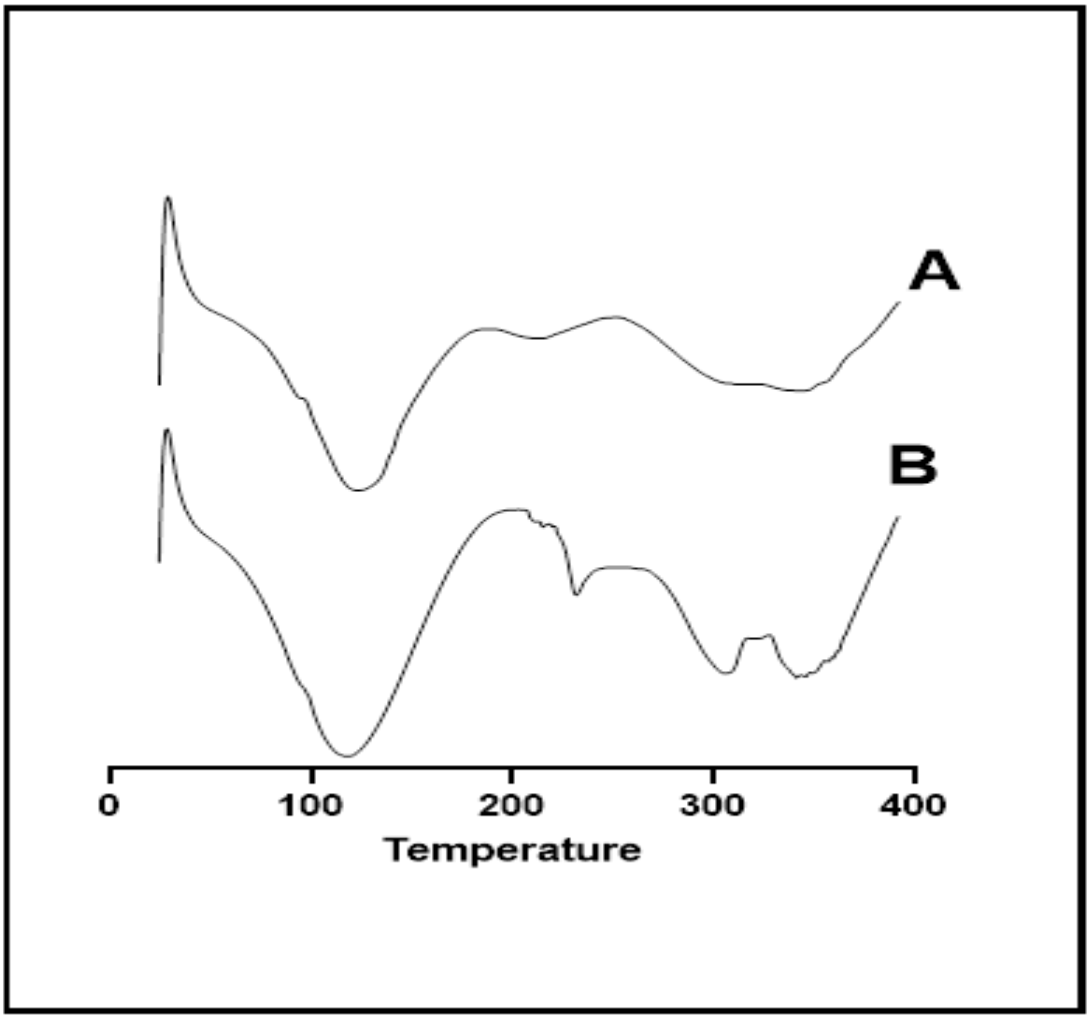

Figure 3. 6: An overlay of the DSC thermograms of the optimum sponge(A) and the Gelfoam® sponge(B).

3.3.5 Hydrolytic degradation test:

Hydrolytic degradation was performed on the gelatine sponge to compare its stability to the Gelfoam® sponge. Figure 3.7 showed the percentage weight remaining of the optimum sponge as a function of time. The data suggested that the gelatine sponge is degrading over time, as the percentage of weight remaining decreases from week to week with a degradation time of more than 6 weeks, which is similar to the reported degradation time (between 4 and 6 weeks) of Gelfoam® sponge.

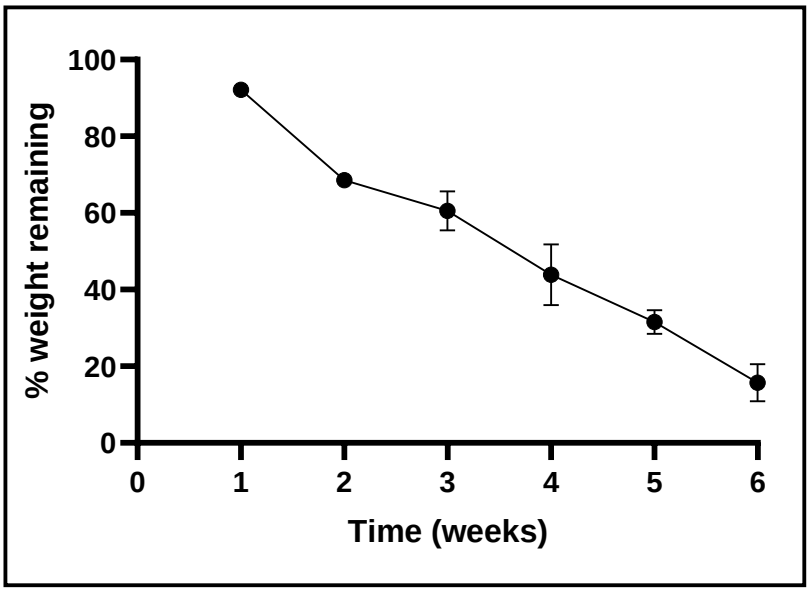

Figure 3. 7: The percent weight remaining of the hydrolysis degradation for the optimum sponge(n=3).

3.3.6 HPLC analysis:

Figure 3.8 depicts the IRN standard curve at seven different IRN concentrations quantified by HPLC. From 10 to 60 µg/ml, the correlation between IRN concentrations and HPLC area under the curve (AUC) was excellent, with a R value of 0.9983.

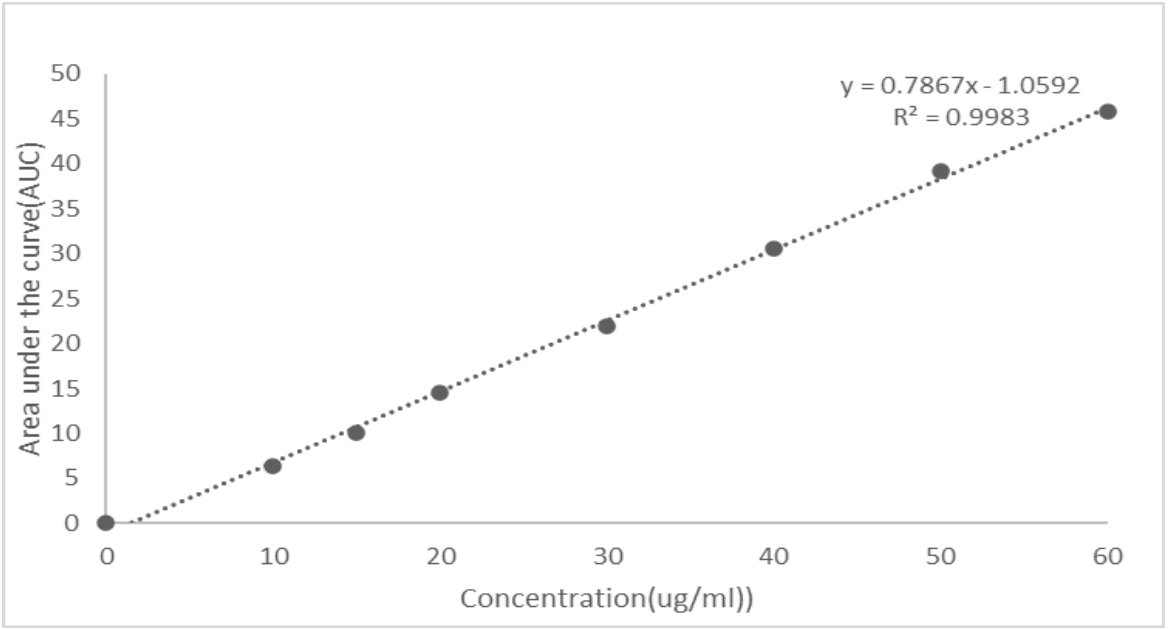

Figure 3. 8: Standard curve for IRN using HPLC (n=3).

3.3.7 Validation of HPLC method:

3.3.7.1 Linearity:

The IRN regression analysis results are presented in Table 3.1. The R2 values for linear regression in IRN analysis were ≥0.999, indicating a linear relationship between drug concentration and peak area. Moreover, the average peak area RSD% values for IRN are greater than 10%, showing that most of the data points are close to the mean.

Table 3. 1: Results of regression analysis for the linearity data of IRN

Conentration(µg/ml)	Concentration (% of analyte target)	Peak area (mean of three injections)	Peak area RSD (%)
10	50	6.41	7.07
15	75	10.03	1.80
20	100	14.51	2.16
30	150	21.93	0.97
40	200	30.61	1.13
50	250	39.21	0.55
60	300	45.83	1.66
Equation for regression line= y = 0.803x - 1.7335		correlation coefficient(r2)= R^2 = 0.999	

Conentration(µg/ml)	Concentration (% of analyte target)	Peak area (mean of three injections)	Peak area RSD (%)
10	50	6.41	7.07
15	75	10.03	1.80
20	100	14.51	2.16
30	150	21.93	0.97
40	200	30.61	1.13
50	250	39.21	0.55
60	300	45.83	1.66
Equation for regression line= y = 0.803x - 1.7335		correlation coefficient(r2)= R^2 = 0.999	

3.3.7.2 LOD and LOQ:

The LOD and LOQ were established at 3.6 and 11 µg/mL, respectively, with RSD% values of less than 1.7% (Table 3.2).

Table 3. 2: LOD and LOQ for HPLC method for IRN.

Test	AUC (mAU)	Concentration(µg/ml)	Found concentration(µg/ml)	Recovery (%)
1	6.41	10	10.14	101.44
2	10.02	15	14.64	97.62
3	14.51	20	20.22	101.14
4	21.93	30	29.46	98.23
5	30.61	40	40.28	100.71
6	39.21	50	50.99	101.98
7	45.83	60	59.23	98.73
Mean				99.98
RSD %				1.74
LOD				3.65
LOQ				11.06

3.3.7.3 Accuracy:

The method's accuracy was validated. Data are presented in table 3-3. The percentage recovery of the method was 97% to 101% for all examined samples and an RSD% of less than 2.

Table 3. 3: The accuracy validation for IRN method(n=3).

sample	percent of nominal (mean of three injections)	spiked concentration(ug/ml)	found concentration(ug/ml)	Recovery(%)
1	75	15	14.64	97.62418708
2	100	20	20.22851806	101.1425903
3	150	30	29.46928186	98.23093953
Mean				98.99923896
SD				1.880825165
RDS%				1.899838003

3.3.8 *In vitro* drug release of IRN from the optimum sponge:

The cumulative percentage release of IRN release from the gelatine sponge is presented in figure 3.9. The graph clearly shows that the cumulative release percentage increases over time, implying that the release is sustained, with the rate of IRN release decreasing over time. After the initial burst of approximately 62% after 1 hour, the percentage increase in IRN release was 16.49% between 1 hour and 3-hour time points, with only 3.82% between 5 hour and 7-hour time points.

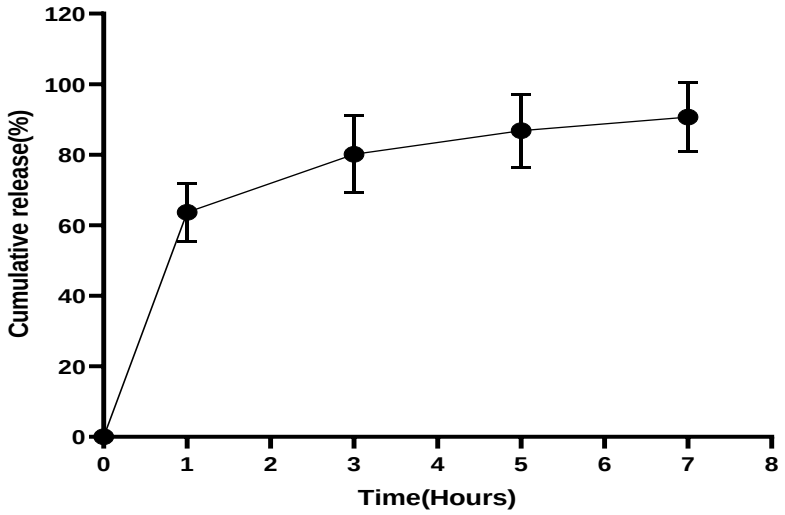

Figure 3. 9:in vitro drug release of IRN from the optimum sponge(n=3).

4. Discussion

In this chapter, the microstructural characteristics, drug distribution, FTIR spectral analysis, thermal properties and hydrolysis degradation for the optimum gelatine and Gelfoam® sponges were examined, with the drug release from the gelatine sponge determined.

The SEM images (figures 3.1and 3.2) revealed a network structure of diverse pores in both sponges. Moreover, the variances in pore size and interior structure of gelatine sponges may indicate differences in heat transmission rates during the hydrogel's freezing process. Because at a greater freezing temperature, fewer ice crystallisation nuclei are initially generated than at a lower freezing temperature, resulting in larger ice crystals (Van Luyn *et al.*, 1991; Kabiri *et*

al., 2010). Additionally, the morphology of the gelatine sponge relied more on the varying content of gelatine and alginate solutions than on the degree of crosslinking. As a result, the gelatine sponge had an interconnected network structure between the gelatine with its membrane-like structure and the alginate with its fibrous structure (Choi *et al.*, 1999). Furthermore, it was reported that, the gelatine sponge's porous structure comprised mostly of elongated pores (Murphy, Haugh and O'Brien, 2010; Kirdponpattara, Phisalaphong and Kongruang, 2017). However, both the gelatine and Gelfoam® sponges showed very porous structure with an average pore size of 100µm. This finding agreed with the SEM micrographs of Gelfoam® reported by Rohanizadeh et al where the porosity varied from 30-700µm (Rohanizadeh, Swain and Mason, 2008). As a highly porous structure would have a higher porosity, the porosity determined using the fluid replacement approach from chapter two was consistent with the SEM morphological analysis.

It is well known that two-dimensional spectroscopic images provide information regarding spatial distribution, with one dimension for spectrum information. In addition, it is essential to ensure the content homogeneity of medications administered in moderate dose (Psimadas *et al.*, 2012). Also, the homogeneous blend of medicines and matrix is particularly critical for spatial control of drug release (Indolfi, Ligorio, David T Ting, *et al.*, 2016). Therefore, to establish the homogeneity of the drug distribution within the sponge, Raman mapping was utilised in this study. The findings demonstrated that IRN was evenly distributed in some areas within both sponges (Figures 3.3A and B). IRN was partially homogenously distributed throughout the sponge matrix. This is demonstrated by the colour coded maps of IRN , the sponge and the blend of both. The same pattern of distribution was found to be common for both sponges.

In this study, glutaraldehyde crosslinking of the gelatine sponge was verified using FTIR spectral analysis. The glutaraldehyde-crosslinked gelatine sponge's FTIR spectrum resembled

that of Gelfoam® sponge with a shift peak associated with the crosslinking process. Furthermore, the characteristic amide A peak at 3300 cm-1, which is related to the N-H stretching mode (Del Gaudio *et al.*, 2017), demonstrated the similarity of the two sponges' spectra. The Amide I and Amide II bands, as well as several partially overlapping components in the fingerprint region between 1500 and 800 cm^{-1}, are characteristic spectral features of polypeptides and are shown in the FTIR absorption spectra of the gelatine and Gelfoam® sponges (Figure 3.5). Additionally, the amide I band is closely related to the backbone conformation and predominantly associated with the C=O stretching vibration (70–85%) (Farris, Song and Huang, 2010). Upon crosslinking reaction, there will be a shift in band position detected for the amide I. For instance, glutaraldehydes have an aldehyde group (-CHO) that interacts with the amino group of lysine residues in proteins such as gelatine (Imani, Rafienia and Emami, 2013). Through a Schiff base reaction, the carbonyl group of glutaraldehyde forms covalent imine bonds with the amino groups of gelatine (Fan *et al.*, 2018). As a result, a peak shift to a higher wavenumber is observed that is directly associated with glutaraldehyde crosslinking (Liu *et al.*, 2014). Moreover, in this study the amide I shift from 1648.44 cm^{-1} (Strong) into 1655.68 cm^{-1} (Wide) indicated the formation of imine functional groups, although partial. Furthermore, it is predicted that a Schiff base's absorption band will be too close to the amide bond absorption, at 1640–1690 cm^{-1} (Jenisha, Theodore David and Priyadharsini, 2015). So, a slight absorption shift was anticipated in this case. By confirming the successful crosslinking of the gelatine sponge with glutaraldehyde, it was possible to conclude that 0.5% glutaraldehyde was sufficient for producing a mechanically stable sponge similar to the control Gelfoam® sponge. Consequently, this was attributed to the blending of sodium alginate and gelatine prior to crosslinking with glutaraldehyde. As a result, less glutaraldehyde (0.5%) was used, thus minimizing the glutaraldehyde associated toxicity. It has

been reported that when used in low concentrations, glutaraldehyde has demonstrated reduced toxicity as an effective crosslinker for gelatine (Farris, Song and Huang, 2010).

The primary purpose of the DSC study was to compare the thermal properties of the gelatine sponge and the Gelfoam® sponge, in relation to the formation of imine crosslinks in the gelatine sponge, which was confirmed by FTIR spectra. The gelatine sponge, as depicted in the figure 3.6A, had a glass temperature of 125.24°C, which was greater than Gelfoam®'s glass temperature of 110°C (figure 3.6 B). This shift in glass temperature from, was due to the creation of an imine bond because of the Schiff base reaction of crosslinking with glutaraldehyde. Chang et al. reported that as the glass transition temperature of gelatine rises, the movement of its polymer chains becomes constrained (Chang *et al.*, 2020). This is primarily explained by the inclusion of imine crosslinks into the gelatine molecule, which restricted the mobility of the molecules and accordingly increased the glass transition of the gelatine sponge. Because of the lack of imine crosslinks in the Gelfoam® sponge, the molecules are free to move, resulting in a lower glass transition temperature than the gelatine sponge. This result was consistent with the results of the FTIR spectrum analysis of both the gelatine sponge and the Gelfoam® sponge.

Hemostat sponges made of biomaterials are required to dissolve into the body after their action is completed (Hong *et al.*, 2001; Imani, Rafienia and Emami, 2013). When dissolved in aqueous systems, gelatine experiences a progressive hydrolytic degradation. To address this issue, gelatine-based biomaterials are typically the result of physical, enzymatic, or chemical cross-linking (Oryan *et al.*, 2018b; Guizzardi *et al.*, 2019). According to the studies, hydrolysis of the Gelfoam® sponge is typically complete within 4–6 weeks after implantation (Holste *et al.*, 2022; Irfan *et al.*, 2022). Therefore, in this study the percentage of the weight remaining of the gelatine sponge was studied over a period of 6 weeks. Figure 3.7 showed that the gelatine sponge degraded rapidly during the first week, then slowly progressed in the following weeks,

specifically, the average percentage of remaining weight was decreased from 92.086% in week 1 to 15.706% in week 6. It is worth mentioning that the gelatine sponge reached to15.706 % weight remaining by week 6 which means that it is very stable, perhaps more than the Gelfoam® sponge. Furthermore, there are two possible scenarios of the degradation of the gelatine sponge that could occur in two different ways. The first is due to hydrolysis, which is influenced mostly by crosslinking and polymer concentration. The second scenario is deterioration caused by the diffusion of the PBS solution via the sponge's porous structure. Additionally, the reason for the gelatine sponge stability is the synergistic effect of both approaches, crosslinking, and polymer blending. It has been reported in the research that the resistance of the sponge to hydrolysis and degradation in PBS is due to the high concentration of gelatine and the presence of crosslinking (Imani, Rafienia and Emami, 2013). Under physiological conditions, this data suggested that the gelatine sponge (4% gelatine concentration, 4% sodium alginate with 0.5% glutaraldehyde) would show good stability.

In this chapter, the HPLC method for IRN measurement was verified utilizing multiple criteria such as linearity and range, LOD and LOQ. Because any new or altered method must be validated to demonstrate that it can produce reproducible and reliable findings when used by many operators employing the same equipment in the same or different laboratory. Validation of an analytical method is defined by the International Organization for Standardization as the investigation and providing of objective proof that the specific requirements for a defined intended use for that method are met (Araujo, 2009).

The linearity of the method must be evaluated to demonstrate a proportional relationship between response and analyte concentration across the working range. To determine the acceptability of linearity data, the correlation coefficient and y-intercept of the linear regression line for the response versus concentration plot are frequently examined (Shabir *et al.*, 2007). The linearity of IRN method was tested in this study over a concentration range of 10-60 µg/mL

(table 3.1). This is equivalent to 50-300% of the nominal concentration. By plotting the peak area (y) versus the IRN concentration, the following regression equation was discovered, y = 0.803x - 1.7335. The correlation coefficient (R^2 = 0.999) for the regression line showed an excellent relationship between peak area and IRN concentration (Figure 3.8). Additionally, LOQ measures the analytical method's selectivity and is defined as the lowest quantifiable concentration of an analyte (Zakeri-Milani *et al.*, 2005; Kowalska *et al.*, 2022). Based on the results (Table 3.2), the LOQ was determined to be a concentration of 11.06µg/ml, with an RSD% of 1.7 which means that the acceptance criteria (RSD%<10%) (Kowalska *et al.*, 2022), was achieved. However, the LOD of IRN method, which is the smallest detectable quantity of analyte in a sample that cannot be quantified precisely, was also confirmed to be 3.65µg/ml as had shown in table 3.2. The LOD and LOQ were calculated using the following equations: LOD = 3.3 × S /SD and LOQ = 10 × S /SD. Furthermore, the accuracy of the method was also tested as part of the validation process. The accuracy of a measurement is the degree of concordance between the acknowledged true value or acceptable reference value and the measured value (Taleuzzaman, Ahmed and Chattopadhyay, 2016; Vidushi, Meenakshi and Bharkatiya, 2017). The analytical procedures were likewise precise and accurate (table 3.3). According to recovery studies, the confidence interval of the average recovery value fell between 97.0 and 101.0% with an RSD % less than 2.

Over the course of seven hours, the IRN showed a biphasic release profile from the gelatine (Figure 3-9). Initially, a rapid 'burst' release was observed, followed by a slower release rate 3 hours later during the second phase of release. At time 3 hours, the cumulative release was 80.09 %, indicating that the rate of release has slowed since the initial surge at time 1 hour. Nonetheless, it is significant that the release is ongoing and not yet complete. It has been reported that drug diffusion was facilitated by the porous structure of the non-crystalline matrix, where water could spread more freely between polymer chains (Peppas *et al.*, 2000;

Alagha, Nourallah and Hariri, 2020). Consequently, IRN was rapidly released due to the amorphous nature of the sponge, as confirmed by the Raman mapping of the gelatine sponge. In addition to the gelatine sponge's swelling ability, which aided in the faster release of IRN.

5. Conclusion

Detailed examination of the optimum gelatine sponge versus the industry standard Gelfoam® sponge has yielded encouraging outcomes. Similar morphological properties, drug distribution pattern in the sponge’s matrix characteristics were observed in the newly developed sponge in comparison to the Gelfoam® sponge. In addition, the results of the characterization demonstrated that the gelatine sponge possessed adequate properties for implantation as part of a device to treat the resection margin of PC. Also, by using several characterisation techniques, such as hydrolytic stability, the gelatine sponge was shown to be as effective as Gelfoam® and to have the potential to serve as a homostat device to enhance the local chemotherapy treatment of PC. FTIR spectral analysis confirmed the crosslinking of the gelatine sponge. Consequently, the Schiff base reaction from glutaraldehyde crosslinking of the gelatine sponge caused elevation of the glass temperature. However, the *in vitro* drug release of IRN from the gelatine sponge, was immediate and not sustained and thus a membrane would be required to control and sustain drug release. The validity of the IRN method was confirmed by its linearity, range, accuracy, LOD, and LOQ during the method's validation.

Chapter 4: Designing and manufacturing of an implantable device using 3D printing

4.1 Introduction

Specific ailments exhibit a localized manifestation within distinct anatomical regions of the human body. Using drug-eluting implants for precise treatment has been proposed as a promising strategy, as indicated by Domsta and Seidlitz's research (Domsta and Seidlitz, 2021). Gao et al. and Domsta and Seidlitz have observed that patients' anatomical characteristics are heterogeneous and may differ depending on the nature and size of their ailments within the body (Gao *et al.*, 2020; Domsta and Seidlitz, 2021). Therefore, it is essential to have customized therapeutic options to attain the best healthcare results, which can be met through the utilization of 3D-printed drug-eluting implants (Domsta and Seidlitz, 2021). The highly customizable and complex nature of 3D printing technology enables the production of medical devices and structures specifically designed to meet the unique requirements of individual patients. According to Anadioti, Kane, and Soulas, intricate structures exist that surpass the production capabilities of conventional manufacturing techniques such as injection moulding, compression, melting, and casting (Anadioti, Kane and Soulas, 2018). The approval of Spritam®, the first 3D-printed tablet, by the FDA has set a precedent for the utilization of 3D printing technology in the development of drug delivery systems (Prasad and Smyth, 2016). As per the existing literature, Ethylene vinyl acetate (EVA) has been employed to manufacture pliable components. Additionally, the low melting point and fast curing properties of EVA render it a more suitable option for AM of flexible structures, as Kumar et al. stated (Kumar *et al.*, 2018). In implanted controlled-release applications, EVA is one of the most popular non-biodegradable polymers. The FDA has authorized this biocompatible, insoluble, non-toxic thermoplastic copolymer of ethylene and vinyl acetate (Genina *et al.*, 2016) .

Because of its shear-thinning behavior and excellent viscoelastic qualities when heated or cooled, thermoplastic polymers find widespread application in AM (Shaqour *et al.*, 2021).

The study aimed to create a post-loaded implantable drug delivery system to deliver FOLFIRINOX chemotherapy to the resection margin of PC at an appropriate clinical time. The primary concept entailed the utilization of a two-part device comprising a catheter port fabricated via 3D printing and a sponge. The catheter port serves as a receptacle for a catheter that extends externally from the patient and encounters the sponge. Following the infusion of the chemotherapeutic solution, the sponge would absorb the solution and maintain the sustained release of the drugs to the resection margin. Furthermore, the sponge that exhibited the most favorable characteristics in chapters two and three demonstrated comparable attributes to the control sponge, Gelfoam®, including mechanical robustness, flexibility, and resilience in the dissolution medium. The gelatine sponge's *in vitro* drug release profile, as presented in chapter three, exhibited an immediate release pattern rather than a sustained one. Consequently, utilizing a membrane to regulate and prolong drug release was postulated. Thus, the subsequent step involved the development of a two-component device utilizing 3D-printing technology. This drug delivery device comprises a catheter port and a membrane to encase the sponge. The requirement to enclose the sponge within the device to maintain its release necessitated stability, which was subsequently achieved. Consequently, the decision was made to utilize the commercially available Gelfoam® sponge to minimize the regulatory pathway necessary to implement Chemo Patch in clinical settings. Furthermore, after consulting with the surgical team, it was concluded that the membrane should be extended beyond the catheter port to facilitate its suturing onto the tissue. The device being developed must exhibit sufficient flexibility to accommodate diverse end-use applications, particularly for suturing the pancreatic resection margin during surgical interventions. The significance of this cannot be

overstated, given the dense nature of the pancreas tissue, as reported by Wex et al. (Wex *et al.*, 2015). The Chemo Patch device was constructed using EVA grade (18.2) material.

4.2 Materials and methods

4.2.1 Materials

Gelfoam® sponge was purchased from AEGIS LIFESCIENCES PVT. LTD, Gujarat, India. Irinotecan hydrochloride, oxaliplatin, and fluorouracil were purchased from LGM Pharma (Memphis, USA). Leucovorin was purchased from Sigma Aldrich (Dorset, UK). Potassium dihydrogen orthophosphate and methanol 99% were purchased from VWR (Leicestershire, UK). Acetonitrile was purchased from Fisher Scientific (Leicestershire, UK). EVA 18.2 % copolymer pellets supplied by Celanese (Irving, Texas, USA). Phosphoric acid and PBS were purchased from Sigma-Aldrich (Dorset, United Kingdom).

4.2.2 Determination of melt viscosity for EVA18.2

Rheology was used to determine melt viscosity and processing parameters for 3D printing as a function of temperature. A discovery HR10 TA rotational rheometer with a Peltier heating system was used for the rheological analysis using a plate-plate geometry with a diameter of 20 mm. Before beginning the experiment, the rheometer was calibrated to zero gap. EVA18.2 pellets in the amount of 400mg, were placed on the lower plate and gently heated until a paste was formed. Following that, a temperature sweeps in the range of 80°C to 200°C was conducted, with a ramp rate of 5°C/min, an oscillation strain of 0.5% and an angular frequency of 0.1°radian/s to determine the viscosity of the sample.

4.2.3 The rationale for chemo patch design

The requirement for a personalized implantable drug delivery device for treating the margin of PC drove the development of the Chemo Patch. Following consultation with the surgical team, a patch-like device was recommended. This is due to the hollow groove shape of the resection margin. Furthermore, because the resection margin is so small, the device cannot contain any extra pieces, such as a pump, to aid in medication transport. As a result, a catheter was

presented as a method of delivering the FOLFIRINOX solution from the outside to the device via passive diffusion, and the concept of local continuous infusion was proposed.

4.2.4 Feasibility study

Prior to the final device manufacture, a few key points were considered in this study. The first was design input, which entailed a conversation with the surgical team about the device's specifications. The second was a quick prototyping based on the surgical team's suggested device shape and size. Finally, the prototype was validated by surgically implanting the initial device to a cadaver pig to check the correct size and shape. This study was done by the surgeon (Rupaly Pande).

4.2.5 3D printing process

The Chemo Patch device was printed on a Pam printer (Pollen) with the Cura® software slicer (Ivry-sur-Seine, France). The printer is a pellet based FDM 3D printer. All designs were created in the CAD software Tinkercad and exported as STL files for slicing and G code generation in the pam Cura® software. One extruder was used for the printing with a nozzle size of 0.6mm. Initially, 12 distinct 3D-printed membranes with various membrane thickness, % infill, membrane pore number, and pore size were printed. After characterizing each membrane, the optimal one was selected, and the final Chemo Patch design was printed. The print speed was 15 mm/s, the print temperature was 110 °C, and the build plate temperature was 55 °C. In addition, the Chemo Patch was printed using the following print settings: the infill pattern was zig zag, travel speed 120mm/sec, flow rate was 35% and layer height was 0.15mm.

4.2.6 HPLC analysis

The samples of the FOLFIRINOX regimen were analyzed using the DIONEX Ultimate 3000 Autosampler (Thermo Scientific) equipped with a quaternary gradient pump and Chromeleon Chromatography Data System software. The FOLFIRINOX regimen was separated by utilising a C18 column (150mm × 4.6 cm) with a particle size of 5 µm (ThermoFisher

Scientific, Loughborough, UK) at a temperature of 25 °C. The subsequent techniques were employed for FOLFIRINOX regimen:

4.2.6.1 HPLC chromatographic condition for oxaliplatin

The experimental setup involved an injection volume of 20 µL, a 10-minute run time, and a 1.00 mL/min flow rate. The mobile phase composition used in the experiment was a mixture of an aqueous acid solution containing 0.01 M phosphoric acid and acetonitrile in a ratio of 95:5 (v/v). The UV wavelength utilized by the detector was configured to 255 nm.

4.2.6.2 HPLC chromatographic condition for fluorouracil

The experimental protocol involved an injection volume of 20 µL, a run time of 10 minutes, and a flow rate of 1.00mL/min. The mobile phase comprised degassed and filtered water. The detector's UV wavelength was configured to 254 nm.

4.2.6.3 HPLC chromatographic condition of leucovorin

The experimental protocol involved an injection volume of 20 µL, a run time of 10 minutes, and a flow rate of 0.8 mL/min. The mobile phase was composed of a mixture of Phosphate Buffer and Acetonitrile in a volumetric ratio of 40:60. The mobile phase underwent filtration and degassing. The UV wavelength of the detector was set to 283 nm.

4.2.6.4 HPLC chromatographic condition of IRN

Chapter 3, section 3.2.8.1, discussed the separation of IRN Briefly, the injection volume was reported to be 20 µL, while the run time and flow rate were 10 minutes and 1 mL/min, respectively. The mobile phase comprises a combination of ethanol, acetonitrile, and 0.02 M potassium dihydrogen orthophosphate, with a pH of 3.5 that has been adjusted using orthophosphoric acid. The proportions of the components are 60% ethanol, 20% acetonitrile, and 20% potassium dihydrogen orthophosphate. The UV wavelength of the detector has been set to 220 nm.

4.2.7 *In vitro* drug release from the membranes

To examine the *in vitro* drug release from different membrane groups, the membrane was suspended and brought into contact with the release media (water PH 6.5) to ensure unidirectional release. The drug solution was introduced from the top, and samples were collected (1 ml) from the release media at alternate intervals over six days. Subsequently, the drug solutions underwent filtration and were subjected to HPLC analysis.

4.2.8 *In vitro* drug release from Chemo Patch and the mathematical modelling

To examine the in vitro drug release from the chemo patch, a solution of FOLFIRINOX regimen measuring 1.5ml was administered via the catheter. Subsequently, the device above was inserted into a Duran flask preloaded with 10 mL of release medium, specifically water, with a pH of 6.5. 1 mL samples were collected periodically at 1, 3, 5, and 7 days and subsequently underwent filtration and analysis via HPLC.

The drug release data obtained from in-vitro experiments were subjected to regression analysis using both linear and nonlinear regression equations. The Excel add-in software program, DDSolver, developed by China Pharmaceutical University in Nanjing, China, offers a comprehensive selection of kinetic release models, including Zero order, First order, Hixon-Crowel and Higuchi models. It calculates the coefficient of determination (R2). A greater value of R2 indicates a stronger degree of goodness of fit for the model.

4.3 Physical characterisation of the Chemo Patch

4.3.1 The Leakage tests

Visual inspection was performed to check for any signs of the drug solution dripping down the walls of the device. In a summary, the Chemo Patch was placed on a tissue, and then a steady infusion of a specified amount of deionized water was performed through the catheter while monitoring the instant leakage of water through the side walls of the device. This test also

helped in determining the exact volume capacity of the Chemo Patch and the drug solution infusion rate.

4.3.2 Tensile strength of the catheter tubing

The force necessary to extract the catheter tubing was measured using a Stable Micro Systems TA-XT2 Texture Analyzer, which was fitted with a 5 kg load cell and Texture Exponent-32® software program. The experiment was performed utilizing a tension mode to measure force, and the return to start option was employed. A trigger force of 5g was applied to a distance of 100 mm. The velocity during the pre-test phase was recorded as 1 mm per second, while the test phase was conducted at a velocity of 3 mm per second. The post-test phase was performed at a velocity of 10 mm per second. Prior to conducting the tensile test, the rig arms underwent calibration to ensure uniformity of the distance between the arms for every sample subjected to testing. The sample was secured by means of self-locking of the catheter tubing via the grip and rotation of its ends. The process of securing the catheter tubing was iterated until a significant portion of the sample's slack was absorbed by the grip. Subsequently, the upper arm was secured with the aid of a screwdriver, following which the test was commenced. A study was conducted to evaluate four distinct Chemo Patch devices, and the mean force was computed. The gram-force measurement of the catheter's maximum pulling force was converted to the Newton unit to obtain the raw peak value. According to the formula provided, one unit of g-force is equivalent to 0.00980665 Newtons (N).

4.4 Results

4.4.1 Melt viscosity of EVA18.2

The diagram in Figure 4.1 displayed the melt viscosity of EVA18.2, thus suggesting that the optimal processing temperature range for EVA 18.2 would be between 84°C and 132°C.

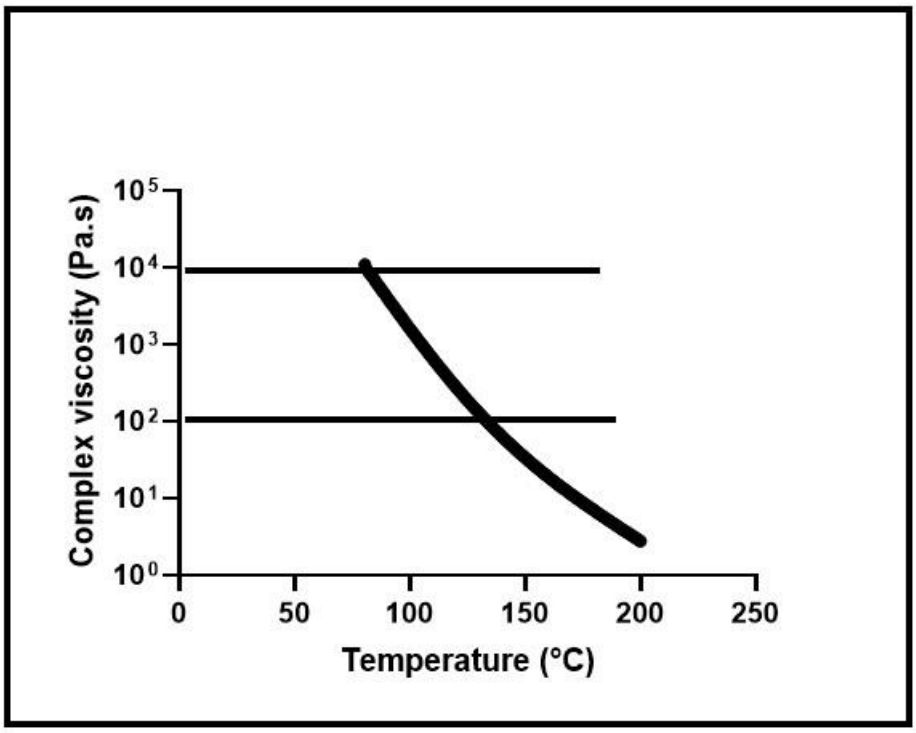

Figure 4. 1: The temperature sweep showing melt viscosity of EVA 18.2 in the range of 80°C to 200°C

4.4.2 The rational of Chemo Patch design

The schematic presentation of the rationale behind the Chemo Patch concept was illustrated in Figure 4.2. The diagrammatic representation demonstrated that the patch configuration would be most suitable for the shape of the resection margin of PC. The presence of a catheter would facilitate multiple infusions as well as the delayed administration when the patient is fit for receiving chemotherapy. Figure 4.3 depicted the preliminary concept of the chemo patch device, comprising a catheter port affixed to a sponge. Additionally, figure 4.4 showed the transition of chemo patch design from the one presented in figure 4.3 to the final one.

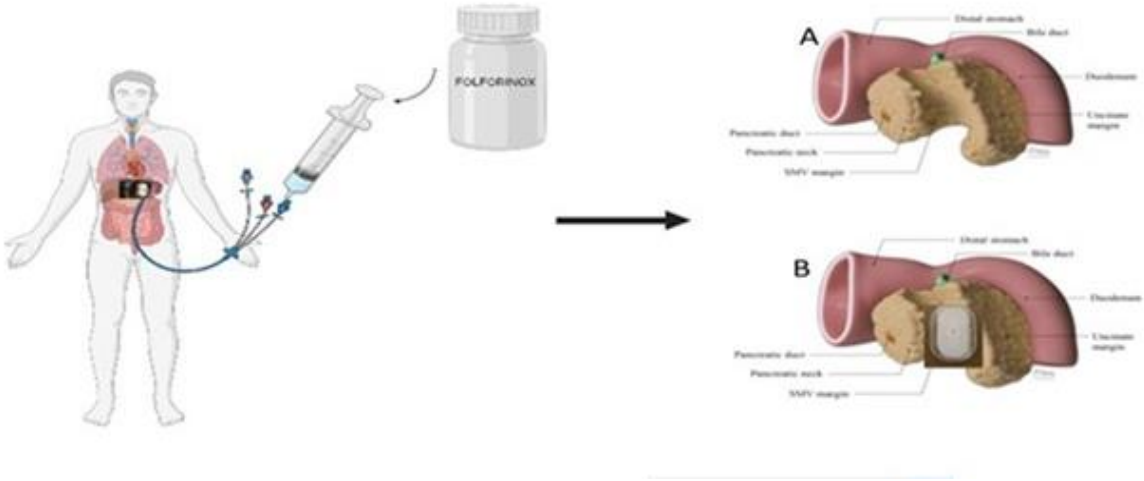

Figure 4. 2: A graphical presentation of the rationale behind chemo patch design, A: the resection margin groove prior to chemo patch implantation, B: the Chemo Patch implantation to the resection margin groove. The demonstration was drown using Biorender software.

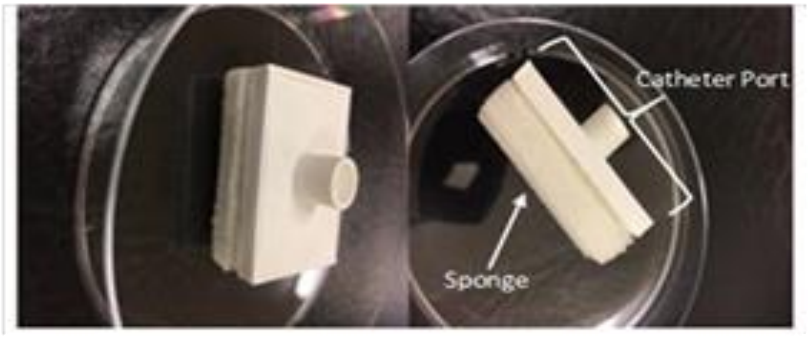

Figure 4. 3: The initial design of Chemo Patch in which it has only one part; the catheter import that was attached to a sponge.

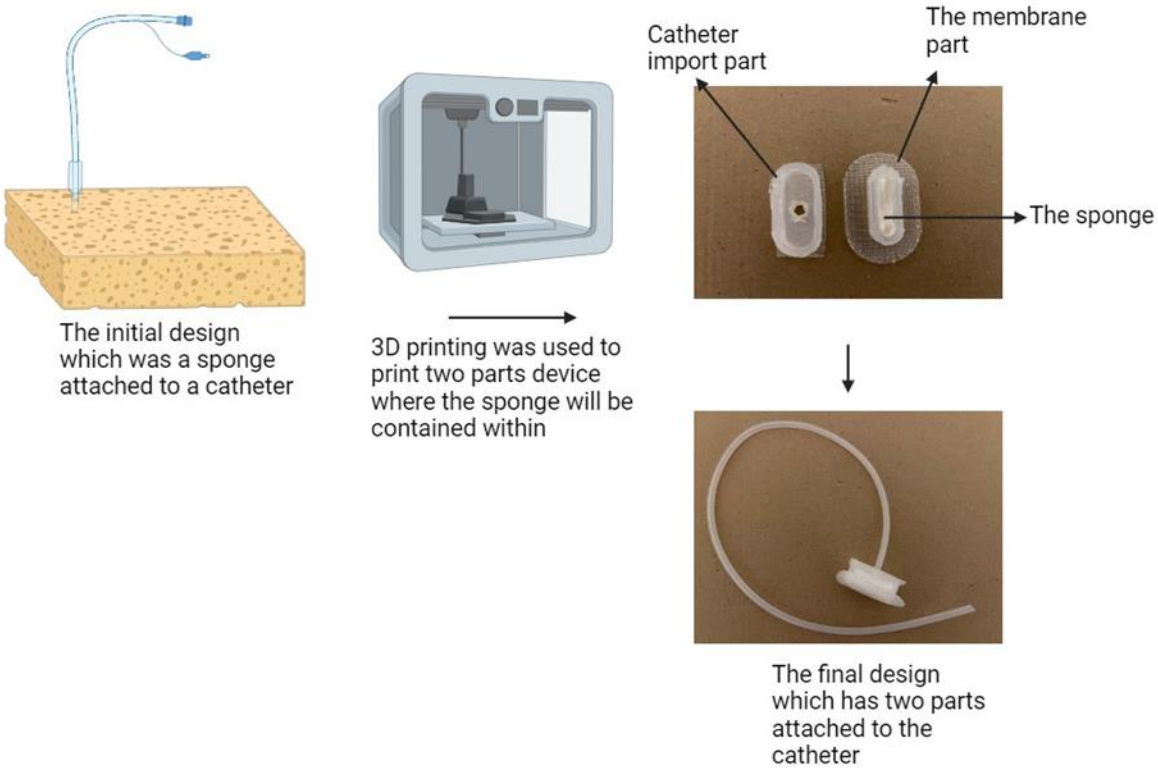

Figure 4. 4: An illustration of the change of chemo patch design from the initial design to the final one.

4.4.3 Feasibility study:

After conducting a feasibility study, two distinct designs (as depicted in Figure 4.5) were developed, featuring differing shapes and proportions. Device A was a square-shaped object measuring 4cm by 4cm, as depicted in the accompanying image (figure 4.5 A). On the other hand, Device B was an elongated object with dimensions of 15mm by 30 mm (figure 4.5 B). The device that conformed to the surgical margin of the cadaver pig was illustrated in Figure 4.6, wherein device B was found to be by the desired geometry and size.

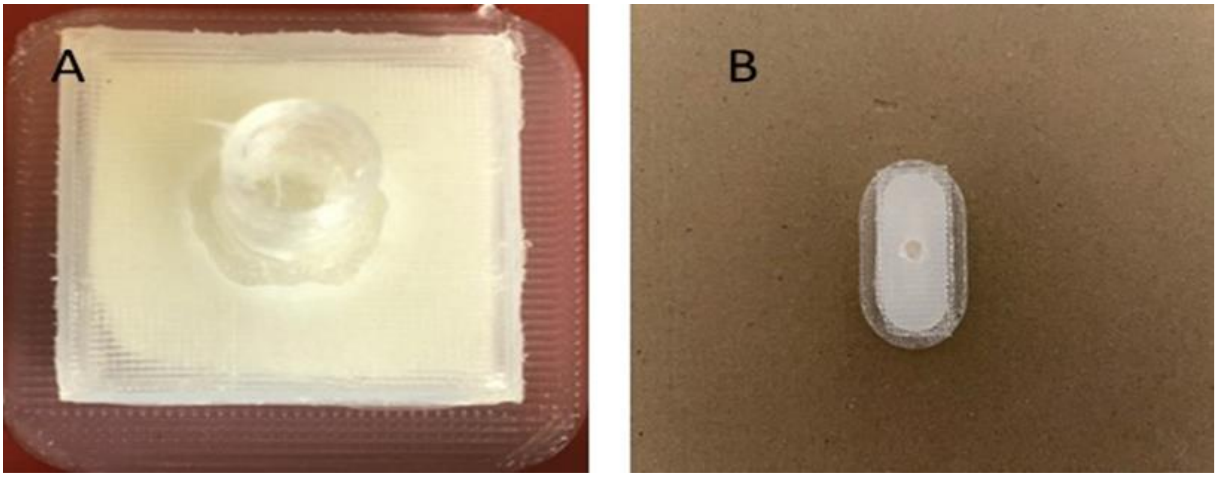

Figure 4. 5: The feasibility study outcome with two devices A and B; A: square shaped bigger device, B: oblong shaped smaller device.

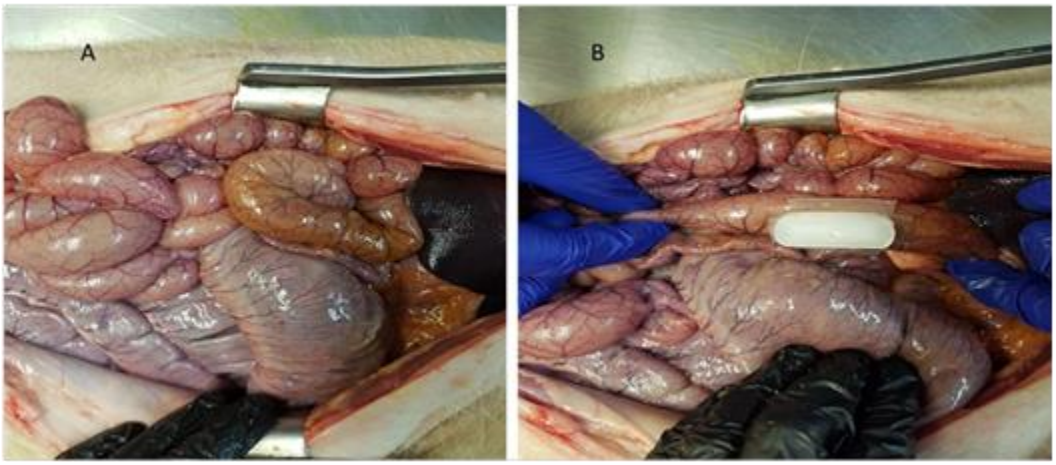

Figure 4. 6: The cadaver fitting of the best device in shape and size (device B), A: preimplantation, B: post implantation

4.4.4 3D printing

The study used 3D printing technology to produce four distinct sets of membranes with differing parameters. These sets were designated as groups A, B, C, and D. Group A involved membranes with varying infill percentages of 100%, 75%, and 50%. Group B consisted of membranes with varying thickness levels of 1mm, 1.5mm, and 2mm. Group C comprised membranes with varying numbers of pores, specifically one pore, two pores, and four pores.

Finally, group D consisted of membranes with varying pore sizes of 3mm, 4mm, and 5mm, as depicted in Figure 4.7 A. The membrane and Chemo Patch designs were generated using Tinker CAD software, as shown in Figure 4.8. Following *in vitro* drug characterization, a membrane thickness of 1mm and an infill of 75% were chosen as a constituent of the Chemo Patch device. Subsequently, the device was fabricated in two distinct parts, namely a membrane and a catheter import part as shown in figure 4.7 C. Additionally, Figure 4.7 B showed the final Chemo Patch design with the catheter attached. Furthermore, an additional component was fabricated via 3D printing. This component, depicted in Figure 4.9, was a circular ring later inserted through the catheter tubing. The primary function of this component was to provide support for the catheter tubing, thereby preventing it from becoming loose and ensuring a more comfortable experience for the patient.

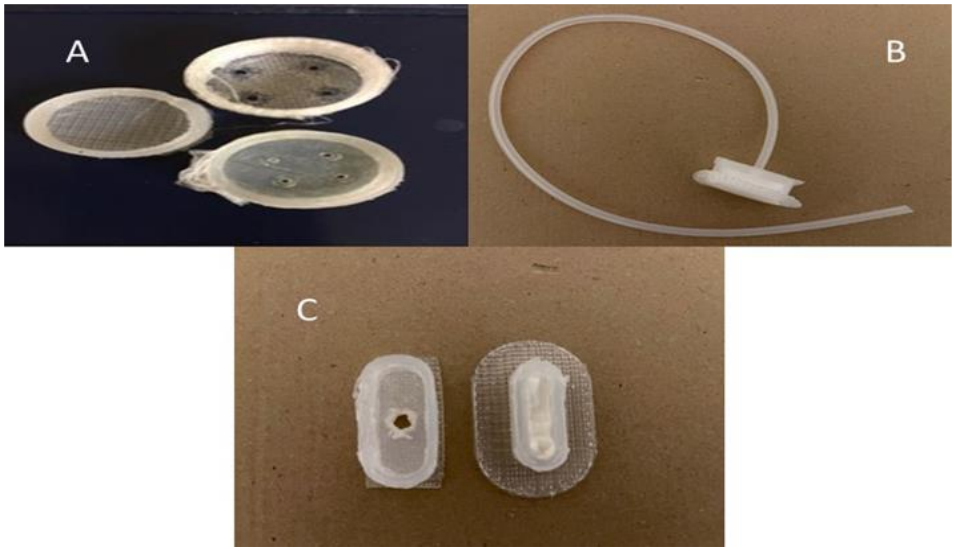

Figure 4. 7:The 3D printing outcomes; A: different membranes, B: the final chemo patch with catheter attached, C: the two parts of the chemo patch being apart with the sponge inside.

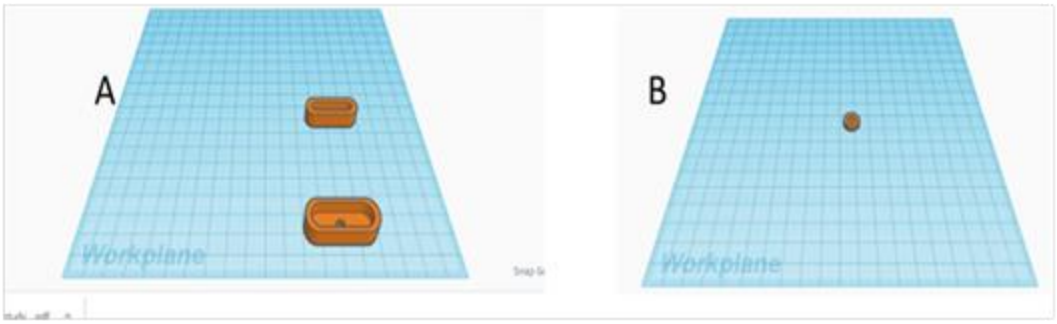

Figure 4. 8: The screen shot from tinker cad software showing; A: the final chemo patch design, B: smaller chemo patch size for mice efficacy study.

Figure 4. 9: The circular ring that was added to the final chemo patch design for extra outside support

4.4.5 The leakage tests

According to the leakage test results, the device's maximum capacity was determined to be 1.5ml. To mitigate lateral seepage, it was imperative to administer the infusion at a reduced rate. Optimally, 0.1 millilitres per second infusion rate was the most effective. As evidenced by visual inspection and tissue dryness, the leakage testing for the final chemo patch device yielded negative results, as depicted in Figure 4.10.

Figure 4. 10: The leakage testing of the Chemo Patch; A: pre infusion, B: during infusion, and C: post infusion.

4.4.6 The tensile strength of the catheter tubing

The study aimed to assess the tensile strength (the maximum axial force needed for catheter detachment from the chemo patch) of four different Chemo Patch devices, as depicted in Figure 4.11. The data presented in table 4.1 indicated that the average tensile strength was 31.95 N, which led to the conclusion that the attachment of the catheter tubing to the chemo patch exhibited an adequate level of strength.

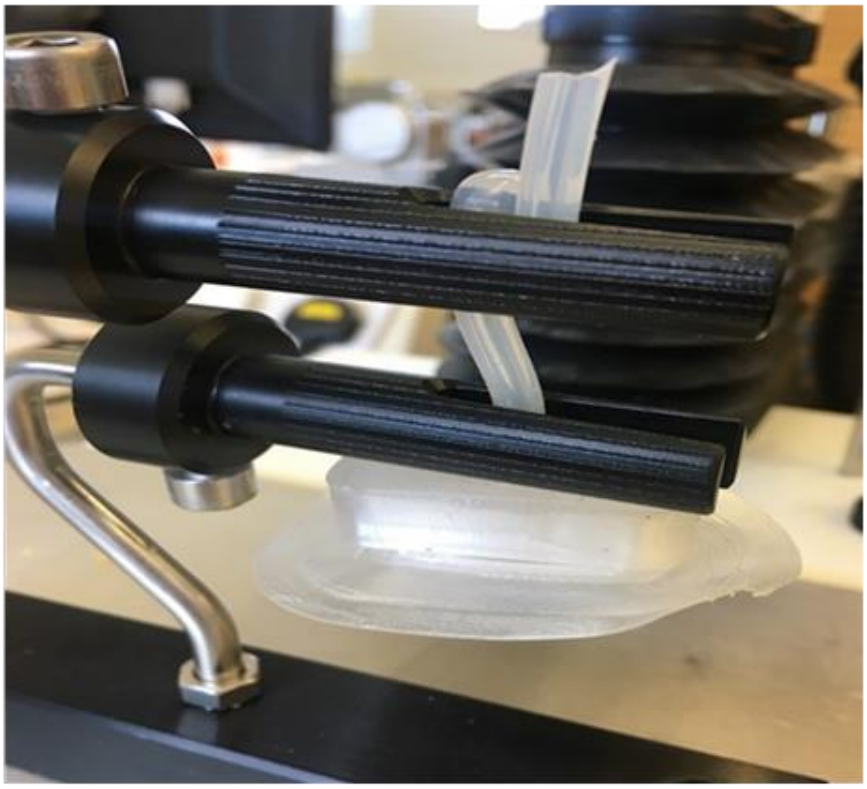

Figure 4. 11: A photograph depicting the process of evaluating the tensile strength of the catheter fastening mechanism on the Chemo Patch device.

Table 4. 1: The tensile strength of catheter attachment to four distinct chemo patch devices.

Sample	Elastic limit/Tensile strength(N)
Device 1	33.5
Device 2	32.17
Device 3	31.27
Device 4	30.68
Average	31.95
S.D.	1.16

4.4.7 *In vitro* drug release from the membranes:

The study's Table 4.2 provides an overview of the characteristics of the four discrete categories of EVA membranes that underwent screening for *in vitro* drug release analysis. The data from the screening study for the 12 membranes was presented in figure 4.12. The study involved Group A, comprising three membranes with varying infill percentages. The results indicated that the maximum release rate was inversely proportional to the infill percentage. Specifically, as the percent of infills increased, the drug release rate decreased. For instance, the 50% infill recorded a release rate of 24%, the 75% infill achieved 18%, and the 100% infill attained 15%. Group B consisted of three membranes with differing thicknesses; on day 7, the 1mm thickness had a greater cumulative release rate (20%) than the 1.5 mm and 2mm thickness, which had a release rate that of 18 % and 12% respectively. In Group C, which consisted of three membranes with varied pores, the release rate increased as the number of pores grew, with one pore reaching 24%, two pores reaching 32%, and four pores reaching 44%. In the final group D, which consisted of three membranes with two pores of differing sizes, the release rate was found to be proportional to the pore size, as depicted in the figure: pore size 3mm was 27%, pore size 4mm was 33%, and pore size 5mm was 50%.

Table 4. 2: The different printed EVA membranes

Membrane code	Thickness (mm)	Infill %	Pore number	Pore size (mm)
Group A membrane 1	1	100	0	-
Group A membrane 2	1	75	0	-
Group A membrane 3	1	50	0	-
Group B membrane 1	1	75	0	-
Group B membrane 2	1.5	75	0	-
Group B membrane 3	2	75	0	-
Group C membrane 1	1	75	1	3
Group C membrane 2	1	75	2	3
Group C membrane 3	1	75	4	3
Group D membrane 1	1	75	2	2
Group D membrane 2	1	75	2	4
Group D membrane 3	1	75	2	5

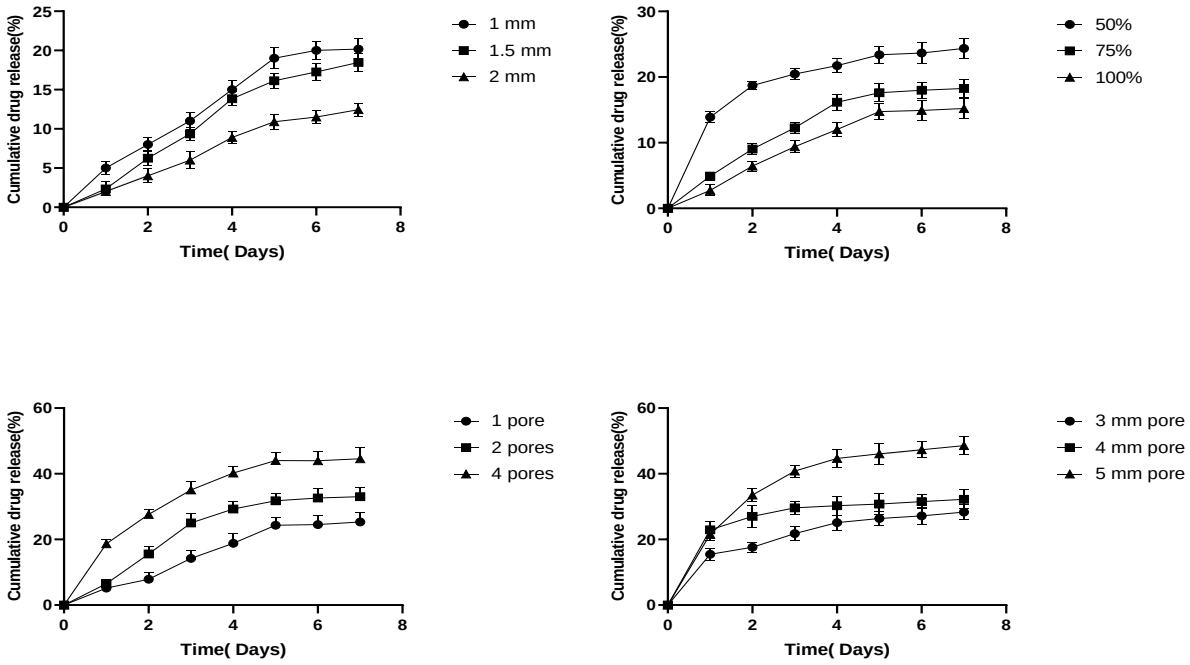

Figure 4. 12: The in vitro drug release of IRN from the four membrane groups in water (PH 6.5) over 7 days at 37°C. Results shown as mean ± SD, n=3.

4.4.8 *In vitro* drug release for FOLFIRINOX from Chemo Patch and the mathematical modelling

Figure 4.13 illustrated the investigation of drug release for the FOLFIRINOX treatment regimen from Chemo Patch device. The initial release of the four drugs was characterized by a sudden and burst release, succeeded by a period of stability indicating a continuous and sustained release for seven days.

The results displayed in Table 4.3 demonstrated that the drug release mechanism may involve a combination of diffusion-controlled release, as explained by the Higuchi model, and first-order kinetics. This conclusion was supported by the greater R^2 values seen for both mechanisms compared to other R^2 for all drugs in the FOLFIRINOX regimen. The previously mentioned finding implied the existence of a complex mechanism for drug release, in which the combined influences of matrix diffusion(sponge), membrane diffusion(the controlling membrane), and maybe additional factors synergistically impact the overall kinetics of drug release.

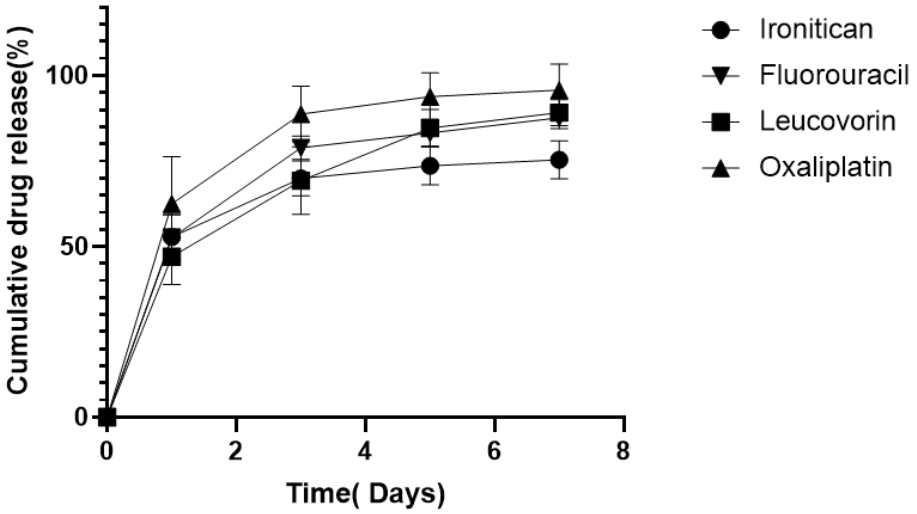

Figure 4. 13: In vitro cumulative drug release of FOLFIRINOX regimen from the Chemo Patch in water (PH 6.5) over 7 days at 37°C. Results shown as mean ± SD, n=3.

Table 0-3: *Results of fitting FOLFIRINOX release data from the chemo patch to different release kinetic models*

Drug	Zero order R^2	First order R^2	Higuchi R^2	Hixon-Crowel R^2
Irinotecan	0.6016	0.7581	0.8486	0.7041
Oxaliplatin	0.6519	0.8266	0.8845	0.7737
Fluorouracil	0.6519	0.8266	0.8968	0.8028
Leucovorin	0.7247	0.9428	0.9308	0.8811

4.5 Discussion

A chronic illness, such as cancer, is characterized by its prolonged and recurring nature. In addition, managing this ailment incurs high costs, mainly when it increases the number of disability-adjusted life years experienced by patients (Bernell and Howard, 2016). Implantable drug delivery systems offer numerous benefits compared to conventional systemic drug delivery in managing chronic diseases. Implementing site-specific implants can circumvent the absorption and dispersion phases associated with oral and peripheral regimens, thereby leading to elevated concentrations of medication in targeted areas (Danckwerts and Fassihi, 1991; Pons-Faudoa *et al.*, 2019). Hence, the placement of implants after surgery can serve as adjunctive therapy for eradicating residual tumours or subclinical lesions, as Wex et al. suggested (Wex *et al.*, 2015). Furthermore, the co-administration of systemic chemotherapy and local sustained-release implantation near a solid tumour with significant drug loading can lead to a focused eradication on cancer in patients with advanced or metastatic malignancies (Chew and Danti, 2017; Hao *et al.*, 2021).

The processability settings of various 3D printing materials rely heavily on the results of rheological studies (Cicala *et al.*, 2018; Mohamdeen *et al.*, 2022). A material's viscosity must

be low enough to guarantee continuous flow through the printing nozzle and high enough to ensure layer adhesion during deposition. Therefore, to provide consistent and reproducible 3D printing, printing parameters, notably printing temperature and speed, are regularly optimised to obtain the desired viscosity (Azad *et al.*, 2020; Tabriz *et al.*, 2021). Additionally, it was discovered that the viscosity of most polymer melts under extrusion varies between 10^2 pa.s and 10^5 pa.s (Campanella *et al.*, 2002). As a result, in this study, a temperature sweep test on the EVA 18.2 was performed to identify the printing temperature range based on the optimum viscosity for extrusion (10^2 Pa.s to 10^5 Pa.s). Figure 4.1 demonstrated that the temperature range corresponding to the optimum viscosity was between 84°C and 132°C. Subsequently, the optimal temperature for 3D printing of EVA 18.2 at this temperature range was determined to be 110°C. This further confirmed that the viscosity measurement at the examined temperature was within the extrudable range. Additionally, EVA 18.2 was selected due to its melting index (MI) of 150g/min. In a previous work by Genina et al., in which several grades of EVA with MI ranging from 1.1 to 500g/10min were attempted for 3D printing, a correlation was discovered between the MI and the printability. The low MI EVA grade did not generate a print of acceptable quality, while the higher MI EVA grade produced droplets, causing the printing to fail (Genina *et al.*, 2016). Therefore, it was decided to conduct an EVA with moderate MI such as EVA 18.2.

In this study, a feasibility analysis was conducted to maximize the likelihood of success of the final Chemo Patch device. The research comprises three primary phases: design input, rapid prototyping, and design proper validation. As per Aitchison et al., developing a successful medical device is commonly attributed to the collaborative efforts of a multidisciplinary team comprising medical engineers, surgeons, and other professionals (Aitchison *et al.*, 2009). Following consultations with the surgical team at Queen Elizabeth Hospital, two device designs were proposed, each in the form of patches that would conform appropriately to the

surgical margin. The circumferential resection margin, as described by Verbeke and Menon, possesses a groove-like shape conducive to accommodating a patch of appropriate size and shape (Verbeke and Menon, 2009). The proposed design's patch shape was based on the underlying rationale depicted in figure 4.2. In addition, the preliminary design we proposed was a patch, illustrated in Figure 4.3, featuring an exposed sponge that has demonstrated a rapid drug release, as discussed in Chapter 3. Therefore, the idea of incorporating a regulating membrane for drug delivery was proposed in this chapter. The device's width is recommended to fall within the 1 to 2 millimetres range. The "1 mm rule" has been substantiated by empirical evidence to classify PC resections as fully accomplished. The findings suggest that a margin clearance of 1 mm had a notable impact on the survival rates of resections with a margin clearance exceeding 1 mm, as opposed to those with a margin clearance below 1 mm. These results were reported in studies conducted by Niesen et al. and Daamen et al. (Niesen *et al.*, 2019; Daamen *et al.*, 2021). Therefore, to guarantee comprehensive coverage of the implantable device, it is recommended that the width falls within the range of 1 to 2 mm. However, the device width of 15mm was implemented to provide a broader coverage of the area surrounding the resection margin, thereby enhancing the device's overall performance. Moreover, the device's functionality would be constrained to a single element without any additional attachments, such as a pumping system, due to the narrow proximity of the resection margin, particularly in the presence of adjacent blood vessels (Nishino *et al.*, 2023). Consequently, the administration of medicine via catheterization was suggested. Subsequently, two prototypes were produced via 3D printing, resulting in two distinct shapes with varying dimensions (refer to Figure 4.4 A and B). Device A exhibited larger physical sizes, measuring 4 cm by 4 cm, compared to Device B, which possessed a smaller rectangular shape with dimensions of 30 mm by 15 mm. Rapid prototyping technologies were incorporated in this feasibility study due to their various applications in the biomedical

sector, such as customized implants and drug delivery systems. This is attributed to its ability to manufacture intricate structures with high precision, as stated by Touri et al. (Touri *et al.*, 2019). The conclusive stage of the feasibility analysis encompassed the verification of the prototype's conformity with the appropriate shape and dimensions before the production of the final Chemo Patch. The process of Design Validation aims to verify that the medical device meets the user's specified requirements, as stated by Aitchison et al. (Aitchison *et al.*, 2009). Furthermore, scholarly sources have indicated that cadaver have been utilized to evaluate surgical equipment, including a hook apparatus affixed to the spinous process of the lumbar vertebrae (Shepherd *et al.*, 2001; Aitchison *et al.*, 2009). The findings depicted in Figure 4.5 illustrated that through cadaver testing, it was observed that device B's dimensions effectively encompassed a significant portion of the tissue diameter proximal to the stomach. Device B was confirmed as the shape and size of the Chemo Patch. Before conducting *in vivo* testing on pigs, an additional component was incorporated into the final chemotherapy patch which is shown in figure 4.8. This component comprised two circular rings of 3D-printed EVA18.2, administered through the catheter. The part mentioned above was designed with the purpose of emulating statlock®, a widely recognized mechanism for securing catheters (Bishop *et al.*, 2007).

Furthermore, the investigation assessed various EVA membranes to regulate drug delivery and determined the most effective EVA membrane for integration into the ultimate Chemo Patch device. Hence, an *in vitro* drug release study was conducted to screen four distinct membrane group parameters, as illustrated in Table 4.2. Figure 4.11 demonstrates that each membrane variant exhibited moderate drug release. The augmentation of the thickness parameter enhanced the membrane's hydrophobicity, thereby decreasing the water absorption rate and permeation through the membranes. The reduced drug release rate was ascribed to the facilitated diffusion across the membrane. According to Liu et al., the membrane's thickness

impacted the release rates of nifedipine monolithic osmotic tablets. Specifically, the release rates decreased as the membrane thickness increased from 85 to 340 µm (Liu *et al.*, 2000). This finding was also supported by Nokhodchi et al. (Nokhodchi *et al.*, 2008). According to Figure 4.11, the drug release rate was higher in the 1mm membrane than in the 1.5mm and 2mm membranes. The graphical representation depicted a decline in the pace of drug release as the infill percentage rises from 50% to 75% to 100%. The phenomenon above can be ascribed to the formation of significant cavities and loosely packed spaces between consecutive layers resulting from the decrease in infill ratio, as indicated by the research conducted by Giri et al. (Giri *et al.*, 2020). The present study evaluated the effect of membrane porosity, including pore quantity and dimensions, on the drug release rate across the membranes. The results presented in Figure 4.11 demonstrated a significant correlation between porosity and the drug release rate. A positive correlation was observed between the quantity and dimensions of pores and the rate of drug release. According to Giri et al., the increased porosity of the membrane allowed for rapid penetration of the dissolution medium into the membrane's core, resulting in the rapid diffusion of the drug solution across the membrane (Giri *et al.*, 2020).

The assessment of the mechanical properties of implants is a critical factor in determining their ability to endure the compressive forces exerted by the adjacent bone and tissue following their insertion into the body (Cui *et al.*, 2021). Therefore, it was imperative to analyse two fundamental mechanical aspects of the Chemo Patch during this investigation. The initial step involved conducting a leakage test to verify the absence of any leakage from either the catheter aperture or the walls of the catheter import component. Moreover, leakage testing facilitated the determination of the solution's device capacity, as any leakage beyond the device's capacity was observed. The second variable under consideration was the tensile strength of the catheter tubing, which was crucial in ensuring that the catheter was not easily dislodged and possessed

the requisite level of attachment strength. The leakage testing results presented in figure 4.9 indicated that the quality of the 3D printing process was satisfactory, as there were no instances of leakage observed either from the walls or from the catheter import opening. According to Auhl et al., achieving successful 3D printing requires the presence of consistent printing behaviour, full layer strength, and a void-free and durable surface (Auhl *et al.*, 2019).

The efficacy of catheter securement plays a crucial role in achieving successful infusion therapy and preventing complications, as noted by Bishop et al. and Rutledge et al. (Bishop *et al.*, 2007; Rutledge *et al.*, 2015). The dislodgement of intravascular catheters, whether partial or total, remains a significant issue in hospital settings, despite implementing contemporary securement methods (Simonova *et al.*, 2012). Therefore, assessing the adhesive properties of the catheter tubing to the Chemo Patch in this investigation was imperative. The results of tensile tests were presented in a tabular format (4.1), indicating that the average force required to extract the catheter tubing from the Chemo Patch was 31.95 N. The findings suggest that the Chemo Patch and catheter tubing exhibited strong adhesion, reducing the likelihood of catheter tubing withdrawal unless a force greater than 31 N was exerted. Laura et al. conducted a comparative study to evaluate the catheter attachment strength of two investigational adhesive securement devices, two commercial securement solutions, and sutures using an *in vivo* animal model (Rutledge *et al.*, 2015). According to Rutledge et al., the results indicated that the mean peak axial pull forces of the two investigational devices were the highest (40-41 N) and were deemed superior to both sutures (28 N) and the securement dressing (17 N) while being like the securement device (37 N) (Rutledge *et al.*, 2015). The results indicated that the attachment force between the catheter and Chemo Patch (31.95 N) was consistent with previous literature, demonstrating the precise pore capabilities of 3D printing technology. This firm attachment has potential implications for the *in vivo* performance of the chemo patch.

The drug release profile of FOLFIRINOX from the Chemo Patch exhibited a biphasic pattern, characterised by an initial burst release on the first day, followed by a sustained drug release as presented in figure 4.12. Implementing burst release offers significant advantages in promoting the effective removal of tumour cells at the resection margins. In addition, Tan et al. have reported that burst release is productive as it allows for prompt administration of the appropriate dosage to the patient after implantation (Tan *et al.*, 2003). Furthermore, pharmaceutical formulations can be designed to exhibit an active burst-release mode, characterised by high drug concentrations at the initial stage, followed by a sustained release at levels adequate for a desired duration. This approach can help maintain therapeutic efficacy while minimising complications, as reported in studies by Yang et al. and Nguyen et al. (Yang *et al.*, 2016; Nguyen *et al.*, 2023). The Chemo Patch device is expected to govern drug release through two distinct mechanisms: passive diffusion across the membrane and matrix erosion via the core sponge. Most drug release profiles observed *in vitro* for gelatine-based sponges loaded with medication displayed an initial burst release, followed by a sustained and gradual release. This indicated that the sponge within the Chemo Patch device acted as the regulator of drug release. The mechanism mentioned above has been reported a beneficial function in eliminating bacterial strains in the wound bed while protecting the wound from any potential microbial infiltration, as posited by Ndlovu et al. (Ndlovu *et al.*, 2021). Therefore, it is expected that a comparison can be made regarding this process, in which chemotherapy is utilised to eradicate any remaining malignant cells and continually protect the surgical margin from any future cancer recurrence and metastasis.

4.6 Conclusion

This investigation aimed to design a device capable of delivering the FOLFIRINOX therapy in a controlled and prolonged manner to address the resection margin of PC. The drug delivery device, commonly known as a Chemo Patch, resembles a patch in its physical appearance.

However, it is comprised of a sponge that has been infused through catheter with drug solution at its core. The fabrication of the device was carried out through the utilization of 3D printing technology. The device comprises two distinct components, namely a cover having the catheter imports and a base that facilitates the release of the membrane. A research investigation was carried out to evaluate the effectiveness of IRN release through 12 distinct membranes. The findings of the screening process suggested that the temporal drug release of EVA membranes produced through 3D printing can be modified through the manipulation of various variables, such as membrane thickness, infill percentage, and porosity. The latter encompasses a range of pores with differing sizes. The optimal membrane was determined to possess a thickness of 1mm, an infill of 75%, and an absence of pores. The analysis of the Chemo Patch device's characteristics indicated that there was no evidence of leakage. Additionally, the attachment of the catheter to the device was deemed satisfactory, and the device's geometry and size were found to be suitable for use with pig cadavers. Furthermore, the Chemo Patch solution capacity was 1.5ml with an optimal infusion rate of 0.1ml/sec. It was postulated that the sponge was responsible for the controlled release of FOLFIRINOX from the Chemo Patch. The observed phenomenon can be attributed to the biphasic drug release profile, characterized by an initial burst release on the first day, followed by a sustained release over 7 days. The phenomenon is frequently documented in scholarly literature as a distinctive attribute of drug release from gelatine sponges.

Chapter 5: The *in vivo* testing of the chemo patch: a local drug delivery device

5.1 Introduction

PC mortality has risen despite a general decline in cancer deaths. PC now ranks fourth in the United States and fifth in Europe among individual cancer organs in terms of mortality (Siegel, Miller and Jemal, 2015; Kruger *et al.*, 2016). Thus, unconventional approaches are required to rectify the current situation. After surgery for resectable PC, chemotherapy has shown to be more and more effective (Zhan *et al.*, 2017). However, surgery for PC is flawed as microscopic cancer is present at the surgical margin in most patients, correlating with both local recurrence and reduced survival (Bockhorn *et al.*, 2014; Zhan *et al.*, 2017). Most patients will experience recurrence after a potentially curative resection, and only up to 25% of patients who undergo a complete resection will survive for 5 years (Siegel, Miller and Jemal, 2015; Kamisawa *et al.*, 2016). Local recurrence after surgery affects around 80% of all patients with locally invasive tumour growth being the cause of death in 30% of patients (Groot *et al.*, 2017; Luu *et al.*, 2021).

To increase the chances of survival from this aggressive cancer, radical resection with a negative margin (R0 resection) must be performed (Yamamoto *et al.*, 2015; Zhan *et al.*, 2017). Moreover, the microenvironment of PC restricts the administration of anticancer medicines, particularly to cells distant from working blood arteries (Olive *et al.*, 2011; Byrne *et al.*, 2018). Furthermore, the hypovascularity of the tumour mass, which is a significant barrier to systemic distribution, enables high retention within the tumour mass in the case of local delivery by preventing drug leakage into the circulation. Thus, converting one of the most significant drawbacks of systemic delivery in PC to a strength for a localised strategy (Indolfi, Ligorio, David T. Ting, *et al.*, 2016).

Therefore, the idea of treating the surgical margin locally among patients undergoing pancreatoduodenectomy for ‘resectable’ PC is highly appealing and will address this area of unmet need as FOLFIRINOX could be administered to all patients, even those who usually

would not receive adjuvant chemotherapy. Further, the Pancreatic anastomosis is the most crucial and hardest phase in the rebuilding of the digestive tract after pancreatoduodenectomy (Yang *et al.*, 2019). Numerous debates have emphasised the reduction of problems, although the benefit of pancreatic anastomosis remains unknown (Loos *et al.*, 2018). The most common serious postoperative consequence is pancreatic fistula, which is typically caused by insufficient anastomosis (Yang *et al.*, 2019). Inflammation at the site of implantation following stenting or any other treatment is highly common, and premature administration of a chemotherapeutic agent may result in adverse effects by impeding healing (Indolfi, Ligorio, David T. Ting, *et al.*, 2016). To solve this issue, catheterization is also advocated in this research so that chemotherapy can be administered after the surgical site has completely healed. Moreover, Herdeg et al. and his colleagues, seeking a safer technique to treat restenosis, introduced the concept of intracoronary drug delivery through catheter in previous investigations. They value the capability of delivering the active material to the entire vessel wall locally. Furthermore, to avoid the so-called "edge effect" of drug-eluting stents, pharmacotherapy can also be utilised to cover the stent edges and neighbouring artery segments (Herdeg *et al.*, 2008). In addition, to mitigate the risk associated with the Chemo Patch for prospective industry partners and sponsors, it is imperative to demonstrate its efficacy and safety *in vivo* before implementation. A future collaborator expressed concern regarding the potential hazards of utilising a sponge in the vicinity of the anastomotic site due to the possibility of abscess formation and subsequent anastomotic breakdown, eventually resulting in the development of a high-grade fistula. Consequently, during the progression of the Chemo Patch device from animal model to clinical product, it is imperative to comprehend the biocompatibility and efficacy of the device. Specifically, the utilisation of rodents is prevalent in preclinical investigations. Nevertheless, it is anticipated that comparatively larger creatures, such as pigs or dogs, would exhibit a more remarkable resemblance to human physiology than

rodents (Beykan *et al.*, 2016, 2019). Therefore, this chapter evaluated the biocompatibility and implantability of the Chemo Patch in pigs. They are considered a superior model for human disease due to their physiological and anatomical similarities ((Hou, Du and Wu, 2022). As a result, it is frequently used as a promising animal model for translational study ((Patterson, Lei and Miller, 2008; Gonzalez, Moeser and Blikslager, 2015). Additionally, the biocompatibility of the Chemo Patch was evaluated by analysing its potential impact on the tissue at the implantation site. This analysis aimed to determine whether the Chemo Patch could hinder the healing of anastomosis and, consequently, contribute to the morbidity associated with pancreatic fistula resulting from the failed anastomosis (Tabatabei and Hashemi, 2015a). On the other hand, preclinical *in vivo* test models are crucial in assessing novel chemotherapeutic drugs and drug delivery technologies. Among these models, xenografts of human cancers in mice are essential (Caysa *et al.*, 2012). Therefore, this study also evaluated the efficacy of the Chemo Patch device compared to intravenous therapy using a patient-derived xenograft mouse model.

5.2 Material and methods

5.2.1 Materials

Chemo Patch, a Flexible, biodegradable, impermeable EVA patch with a collagen-based sponge and an EVA catheter port. The chemo patch was manufactured and supplied by our lab (University of Birmingham, Pharmacy school, Birmingham, UK). Gelfoam® sponge was purchased from AEGIS LIFESCIENCES PVT. LTD, Gujarat, India. Irinotecan hydrochloride, oxaliplatin, and fluorouracil were purchased from LGM Pharma (Memphis, USA). Leucovorin was purchased from Sigma Aldrich (Dorset, UK). The FOLFIRINOX was supplied as a solution containing the following concentrations: Leucovorin (1.08 mg/mL), Oxaliplatin (0.23 mg/mL), Irinotecan (0.486 mg/mL), and 5-fluorouracil (1.081 mg/mL). six females, Large white/ Landrace/ Hampshire crossbred pig (Sus scrofa domestica) each weighing 60 kilograms (Kg), Rollins Farm, St. Ives Road, Somersham, Huntingdon, Cambridgeshire.

5.2.2 Pig study

5.2.2.1 Study design

The pig study was performed by the surgeon Rupaly Pande from Queen Elizabeth hospital, hospital university Birmingham. The study was performed at the Griffin institute, London and the ethical approval number was 839758.

The study comprised of 6 animals. For each animal, at laparotomy, the pig had three anastomoses, representing the 3 test sites. At the first and second anastomoses, one Chemo Patch per anastomoses was sutured onto the bowel. The third anastomoses had no Chemo Patch device attached(control). For CP1-5, on study day 7, chemotherapy (FOLFIRINOX) was infused into the Chemo Patch at site 1(test) and sterile water was infused into site 2(control) through the infusion line tunnelled through the skin. For CP6, it could not be determined whether the Chemo Patch was still attached to the infusion line at the time of infusion. All animals were recovered for 14 days.

5.2.2.2 Procedures pre surgery

The general health of the animal was observed from prior to the surgery and findings were reported on animal record. The animal was weighed one day prior to surgery. Each step was the same in all animals unless stated otherwise.

5.2.2.3 Anaesthesia

Diazepam tablets (10 mg/10kg) and Acepromazine tablets (10 mg/10kg) (CP1-5) was administered orally in a piece of banana or diet approximately 30-60 minutes prior to other administrations. Pre-medication: Ketamine (5 mg/kg)/ Xylazine (1 mg/kg) was administered intramuscularly with standard operating procedure (SOP) (8:3:3). General anaesthesia was induced with oxygen over Isoflurane, delivered via a close-fitting face mask. Then, the animal was transferred to the appropriate operating theatre. The animal was intubated with a cuffed endotracheal tube. After intubation, anaesthesia was maintained using oxygen over isoflurane,

with respiration controlled via a ventilator (SOP 8:2:38). Oxygen saturation, pulse rate, oesophageal temperature, expired CO_2, and respiratory rate were measured and recorded.

5.2.2.4 Animal preparation for surgery

The outer aspect of one ear was marked with the animal ID using a tattoo (CP1-3) or marker pen (CP4-6). The analgesic Carprofen (4 mg/kg) was administered subcutaneously. The long-lasting antibiotic Betamox LA (1 mL/kg) was administered intramuscularly (CP1-3). A continuous intravenous drip of Hartmann's solution (Baxter) was delivered via the ear vein throughout the procedure and the volume recorded. The animal was clipped of hair from the abdomen and flank. The exposed skin was cleaned with Chlorhexidine and Povidone Iodine. The animal was covered with sterile drapes in such a way, to leave only the operative site exposed. All procedures were performed using aseptic technique from this point on.

5.2.2.5 Surgical procedure

The first day of surgery for each animal was considered to be study day 0. An incision was made into the peritoneal cavity at the midline position. The jejunum was located and exposed in sections. Any exposed tissue not being operated on was covered with moist swabs. 1% Lidocaine in 5 mL boluses (2 mL Lidocaine in 18 mL sterile water in total) were administrated intradermally left and right of the incision (CP2, CP3 & CP5). Three anastomoses were made in the jejunum at a 20 cm distance from one another. The anastomoses were sutured using 3.0 polydioxanone suture (PDS). 1% Lidocaine in 5 mL boluses (2 mL Lidocaine in 18 mL sterile water in total) were administrated intradermally left and right of the incision (CP6). Pressure tests were performed after each anastomosis to visually inspect signs of leakage. The test devices were sutured to the bowel using 3.0 PDS adjacent to two of the anastomoses as follows (the 3rd anastomosis did not receive a device):

- 1st anastomosis ("Site 1"): Chemo Patch (Test) with infusion tubing attached.
- 2nd anastomosis ("Site 2"): Chemo Patch (Control) with infusion tubing attached.

- 3rd anastomosis (“Site 3”): No Chemo Patch and no tubing.

The anastomosis sites were washed with saline. The infusion tubing was tunnelled through the subcutaneous and skin layers of the abdominal flank, emerging between the pelvis and ribs. Tubing was cut to an appropriate length and sutured in place with 2/0 Prolene. An infusion port was attached to the exterior end of each tube. The abdomen was washed with saline. The subcutaneous layers of the abdomen were sutured with 1.0 PDS. 10 mL of Bupivacaine (0.5%) was either injected into the parthenium (CP2), dropped onto the muscle layer (CP3), or given intramuscularly (CP4, CP5 and CP6) before closing. 1% Lidocaine in 5 mL boluses (2 mL Lidocaine in 18 mL sterile water in total) were administrated intradermally left and right of the incision (CP1 & CP4). The skin was closed with staples. Veterinary Wound Powder and Opsite were administered to the closed wound sites. The tubing was covered with a dressing (Tegaderm). The ear cannula was left in place to be used for post-surgery procedures (CP2, CP3, CP4, CP5 & CP6). The animal was allowed to recover and taken back to the animal accommodation area.

5.2.2.6 Treatment

For CP1-5, on study day 7, FOLFIRINOX was infused to the test item at site 1 and sterile water was infused to the test item at site 2 at an approximate rate of 0.1 mL/sec. Ports were wiped with Clinell wipes immediately before and after infusion. For CP6, as the device had detached from the tubing by study day 14 at post-mortem, it cannot be confirmed whether the chemotherapy or sterile water infused into the test item. Air was pumped into the tube to facilitate infusion and the ports were capped.

5.2.2.7 Histology

Tissue samples were placed into 10% neutral buffered formalin for a minimum of 48 hours. Tissue samples were orientated to show the implantation site (where the surface of the patch encountered the bowel) and the anastomoses. Three sections were cut across each of the

anastomotic sites. Tissue samples were processed by routine automated procedures and then embedded to paraffin wax (SOP 6:1:3 and 6:1:4). One 5-micron section from the tissue wax blocks was cut (SOP 6:1:6). These were stained with haematoxylin and eosin (H&E, SOP 6:1:7). A board-certified histopathologist performed the histopathological evaluation. Histological slides were evaluated to see if the implant or chemotherapy caused tissue damage. 57 tissue slides stained with H&E, including Transmural duodenal samples from six pigs (CP 1-6) submitted for histological assessment. The duodenal wall, including the surgical anastomosis site, was sampled sagittally. Inflammation and fibrosis are the two parameters that were measured.

5.2.2.8 Burst strength ex vivo evaluation

To assess intestinal anastomotic integrity, burst strength was used as a surrogate metric. The test was carried out on postmortem pigs, and the burst strength of each anastomosis was visually measured by physically pressurizing and palpating the anastomosis at each site. Burst strength was classified as positive (secretions or leakage noted at anastomosis under manual pressure) or negative (no secretions or leakage observed). Positive signifies there was a leak and the anastomosis failed, whereas negative means there was no leak, and the anastomosis was successful.

5.2.2.9 Statistical analysis

The Kruskall-Walli's test was utilized to perform statistical analysis on the semiquantitative histological findings. Dunn's post-hoc comparison test was then employed for post-hoc statistical testing. A statistically significant level was determined to be a P-value of <0.05.

5.2.3 Mice study

5.2.3.1 Xenograft mouse model

The mice study was performed by Prof Jen Jen Yeh, MD and Dr Gabriela Herrera, University of North Carolina, School of Medicine, Department of Pharmacology. The ethical approval number of the study was 1701757. One million mCherry expressing PDX cells were injected

subcutaneously into the flank of each NSG mouse with Matrigel. Tumours were measured twice weekly by caliper, and after they reached measurable size 9mm-1cm in diameter, mice were scheduled for biopsies and device implantation. As usual, tumors grew at slightly different rates, so the biopsies were divided into three batches, where the treatment groups were distributed evenly and assigned at random. The tumor was exciseded and reduced to a size of 4mmx4mm and placed back into the original pocket. Five mice were found to have tumours that had invaded part of the peritoneal wall. In those cases, it was dangerous to attempt to remove and reduce the tumour to the intended size, so the tumour was reduced to 7mmx5mm. Those five mice were distributed at random to each treatment group. One of the mice did not recover after the surgery so the total number of mice was 27. The wound clips were removed a week later once the incision had healed.

5.2.3.2 Monitoring measurements

There are three measurements that were taken as part of the monitoring process. Tumors were measured with a caliper on a biweekly basis. In addition to the fluorescence imaging, weekly measurements of the weight of the mice were taken.

5.2.3.3 Treatment

Pharmaceutical-grade chemotherapeutics were used in the study. These drugs are available in solution. Because of the concentration of the solutions and the device reservoir capacity, we established that the device treatment mice would receive 15% of the normal cumulative dose (15% of the standard amount received throughout the study). An additional systemic regimen group was added at the 15% standard dose to achieve a fair comparison between the different doses. The standard weekly dose for each regimen component is the following:100 mg/kg Leucovorin, 50 mg/kg 5-Fluorouracil, 5 mg/kg Oxaliplatin, and 50 mg/kg Irinotecan. The calculation of both 100% and 15% systemic doses are presented in table 5.2. Additionally, For

the mice on the device arms, the devices were prepared with the drugs immediately prior to implantation. The drugs were added to the device sponge in the concentrations shown in table 5.3 and given a couple minutes to fully be absorbed by the sponge before closing the cap. Mice undergoing systemic treatment were dosed approximately 3 hours after biopsy. To achieve a fair comparison between the different doses an additional systemic regimen group was added at the 15% standard dose. The groups were set up as shown in table 5.1.

Table 5. 1:The mice group set up including number per group, frequency of dosing, type and percentage

Type	Arm	Dose	Frequency	Mice
Systemic	drug	Standard dose	weekly	5
Systemic	drug	15% of standard	weekly	5
Systemic	vehicle	(placebo)	weekly	5
Device	drug	15% cummulative	once	8
Device	vehicle	(placebo)	once	5

Drug calculations for a 25g mouse are shown below:

Table 5. 2:The calculation of both systemic doses 100% (standard) and 15%.

Systemic Delivery (Standard)

Drug	Phamaceutical concentration	Systemic solution	Single dose (mg) 100%	Single dose (ul) 100%	Schedule	Total (mg) 100%	Total (ul) 100%
Leucovorin	50 powder	25 mg/ml	2.500	100	Weekly	10	400
5FU	50 mg/ml	12.5 mg/ml	1.250	100	Weekly	5	400
Irinotecan	20 mg/ml	10 mg/ml	1.250	125	Weekly	5	500
Oxaliplatin	5 mg/ml	1.25 mg/ml	0.125	100	Weekly	0.5	400
					Total:	***20.5***	***1700***

Systemic Delivery (15% of standard)

Drug	Phamaceutical concentration	Systemic solution	Single dose (mg) 15%	Single dose (ul) 15%	Schedule	Total (mg) 15%	Total (ul) 15%
Leucovorin	50 powder	3 mg/ml	0.375	125	Weekly	1.5	500
5FU	50 mg/ml	1.5 mg/ml	0.188	125	Weekly	0.75	500
Irinotecan	20 mg/ml	1.5 mg/ml	0.188	125	Weekly	0.75	500
Oxaliplatin	5 mg/ml	0.15 mg/ml	0.019	125	Weekly	0.075	500
					Total:	***3.075***	***2000***

Table 5. 3: The dose calculation of the 15% FOLFIRINOX locally delivered by Chemo Patch.

Device directed delivery (15% of standard)

Drug	Phamaceutical concentration	Device solution		Single dose (mg) 15%	Single dose (ul) 15%	Schedule	Total (mg) 15%	Total (ul) 15%
Leucovorin	50 powder	100	mg/ml	0.375	3.75	Once	1.5	15
5FU	50 mg/ml	50	mg/ml	0.188	3.75	Once	0.75	15
Irinotecan	20 mg/ml	20	mg/ml	0.188	9.375	Once	0.75	37.5
Oxaliplatin	5 mg/ml	5	mg/ml	0.019	3.75	Once	0.075	15
						Total:	***3.075***	***82.5***

5.2.3.4 Tumor harvesting

The tumors were harvested at the 4-hour mark after the final therapeutic intervention. Subsequently, the obtained tumor was split into two portions, one for formalin fixation and the other for rapid freezing. Later, the tissues were processed according to established clinical histology procedures. The specimens were processed by embedding formalin-fixed tissues in paraffin and subsequently sectioned to a thickness of 5µm. The resulting sections were then affixed to glass slides and subjected to staining with H&E for histopathological examination.

5.2.3.5 Statistical analysis

Fluorescence signals in tumor and normal tissue was compared using the Mann-Whitney test. A P-value of <0.05 was considered statistically significant.

5.3 Results

5.3.1 Pig study

5.3.1.1 Histopathology

The tabulated data in Table 5.4 summarises the semiquantitative scoring outcomes of the sections categorized by animal and by data set on table 5.5. The scores for any semiquantitative parameter are allocated as follows: 0=absent (0%); 1= minimal (0-1%); 2=mild (1-5%); 3=moderate (5-20%); 4=severe (>20%).

Each of the sections was found to have varying degrees of inflammation and fibrosis (i.e., mature fibrosis), and the majority also showed evidence of superimposed fibroplasia (i.e., ongoing fibrosis). These sores always appeared in the serosa and were linked to a mild to moderate

eosinophilic enteritis. Sections where there was no other inflammatory infiltration type typically contained foreign body granulomas in the serosa, which accounted for consistent low inflammatory scores across the sample set. As a qualitative variable, further inflammatory infiltrates were documented. Individual variability in semiquantitative scores was collected for all factors evaluated in accordance with individual variability across all groups. In this regard, it is essential to note that the presentation of site 1 in animal 1 is atypical among the sample set, as necrosis of the inner aspect of the serosal pocket and intralesional bacterial cocci were observed. This is consistent with an infection at the surgical site in question.

Regarding semiquantitative overall differences between groups, there were significant differences in fibrosis scores (figure 5.1). In a post-hoc test the significant differences were noted between site 3 (control) and site 1 (test). However, there were no significant differences between groups for inflammation and fibroplasia scores.

Table 5.4: Summary statistics of semi-quantitative histological scores by animal; Avg: Average; SD: standard deviation.

	Inflammation					
	Site 1		**Site 2**		**Site 3**	
Animal	**Avg**	**SD**	**Avg**	**SD**	**Avg**	**SD**
1	2.0	1.0	1.3	1.2	2.3	0.6
2	2.0	0.0	1.7	0.6	1.3	1.2
3	2.3	1.2	2.7	1.2	1.7	1.2
4	3.3	0.6	3.0	1.0	2.3	1.2
5	4.0	0.0	3.0	1.0	3.0	0.0
6	2.3	1.2	3.3	0.6	3.0	0.0

	Fibrosis					
	Site 1		**Site 2**		**Site 3**	
Animal	**Avg**	**SD**	**Avg**	**SD**	**Avg**	**SD**
1	3.7	0.6	3.3	0.6	3.3	0.6
2	3.3	0.6	3.3	0.6	2.7	0.6
3	2.7	1.5	2.7	1.2	1.3	1.5
4	3.7	0.6	2.7	2.3	1.0	0.0
5	4.0	0.0	3.0	1.0	3.0	0.0
6	3.3	0.6	3.3	0.6	1.3	0.6

	Fibroplasia					
	Site 1		**Site 2**		**Site 3**	
Animal	**Avg**	**SD**	**Avg**	**SD**	**Avg**	**SD**
1	0.0	0.0	0.0	0.0	1.3	1.2
2	0.3	0.6	1.0	1.0	2.3	0.6
3	1.7	0.6	0.7	1.2	1.7	1.2
4	2.3	0.6	2.3	0.6	2.7	0.6
5	2.7	0.6	2.3	1.2	1.3	1.2
6	1.7	0.6	2.0	0.0	1.7	1.2

Table 5.5: Summary of semiquantitative analysis by dataset; Avg: average, SD: standard deviation

Lesion Type	Site 1		Site 2		Site 3	
	Avg	**SD**	**Avg**	**SD**	**Avg**	**SD**
Inflammation	2.7	0.8	2.5	0.8	2.3	0.7
Fibrosis	3.4	0.5	3.1	0.3	2.1	1.0
Fibroplasia	1.4	1.1	1.4	1.0	1.8	0.5

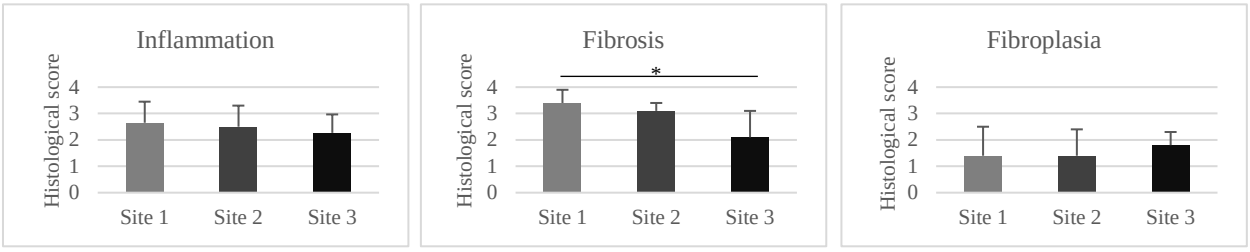

Figure 5.1: Summary of semiquantitative histological findings for the three anastomosis sites. Data presented as mean ± standard deviation. An asterisk in the title indicates p<0.05 in Kruskall Wallis test (i.e., there are statistically significant differences between the groups).

5.3.1.2 Burst strength ex vivo:

Table 5.6 represented the burst strength values obtained from various anastomosis sites. The findings indicated no leakage for CP4, CP5, and CP6, thus suggesting that the anastomosis was successful. No instances of leakage were reported from Site 1 (Test) or Site 3 (control) for CP1. Furthermore, the observation of leakage for site 2 (placebo) was challenging owing to the site's reddish appearance. The results of the CP3 assessment indicated that sites 1 and 2 exhibited no evidence of leakage, while site 3 presented challenges in terms of inspection. The absence of data for CP2 can be attributed to uncertainty regarding the proper attachment of the Chemo Patch device.

Table 5. 6: The burst strength observations from the three anastomosis sites for each animal

Animal ID	Burst strength		
	Site1 (ChemoPatch & Chemotherapy)	Site 2 (ChemoPatch & Sterile water)	Site 3 (No ChemoPatch or Infusion)
CP1	Negative	Could not inspect leakage. Site was more red than other two sites	Negative
CP2	N/A	N/A	N/A
CP3	Negative	Negative	Could not inspect leakage.
CP4	Negative	Negative	Negative
CP5	Negative	Negative	Negative
CP6	Negative	Negative	Negative

5.3.2 Mice study

The *in vivo* efficacy was investigated by comparing the tumour burden in mice administered an intravenous injection of FOLFIRINOX with 100% and 15% doses to those administered a 15% dose via a local delivery device (Chemo Patch). Furthermore, the study incorporated two placebo groups as means of controls. The first group received local saline delivery through Chemo Patch device, while the second group received systemic saline delivery. During treatment, tumour burden was evaluated by fluorescence imaging and ex vivo pancreatic tumour volume measurements as shown in figures 5.2, 5.3 and 5.4.

The results in Figure 5.4 demonstrate the fluorescence imaging obtained for the three FOLFIRINOX treated groups, indicating a decrease in fluorescence intensity over time. The values of the tumour growth from figure 5.4 were illustrated in figure 5.2 to facilitate visualization. Furthermore, Figure 5.2 depicted the log change in tumour volume of PC xenografts relative to the tumour volume on day 0 (the day of FOLFIRINOX administration) for the three FOLFIRINOX treated groups. All the FOLFIRINOX treated arms resulted in noticeably reduced tumours at each of the analysed time points, beginning in the day 8 following administration and continuing through day 28, when the trial was terminated. Also, the results revealed that Chemo Patch (the device with a 15% dose) suppressed tumour growth more effectively than the other two groups (FOLFIRINOX-100%-systemic and FLOFIRINOX-15%-systemic).

Conversely, it can be observed from Figure 5.3 and 5.5 that the groups administered with placebos exhibited a rise in the growth of tumours. The tumour growth values from figure 5.3 were shown in figure 5.5 to enhance clarity in visualisation. Furthermore, the statistical analysis conducted on the FOLFIRINOX group on day 28 indicated a significant difference between the Chemo Patch, the 15% and 100% systemic dose, with a p-value of 0.04 as presented in figure 5.6. Furthermore, the statistical analysis conducted on the device group comprising the

Chemo patch with 15% FOLFIRINOX and Chemo Patch with saline revealed a visual comparison in tumour growth inhibition, as illustrated in Figure 5.7. However, this difference did not attain statistical significance (P-value 0.49).

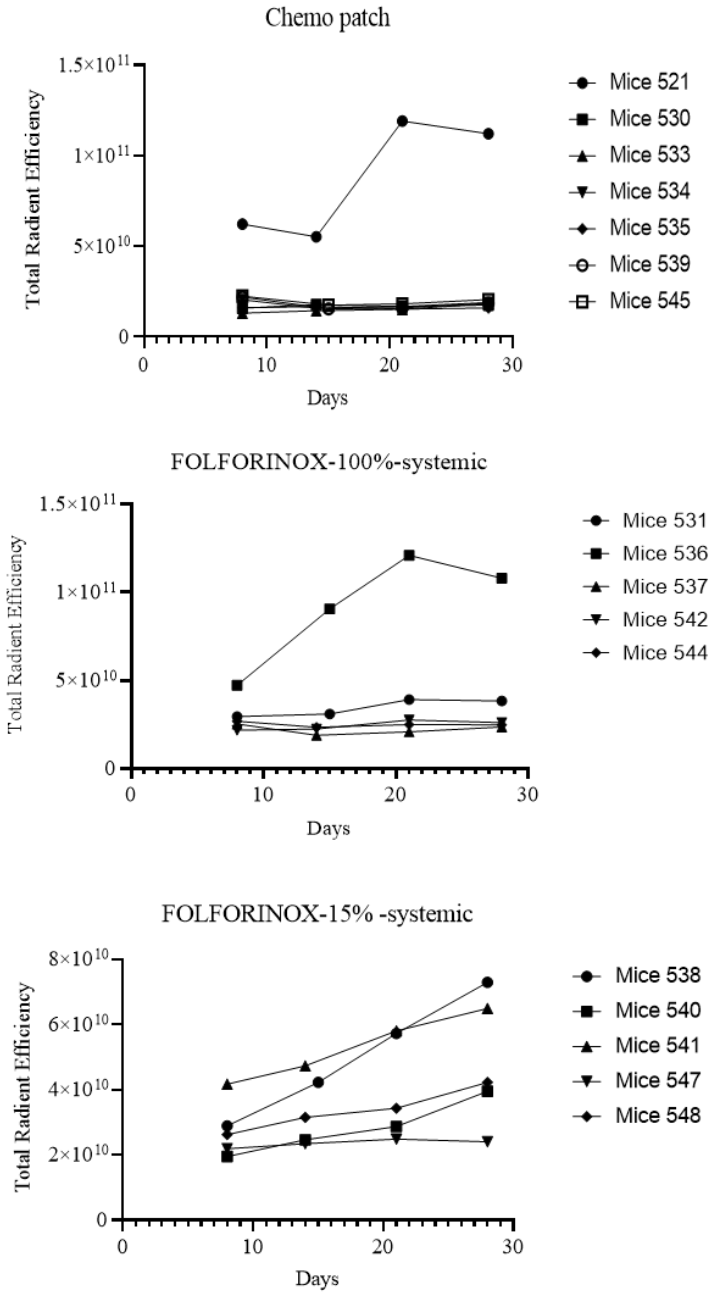

Figure 5.2: Profile plots on the natural log scale (per-mouse intraperitoneal tumour area trajectories measured via fluorescence imaging) for all FOLFIRINOX treated groups (Chemo Patch (device FOLFORINOX 15%), FOLFIRINOX- 100% -systemic, and FOLFIRINOX - 15% -systemic.

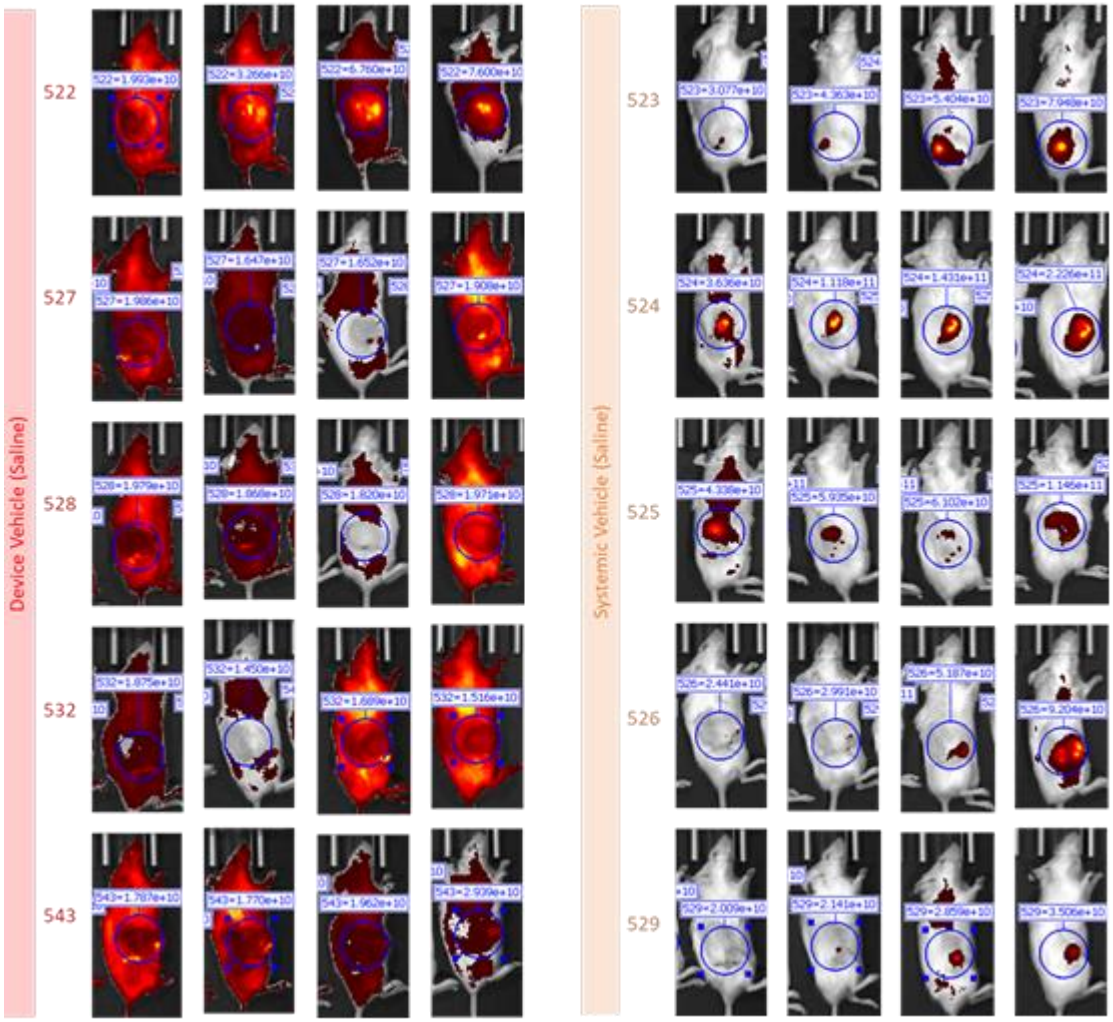

Figure 5.3: Whole-body dorsal fluorescence pictures of the placebo groups with subcutaneous tumours at various time points following the implantation of a Chemo Patch (left) with infusion of saline, and infusion of systemic saline(right). The red colour is the fluorescence, the circles are the tumour, and the values are the mice numbers.

Figure 5.4: Whole-body dorsal fluorescence pictures of nu/nu mice with subcutaneous tumours at various time points following the implantation of a Chemo Patch and infusion of the FOLFIRINOX regimen. The red colour is the fluorescence, the circles are the tumour, and the values are the mice numbers.

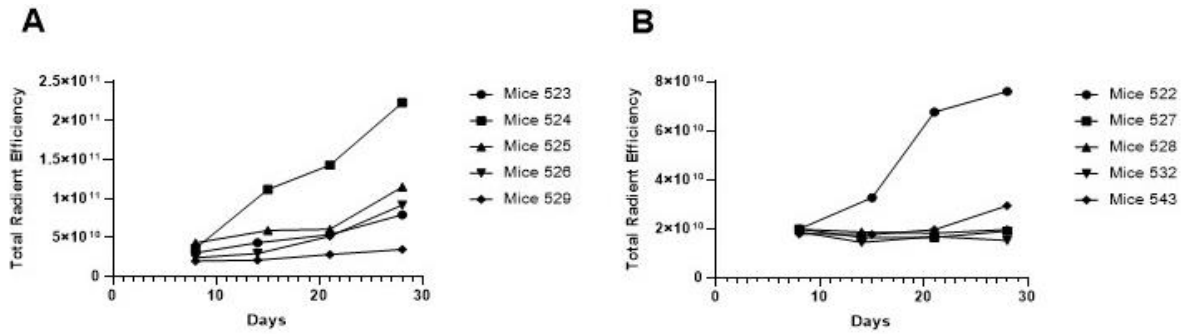

Figure 5.5: Profile plots on the natural log scale (per-mouse intraperitoneal tumour area trajectories measured via fluorescence imaging) for the placebo groups; A: systemic saline, B: Chemo Patch saline.

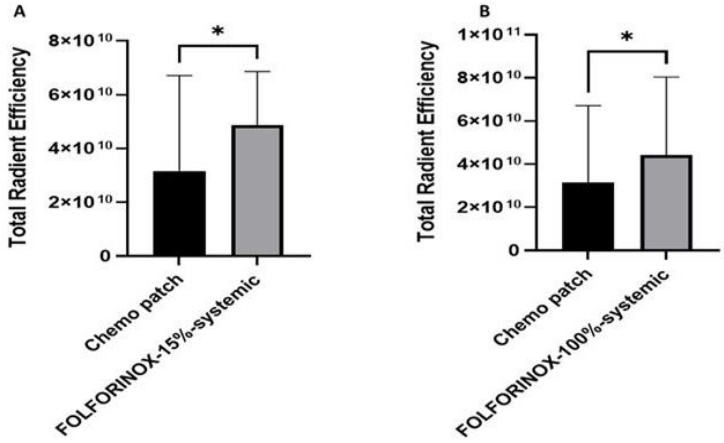

Figure 5.6: In vivo efficacy of Chemo Patch device. Tumour growth inhibition at day 28; A: Chemo Patch Vs FOLFIRINOX-15%-systemic, B: Chemo Patch Vs FOLFIRINOX-100%-systemic. Data presented as mean ± standard deviation. The test was Mann Whitney test with p value (0.048) for both comparisons.

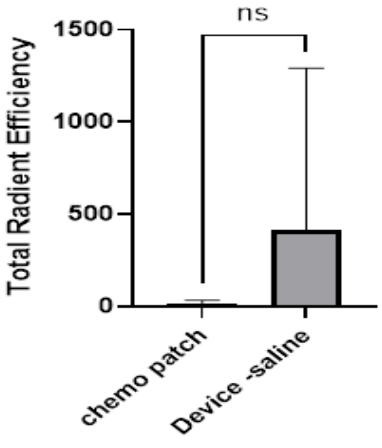

Figure 5. 7: A statistical comparison between the two-device group; Chemo patch with 15% FOLFIRINOX and Chemo Patch with saline. Data presented as mean ± standard deviation.

Figure 5.8 shows H&E-stained images of murine tissue from FOLFIRINOX-treated groups, corroborating the results of the pig study by demonstrating the presence of inflammatory infiltrates and fibrosis.

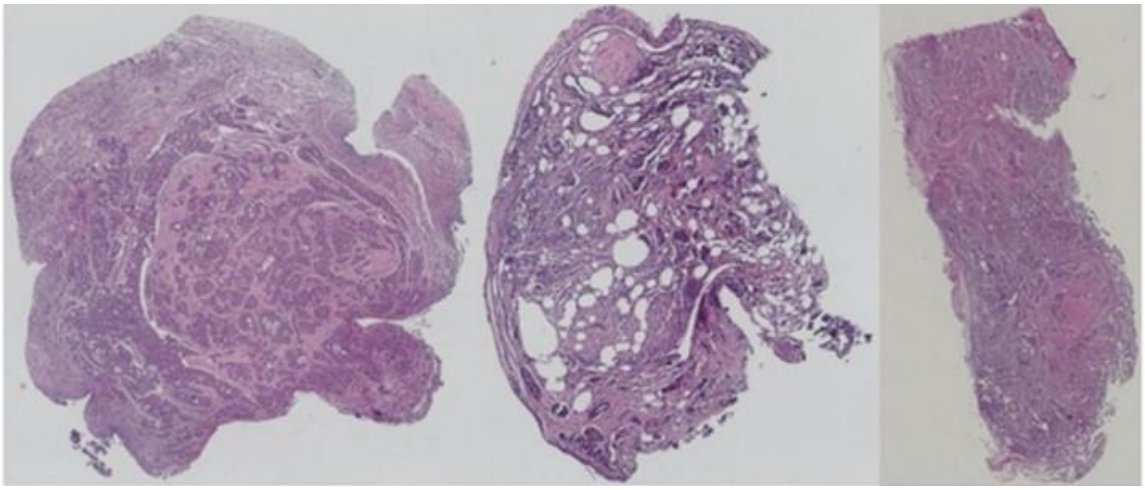

Figure 5. 8: Histology slides from the tumour tissue for the (from right to left) device plus 15% FOLFIRINOX, 100% systemic FOLFIRINOX and 15% systemic groups.

5.4 Discussion

5.4.1 Pig study

The standard treatment for PC and certain benign pancreatic diseases is surgical resection. However, pancreatic leakage and fistula development is currently the leading cause of morbidity and mortality following pancreatectomy (Shrikhande and D'Souza, 2008). The surgical procedure of pancreaticoduodenectomy comprises two distinct phases. The first phase involves resecting the pancreatic head, duodenum, gallbladder, distal bile duct, and proximal jejunum, with or without pylorus preservation. The second phase consists of the reconstruction phase, creating three anastomoses (Florentin *et al.*, 2022) . Furthermore, the procedure involves the creation of three anastomoses, namely the anastomosis connecting the pancreas and alimentary tract (known as pancreatic-jejunal or pancreaticogastrostomy anastomosis), the anastomosis connecting the biliary tract and the intestine, and the gastrojejunal or duodenojejunal anastomosis. The initial anastomosis type exhibits a higher probability of

anastomotic leakage, consequently linked to elevated morbidity and mortality rates (Veillette *et al.*, 2008; Tabatabei and Hashemi, 2015b). The conventional form of pancreatic anastomosis involves a dual-layered approach, utilizing an end-to-side connection between the pancreatic duct and the mucosa of the jejunum, Warren and Catell were the first to introduce this technique (Luu *et al.*, 2021). Therefore, it was necessary in this chapter to investigate the likelihood that the Chemo Patch could cause pancreatic-jejunal anastomosis leakage and pancreatic fistula. The possibility of the Chemo Patch triggering toxicity and an inflammatory reaction at the implantation site was also evaluated. Additionally, intestinal anastomoses are often tested for integrity with a burst strength test. Maximum intraluminal pressure (ILP) reached during inflation of the anastomosed intestinal segment prior to disruption is a reliable indicator of gastrointestinal healing failure (Norbury *et al.*, 2012).

Three anastomosis locations on each animal were examined for tissue toxicity and burst strength. This was done to compare the Chemo Patch group to the placebo groups regarding anastomosis leak growth and tissue biocompatibility. Throughout the study period, it was observed that no humane endpoints were attained for any of the animals. Furthermore, all the animals survived without significant complications or weight loss. The post-mortem analysis findings revealed that, except for one animal (16.6%), the external wounds had an absence of redness and exudation. The results of the semiquantitative analysis indicated the presence of three distinct lesions, namely fibrosis, inflammation, and fibroplasia. Fibrosis is frequently described as an uncontrolled wound-healing response (Wynn, 2007). The condition of fibrosis is characterised by the excessive accumulation of extracellular matrix components, mainly collagen, resulting in various tissues' overgrowth, hardening, and scarring (Dees, Chakraborty and Distler, 2021). The study revealed a higher incidence of fibrosis at site one (test) as presented in table 5.4, where Chemo Patches and FOLFIRINOX were administered. Moreover, as depicted in Figure 5.4, a post-hoc comparison test was conducted for the semiquantitative

analysis of the groups, revealing a statistically significant difference in fibrosis levels. Specifically, the fibrosis levels were higher for site 1 (test) compared to site 3 (control), while no significant difference was observed between site two and the other groups. Importantly, however, examination of table 5.4 and figure 5.4 suggests that despite a lack of statistically significant results, fibrosis is also comparatively higher in site 2 than in site 3. Furthermore, empty cavities lined by fibrosis and inflammation or bands of serosal inflammation were noted in 83.3% of animals at site 1 (Chemo Patch + chemotherapy) and in 66.6% of animals at site 2 (Chemo Patch + saline), but not in any animal at site 3 (no treatment).

Nevertheless, the augmentation of fibrosis linked to this location (site 1) does not indicate an adverse outcome. Because, according to Parra-Membrives et al.'s findings, weakened wound healing can be attributed to reduced fibrosis formation or collagen synthesis following selective devascularization, as indicated by histologic examination (Parra-Membrives *et al.*, 2007). Additionally, PC is characterised by highly dense stroma tissue, while fibrosis is typically induced by chemotherapy (Thomas and Radhakrishnan, 2019). Moreover, Chun et al. who employed a new method to examine the fibrotic regions in PC tissues of patients receiving neoadjuvant therapy, discovered that an elevated level of fibrosis was associated with a good prognosis (Matsuda *et al.*, 2019). Additionally, PSC, also known as myofibroblast-like cells, are stimulated by cancer cells to generate fibrosis in the vicinity of the tumour (Vonlaufen *et al.*, 2008; Ho, Jaffee and Zheng, 2020). Furthermore, the Chemo Patch is an additional factor contributing to inflammation and fibrosis. Moreover, several approved EVA-based implants, including the contraceptive implant (Nexplanon), have been linked to reports of foreign body reactions. For example, a study on 4373 Nexplanon removals conducted revealed that the implant was encased in fibrotic tissue and that some patients had late-onset antibiotic resistance at the implantation site (Chaudhry, 2013; Serati *et al.*, 2015; Fayzullin, Bakulina, *et al.*, 2021). Additionally, Previous animal studies have shown that the injection of Gelfoam® leads to

the developing of a foreign body reaction within the vessel wall, with the highest reaction occurring at the 20-day mark (Barth, Strandberg and White, 1977; Kumar *et al.*, 2013). However, the cellular response becomes absent within 45 days (Laurent, 2007; Kumar *et al.*, 2013). Recently, various studies have shown that the mechanisms involved in wound healing and tumour fibrosis exhibit significant similarities (Piersma, Hayward and Weaver, 2020; Huang, Iovanna and Santofimia-Castaño, 2021). Thus, it can be deduced that the wound-healing process contributes to heightened fibrosis, which is a favourable outcome rather than an unfavourable one.

Generally, the implantable drug delivery systems have been observed to elicit a localised immune response commonly referred to as the foreign body reaction (Coleman, King and Andrade, 1974; Kleiner, Wright and Wang, 2014; Fayzullin, Churbanov, *et al.*, 2021). According to the study design, the histological appearance of these samples is compatible with a surgical anastomosis site. This is evidenced by the presence of serosal fibrosis/fibroplasia and intralesional suture granulomas (foreign body granulomas) in all samples. The eosinophilic infiltration noted in all groups was likely secondary to surgery too. Nonetheless, eosinophilic infiltration may be secondary to the treatment of FOLFIRINOX. A clinical study revealed the presence of eosinophils in a 68-year-old female patient with PDAC who lacked an allergy or autoimmune illness. The abdomen computed tomography revealed a lump in the neck of the pancreas, and the fine needle aspiration biopsy confirmed the patient's adenocarcinoma. The patient was administered FOLFIRINOX, resulting in the eosinophilia's resolution (Manohar *et al.*, 2021). Eosinophilic enteritis was also reported in a 70-year-old lady treated with folinic acid, fluorouracil, and oxaliplatin (FOLFOX) for recurrent colon cancer with lung metastases. Colonoscopy and double-balloon small bowel enteroscopy revealed ileal stenosis; a subsequent biopsy indicated small bowel eosinophilic enteritis (Pearson and Mennel, 2013). In some samples, there were occasional fragments of vegetal material in the serosa with no

inflammation associated, which are interpreted as artefacts of the post-mortem sampling of these tissues. Site 1 of animal 1 displayed a high quantity of intralesional bacteria, consistent with surgical site infection. It has been noted that intra-abdominal contamination is common even in straightforward pancreatectomy and may increase the incidence of pancreatic fistula infection following surgery (Loos *et al.*, 2018). This presentation was exclusive to this location/animal, suggesting that these results may not be applicable to group comparisons. Additionally, this result did not impact the anastomosis as evidenced by the negative burst strength from this site. However, because these data did not reveal any surprising variations from the rest of the sample set other than the presence of bacteria in the lesion, they have been included in our study. Importantly, the inflammation and bacterial pocket observed did not involve the muscularis, submucosa, or mucosa, indicating that bacterial contamination may have resulted from a contaminated implant or chemotherapeutic agent, and not from an anastomosis failure, where extension from an unresolved mural cleft would have been expected.

In experimental settings, two mechanical parameters, namely bursting pressure and breaking strength, are commonly utilised to evaluate the strength of anastomosis. The bursting pressure metric indicates intestinal anastomosis's capacity to withstand heightened ILP. In contrast, the breaking strength metric is meaningful for the intestinal's ability to resist longitudinal forces (Hendriks and Mastboom, 1990; Durães *et al.*, 2013). However, Dueaes et al. conducted a correlation study between the bursting pressure and breaking strength. The study suggests that the bursting pressure test is the most appropriate method for evaluating the integrity of the anastomosis and the potential for leaks (Durães *et al.*, 2013). Furthermore, burst strength is a more suitable parameter for the phase of inflammatory healing (Ikeuchi *et al.*, 2000; Durães *et al.*, 2013). The study ascertained that the anastomosis displayed a negative burst strength of 83% for site 1 (test), as indicated in Table 5.2, in contrast to sites 2 and 3, which exhibited 66%

each. The residual proportion of 33% did not show an anastomotic failure but instead attributed to the inability to quantify the burst strength in certain specimens. Thus, it can be inferred that the anastomotic procedure was successful. This implies that the Chemo Patch did not exhibit any negative impact on the anastomosis.

5.4.2 Mice study

Murine models utilized in experiments have proven to be valuable resources in advancing and refining targeted therapies for PC (Mallya *et al.*, 2021). The present study aimed to assess the efficacy of administering FOLFIRINOX locally via the Chemo Patch in inhibiting tumour growth. This was accomplished through fluorescence imaging and *ex vivo* tumour measurement via calliper.

The fluorescence imaging of tumour growth monitoring in all treated FOLFIRINOX groups was illustrated in Figure 5.2, 5.3. The study findings indicated that the FOLFORINOX Chemo Patch device administered at a 15% dose exhibited the highest efficacy in inhibiting tumour growth among all treated groups. Subsequently, both systemic treated groups of FOLFORINOX at 100% and 15% also demonstrated some effectiveness. However, the superiority of the FOLFORINOX Chemo Patch device with a 15% dose is evident from this result. This finding was consistent with that of Zhan et al. , who have reported that the localized delivery of low-dose FOLFORINOX from a drug-eluting scaffold in an orthotopic murine model have shown efficacy (Zhan *et al.*, 2013). Furthermore, It is widely acknowledged that a limited fraction of the administered dose of an anticancer medication via intraperitoneal injection effectively reaches the intended cancerous cells (Cheng *et al.*, 2012; Wang, Langer and Farokhzad, 2012; Zhan *et al.*, 2013). Therefore, 15% FOLFIRINOX administered locally through Chemo Patch device was sufficient to supress the tumour growth. Furthermore, upon comparing the tumour growth pattern exhibited by the placebo group, as depicted in Figures 5.4 and 5.5 the findings provided additional evidence to substantiate the efficacy of the Chemo

Patch device with 15% FOLFIRINOX dose delivery. Notably, the minimal suppression of tumour growth observed in the placebo group further underscores the effectiveness of the Chemo Patch device. Additionally, the FOLFIRINOX cohort underwent a statistical examination on day 28, revealing a noteworthy difference among the Chemo Patch, the 15% and 100% systemic groups. This was supported by a p-value of 0.04, as illustrated in Figure 5.6. On the other hand, the statistical examination carried out on the cohort of devices consisting of the Chemo patch delivering 15% FOLFIRINOX and the Chemo Patch delivering saline demonstrated a visual contrast in the suppression of tumour growth, as depicted in Figure 5.7. Nevertheless, this disparity did not achieve statistical significance (p -value 0.49). Moreover, out of the 6 mice in the device group only 2 (33.3%) had tumour tissue present after 28 days, while in the 100% FOLFIRINOX group all 6 mice (100%) had tumour tissue present. Furthermore, one mouse died in the 100% FOLFIRINOX systemic arm from the treatment. This finding further supports the efficacy and safety of the 15% FOLFIRINOX administered through Chemo Patch.

Histology analysis of the tumour tissue from each treatment group (Figure 5.8) in the device plus 15% FOLFIRINOX demonstrated 20 to 30% stroma cells and approximately 40% fibrosis, while the 100% systemic FOLFIRINOX group showed between 40 and 80% stroma cells, 20 to 30% fibrosis, with up 90% necrosis. The histology of the 15% systemic FOLFIRINOX demonstrated a large amount of infiltrating stroma tissue, with approximately 10 to 20% fibrosis. PC is characterised by extremely dense stroma tissue, while the fibrosis is typically induced by chemotherapy. Therefore, the reduced stroma tissue and increased fibrosis in the device plus 15% FOLFIRINOX group compared to the 15% and 100% systemic FOLFIRINOX groups further demonstrates the improved efficacy of the localised delivery of low dose FOLFIRINOX, with more of the dose reaching the tumour tissue compared to systemic FOLFIRINOX.

5.5 Conclusion

To demonstrate the feasibility of administering the FOLFIRINOX regimen through catheterization in a localized manner, a 3D-printed apparatus was utilized and subjected to in vivo testing in this chapter. Furthermore, we successfully developed a platform technology that combines the benefits of porous materials and 3D printing, allowing the implantability to be precisely modified by modifying the geometry of the printed object. Therefore, it was essential to test the biocompatibility and safety in pigs as they are the best surgical model of human. Overall, these results indicate that in this experimental setting, the presence of the implant with no added chemotherapy treatment (site 2) is associated with more fibrosis than the no treatment control (site 1) at the anastomosing site, and that this fibrosis is even more prominent after administration of FOLFIRINOX through the implant (site 1). Also, this fibrosis is associated with serosal cavitation and an inflammatory response that is also absent from no treatment controls (site 3), and more frequent after chemotherapeutant treatment in animals with an implant man. The study findings suggested that using Chemo Patch for administering a lower local dose is more productive, resulting in decreased adverse effects compared to the systemic administration of 100% FOLFIRINOX. According to the efficacy data, the utilisation of low-dose (15%) local FOLFIRINOX exhibited greater effectiveness in comparison to low-dose (15%) systemic FOLFIRINOX while maintaining comparable efficacy to the standard dose (100%) systemic FOLFIRINOX. Thus, we contend that Chemo Patch holds promise in enhancing the survival rates of individuals who have PC.

Chapter 6: General discussion and future work

6.1 Discussion

The incidence of PC is rapidly increasing globally, and it is anticipated to become the second most prevalent cause of cancer-associated mortality by the year 2030 (Olajubutu *et al.*, 2023). Despite notable advancements in healthcare overall and in the domain of cancer treatment expressly, the positive effects of these progressions have been limited for individuals with PC (Edwards *et al.*, 2010; Poruk *et al.*, 2013). Furthermore, the difficulties linked to suboptimal clinical results in PC include rapid metastasis, elevated recurrence frequency, and inadequate reaction to current therapeutic modalities (Mallya *et al.*, 2021). Although surgical resection provides a distinct advantage in terms of survival and enhances the 5-year survival rate to 25%, a significant proportion of patients exhibit metastasised and locally advanced disease, which renders them ineligible for resection. Despite undergoing surgery to cure the disease, a significant proportion of patients (80%) will experience a relapse and ultimately succumb to the illness (Rahib *et al.*, 2014). This phenomenon can be attributed, at least in part, to the challenge of accurately visualizing surgical margins, the complexities involved in executing an extended resection due to the proximity of neighbouring blood vessels, particularly in the uncinate process, and sub microscopi metastatic disease (Nishino *et al.*, 2023) . Therefore, the majority of patients are administered with traditional chemotherapy. Although chemotherapy has been found to offer a survival advantage for both resectable and non-resectable forms of the disease, the benefits are limited due to the presence of drug resistance in nearly all patients (Sultana *et al.*, 2007; Principe *et al.*, 2021). Furthermore, the treatment paradigm for PC was altered by introducing FOLFIRINOX chemotherapy, consisting of fluorouracil, leucovorin, IRN, and oxaliplatin. This novel approach was initially presented at the 2010 American Society of Clinical Oncology conference (Conroy *et al.*, 2011; Choi, Razzaque and Kim, 2012). Subsequently, it emerged as the initial therapeutic approach for locally advanced and metastatic PC (Conroy *et al.*, 2011; Vary *et al.*, 2021). Notwithstanding its efficacy, this treatment

protocol elicits considerable toxicities, including haematological and gastrointestinal adverse effects and cumulative peripheral neuropathy primarily induced by oxaliplatin. As a result, the treatment is typically discontinued after a median of seven cycles (Vary *et al.*, 2021). Furthermore, the aggressive tumour biology of PC, characterized by significant local invasion and early metastasis, limits the number of patients eligible for resection to only 10-20%. The literature reports a considerable variation in the occurrence of a microscopically positive resection margin (R1) within this patient cohort, with rates ranging from less than 20% to greater than 80% (Fatima *et al.*, 2010; Rau *et al.*, 2012). On the other hand, implantable drug delivery platforms have demonstrated greater efficacy than conventional drug delivery systems. Local delivery of highly toxic drugs, such as chemotherapy, offers the advantage of maximum effectiveness and low toxicity. Several types of cancer, including brain and PC, exhibit a more significant response to chemotherapy when administered through local drug delivery. The former displays a formidable obstacle in the form of the blood-brain barrier, impeding drug delivery to the brain. At the same time, the latter is plagued by residual malignant cells at the resection margin, leading to recurrence. In addition, Byrne et al. have developed an implantable iontophoretic device as a potential solution to address the challenges associated with restricted drug transport into PC. This device has been designed to facilitate the targeted delivery of FOLFIRINOX directly to the tumours, which has shown promising results (Byrne *et al.*, 2018). Therefore, this research introduced a novel treatment concept for PC in which FOLFIRINOX regimen was delivered locally to the resection margin of PC. Moreover, this study aimed to create a drug delivery system that can be implanted to address the resection margin of PC. The pharmaceutical industry employs various technologies, including 3D printing, to produce implantable drug delivery systems. The conceptual basis of this project involved an integration of the benefits of porous systems, such as sponges, with the durability and resilience of 3D printing technology. Consequently, a novel Chemo Patch device

was developed, comprising two distinct 3D printed components: a catheter inlet component and a drug releasing membrane, the device contained also a Gelfoam® sponge that absorbs the drug solution within the device's core. The drug delivery system (Chemo Patch) utilized in our investigation was developed explicitly for the localized administration of FOLFIRINOX after surgical resection, targeting the margins of the tumour resection.

The initial experimental chapter of this study involved endeavours in fabricating a gelatine sponge possessing favourable mechanical characteristics for integration into the Chemo Patch device using freeze drying technique. Porous materials like sponges have garnered significant attention in drug delivery systems due to their distinctive features, including porosity, augmented surface area, and reduced density (Singhvi *et al.*, 2019; Zhang *et al.*, 2021). The incorporation of a sponge into the core of the Chemo Patch device was an appealing idea for two primary reasons: firstly, to regulate the release of FOLFIRINOX solution, and secondly, to prevent the burst release of the drug in the event of accidental device displacement. Furthermore, the study used Gelfoam® sponge, a commonly employed commercial sponge in drug delivery and implantation (Rohanizadeh, Swain and Mason, 2008), to deduce the optimal mechanical properties of the sponge. The primary mechanical properties evaluated encompassed hardness, elasticity, swelling ratio, and porosity in dry and hydrated conditions. Gelatine was selected as the polymer of choice due to its biocompatible properties. However, it was observed that the gelatine sponge exhibited rapid *in vivo* degradation (Cortesi, Nastruzzi and Davis, 1998; Ulubayram *et al.*, 2002). Therefore, to improve the mechanical properties of the gelatine sponge, two approaches were implemented due to the inherent limitations of the gelatine mechanical characteristics. The two approaches under consideration were crosslinking and blending. The investigation encompassed an examination of various concentrations of gelatine (1%, 4%, 7%, and 10%) and sodium alginate (1% and 4%) in conjunction with gelatine concentrations (4%, 7%, and

10%). Consequently, the 4% sodium alginate and 4% gelatine composite were crosslinked with glutaraldehyde (0.1%, 0.5%, and 1%) to achieve comparable mechanical properties to the Gelfoam® sponge. Moreover, the gelatine sponge can be characterized as a freeze-dried derivative of gelatine hydrogel. Consequently, it is imperative to initiate the preparation of the gel (Haiyan *et al.*, 2017). As a result, it was crucial to analyse the precursor hydrogels to investigate the impact of the gel's properties on the mechanical properties of the sponges. Therefore, the effect of gelatine concentration and blending with sodium alginate on the rheological properties of the precursor hydrogels were studied. The results indicated that an increase in gelatine concentration was associated with high moduli, decreased LVER, and reduced yield strain. Additionally, the samples can withstand lower stress levels before undergoing deconstruction behaviour at higher stresses. The results showed a prevalence of the storage modulus G' over the loss modulus G" as the gelatine content increased, implying a more pronounced hydrogel performance. Similarly, a positive correlation has been observed between the concentration of sodium alginate and the moduli, with a simultaneous increase in the LVER. This suggested that the storage modulus G$^{'}$ dominates over the loss modulus G" as the concentration of sodium alginate increases, indicating a more robust hydrogel behaviour.

The mechanical properties of the Gelfoam® sponge were initially assessed to determine the optimal values required for our sponge. The dry Gelfoam® sponge exhibited a hardness of 2703.18 g±35.0, whereas the hydrated sponge displayed a hardness of 869.81 g±117.7. The Gelfoam® sponge in its dry state showed an elasticity ratio of 78.71%±1.9, while in its hydrated form, the sponge demonstrated a value of 12.14%±1.7. The findings indicated that an increase in gelatine concentration leads to an increase in the hardness of the sponges for both dry and hydrated states. Specifically, the sponges with 1% and 2% gelatine concentration exhibited low hardness compared to the Gelfoam® sponge, whereas those with 4% and 10% gelatine concentration demonstrated superior hardness relative to the Gelfoam® sponge.

Conversely, a rise in the gelatine concentration leads to a reduction in the elasticity of the prepared sponges, with 1% being greater than Gelfoam® and 4% being less than Gelfoam®. Additionally, the augmentation of gelatine concentration results in a reduction in both porosity and swelling ratio. Moreover, Elevated concentrations of polymer blends (gelatine and sodium alginate) resulted in heightened hardness levels and reduced elasticity in dry and hydrated sponge specimens. The porosity and swelling ratio exhibited a negative correlation with the concentration of the blend, whereby an increase in the latter results in a decrease in the former. Furthermore, increase concentrations of glutaraldehyde resulted in increased levels of hardness and elasticity in both dry and hydrated sponge specimens. Likewise, the increase of glutaraldehyde concentration resulted in a reduction of porosity and swelling ratio.

We successfully created a gelatine-sodium alginate composite sponge crosslinked with glutaraldehyde (4% gelatine, 4% sodium alginate, 0.5% glutaraldehyde) to enhance its properties, particularly mechanical strength and degradation resistance, without altering other physicochemical properties. The physicochemical properties of the novel gelatine sponges cross-linked with glutaraldehyde support their suitability for use as part of the Chemo Patch device, where they must be biocompatible, biodegradable, haemostatic, and stable. In chapter 3 of this research, the gelatine sponge was characterised for microstructural, drug distribution, FTIR spectral analysis, thermal properties and hydrolysis degradation in comparison to Gelfoam® control sponge as well as the *in vitro* drug release of IRN from FOLFIRINOX regimen. The results revealed that a diverse pore structure in SEM for both sponges with an average pore size of 100µm , this diversity of the porous structure is attributed to the variation in heat transmission during freezing of hydrogels (Van Luyn *et al.*, 1991; Kabiri *et al.*, 2010). Additionally, the prominent microstructure was mainly membrane like (for gelatine) and fibrous like (for alginate), which was in agreement with the literature (Choi *et al.*, 1999). The spatial distribution of IRN through Raman mapping revealed a homogenous distribution

throughout both sponges' matrices. Furthermore, the crosslinking of the gelatine sponge was confirmed by FTIR analysis, it showed a shifted peak for the Amide I from 1648.44 cm^{-1} to 1655.68 $cm^{-1,}$ indicating the partial formation of imine functional groups and successful crosslinking of the composite sponge by glutaraldehyde. The DSC analysis revealed that the gelatine sponge exhibited a glass transition temperature of 125.24°C, surpassing that of Gelfoam® one, measured at 110°C. This finding supports the FTIR results for crosslinking , because it has been previously indicated that an increase in glass transition temperature indicates restricted polymer chain mobility resulting from cross-linking (Chang *et al.*, 2020). In addition, the hydrolysis study showed that the gelatine sponge was stable for up to 6 weeks, which is comparable to the reported stability of Gelfoam® *in vivo* (4-6 weeks) as presented in the literature (Holste *et al.*, 2022; Irfan *et al.*, 2022). The drug release profile of IRN from the gelatine sponge demonstrated a biphasic pattern extending for seven hours. Furthermore, the validation of the IRN method was validated through an evaluation of its linearity, range, accuracy, LOD, and LOQ.

In chapter four of this research the process of manufacturing the Chemo Patch involved the initial digital design using Tinker CAD software then followed by 3D printing using FDM printer. the Chemo Patch was printed using EVA 18.2 which is a well-documented polymer used for implants manufacturing. The melt viscosity of EVA 18.2 polymer was determined as preliminary step to determine the processing temperature of 3D printing. The results of melt rheology revealed that the printing temperature would fill in the range of 84°C to 132°C, which was later confirmed to be 110°C. The initial step involved a feasibility study in which trying two different designs a squared and an oblong one. The square-shaped device measured 4cm by 4cm and the elongated device with dimensions of 15mm by 30 mm which was the device that conformed to the surgical margin of the cadaver pig, it was found to be by the desired geometry and size. Furthermore, twelve 3D-printed membranes with different thicknesses,

infill, pore numbers, and sizes were printed. After characterizing each membrane, the best was chosen (1 mm thickness and 75% infill) and then the final Chemo Patch design was created. Print speed was 15 mm/s, print temperature 110 °C, and build plate 55 °C. The Chemo Patch was printed with zig zag infill, 120mm/sec travel speed, 35% flow rate, and 0.15mm layer height. Furthermore, the physical characterisation of Chemo Patch device included leakage testing, tensile strength of the catheter tubing, as well as *in vitro* drug release of FOLFIRINOX. the results revealed that from leakage test, the maximum capacity of the device was 1.5ml with a recommended flow rate of 0.1ml/sec. Additionally, the average tensile strength of the catheter tubing was 31.951 N, which demonstrated good attachment strength as reported by previous literature (Rutledge *et al.*, 2015). The Chemo Patch's drug release profile of FOLFIRINOX displayed a biphasic pattern, featuring an initial burst release during the first day, succeeded by a continuous drug release over seven days.

The Chemo Patch has been developed with a focus on end-user engagement and possesses a malleable structure and dimensions that enable detailed stitching into position. Consequently, the implantation process of the device has been simplified. The device does not elicit any toxicological concerns or escalate the likelihood of fistula formation in pig model. The administration of a low dose (15%) of FOLFIRINOX via local delivery does not result in any toxicity concerns or elevate the likelihood of a fistula. Furthermore, the data on efficacy indicated that the administration of low dose (15%) FOLFIRINOX locally is superior in effectiveness to low dose (15%) FOLFIRINOX systemically while being equally as effective as the standard dose (100%) of systemic FOLFIRINOX. Our results on animal models have indicated that the Chemo Patch effectively produced anti-tumour effects in orthotopic mouse models of PC, as evidenced by fluorescence imaging and tumour volume measurements. Nonetheless, the biocompatibility study in pigs revealed the implantation of Chemo Patch did not elicit any severe immunological response, however, fibrosis and some inflammations were

observed. The recruited fibroblasts in cancer are a fundamental component of granulation tissue that plays a crucial role in wound healing and chronic inflammation (Hanahan and Weinberg, 2011; Karagiannis *et al.*, 2012). PC is characterised by significant fibrosis at the primary tumour locations, a phenomenon referred to as desmoplasia (Ayala *et al.*, 2003; Ren *et al.*, 2018).

To conclude, the results of this study provide proof-of-concept that the combination of 3D printing, porous materials, and catheterization can effectively overcome intrinsic and extrinsic PC chemoresistance to deliver the highly toxic regimen FOLFIRINOX, thereby paving the way for novel strategies to treat patients with PC.

6.2 Future work

The forthcoming task involves accomplishing the scale-up of the manufacturing process and exploring the feasibility of utilizing injection moulding to produce Chemo patch. Additionally, it is necessary to evaluate the potential toxicity of crosslinking by conducting an *in vitro* cytotoxicity analysis of the gelatine sponge. Additional tests such as cell viability, proliferation, and *in vitro* wound-healing assays with gelatine sponges are required to establish their biocompatibility and wound-healing characteristics.

The enzymatic degradation test should be conducted to investigate the impact of the enzymatic environment of the pancreas on the degradation process of the sponge. To comprehensively assess the impact of device protection on the sponge, it is recommended to conduct experiments both with the sponge within and outside the device. This approach will provide a more thorough understanding of how the device's coverage influences the sponge's mechanical stability.

The next thesis will conduct a comprehensive examination of infections linked to indwelling catheters, spanning several types typically employed in healthcare facilities. The primary

objective of this study is to comprehensively comprehend the complex microbial dynamics associated with catheters, while also shedding light on the various risk factors, colonization patterns, and the fundamental mechanisms that contribute to infections. Particular emphasis will be placed on the progression of infections associated with catheters, including those affecting the abdomen and skin. The proposed research approach entails a methodical examination of preventative measures, with a particular focus on aseptic techniques employed during the insertion and maintenance of catheters. The primary objective is to acquire a thorough comprehension of catheter-associated infections, regardless of the particular kind of catheter, to inform behaviors based on evidence and enhancing patient safety in healthcare settings.

The good manufacturing practice will be essential to be implemented in the 3D printing process, particularly in ensuring that the 3D-printed implantable drug delivery device adheres to its intended specifications. This can be achieved by incorporating design controls, which involve documenting the design inputs, and outputs, as well as verification and validation activities. Additionally, a process validation strategy will be established for the 3D printing process to validate crucial phases and assure the maintenance of consistency and reliability. This process may entail the examination and experimentation of several 3D printing settings, including but not limited to temperature, speed, and layer thickness.

References

Abada, H. T. and Golzarian, J. (2007) 'Gelatine sponge particles: handling characteristics for endovascular use', *Techniques in vascular and interventional radiology*. Tech Vasc Interv Radiol, 10(4), pp. 257–260. doi: 10.1053/J.TVIR.2008.03.002.

Abd El-Aziz, M. F. *et al.* (2020) 'Alfuzosin hydrochloride-loaded low-density gastroretentive sponges: development, in vitro characterization and gastroretentive monitoring in healthy

volunteers via MRI', *Pharmaceutical Development and Technology*. Taylor & Francis, 25(5), pp. 566–578. doi: 10.1080/10837450.2020.1720235.

Abdelwahed, W. *et al.* (2006) 'Freeze-drying of nanoparticles: Formulation, process and storage considerations', *Advanced Drug Delivery Reviews*, 58(15), pp. 1688–1713. doi: 10.1016/j.addr.2006.09.017.

Abdul Khalil, H. P. S. *et al.* (2023) 'Biopolymers based aerogels: A review on revolutionary solutions for smart therapeutics delivery', *Progress in Materials Science*. Elsevier Ltd. doi: 10.1016/j.pmatsci.2022.101014.

Abeer, M. M., Mohd Amin, M. C. I. and Martin, C. (2014) 'A review of bacterial cellulose-based drug delivery systems: Their biochemistry, current approaches and future prospects', *Journal of Pharmacy and Pharmacology*. Blackwell Publishing Ltd, pp. 1047–1061. doi: 10.1111/jphp.12234.

Ahmady, A. and Abu Samah, N. H. (2021) 'A review: Gelatine as a bioadhesive material for medical and pharmaceutical applications', *International Journal of Pharmaceutics*. Elsevier B.V., 608(August), p. 121037. doi: 10.1016/j.ijpharm.2021.121037.

Ahn, J. M. and Oh, J. S. (2020) 'Gelfoam embolization technique to prevent bone cement leakage during percutaneous vertebroplasty: Comparative study of gelfoam only vs. gelfoam with venography', *Korean Journal of Neurotrauma*, 16(2), pp. 200–206. doi: 10.13004/KJNT.2020.16.E46.

Aitchison, G. . *et al.* (2009) 'A Review of the Design Process for Implantable Orthopedic Medical Devices', *The Open Biomedical Engineering Journal*, 3(1), pp. 21–27. doi: 10.2174/1874120700903010021.

Alagha, A., Nourallah, A. and Hariri, S. (2020) 'Characterization of dexamethasone loaded collagen-chitosan sponge and in vitro release study', *Journal of Drug Delivery Science and Technology*. Elsevier, 55(November 2019), p. 101449. doi: 10.1016/j.jddst.2019.101449.

Alam, A. U. *et al.* (2018) 'Polymers and organic materials-based pH sensors for healthcare applications', *Progress in Materials Science*. Elsevier Ltd, pp. 174–216. doi: 10.1016/j.pmatsci.2018.03.008.

Aldana, A. A. *et al.* (2021) 'Development of 3D bioprinted GelMA-alginate hydrogels with tunable mechanical properties', *Bioprinting*. Elsevier Ltd, 21(September 2020), p. e00105. doi: 10.1016/j.bprint.2020.e00105.

Alexakis, N. *et al.* (2004) 'Current standards of surgery for pancreatic cancer', pp. 1410–1427. doi: 10.1002/bjs.4794.

Ali, A. *et al.* (2020) 'Clinical situations for which 3D printing is considered an appropriate representation or extension of data contained in a medical imaging examination: adult cardiac conditions', *3D Printing in Medicine*. 3D Printing in Medicine, 6(1), pp. 1–7. doi: 10.1186/s41205-020-00078-1.

Anadioti, E., Kane, B. and Soulas, E. (2018) 'Current and Emerging Applications of 3D Printing in Restorative Dentistry', *Current Oral Health Reports*. IOP Publishing, 5(2), pp. 133–139. doi: 10.1007/s40496-018-0181-3.

Aquib, M. *et al.* (2020) 'Advances in local and systemic drug delivery systems for post-surgical cancer treatment', *J. Mater. Chem. B*, 8, p. 8507. doi: 10.1039/d0tb00987c.

Araujo, P. (2009) ‘Key aspects of analytical method validation and linearity evaluation’, *Journal of Chromatography B: Analytical Technologies in the Biomedical and Life Sciences*, 877(23), pp. 2224–2234. doi: 10.1016/j.jchromb.2008.09.030.

Arif, M. M. A. *et al.* (2020) ‘Fabrication of bio-based gelatin sponge for potential use as a functional acellular skin substitute’, *Polymers*, 12(11), pp. 1–19. doi: 10.3390/polym12112678.

Artinyan, A. *et al.* (2008) ‘The anatomic location of pancreatic cancer is a prognostic factor for survival’, *Hpb*. Elsevier Masson SAS, 10(5), pp. 371–376. doi: 10.1080/13651820802291233.

Ashour, A. A. *et al.* (2018) ‘Gelfoam haemostatic agent with or without autologous bone marrow-derived stem cells for the regeneration of critical-size mandibular defects in the rabbit’, *International Journal of Oral and Maxillofacial Surgery*. Churchill Livingstone, 47(11), pp. 1488–1494. doi: 10.1016/J.IJOM.2018.04.021.

Aslan, M. *et al.* (2018) ‘Targeted therapies for pancreatic cancer and hurdles ahead’, *Anticancer Research*, 38(12), pp. 6591–6606. doi: 10.21873/anticanres.13026.

Auhl, D. *et al.* (2019) ‘3D-printing quality in relation to melt flow and fusion behavior of polymer materials’, *AIP Conference Proceedings*, 2107(May). doi: 10.1063/1.5109498.

Ayala, G. *et al.* (2003) ‘Reactive Stroma as a Predictor of Biochemical-Free Recurrence in Prostate Cancer’, *Clinical Cancer Research*, 9(13), pp. 4792–4801.

Azad, M. A. *et al.* (2020) *Polymers for extrusion-based 3D printing of pharmaceuticals: A holistic materials–process perspective, Pharmaceutics*. doi: 10.3390/pharmaceutics12020124.

Azum, N. *et al.* (2021) ‘Aerogel applications and future aspects’, in *Advances in Aerogel Composites for Environmental Remediation*. Elsevier, pp. 357–367. doi: 10.1016/B978-0-12-820732-1.00019-9.

Bachmann, J. *et al.* (2006) ‘Pancreatic resection for pancreatic cancer’. doi: 10.1080/13651820600803981.

Badger, S. A. *et al.* (2010) ‘The role of surgery for pancreatic cancer: A 12-year review of patient outcome’, *Ulster Medical Journal*, 79(2), pp. 70–75.

Badowska-kozakiewicz, A. *et al.* (2023) ‘New Treatment Options in Metastatic Pancreatic Cancer’, pp. 1–18.

Baghani, Z. and Kadkhodazadeh, M. (2013) ‘Periodontal dressing: a review article’, *Journal of dental research, dental clinics, dental prospects*. J Dent Res Dent Clin Dent Prospects, 7(4), pp. 183–191. doi: 10.5681/JODDD.2013.040.

Barbosa, O. *et al.* (2014) ‘Glutaraldehyde in bio-catalysts design: A useful crosslinker and a versatile tool in enzyme immobilization’, *RSC Advances*, 4(4), pp. 1583–1600. doi: 10.1039/c3ra45991h.

Barros, A. *et al.* (2016) ‘Hybrid Alginate-Based Cryogels for Life Science Applications’, *Chemie-Ingenieur-Technik*, 88(11), pp. 1770–1778. doi: 10.1002/cite.201600096.

Barth, K. H., Strandberg, J. D. and White, R. I. (1977) ‘Long term follow-up of transcatheter embolization with autologous clot, oxycel and gelfoam in domestic swine’, *Investigative*

radiology. Invest Radiol, 12(3), pp. 273–280. doi: 10.1097/00004424-197705000-00012.

Baumann, P. *et al.* (2009) 'A randomized, controlled, prospective trial to evaluate the haemostatic effect of Lyostypt versus Surgicel in arterial bypass anastomosis: "COBBANA" trial', *Trials*, 10, p. 91. doi: 10.1186/1745-6215-10-91.

Bazeed, A. Y., Day, C. M. and Garg, S. (2022) 'Pancreatic Cancer: Challenges and Opportunities in Locoregional Therapies', *Cancers*, 14(17). doi: 10.3390/cancers14174257.

Beck, R. C. R. *et al.* (2017) '3D printed tablets loaded with polymeric nanocapsules: An innovative approach to produce customized drug delivery systems', *International Journal of Pharmaceutics*. Elsevier B.V., 528(1–2), pp. 268–279. doi: 10.1016/j.ijpharm.2017.05.074.

Becker, A. E. *et al.* (2014) 'Pancreatic ductal adenocarcinoma: Risk factors, screening, and early detection', *World Journal of Gastroenterology*, 20(32), pp. 11182–11198. doi: 10.3748/wjg.v20.i32.11182.

Bengtsson, A., Andersson, R. and Ansari, D. (2020) 'The actual 5-year survivors of pancreatic ductal adenocarcinoma based on real-world data', *Scientific Reports*. Nature Publishing Group UK, 10(1), pp. 1–9. doi: 10.1038/s41598-020-73525-y.

Bernell, S. and Howard, S. W. (2016) 'Use Your Words Carefully: What Is a Chronic Disease?', *Frontiers in Public Health*. Frontiers Media SA, 4, p. 159. doi: 10.3389/FPUBH.2016.00159.

Bertram, U. and Bodmeier, R. (2012) 'Effect of polymer molecular weight and of polymer blends on the properties of rapidly gelling nasal inserts', *Drug Development and Industrial Pharmacy*, 38(6), pp. 659–669. doi: 10.3109/03639045.2011.598536.

Beykan, S. *et al.* (2016) '177Lu-OPS201 targeting somatostatin receptors: in vivo biodistribution and dosimetry in a pig model', *EJNMMI Research*. EJNMMI Research, 6(1), pp. 1–9. doi: 10.1186/s13550-016-0204-9.

Beykan, S. *et al.* (2019) 'In vivo biokinetics of 177Lu-OPS201 in mice and pigs as a model for predicting human dosimetry', *Contrast Media and Molecular Imaging*, 2019, pp. 5–7. doi: 10.1155/2019/6438196.

Bhattarai, S. R. *et al.* (2004) 'Novel biodegradable electrospun membrane: Scaffold for tissue engineering', *Biomaterials*. Elsevier BV, 25(13), pp. 2595–2602. doi: 10.1016/j.biomaterials.2003.09.043.

Bishehsari, F. (2021) 'Organ-Chip Models : Opportunities for Precision Medicine in Pancreatic Cancer', pp. 1–14.

Bishop, L. *et al.* (2007) 'Guidelines on the insertion and management of central venous access devices in adults', *International Journal of Laboratory Hematology*, 29(4), pp. 261–278. doi: 10.1111/j.1751-553X.2007.00931.x.

Blaker, J. J., Knowles, J. C. and Day, R. M. (2008) 'Novel fabrication techniques to produce microspheres by thermally induced phase separation for tissue engineering and drug delivery', *Acta biomaterialia*. Acta Biomater, 4(2), pp. 264–272. doi: 10.1016/J.ACTBIO.2007.09.011.

Bockhorn, M. *et al.* (2014) 'Borderline resectable pancreatic cancer: a consensus statement by the International Study Group of Pancreatic Surgery (ISGPS)', *Surgery*. Surgery, 155(6), pp. 977–988. doi: 10.1016/J.SURG.2014.02.001.

Brem, H. *et al.* (1995) ‘Placebo-controlled trial of safety and efficacy of intraoperative controlled delivery by biodegradable polymers of chemotherapy for recurrent gliomas’, *The Lancet*, 345(8956), pp. 1008–1012. doi: 10.1016/S0140-6736(95)90755-6.

Brennan, M. F., Moccia, R. D. and Klimstra, D. (1996) ‘Management of adenocarcinoma of the body and tail of the pancreas’, *Annals of Surgery*, 223(5), pp. 506–512. doi: 10.1097/00000658-199605000-00006.

Budyanto, L., Goh, Y. Q. and Ooi, C. P. (2009) ‘Fabrication of porous poly(L-lactide) (PLLA) scaffolds for tissue engineering using liquid-liquid phase separation and freeze extraction’, *Journal of materials science. Materials in medicine*. J Mater Sci Mater Med, 20(1), pp. 105–111. doi: 10.1007/S10856-008-3545-8.

Burris, H. A. *et al.* (1997) ‘Improvements in survival and clinical benefit with gemcitabine as first-line therapy for patients with advanced pancreas cancer: a randomized trial’, *Journal of clinical oncology : official journal of the American Society of Clinical Oncology*. J Clin Oncol, 15(6), pp. 2403–2413. doi: 10.1200/JCO.1997.15.6.2403.

Byrne, J. D. *et al.* (2016) ‘Iontophoretic device delivery for the localized treatment of pancreatic ductal adenocarcinoma’, *Proceedings of the National Academy of Sciences of the United States of America*, 113(8), pp. 2200–2205. doi: 10.1073/pnas.1600421113.

Byrne, J. D. *et al.* (2018) ‘Impact of formulation on the iontophoretic delivery of the FOLFIRINOX regimen for the treatment of pancreatic cancer’, 81, pp. 991–998. doi: 10.1007/s00280-018-3570-3.

Campanella, O. H. *et al.* (2002) ‘The role of rheology in extrusion’, *Engineering and Food for the 21st Century*, (January), pp. 393–413. doi: 10.1201/9781420010169-34.

de Carvalho Rodrigues, V. *et al.* (2022) ‘3D-Printed EVA Devices for Antiviral Delivery and Herpes Virus Control in Genital Infection’, *Viruses*, 14(11), p. 2501. doi: 10.3390/v14112501.

Catanzano, O. *et al.* (2018) ‘Composite Alginate-Hyaluronan Sponges for the Delivery of Tranexamic Acid in Postextractive Alveolar Wounds’, *Journal of Pharmaceutical Sciences*. American Pharmacists Association, 107(2), pp. 654–661. doi: 10.1016/j.xphs.2017.09.026.

Caysa, H. *et al.* (2012) ‘Monitoring of Xenograft Tumor Growth and Response to Chemotherapy by Non-Invasive In Vivo Multispectral Fluorescence Imaging’, *PLoS ONE*, 7(10). doi: 10.1371/journal.pone.0047927.

Cenni, E. *et al.* (2000) ‘Biocompatibility and performance in vitro of a hemostatic gelatin sponge’, *Journal of Biomaterials Science, Polymer Edition*, 11(7), pp. 685–699. doi: 10.1163/156856200743959.

Chang, Y. C. *et al.* (2020) ‘A Green Strategy for Developing a Self-Healing Gelatin Resistive Memory Device’, *ACS Applied Polymer Materials*, 2(11), pp. 5318–5326. doi: 10.1021/acsapm.0c01119.

Chanu, N. R. *et al.* (2022) ‘Evaluation of a novel melatonin-loaded gelatin sponge as a wound dressing’, *Journal of Vascular Nursing*. Elsevier Inc., 40(1), pp. 2–10. doi: 10.1016/j.jvn.2021.09.004.

Chashchin, I. S. *et al.* (2021) ‘Microstructure and Mechanical Strength Properties of Chitosan Sponges Obtained from Polymer Solutions in Carbonic Acid’, *Polymer Science - Series A*, 63(6), pp. 749–756. doi: 10.1134/S0965545X21060018.

Chaudhry, F. (2013) ‘Adverse reaction to Nexplanon®’, *Journal of Family Planning and Reproductive Health Care*, 39(3), pp. 231–232. doi: 10.1136/jfprhc-2013-100633.

Chen, C. *et al.* (2013) ‘Bubble template fabrication of chitosan/poly(vinyl alcohol) sponges for wound dressing applications’, *International journal of biological macromolecules*. Int J Biol Macromol, 62, pp. 188–193. doi: 10.1016/J.IJBIOMAC.2013.08.042.

Cheng, Z. *et al.* (2012) ‘Multifunctional nanoparticles: Cost versus benefit of adding targeting and imaging capabilities’, *Science*, 338(6109), pp. 903–910. doi: 10.1126/science.1226338.

Chew, S. A. and Danti, S. (2017) ‘Biomaterial-Based Implantable Devices for Cancer Therapy’, *Advanced Healthcare Materials*. John Wiley & Sons, Ltd, 6(2), p. 1600766. doi: 10.1002/ADHM.201600766.

Choi, M., Razzaque, S. and Kim, R. (2012) ‘Systemic therapy of advanced pancreatic cancer: Has the landscape changed?’, *Clinical Advances in Hematology and Oncology*, 10(7), pp. 442–451.

Choi, Y. S. *et al.* (1999) ‘Study on gelatin-containing artificial skin: I. Preparation and characteristics of novel gelatin-alginate sponge’, *Biomaterials*, 20(5), pp. 409–417. doi: 10.1016/S0142-9612(98)00180-X.

Chronopoulos, A. *et al.* (2016) ‘ATRA mechanically reprograms pancreatic stellate cells to suppress matrix remodelling and inhibit cancer cell invasion’, *Nature Communications*, 7. doi: 10.1038/ncomms12630.

Chung, J. W. *et al.* (1998) ‘Transcatheter oily chemoembolization of the inferior phrenic artery in hepatocellular carcinoma: the safety and potential therapeutic role’, *Journal of vascular and interventional radiology : JVIR*. J Vasc Interv Radiol, 9(3), pp. 495–500. doi: 10.1016/S1051-0443(98)70306-9.

Chung, S. *et al.* (2010) ‘Bioresorbable elastomeric vascular tissue engineering scaffolds via melt spinning and electrospinning’, *Acta Biomaterialia*. Elsevier, 6(6), pp. 1958–1967. doi: 10.1016/J.ACTBIO.2009.12.007.

Chvapil, M. (1977) ‘Collagen sponge: Theory and practice of medical applications’, *Journal of Biomedical Materials Research*, 11(5), pp. 721–741. doi: 10.1002/jbm.820110508.

Cicala, G. *et al.* (2018) ‘Polylactide (PLA) Filaments a Biobased Solution for Additive Manufacturing: Correlating Rheology and Thermomechanical Properties with Printing Quality’, *Materials 2018, Vol. 11, Page 1191*. Multidisciplinary Digital Publishing Institute, 11(7), p. 1191. doi: 10.3390/MA11071191.

Clinic, M. *et al.* (1984) ‘Pancreatic Cancer’, (Table 1).

Colaris, M. J. L. *et al.* (2017) ‘Two hundreds cases of ASIA syndrome following silicone implants: a comparative study of 30 years and a review of current literature’, *Immunologic Research*. Springer US, 65(1), pp. 120–128. doi: 10.1007/s12026-016-8821-y.

Coleman, D. L., King, R. N. and Andrade, J. D. (1974) ‘The foreign body reaction: a chronic inflammatory response’, *Journal of biomedical materials research*. J Biomed Mater Res, 8(5), pp. 199–211. doi: 10.1002/JBM.820080503.

Colon, G. P. *et al.* (1996) ‘Thrombin-soaked gelatin sponge and brain edema in rats’, *Journal of neurosurgery*. J Neurosurg, 85(2), pp. 335–339. doi: 10.3171/JNS.1996.85.2.0335.

Conoscenti, G., Carrubba, V. La and Brucato, V. (2017) 'A Versatile Technique to Produce Porous Polymeric Scaffolds: The Thermally Induced Phase Separation (TIPS) Method', *Archives in Chemical Research*, 01(02), pp. 10–12. doi: 10.21767/2572-4657.100012.

Conroy, T. *et al.* (2011) 'FOLFIRINOX versus Gemcitabine for Metastatic Pancreatic Cancer', *n engl j med*, 364, pp. 1817–1842.

Cortesi, R., Nastruzzi, C. and Davis, S. S. (1998) 'Sugar cross-linked gelatin for controlled release: microspheres and disks', *Biomaterials*. Biomaterials, 19(18), pp. 1641–1649. doi: 10.1016/S0142-9612(98)00034-9.

Crowe, J. H., Crowe, L. M. and Chapman, D. (1984) 'Preservation of membranes in anhydrobiotic organisms: The role of trehalose', *Science*, 223(4637), pp. 701–703. doi: 10.1126/science.223.4637.701.

Cui, M. *et al.* (2021) 'Exploration and Preparation of Patient-specific Ciprofloxacin Implants Drug Delivery System Via 3D Printing Technologies', *Journal of Pharmaceutical Sciences*, 110(11), pp. 3678–3689. doi: 10.1016/j.xphs.2021.08.004.

Daamen, L. A. *et al.* (2021) 'Microscopic resection margin status in pancreatic ductal adenocarcinoma – A nationwide analysis', *European Journal of Surgical Oncology*. W.B. Saunders Ltd, 47(3), pp. 708–716. doi: 10.1016/J.EJSO.2020.11.145.

Dai, Z. (2019) 'Preparation and Characterization of Capsaicin-Collagen Sponge', *Biomedical Journal of Scientific & Technical Research*, 16(5), pp. 12353–12360. doi: 10.26717/bjstr.2019.16.002912.

Danckwerts, M. and Fassihi, A. (1991) 'Implantable Controlled Release Drug Delivery Systems: A Review', *Drug Development and Industrial Pharmacy*. Informa Healthcare, 17(11), pp. 1465–1502. doi: 10.3109/03639049109026629.

Dash, A. K. and Cudworth, G. C. (1998) 'Therapeutic applications of implantable drug delivery systems', *Journal of Pharmacological and Toxicological Methods*, 40(1), pp. 1–12. doi: 10.1016/S1056-8719(98)00027-6.

Dees, C., Chakraborty, D. and Distler, J. H. W. (2021) 'Cellular and molecular mechanisms in fibrosis', *Experimental Dermatology*, 30(1), pp. 121–131. doi: 10.1111/exd.14193.

Delpero, J. R. *et al.* (2017) 'Prognostic Value of Resection Margin Involvement After Pancreaticoduodenectomy for Ductal Adenocarcinoma: Updates From a French Prospective Multicenter Study', *Annals of surgery*. Ann Surg, 266(5), pp. 787–796. doi: 10.1097/SLA.0000000000002432.

Derkach, S. R. *et al.* (2020) 'Interactions between gelatin and sodium alginate: UV and FTIR studies', *Journal of Dispersion Science and Technology*. Taylor & Francis, 41(5), pp. 690–698. doi: 10.1080/01932691.2019.1611437.

Deshmane, S. *et al.* (2021) 'Stereolithography 3D printing technology in pharmaceuticals: a review', *Drug Development and Industrial Pharmacy*. Taylor & Francis, 47(9), pp. 1362–1372. doi: 10.1080/03639045.2021.1994990.

Dindo, D., Demartines, N. and Clavien, P. A. (2004) 'Classification of surgical complications: A new proposal with evaluation in a cohort of 6336 patients and results of a survey', *Annals of Surgery*, 240(2), pp. 205–213. doi: 10.1097/01.sla.0000133083.54934.ae.

Distler, M. *et al.* (2014) 'Precursor lesions for sporadic pancreatic cancer: PanIN, IPMN, and

MCN', *BioMed research international*. Biomed Res Int, 2014. doi: 10.1155/2014/474905.

Domsta, V. and Seidlitz, A. (2021) '3d-printing of drug-eluting implants: An overview of the current developments described in the literature', *Molecules*, 26(13). doi: 10.3390/molecules26134066.

Dörr, D., Kuhn, U. and Altstädt, V. (2020) 'Rheological study of gelation and crosslinking in chemical modified polyamide 12 using a multiwave technique', *Polymers*, 12(4), pp. 7–9. doi: 10.3390/POLYM12040855.

Duan, G. *et al.* (2017) 'Exploration of Macroporous Polymeric Sponges As Drug Carriers', *Biomacromolecules*. doi: 10.1021/acs.biomac.7b00852.

Durães, L. de C. *et al.* (2013) 'Correlation between bursting pressure and breaking strength in colonic anastomosis', *Acta Cirurgica Brasileira*, 28(6), pp. 447–452. doi: 10.1590/S0102-86502013000600008.

Edwards, B. K. *et al.* (2010) 'Annual report to the nation on the status of cancer, 1975-2006, featuring colorectal cancer trends and impact of interventions (risk factors, screening, and treatment) to reduce future rates', *Cancer*, 116(3), pp. 544–573. doi: 10.1002/cncr.24760.

Eissa, M. A. L. *et al.* (2019) 'Promoter methylation of ADAMTS1 and BNC1 as potential biomarkers for early detection of pancreatic cancer in blood', *Clinical Epigenetics*. Clinical Epigenetics, 11(1), pp. 1–10. doi: 10.1186/s13148-019-0650-0.

Erkan, M. *et al.* (2012) 'The role of stroma in pancreatic cancer: Diagnostic and therapeutic implications', *Nature Reviews Gastroenterology and Hepatology*. Nature Publishing Group, 9(8), pp. 454–467. doi: 10.1038/nrgastro.2012.115.

Esposito, E., Cortesi, R. and Nastruzzi, C. (1996) 'Gelatin microspheres: Influence of preparation parameters and thermal treatment on chemico-physical and biopharmaceutical properties', *Biomaterials*. Elsevier Ltd, 17(20), pp. 2009–2020. doi: 10.1016/0142-9612(95)00325-8.

Fan, H. Y. *et al.* (2018) 'Salmon skin gelatin-corn zein composite films produced via crosslinking with glutaraldehyde: Optimization using response surface methodology and characterization', *International Journal of Biological Macromolecules*, 120, pp. 263–273. doi: 10.1016/j.ijbiomac.2018.08.084.

Farris, S., Song, J. and Huang, Q. (2010) 'Alternative reaction mechanism for the cross-linking of gelatin with glutaraldehyde', *Journal of Agricultural and Food Chemistry*, 58(2), pp. 998–1003. doi: 10.1021/jf9031603.

Fatima, J. *et al.* (2010) 'Pancreatoduodenectomy for Ductal Adenocarcinoma', *Archives of Surgery*, 145(2), p. 167. doi: 10.1001/archsurg.2009.282.

Fayzullin, A., Bakulina, A., *et al.* (2021) 'Implantable drug delivery systems and foreign body reaction: Traversing the current clinical landscape', *Bioengineering*, 8(12), pp. 1–27. doi: 10.3390/bioengineering8120205.

Fayzullin, A., Churbanov, S., *et al.* (2021) 'Local delivery of pirfenidone by pla implants modifies foreign body reaction and prevents fibrosis', *Biomedicines*, 9(8), pp. 1–33. doi: 10.3390/biomedicines9080853.

Fialho, S. L. and Da Silva Cunha, A. (2005) 'Manufacturing techniques of biodegradable implants intended for intraocular application', *Drug Delivery: Journal of Delivery and*

Targeting of Therapeutic Agents, 12(2), pp. 109–116. doi: 10.1080/10717540590921432.

Florentin, L. M. *et al.* (2022) 'Imaging assessment after pancreaticoduodenectomy: reconstruction techniques—normal findings and complications', *Insights into Imaging*. Springer Vienna, 13(1). doi: 10.1186/s13244-022-01306-4.

Foda, N. H., El-Laithy, H. M. and Tadros, M. I. (2004) 'Optimization of biodegradable sponges as controlled release drug matrices. I. Effect of moisture level on chitosan sponge mechanical properties', *Drug Development and Industrial Pharmacy*, 30(4), pp. 369–379. doi: 10.1081/DDC-120030931.

Freag, M. S., Saleh, W. M. and Abdallah, O. Y. (2018) 'Exploiting polymer blending approach for fabrication of buccal chitosan-based composite sponges with augmented mucoadhesive characteristics', *European Journal of Pharmaceutical Sciences*. Elsevier, 120(February), pp. 10–19. doi: 10.1016/j.ejps.2018.04.041.

Friess, W. (1998) 'Collagen – biomaterial for drug delivery', *European Journal of Pharmaceutics and Biopharmaceutics*. Elsevier, 45(2), pp. 113–136. doi: 10.1016/S0939-6411(98)00017-4.

Fuenmayor, E. *et al.* (2018) 'Material considerations for fused-filament fabrication of solid dosage forms', *Pharmaceutics*, 10(2), pp. 1–27. doi: 10.3390/pharmaceutics10020044.

Gao, Z. *et al.* (2020) 'High variability of postsurgical anatomy supports the need for individualized drug-eluting implants to treat chronic rhinosinusitis', *Life*, 10(12), pp. 1–10. doi: 10.3390/life10120353.

Garg, T. *et al.* (2012) 'Scaffold: a novel carrier for cell and drug delivery.', *Critical reviews in therapeutic drug carrier systems*.

Del Gaudio, C. *et al.* (2017) 'Natural polymeric microspheres for modulated drug delivery', *Materials Science and Engineering C*. Elsevier B.V., 75, pp. 408–417. doi: 10.1016/j.msec.2017.02.051.

Gebhardt, A., Kessler, J. and Thurn, L. (2018) 'Basics of 3D Printing Technology', *3D Printing*, pp. 1–32. doi: 10.3139/9781569907030.001.

Geidobler, R. and Winter, G. (2013) 'Controlled ice nucleation in the field of freeze-drying: Fundamentals and technology review', *European Journal of Pharmaceutics and Biopharmaceutics*. Elsevier, 85(2), pp. 214–222. doi: 10.1016/j.ejpb.2013.04.014.

Geng, G. *et al.* (2015) 'Establishment of a New Zealand rabbit model of spinal tuberculosis', *Journal of Spinal Disorders and Techniques*, 28(3), pp. E140–E145. doi: 10.1097/BSD.0000000000000191.

Genina, N. *et al.* (2016) 'Ethylene vinyl acetate (EVA) as a new drug carrier for 3D printed medical drug delivery devices', *European Journal of Pharmaceutical Sciences*. Elsevier B.V., 90, pp. 53–63. doi: 10.1016/j.ejps.2015.11.005.

Gheorghe, G. *et al.* (2020) 'Early diagnosis of pancreatic cancer: The key for survival', *Diagnostics*, 10(11), pp. 1–17. doi: 10.3390/diagnostics10110869.

Ghosn, M. *et al.* (2016) 'Dilemma of first line regimens in metastatic pancreatic adenocarcinoma', *World Journal of Gastroenterology*. Baishideng Publishing Group Co, 22(46), pp. 10124–10130. doi: 10.3748/wjg.v22.i46.10124.

Giri, B. R. *et al.* (2020) 'Fabrication of intragastric floating, controlled release 3D printed theophylline tablets using hot-melt extrusion and fused deposition modeling', *Pharmaceutics*, 12(1). doi: 10.3390/pharmaceutics12010077.

Gomez-Guillen, M. C. *et al.* (2011) 'Functional and bioactive properties of collagen and gelatin from alternative sources: A review', *Food Hydrocolloids*. Elsevier, 25(8), pp. 1813–1827. doi: 10.1016/J.FOODHYD.2011.02.007.

Gonzalez, L. M., Moeser, A. J. and Blikslager, A. T. (2015) 'Porcine models of digestive disease: the future of large animal translational research', *Translational research : the journal of laboratory and clinical medicine*. Transl Res, 166(1), pp. 12–27. doi: 10.1016/J.TRSL.2015.01.004.

Goral, V. (2015) 'Pancreatic cancer: Pathogenesis and diagnosis', *Asian Pacific Journal of Cancer Prevention*, 16(14), pp. 5619–5624. doi: 10.7314/APJCP.2015.16.14.5619.

Gouma, D. J. *et al.* (1999) 'Surgical palliative treatment in bilio-pancreatic malignancy', *Annals of Oncology*. Elsevier Masson SAS, 10(SUPPL. 4), pp. S269–S272. doi: 10.1093/annonc/10.suppl_4.S269.

Gourgou-Bourgade, S. *et al.* (2013) 'Impact of FOLFIRINOX compared with gemcitabine on quality of life in patients with metastatic pancreatic cancer: Results from the PRODIGE 4/ACCORD 11 randomized trial', *Journal of Clinical Oncology*, 31(1), pp. 23–29. doi: 10.1200/JCO.2012.44.4869.

Gray, S. *et al.* (2022) 'Clinical challenges associated with utility of neoadjuvant treatment in patients with pancreatic ductal adenocarcinoma', *European Journal of Surgical Oncology*, 48(6), pp. 1198–1208. doi: 10.1016/j.ejso.2022.02.014.

Greenlee, R. T. *et al.* (2000) 'Cancer Statistics , 2000', pp. 7–33.

Groot, V. P. *et al.* (2017) 'Systematic review on the treatment of isolated local recurrence of pancreatic cancer after surgery; re-resection, chemoradiotherapy and SBRT', *Hpb*, 19(2), pp. 83–92. doi: 10.1016/j.hpb.2016.11.001.

Guidoin, R. *et al.* (1994) 'The benefits of fluoropassivation of polyester arterial prostheses as observed in a canine model.', *ASAIO Journal (American Society for Artificial Internal Organs : 1992)*. J.B. Lippincott Co, 40(3), pp. M870-9. doi: 10.1097/00002480-199407000-00121.

Guizzardi, R. *et al.* (2019) 'Gelatin-based hydrogels through homobifunctional triazolinediones targeting tyrosine residues', *Molecules*, 24(3). doi: 10.3390/molecules24030589.

Haiyan, L. *et al.* (2017) 'PreparSation and characteristics of gelatin sponges crosslinked by microbial transglutaminase', *PeerJ*, 2017(8), p. 3665. doi: 10.7717/peerj.3665.

Haleem, A., Javaid, M. and Vaishya, R. (2020) '3D printing applications for the treatment of cancer', *Clinical Epidemiology and Global Health*. Elsevier, 8(4), pp. 1072–1076. doi: 10.1016/j.cegh.2020.03.022.

Hamad, K. *et al.* (2014) 'Biodegradable polymer blends and composites: An overview', *Polymer Science - Series A*, 56(6), pp. 812–829. doi: 10.1134/S0965545X14060054.

Hanahan, D. and Weinberg, R. A. (2011) 'Hallmarks of cancer: The next generation', *Cell*. Elsevier Inc., 144(5), pp. 646–674. doi: 10.1016/j.cell.2011.02.013.

Hani, U. *et al.* (2021) ‘A systematic study of novel drug delivery mechanisms and treatment strategies for pancreatic cancer’, *Journal of Drug Delivery Science and Technology*. Elsevier B.V., 63(April), p. 102539. doi: 10.1016/j.jddst.2021.102539.

Hao, W. *et al.* (2021) ‘3D printing-based drug-loaded implanted prosthesis to prevent breast cancer recurrence post-conserving surgery’, *Asian Journal of Pharmaceutical Sciences*. Elsevier B.V., 16(1), pp. 86–96. doi: 10.1016/j.ajps.2020.06.002.

Haws, M. *et al.* (1994) ‘Vitamin A-soaked gelfoam sponges and wound healing in steroid-treated animals’, *Annals of plastic surgery*. Ann Plast Surg, 32(4), pp. 418–422. doi: 10.1097/00000637-199404000-00017.

Hendriks, T. and Mastboom, W. J. B. (1990) ‘Healing of experimental intestinal anastomoses. Parameters for repair’, *Diseases of the colon and rectum*. Dis Colon Rectum, 33(10), pp. 891–901. doi: 10.1007/BF02051930.

Herdeg, C. *et al.* (2008) ‘Local catheter-based delivery of antithrombotic or antiproliferative drugs: A new concept for prevention of restenosis’, *Thrombosis Research*. Elsevier Ltd, 123(2), pp. 236–243. doi: 10.1016/j.thromres.2008.02.015.

Hidalgo, M. *et al.* (2015) ‘Addressing the challenges of pancreatic cancer: Future directions for improving outcomes’, *Pancreatology*, 15(1), pp. 8–18. doi: 10.1016/j.pan.2014.10.001.

Hinni, M. L. *et al.* (2013) ‘Surgical margins in head and neck cancer: a contemporary review’, *Head & neck*. Head Neck, 35(9), pp. 1362–1370. doi: 10.1002/HED.23110.

Hishinuma, S. *et al.* (2006) ‘Patterns of Recurrence After Curative Resection of Pancreatic Cancer, Based on Autopsy Findings’, *Journal of Gastrointestinal Surgery*, 10(4), pp. 511–518. doi: 10.1016/j.gassur.2005.09.016.

Ho, W. J., Jaffee, E. M. and Zheng, L. (2020) ‘The tumour microenvironment’, *Nature Reviews Clinical Oncology*. Springer US, 17(September). doi: 10.1038/s41571-020-0363-5.

Holste, K. G. *et al.* (2022) ‘Conservative management of intraventricular migration of a gelatin sponge: illustrative case’, *Journal of Neurosurgery: Case Lessons*, 3(20), pp. 15–17. doi: 10.3171/case22126.

Hong, S. R. *et al.* (2001) ‘Study on gelatin-containing artificial skin IV: A comparative study on the effect of antibiotic and EGF on cell proliferation during epidermal healing’, *Biomaterials*. Biomaterials, 22(20), pp. 2777–2783. doi: 10.1016/S0142-9612(01)00021-7.

Hou, N., Du, X. and Wu, S. (2022) ‘Advances in pig models of human diseases’, *Animal Models and Experimental Medicine*, 5(2), pp. 141–152. doi: 10.1002/ame2.12223.

Huang, B. and Bártolo, P. J. (2018) ‘Rheological characterization of polymer/ceramic blends for 3D printing of bone scaffolds’, *Polymer Testing*. Elsevier, 68(February), pp. 365–378. doi: 10.1016/j.polymertesting.2018.04.033.

Huang, C., Iovanna, J. and Santofimia-Castaño, P. (2021) ‘Targeting fibrosis: The bridge that connects pancreatitis and pancreatic cancer’, *International Journal of Molecular Sciences*, 22(9). doi: 10.3390/ijms22094970.

Huang, J. *et al.* (2017) ‘3D printing guiding stent graft fenestration: A novel technique for fenestration in endovascular aneurysm repair’, *Vascular*, 25(4), pp. 442–446. doi: 10.1177/1708538116682913.

Huang, W. *et al.* (2018) 'Preliminary application of 3D-printed coplanar template for iodine-125 seed implantation therapy in patients with advanced pancreatic cancer', *World Journal of Gastroenterology*, 24(46), pp. 5280–5287. doi: 10.3748/wjg.v24.i46.5280.

Ikeda, O. *et al.* (2005) 'Randomized comparison of intra-arterial chemotherapy versus intra-arterial chemotherapy and gelfoam embolization for treatment of advanced cervical carcinoma', *CardioVascular and Interventional Radiology*, 28(6), pp. 736–743. doi: 10.1007/s00270-004-4178-z.

Ikeuchi, D. *et al.* (2000) 'Correlation of Tensile Strength with Bursting Pressure in the Evaluation of Intestinal Anastomosis', *Digestive Surgery*. S. Karger AG, 16(6), pp. 478–485. doi: 10.1159/000018773.

Ilic, M. and Ilic, I. (2016) 'Epidemiology of pancreatic cancer', *World journal of gastroenterology*. World J Gastroenterol, 22(44), pp. 9694–9705. doi: 10.3748/WJG.V22.I44.9694.

Imani, R., Rafienia, M. and Emami, S. H. (2013) 'Synthesis and characterization of glutaraldehyde-based crosslinked gelatin as a local hemostat sponge in surgery: an in vitro study.', *Bio-medical materials and engineering*, 23(3), pp. 211–224. doi: 10.3233/bme-130745.

Indolfi, L., Ligorio, M., Ting, D. T., *et al.* (2016) 'A tunable delivery platform to provide local chemotherapy for pancreatic ductal adenocarcinoma', *Biomaterials*. doi: 10.1016/j.biomaterials.2016.03.044.

Indolfi, L., Ligorio, M., Ting, D. T., *et al.* (2016) 'A Tunable Delivery Platform to Provide Local Chemotherapy for Pancreatic Ductal Adenocarcinoma HHS Public Access', *Biomaterials*, 93, pp. 71–82. doi: 10.1016/j.biomaterials.2016.03.044.

Irfan, N. I. *et al.* (2022) 'Gelatin-based hemostatic agents for medical and dental application at a glance: A narrative literature review', *Saudi Dental Journal*. King Saud University, 34(8), pp. 699–707. doi: 10.1016/j.sdentj.2022.11.007.

Jacobetz, M. A. *et al.* (2013) 'Hyaluronan impairs vascular function and drug delivery in a mouse model of pancreatic cancer', *Gut*, 62(1), pp. 112–120. doi: 10.1136/gutjnl-2012-302529.

Jakubowska, E. and Lulek, J. (2021) 'The application of freeze-drying as a production method of drug nanocrystals and solid dispersions – A review', *Journal of Drug Delivery Science and Technology*. Editions de Sante. doi: 10.1016/j.jddst.2021.102357.

Jamiyan, T. *et al.* (2020) 'Clinical impacts of resection margin status and clinicopathologic parameters on pancreatic ductal adenocarcinoma', *World Journal of Surgical Oncology*. World Journal of Surgical Oncology, 18(1), pp. 1–11. doi: 10.1186/s12957-020-01900-0.

Jayakrishnan, A. and Jameela, S. R. (1996) 'Glutaraldehyde as a fixative in bioprostheses and drug delivery matrices', *Biomaterials*. Elsevier Science Ltd, 17(5), pp. 471–484. doi: 10.1016/0142-9612(96)82721-9.

Jemal, A. *et al.* (2009) 'Cancer Statistics , 2009 BOTH SEXES FEMALE BOTH SEXES ESTIMATED DEATHS', *CA Cancer J Clin*, 59(4), pp. 1–25. doi: 10.1002/caac.20073.Available.

Jenisha, Theodore David, S. and Priyadharsini, J. . (2015) 'Schiff Base Ligand Its Complexes and Their Ft-Ir Spectroscopy Studies', *International Journal on Applied Bio-Engineering*,

9(1), pp. 1–4. doi: 10.18000/ijabeg.10124.

JENKINS, H. P. and JANDA, R. (1946) ‘Studies on the use of gelatin sponge or foam as an hemostatic agent in experimental liver resections and injuries to large veins.’, *Annals of surgery*, 124, pp. 952–961. doi: 10.1097/00000658-194611000-00010.

Jiang, B. *et al.* (2020) ‘Stroma-Targeting Therapy in Pancreatic Cancer: One Coin With Two Sides?’, *Frontiers in Oncology*, 10(October), pp. 1–9. doi: 10.3389/fonc.2020.576399.

Jin, S. *et al.* (2021) ‘A double-layer dura mater based on poly(caprolactone-: Co -lactide) film and polyurethane sponge: Preparation, characterization, and biodegradation study’, *Journal of Materials Chemistry B*. Royal Society of Chemistry, 9(18), pp. 3863–3873. doi: 10.1039/d1tb00454a.

Jones, S. *et al.* (2008) ‘Core signaling pathways in human pancreatic cancers revealed by global genomic analyses’, *Science*, 321(5897), pp. 1801–1806. doi: 10.1126/science.1164368.

Kabiri, M. *et al.* (2010) ‘Preparation and characterization of absorbable hemostat crosslinked gelatin sponges for surgical applications’. doi: 10.1016/j.cap.2010.08.031.

Kaifi, J. T. *et al.* (2015) ‘Circulating tumor cell isolation during resection of colorectal cancer lung and liver metastases: a prospective trial with different detection techniques’, *Cancer biology & therapy*. Cancer Biol Ther, 16(5), pp. 699–708. doi: 10.1080/15384047.2015.1030556.

Kamisawa, T. *et al.* (2016) ‘Pancreatic cancer’, *The Lancet*. Elsevier Ltd, 388(10039), pp. 73–85. doi: 10.1016/S0140-6736(16)00141-0.

Karagiannis, G. S. *et al.* (2012) ‘Cancer-associated fibroblasts drive the progression of metastasis through both paracrine and mechanical pressure on cancer tissue’, *Molecular Cancer Research*, 10(11), pp. 1403–1418. doi: 10.1158/1541-7786.MCR-12-0307.

Kassem, M. A. A., ElMeshad, A. N. and Fares, A. R. (2015) ‘Lyophilized Sustained Release Mucoadhesive Chitosan Sponges for Buccal Buspirone Hydrochloride Delivery: Formulation and In Vitro Evaluation’, *AAPS PharmSciTech*, 16(3), pp. 537–547. doi: 10.1208/s12249-014-0243-3.

Katz, M. H. G. *et al.* (2017) ‘Alliance for clinical trials in oncology (ALLIANCE) trial A021501: Preoperative extended chemotherapy vs. chemotherapy plus hypofractionated radiation therapy for borderline resectable adenocarcinoma of the head of the pancreas’, *BMC Cancer*. BMC Cancer, 17(1), pp. 1–8. doi: 10.1186/s12885-017-3441-z.

Kaur, N. *et al.* (2016) ‘Formulation, optimization and evaluation of curcumin-β-cyclodextrin-loaded sponge for effective drug delivery in thermal burns chemotherapy’, *Drug Delivery*, 23(7), pp. 2245–2254. doi: 10.3109/10717544.2014.963900.

Kaurav, H. and Kapoor, D. N. (2017) ‘Implantable systems for drug delivery to the brain’, *https://doi.org/10.4155/tde-2017-0082*. Future Science Ltd London, UK , 8(12), pp. 1097–1107. doi: 10.4155/TDE-2017-0082.

Kawasaki, S. *et al.* (2017) ‘Comparison of TachoSil and TachoComb in patients undergoing liver resection—a randomized, double-blind, non-inferiority trial’, *Langenbeck’s Archives of Surgery*. Springer, 402(4), p. 591. doi: 10.1007/S00423-017-1571-Z.

Khdhir, R., Belghith, A. and Othmen, S. (2023) ‘Pancreatic Cancer Segmentation and

Classification in CT Imaging using Antlion Optimization and Deep Learning Mechanism', *International Journal of Advanced Computer Science and Applications*, 14(3), pp. 50–61. doi: 10.14569/IJACSA.2023.0140307.

Kim, D. S. *et al.* (2014) 'Lumbar Nerve Root Compression due to Leakage of Bone Cement after Vertebroplasty', *Korean Journal of Neurotrauma*, 10(2), p. 155. doi: 10.13004/kjnt.2014.10.2.155.

Kim, V. M. and Ahuja, N. (2015) 'Early detection of pancreatic cancer', *Chinese Journal of Cancer Research*, 27(4), pp. 321–331. doi: 10.3978/j.issn.1000-9604.2015.07.03.

Kirdponpattara, S., Phisalaphong, M. and Kongruang, S. (2017) 'Gelatin-bacterial cellulose composite sponges thermally cross-linked with glucose for tissue engineering applications'. doi: 10.1016/j.carbpol.2017.08.094.

Kizilay, E., Kayitmazer, A. B. and Dubin, P. L. (2011) 'Complexation and coacervation of polyelectrolytes with oppositely charged colloids', *Advances in Colloid and Interface Science*. Elsevier B.V., 167(1–2), pp. 24–37. doi: 10.1016/j.cis.2011.06.006.

Klaassen, D. J. *et al.* (1985) 'Treatment of locally unresectable cancer of the stomach and pancreas: a randomized comparison of 5-fluorouracil alone with radiation plus concurrent and maintenance 5-fluorouracil--an Eastern Cooperative Oncology Group study.', *Journal of clinical oncology : official journal of the American Society of Clinical Oncology*, 3(3), pp. 373–8. doi: 10.1200/JCO.1985.3.3.373.

Kleiner, L. W., Wright, J. C. and Wang, Y. (2014) 'Evolution of implantable and insertable drug delivery systems', *Journal of controlled release : official journal of the Controlled Release Society*. J Control Release, 181(1), pp. 1–10. doi: 10.1016/J.JCONREL.2014.02.006.

Klimstra, D. S. and Adsay, N. V. (2009) *Tumors of the Pancreas and Ampulla of Vater*. Second Edi, *Surgical Pathology of the GI Tract, Liver, Biliary Tract and Pancreas*. Second Edi. Elsevier Inc. doi: 10.1016/B978-141604059-0.50038-2.

Klose, J., Ronellenfitsch, U. and Kleeff, J. (2021) 'Management problems in patients with pancreatic cancer from a surgeon's perspective', *Seminars in Oncology*. Elsevier Inc., 48(1), pp. 76–83. doi: 10.1053/j.seminoncol.2021.02.008.

Kowalska, M. *et al.* (2022) 'Management of validation of HPLC method for determination of acetylsalicylic acid impurities in a new pharmaceutical product', *Scientific Reports*. Nature Publishing Group UK, 12(1), pp. 1–9. doi: 10.1038/s41598-021-99269-x.

Kruger, S. *et al.* (2016) 'Isolated pulmonary metastases define a favorable subgroup in metastatic pancreatic cancer'. doi: 10.1016/j.pan.2016.03.016.

Kumar, M. *et al.* (2013) 'Percutaneous trans-hepatic gelfoam-cyanoacrylate glue embolization for ruptured post-traumatic hepatic artery pseudo-aneurysm in a limited-resource scenario', *Pediatric Surgery International*, 29(5), pp. 465–469. doi: 10.1007/s00383-013-3291-y.

Kumar, N. *et al.* (2018) '3D printing of flexible parts using eva material', *Materials Physics and Mechanics*, 37(2), pp. 124–132. doi: 10.18720/MPM.3722018-3.

Kumar, R. B. (2012) 'A review on freeze drying process and technologies', *International Journal of Pharmacy and Technology*, 4(3), pp. 2215–2243.

Kurita, H. *et al.* (2006) 'Intraoperative digital microscopic assessment of the deep surgical

margins in oral carcinoma surgery: a preliminary report', *American journal of surgery*. Am J Surg, 191(1), pp. 84–88. doi: 10.1016/J.AMJSURG.2005.10.006.

Kutlehria, S. *et al.* (2022) 'Role of 3D Printing in the Development of Biodegradable Implants for Central Nervous System Drug Delivery', *Molecular Pharmaceutics*, 19(12), pp. 4411–4427. doi: 10.1021/acs.molpharmaceut.2c00344.

Lambert, A. *et al.* (2019) 'An update on treatment options for pancreatic adenocarcinoma', *Therapeutic Advances in Medical Oncology*, 11. doi: 10.1177/1758835919875568.

Lambert, A. *et al.* (2021) 'Neoadjuvant treatment strategies in resectable pancreatic cancer', *Cancers*, 13(18), pp. 1–19. doi: 10.3390/cancers13184724.

Laplane, L. *et al.* (2019) 'Beyond the tumour microenvironment', *International Journal of Cancer*, 145(10), pp. 2611–2618. doi: 10.1002/ijc.32343.

Laurent, A. (2007) 'Microspheres and nonspherical particles for embolization', *Techniques in vascular and interventional radiology*. Tech Vasc Interv Radiol, 10(4), pp. 248–256. doi: 10.1053/J.TVIR.2008.03.010.

Ledermann, H. P. *et al.* (1998) 'Superselective coil embolization in acute gastrointestinal hemorrhage: personal experience in 10 patients and review of the literature', *Journal of vascular and interventional radiology : JVIR*. J Vasc Interv Radiol, 9(5), pp. 753–760. doi: 10.1016/S1051-0443(98)70387-2.

Leffler, C. C. and Mü, B. W. (2000) 'Influence of the acid type on the physical and drug liberation properties of chitosan-gelatin sponges', *International Journal of Pharmaceutics*, 194. Available at: www.elsevier.com/locate/ijpharm (Accessed: 24 October 2022).

Li, F. *et al.* (2015) 'Multiple layer-by-layer lipid-polymer hybrid nanoparticles for improved folfirinox chemotherapy in pancreatic tumor models', *Advanced Functional Materials*, 25(5), pp. 788–798. doi: 10.1002/adfm.201401583.

Liening, D. A. *et al.* (1997) 'A comparison of the biocompatibility of three absorbable hemostatic agents in the rat middle ear', *Otolaryngology--head and neck surgery : official journal of American Academy of Otolaryngology-Head and Neck Surgery*. Otolaryngol Head Neck Surg, 116(4), pp. 454–457. doi: 10.1016/S0194-59989770294-8.

Lin, F. H. *et al.* (1998) 'Biological effects and cytotoxicity of the composite composed by tricalcium phosphate and glutaraldehyde cross-linked gelatin', *Biomaterials*. Biomaterials, 19(10), pp. 905–917. doi: 10.1016/S0142-9612(97)00202-0.

Lindegaard, J. C. *et al.* (2016) 'Individualised 3D printed vaginal template for MRI guided brachytherapy in locally advanced cervical cancer', *Radiotherapy and Oncology*. Elsevier Ireland Ltd, 118(1), pp. 173–175. doi: 10.1016/j.radonc.2015.12.012.

Liu, H. *et al.* (2014) 'Modification of fish skin collagen film and absorption property of tannic acid', *Journal of Food Science and Technology*. Springer, 51(6), pp. 1102–1109. doi: 10.1007/S13197-011-0599-2/FIGURES/8.

Liu, J. (2006) 'Physical characterization of pharmaceutical formulations in frozen and freeze-dried solid states: Techniques and applications in freeze-drying development', *Pharmaceutical Development and Technology*, 11(1), pp. 3–28. doi: 10.1080/10837450500463729.

Liu, J. *et al.* (2007) 'A novel trans-lymphatic drug delivery system: Implantable gelatin

sponge impregnated with PLGA-paclitaxel microspheres', *Biomaterials*, 28(21), pp. 3236–3244. doi: 10.1016/j.biomaterials.2007.03.022.

Liu, J. *et al.* (2009) 'Translymphatic chemotherapy by intrapleural placement of gelatin sponge containing biodegradable paclitaxel colloids controls lymphatic metastasis in lung cancer', *Cancer Research*, 69(3), pp. 1174–1181. doi: 10.1158/0008-5472.CAN-08-1753.

Liu, L. *et al.* (2000) 'Monolithic osmotic tablet system for nifedipine delivery', *Journal of Controlled Release*, 67(2–3), pp. 309–322. doi: 10.1016/S0168-3659(00)00222-4.

Liu, S. L. *et al.* (2019) 'Establishment and application of an artificial intelligence diagnosis system for pancreatic cancer with a faster region-based convolutional neural network', *Chinese Medical Journal*, 132(23), pp. 2795–2803. doi: 10.1097/CM9.0000000000000544.

Liu, X. *et al.* (2020) 'Safety Considerations of Cancer Nanomedicine—A Key Step toward Translation', *Small*, 16(36). doi: 10.1002/smll.202000673.

Logothetidis, S. (2018) 'Polymer Blends and Composites', *Springer Series in Surface Sciences*, 52, pp. 271–294. doi: 10.1007/978-3-319-75895-4_12.

Loh, Q. L. and Choong, C. (2013) 'Three-dimensional scaffolds for tissue engineering applications: Role of porosity and pore size', *Tissue Engineering - Part B: Reviews*, 19(6), pp. 485–502. doi: 10.1089/ten.teb.2012.0437.

Loos, M. *et al.* (2008) 'Surgical treatment of pancreatic cancer', *Annals of the New York Academy of Sciences*, 1138, pp. 169–180. doi: 10.1196/annals.1414.024.

Loos, M. *et al.* (2018) 'Postoperative pancreatic fistula: Microbial growth determines outcome', *Surgery*. Mosby, 164(6), pp. 1185–1190. doi: 10.1016/J.SURG.2018.07.024.

Lu, T., Li, Y. and Chen, T. (2013) 'Techniques for fabrication and construction of three-dimensional scaffolds for tissue engineering', *International Journal of Nanomedicine*, 8, pp. 337–350. doi: 10.2147/IJN.S38635.

Luu, A. M. *et al.* (2021) 'Late recurrences of pancreatic cancer in patients with long-term survival after pancreaticoduodenectomy', *Journal of Gastrointestinal Oncology*, 12(2), pp. 474–483. doi: 10.21037/jgo-20-433.

Van Luyn, M. J. A. *et al.* (1991) 'Methylcellulose cell culture as a new cytotoxicity test system for biomaterials', *Journal of Materials Science: Materials in Medicine*. Kluwer Academic Publishers, 2(3), pp. 142–148. doi: 10.1007/BF00692972/METRICS.

Mahadevan, D. and Von Hoff, D. D. (2007) 'Tumor-stroma interactions in pancreatic ductal adenocarcinoma', *Molecular Cancer Therapeutics*, 6(4), pp. 1186–1197. doi: 10.1158/1535-7163.MCT-06-0686.

Mahadevan, V. (2019) 'Anatomy of the pancreas and spleen', *Surgery (United Kingdom)*. Elsevier Ltd, 37(6), pp. 297–301. doi: 10.1016/j.mpsur.2019.04.008.

Mallakpour, S. and khodadadzadeh, L. (2018) 'Ultrasonic-assisted fabrication of starch/MWCNT-glucose nanocomposites for drug delivery', *Ultrasonics Sonochemistry*. Elsevier B.V., 40, pp. 402–409. doi: 10.1016/j.ultsonch.2017.07.033.

Mallya, K. *et al.* (2021) 'Modeling pancreatic cancer in mice for experimental therapeutics', *Biochimica et Biophysica Acta - Reviews on Cancer*. Elsevier B.V., 1876(1), p. 188554. doi: 10.1016/j.bbcan.2021.188554.

Maman, S. and Witz, I. P. (2018) ‘A history of exploring cancer in context’, *Nature reviews. Cancer*. Nat Rev Cancer, 18(6), pp. 359–376. doi: 10.1038/S41568-018-0006-7.

Mania, S. *et al.* (2019) ‘Obtaining and characterization of the PLA/chitosan foams with antimicrobial properties achieved by the emulsification combined with the dissolution of chitosan by CO2 saturation’, *Molecules*. MDPI AG, 24(24). doi: 10.3390/molecules24244532.

Manohar, M. *et al.* (2021) ‘Eosinophils in the pathogenesis of pancreatic disorders’, *Seminars in Immunopathology*. Seminars in Immunopathology, 43(3), pp. 411–422. doi: 10.1007/s00281-021-00853-0.

Marconi, S. *et al.* (2016) ‘An innovative strategy for the identification and 3D reconstruction of pancreatic cancer from CT images’, *Updates in Surgery*. Springer Milan, 68(3), pp. 273–278. doi: 10.1007/s13304-016-0394-8.

Marconi, S. *et al.* (2017) ‘Value of 3D printing for the comprehension of surgical anatomy’, *Surgical Endoscopy*. Springer US, 31(10), pp. 4102–4110. doi: 10.1007/s00464-017-5457-5.

Marsh, R. D. W. *et al.* (2015) ‘Pancreatic cancer and FOLFIRINOX: A new era and new questions’, *Cancer Medicine*, 4(6), pp. 853–863. doi: 10.1002/cam4.433.

Martinez-bosch, N. (2018) ‘Immune Evasion in Pancreatic Cancer ’:, pp. 1–16. doi: 10.3390/cancers10010006.

Matsuda, Y. *et al.* (2019) ‘Encapsulating fibrosis following neoadjuvant chemotherapy is correlated with outcomes in patients with pancreatic cancer’, *PLoS ONE*, 14(9), pp. 1–18. doi: 10.1371/journal.pone.0222155.

McGuigan, A. *et al.* (2018) ‘Pancreatic cancer: A review of clinical diagnosis, epidemiology, treatment and outcomes’, *World Journal of Gastroenterology*. Baishideng Publishing Group Co, 24(43), pp. 4846–4861. doi: 10.3748/WJG.V24.I43.4846.

Miller, A. L., Garcia, P. L. and Yoon, K. J. (2020) ‘Developing effective combination therapy for pancreatic cancer: An overview’, *Pharmacological Research*, 155(February). doi: 10.1016/j.phrs.2020.104740.

Min, K. K. M. *et al.* (2023) ‘Overcoming the Fibrotic Fortress in Pancreatic Ductal Adenocarcinoma : Challenges and Opportunities’, pp. 1–19.

Mohamdeen, Y. M. G. *et al.* (2022) ‘Development of 3D printed drug-eluting contact lenses’, *The Journal of pharmacy and pharmacology*, 74(10), pp. 1467–1476. doi: 10.1093/jpp/rgab173.

Mohammed, A. A. *et al.* (2021) ‘3D Printing in medicine: Technology overview and drug delivery applications’, *Annals of 3D Printed Medicine*. Elsevier Masson SAS, 4, p. 100037. doi: 10.1016/j.stlm.2021.100037.

Mondal, A. *et al.* (2019) ‘Characterization and printability of Sodium alginate -Gelatin hydrogel for bioprinting NSCLC co-culture’, *Scientific Reports*, 9(1), pp. 1–12. doi: 10.1038/s41598-019-55034-9.

Mostafa, M. E. *et al.* (2017) ‘Pathologic classification of “pancreatic cancers”: Current concepts and challenges’, *Chinese Clinical Oncology*, 6(6). doi: 10.21037/cco.2017.12.01.

Moysan, E., Bastiat, G. and Benoit, J. P. (2013) ‘Gemcitabine versus modified gemcitabine:

A review of several promising chemical modifications', *Molecular Pharmaceutics*, 10(2), pp. 430–444. doi: 10.1021/mp300370t.

Muñoz, A. R. *et al.* (2017) 'Pancreatic Cancer: Current Status and Challenges', *Current Pharmacology Reports*. Current Pharmacology Reports, 3(6), pp. 396–408. doi: 10.1007/s40495-017-0112-3.

Murphy, C. M., Haugh, M. G. and O'Brien, F. J. (2010) 'The effect of mean pore size on cell attachment, proliferation and migration in collagen-glycosaminoglycan scaffolds for bone tissue engineering', *Biomaterials*. Biomaterials, 31(3), pp. 461–466. doi: 10.1016/J.BIOMATERIALS.2009.09.063.

Muthukumar, T. *et al.* (2014) 'Fish scale collagen sponge incorporated with Macrotyloma uniflorum plant extract as a possible wound/burn dressing material', *Colloids and surfaces. B, Biointerfaces*. Colloids Surf B Biointerfaces, 113, pp. 207–212. doi: 10.1016/J.COLSURFB.2013.09.019.

Nagahama, K., Ouchi, T. and Ohya, Y. (2008) 'Temperature-Induced Hydrogels Through Self-Assembly of Cholesterol-Substituted Star PEG-b-PLLA Copolymers: An Injectable Scaffold for Tissue Engineering', *Advanced Functional Materials*. John Wiley & Sons, Ltd, 18(8), pp. 1220–1231. doi: 10.1002/ADFM.200700587.

Nagarajan, S. *et al.* (2019) 'Overview of Protein-Based Biopolymers for Biomedical Application', *Macromolecular Chemistry and Physics*, 220(14), pp. 1–16. doi: 10.1002/macp.201900126.

Nagata, Y. *et al.* (1998) 'Transcatheter arterial embolization for malignant osseous and soft-tissue sarcomas. I. A rabbit experimental model', *Cardiovascular and interventional radiology*. Cardiovasc Intervent Radiol, 21(3), pp. 205–207. doi: 10.1007/S002709900245.

Ndlovu, S. P. *et al.* (2021) 'Gelatin-based hybrid scaffolds: Promising wound dressings', *Polymers*, 13(17). doi: 10.3390/polym13172959.

Neoptolemos, J. P. *et al.* (2004) 'A Randomized Trial of Chemoradiotherapy and Chemotherapy after Resection of Pancreatic Cancer', *New England Journal of Medicine*, 350(12), pp. 1200–1210. doi: 10.1056/nejmoa032295.

Nguyen, D. D. *et al.* (2023) 'Amination-mediated nano eye-drops with enhanced corneal permeability and effective burst release for acute glaucoma treatment', *Chemical Engineering Journal*. Elsevier B.V., 451(P1), p. 138620. doi: 10.1016/j.cej.2022.138620.

Niesen, W. *et al.* (2019) 'Local radicality and survival outcome of pancreatic cancer surgery', *Annals of Gastroenterological Surgery*. Wiley-Blackwell Publishing Ltd, 3(5), pp. 464–475. doi: 10.1002/AGS3.12273.

Nishino, H. *et al.* (2023) 'Proof of Principle of Combining Fluorescence-Guided Surgery with Photoimmunotherapy to Improve the Outcome of Pancreatic Cancer Therapy in an Orthotopic Mouse Model', *Oncol*, 30, pp. 618–625. doi: 10.1245/s10434-022-12466-4.

Nita, L. E. *et al.* (2020) 'New trends in bio-based aerogels', *Pharmaceutics*. MDPI AG. doi: 10.3390/pharmaceutics12050449.

Noble, S. and Goa, K. L. (1997) 'Gemcitabine. A review of its pharmacology and clinical potential in non-small cell lung cancer and pancreatic cancer', *Drugs*. Drugs, 54(3), pp. 447–472. doi: 10.2165/00003495-199754030-00009.

Nokhodchi, A. *et al.* (2008) 'Factors Affecting the Release of Nifedipine from a Swellable Elementary Osmotic Pump', *Drug Delivery*, 15(1), pp. 43–48. doi: 10.1080/10717540701829028.

Norbury, K. C. *et al.* (2012) 'Burst strength testing of porcine intestinal anastomoses following negative pressure therapy', *Surgical Innovation*, 19(2), pp. 181–186. doi: 10.1177/1553350611418254.

Nori, D., Li, X. and Pugkhem, T. (1995) 'Intraoperative brachytherapy using gelfoam radioactive plaque implants for resected stage iii non-small cell lung cancer with positive margin: A pilot study', *Journal of Surgical Oncology*. John Wiley & Sons, Ltd, 60(4), pp. 257–261. doi: 10.1002/JSO.2930600409.

O'Brien, F. J. (2011) 'Biomaterials & scaffolds for tissue engineering', *Materials Today*. Elsevier Ltd, 14(3), pp. 88–95. doi: 10.1016/S1369-7021(11)70058-X.

Olajubutu, O. *et al.* (2023) 'Drug Delivery Strategies for the Treatment of Pancreatic Cancer'.

Olive, K. P. *et al.* (2011) 'Inhibition of Hedgehog Signaling', *Science*, 324(June), pp. 1457–61.

Ooi, S. Y., Ahmad, I. and Amin, M. C. I. M. (2016) 'Cellulose nanocrystals extracted from rice husks as a reinforcing material in gelatin hydrogels for use in controlled drug delivery systems', *Industrial Crops and Products*. Elsevier, 93, pp. 227–234. doi: 10.1016/J.INDCROP.2015.11.082.

Orth, M. *et al.* (2019) 'Pancreatic ductal adenocarcinoma: biological hallmarks, current status, and future perspectives of combined modality treatment approaches', *Radiation Oncology 2019 14:1*. BioMed Central, 14(1), pp. 1–20. doi: 10.1186/S13014-019-1345-6.

Oryan, A. *et al.* (2018a) 'Chemical crosslinking of biopolymeric scaffolds: Current knowledge and future directions of crosslinked engineered bone scaffolds', *International journal of biological macromolecules*. Int J Biol Macromol, 107(Pt A), pp. 678–688. doi: 10.1016/J.IJBIOMAC.2017.08.184.

Oryan, A. *et al.* (2018b) 'Chemical crosslinking of biopolymeric scaffolds: Current knowledge and future directions of crosslinked engineered bone scaffolds', *International Journal of Biological Macromolecules*. Elsevier B.V., 107(PartA), pp. 678–688. doi: 10.1016/j.ijbiomac.2017.08.184.

Ozols, R. F. (2005) 'Gemcitabine and carboplatin in second-line ovarian cancer', *Seminars in oncology*. Semin Oncol, 32(4 Suppl 6), p. 4. doi: 10.1053/J.SEMINONCOL.2005.06.023.

Pan, M. *et al.* (2023) 'Absorbable 3D-printed pancreaticojejunostomy device with a dual-layer drug coating for the prevention of postoperative local recurrence of pancreatic cancer', *Journal of Materials Science and Technology*. Elsevier Ltd, 154, pp. 178–188. doi: 10.1016/j.jmst.2023.01.016.

Park, S. H. *et al.* (2017) 'Design and Fabrication of a Thin-Walled Free-Form Scaffold on the Basis of Medical Image Data and a 3D Printed Template: Its Potential Use in Bile Duct Regeneration', *ACS Applied Materials and Interfaces*, 9(14), pp. 12290–12298. doi: 10.1021/acsami.7b00849.

Parra-Membrives, P. *et al.* (2007) 'Effect of pentoxifylline on the healing of ischemic colorectal anastomoses', *Diseases of the Colon and Rectum*, 50(3), pp. 369–375. doi:

10.1007/s10350-006-0803-z.

Patterson, J. K., Lei, X. G. and Miller, D. D. (2008) ‘The pig as an experimental model for elucidating the mechanisms governing dietary influence on mineral absorption’, *Experimental Biology and Medicine*, 233(6), pp. 651–664. doi: 10.3181/0709-MR-262.

Pawar, S. N. and Edgar, K. J. (2012) ‘Alginate derivatization: a review of chemistry, properties and applications’, *Biomaterials*. Biomaterials, 33(11), pp. 3279–3305. doi: 10.1016/J.BIOMATERIALS.2012.01.007.

Pawar, V. and Srivastava, R. (2019) ‘Chitosan-polycaprolactone blend sponges for management of chronic osteomyelitis: A preliminary characterization and in vitro evaluation’, *International Journal of Pharmaceutics*. Elsevier, 568(July), p. 118553. doi: 10.1016/j.ijpharm.2019.118553.

Pearson, E. J. and Mennel, R. (2013) ‘Eosinophilic Small Bowel Enteritis in Response to Folinic Acid, Fluorouracil, and Oxaliplatin Chemotherapy’, *Baylor University Medical Center Proceedings*, 26(3), pp. 288–289. doi: 10.1080/08998280.2013.11928986.

Peck, M. *et al.* (2011) ‘Tissue engineering by self-assembly’, *Materials Today*. Elsevier, 14(5), pp. 218–224. doi: 10.1016/S1369-7021(11)70117-1.

Pelosi, E., Castelli, G. and Testa, U. (2017) ‘Pancreatic cancer: Molecular characterization, clonal evolution and cancer stem cells’, *Biomedicines*, 5(4). doi: 10.3390/biomedicines5040065.

Penumadu, P. *et al.* (2015) ‘Pancreatoduodenectomy - Preventing Complications’, *Indian Journal of Surgical Oncology*, 6(1), pp. 6–15. doi: 10.1007/s13193-013-0286-z.

Peppas, N. A. *et al.* (2000) ‘Hydrogels in pharmaceutical formulations’, *European Journal of Pharmaceutics and Biopharmaceutics*, 50(1), pp. 27–46. doi: 10.1016/S0939-6411(00)00090-4.

Perspectives, F. (2019) ‘3D Printing of Bioceramic Sca ff olds — Barriers to the Clinical Translation : From Promise to Reality ’, *Materials*, 12(17), p. 2660.

Piersma, B., Hayward, M. K. and Weaver, V. M. (2020) ‘Fibrosis and cancer: A strained relationship’, *Biochimica et Biophysica Acta - Reviews on Cancer*. Elsevier B.V., 1873(2), p. 188356. doi: 10.1016/j.bbcan.2020.188356.

Pliarchopoulou, K. and Pectasides, D. (2009) ‘Pancreatic cancer: Current and future treatment strategies’, *Cancer Treatment Reviews*. Elsevier Ltd, 35(5), pp. 431–436. doi: 10.1016/j.ctrv.2009.02.005.

Pons-Faudoa, F. P. *et al.* (2019) ‘Advanced implantable drug delivery technologies: transforming the clinical landscape of therapeutics for chronic diseases’, *Biomedical Microdevices*. Biomedical Microdevices, 21(2). doi: 10.1007/s10544-019-0389-6.

Poruk, K. E. *et al.* (2013) ‘Screening for pancreatic cancer: Why, how, and who?’, *Annals of Surgery*, 257(1), pp. 17–26. doi: 10.1097/SLA.0b013e31825ffbfb.

Prasad, L. K. and Smyth, H. (2016) ‘3D Printing technologies for drug delivery: a review’, *Drug Development and Industrial Pharmacy*, 42(7), pp. 1019–1031. doi: 10.3109/03639045.2015.1120743.

Principe, D. R. *et al.* (2021) ‘The Current Treatment Paradigm for Pancreatic Ductal

Adenocarcinoma and Barriers to Therapeutic Efficacy', *Frontiers in Oncology*, 11(July), pp. 1–25. doi: 10.3389/fonc.2021.688377.

Psimadas, D. *et al.* (2012) 'Molecular Nanomedicine Towards Cancer ':, *Journal of pharmaceutical sciences*, 101(7), pp. 2271–2280. doi: 10.1002/jps.

Puertas-Bartolomé, M., Mora-Boza, A. and García-Fernández, L. (2021) 'Emerging biofabrication techniques: A review on natural polymers for biomedical applications', *Polymers*, 13(8), pp. 1–26. doi: 10.3390/polym13081209.

Rahib, L. *et al.* (2014) 'Projecting cancer incidence and deaths to 2030: The unexpected burden of thyroid, liver, and pancreas cancers in the united states', *Cancer Research*, 74(11), pp. 2913–2921. doi: 10.1158/0008-5472.CAN-14-0155.

Rajgor, N., Patel, M. and Bhaskar, V. H. (2011) 'Implantable drug delivery systems: An overview', *Systematic Reviews in Pharmacy*, 2(2), pp. 91–95. doi: 10.4103/0975-8453.86297.

Ramot, Y. *et al.* (2016) 'Preclinical Safety Evaluation in Rats of a Polymeric Matrix Containing an siRNA Drug Used as a Local and Prolonged Delivery System for Pancreatic Cancer Therapy', *Toxicologic Pathology*, 44(6), pp. 856–865. doi: 10.1177/0192623316645860.

Rau, B. M. *et al.* (2012) 'R1 resection in pancreatic cancer has significant impact on long-term outcome in standardized pathology modified for routine use', *Surgery (United States)*. Mosby, Inc., 152(3 SUPPL.), pp. S103–S111. doi: 10.1016/j.surg.2012.05.015.

Rault, I. *et al.* (1996) 'Evaluation of different chemical methods for cross-linking collagen gel, films and sponges', *Journal of Materials Science: Materials in Medicine*, 7(4), pp. 215–221. doi: 10.1007/BF00119733.

Real, F. X. (2003) 'A "catastrophic hypothesis" for pancreas cancer progression', *Gastroenterology*. W.B. Saunders, 124(7), pp. 1958–1964. doi: 10.1016/S0016-5085(03)00389-5.

Real, F. X., Cibrián-Uhalte, E. and Martinelli, P. (2008) 'Pancreatic Cancer Development and Progression: Remodeling the Model', *Gastroenterology*. W.B. Saunders, 135(3), pp. 724–728. doi: 10.1053/J.GASTRO.2008.07.033.

Reddy, N., Reddy, R. and Jiang, Q. (2015) 'Crosslinking biopolymers for biomedical applications', *Trends in Biotechnology*. doi: 10.1016/j.tibtech.2015.03.008.

Refai, H. and Tag, R. (2011) 'Development and characterization of sponge-like acyclovir ocular minitablets', *Drug delivery*. Drug Deliv, 18(1), pp. 38–45. doi: 10.3109/10717544.2010.509364.

Ren, B. *et al.* (2018) 'Tumor microenvironment participates in metastasis of pancreatic cancer', *Molecular Cancer*. Molecular Cancer, 17(1), pp. 1–15. doi: 10.1186/s12943-018-0858-1.

Rodriguez, I. A. *et al.* (2013) 'A preliminary evaluation of lyophilized gelatin sponges, enhanced with platelet-rich plasma, hydroxyapatite and chitin whiskers for bone regeneration', *Cells*, 2(2), pp. 244–265. doi: 10.3390/cells2020244.

Roeth, A. A. *et al.* (2021) '3D-Printed Replica and Porcine Explants for Pre-Clinical Optimization of Endoscopic Tumor Treatment By Magnetic Targeting', *Cancers*, 13(21). doi: 10.3390/cancers13215496.

Rohanizadeh, R., Swain, M. V. and Mason, R. S. (2008) 'Gelatin sponges (Gelfoam®) as a scaffold for osteoblasts', *Journal of Materials Science: Materials in Medicine*, 19(3), pp. 1173–1182. doi: 10.1007/s10856-007-3154-y.

Rossi, S. *et al.* (2012) 'Development of sponge-like dressings for mucosal/transmucosal drug delivery into vaginal cavity', *Pharmaceutical Development and Technology*, 17(2), pp. 219–226. doi: 10.3109/10837450.2010.531736.

Roth, M. T. and Berlin, J. D. (2018) 'Current Concepts in the Treatment of Resectable Pancreatic Cancer', *Current Oncology Reports*. doi: 10.1007/s11912-018-0685-y.

Rutledge, L. F. *et al.* (2015) 'Catheter securement systems: comparison of two investigational devices to a sutureless securement device, a securement dressing, and sutures in a pig model', *Intensive Care Medicine Experimental* . Intensive Care Medicine Experimental, 3(1). doi: 10.1186/s40635-015-0060-3.

Safhi, A. Y. (2022) 'Three-Dimensional (3D) Printing in Cancer Therapy and Diagnostics: Current Status and Future Perspectives', *Pharmaceuticals*, 15(6). doi: 10.3390/ph15060678.

Santin, M. *et al.* (1996) 'Synthesis and characterization of a new interpenetrated poly(2-hydroxyethylmethacrylate)-gelatin composite polymer', *Biomaterials*. Elsevier Science Ltd, 17(15), pp. 1459–1467. doi: 10.1016/0142-9612(96)89769-9.

Schlitter, A. M. *et al.* (2010) 'Definition of Microscopic Tumor Clearance (R0) in Pancreatic Cancer Resections', *Cancers*. Molecular Diversity Preservation International, 2(4), pp. 2001–2010. doi: 10.3390/cancers2042001.

Seo, Y. D. and Katz, M. H. G. (2022) 'Preoperative therapy for pancreatic adenocarcinoma—precision beyond anatomy', *Cancer*, 128(16), pp. 3041–3056. doi: 10.1002/cncr.34273.

Serati, M. *et al.* (2015) 'Delayed-type hypersensitivity reaction against Nexplanon®', *Contraception*. Elsevier Inc., 91(1), pp. 91–92. doi: 10.1016/j.contraception.2014.08.014.

Serrano, D. R., Terres, M. C. and Lalatsa, A. (2018) 'Applications of 3D printing in cancer', *Journal of 3D Printing in Medicine*. 3D Printing in Medicine, 2(3), pp. 115–127. doi: 10.2217/3dp-2018-0007.

Shabir, G. A. *et al.* (2007) 'Evaluation and application of best practice in analytical method validation', *Journal of Liquid Chromatography and Related Technologies*, 30(3), pp. 311–333. doi: 10.1080/10826070601084753.

Shah, A. K. (2018) 'Postoperative pathologic assessment of surgical margins in oral cancer: A contemporary review'. doi: 10.4103/jomfp.JOMFP_185_16.

Shaqour, B. *et al.* (2021) 'Gaining a better understanding of the extrusion process in fused filament fabrication 3D printing: a review', *International Journal of Advanced Manufacturing Technology*. The International Journal of Advanced Manufacturing Technology, 114(5–6), pp. 1279–1291. doi: 10.1007/s00170-021-06918-6.

Shariatinia, Z. and Mazloom-Jalali, A. (2019) 'Chitosan nanocomposite drug delivery systems designed for the ifosfamide anticancer drug using molecular dynamics simulations', *Journal of Molecular Liquids*. Elsevier B.V., 273, pp. 346–367. doi: 10.1016/j.molliq.2018.10.047.

Shepherd, D. E. T. *et al.* (2001) 'Slippage of a spinous process hook during flexion in a flexible fixation system for the lumbar spine', *Medical Engineering and Physics*, 23(2), pp.

135–141. doi: 10.1016/S1350-4533(01)00029-7.

Shinde, S. S. (2022) ‘Lyophilization of Parenteral Dosage Form Shrutika S Shinde’, *International Journal of Pharmaceutical Research and Applications*, 7(3), p. 758. doi: 10.35629/7781-0703758764.

Shitara, K. *et al.* (2008) ‘Pilot study of combination chemotherapy using irinotecan plus S-1 for metastatic pancreatic cancer’, *Oncology*. Oncology, 75(1–2), pp. 67–70. doi: 10.1159/000151742.

Shrikhande, S. V. and D’Souza, M. A. (2008) ‘Pancreatic fistula after pancreatectomy: Evolving definitions, preventive strategies and modern management’, *World Journal of Gastroenterology*, 14(38), pp. 5789–5796. doi: 10.3748/wjg.14.5789.

Shukla, A. *et al.* (2012) ‘Release of vancomycin from multilayer coated absorbent gelatin sponges’, *Journal of Controlled Release*. Elsevier B.V., 157(1), pp. 64–71. doi: 10.1016/j.jconrel.2011.09.062.

Siegel, R. L. *et al.* (2021) ‘Cancer Statistics, 2021’, *CA: A Cancer Journal for Clinicians*, 71(1), pp. 7–33. doi: 10.3322/caac.21654.

Siegel, R. L., Miller, K. D. and Jemal, A. (2015) ‘Cancer statistics, 2015’, *CA: A Cancer Journal for Clinicians*. American Cancer Society, 65(1), pp. 5–29. doi: 10.3322/CAAC.21254.

Siegel, R. L., Miller, K. D. and Jemal, A. (2018) ‘Cancer statistics, 2018’, *CA: A Cancer Journal for Clinicians*, 68(1), pp. 7–30. doi: 10.3322/caac.21442.

Simonova, G. *et al.* (2012) ‘Cyanoacrylate tissue adhesives - Effective securement technique for intravascular catheters: In vitro testing of safety and feasibility’, *Anaesthesia and Intensive Care*, 40(3), pp. 460–466. doi: 10.1177/0310057x1204000311.

Singamneni, S. *et al.* (2018) ‘Extrusion 3D printing of polybutyrate-adipate-terephthalate-polymer composites in the pellet form’, *Polymers*, 10(8). doi: 10.3390/polym10080922.

Singhvi, G. *et al.* (2019) ‘Microsponge: An emerging drug delivery strategy’, *Drug Development Research*, 80(2), pp. 200–208. doi: 10.1002/ddr.21492.

Sionkowska, A. (2021) ‘Collagen blended with natural polymers: Recent advances and trends’, *Progress in Polymer Science*. Elsevier B.V., 122, p. 101452. doi: 10.1016/j.progpolymsci.2021.101452.

Skovrlj, B. *et al.* (2014) ‘Fatal intraoperative cardiac arrest after application of surgifoam into a bleeding iliac screw defect’, *Spine*, 39(20), pp. E1239–E1242. doi: 10.1097/BRS.0000000000000513.

Soliman, S. *et al.* (2010) ‘Multiscale three-dimensional scaffolds for soft tissue engineering via multimodal electrospinning’, *Acta Biomaterialia*. Elsevier Ltd, 6(4), pp. 1227–1237. doi: 10.1016/J.ACTBIO.2009.10.051.

Stergar, J. and Maver, U. (2016) ‘Review of aerogel-based materials in biomedical applications’, *Journal of Sol-Gel Science and Technology 2016 77:3*. Springer, 77(3), pp. 738–752. doi: 10.1007/S10971-016-3968-5.

Stewart, S. A. *et al.* (2018) ‘Implantable polymeric drug delivery devices: Classification, manufacture, materials, and clinical applications’, *Polymers*, 10(12). doi:

10.3390/polym10121379.

Stewart, S. A. *et al.* (2020) ‘Development of a biodegradable subcutaneous implant for prolonged drug delivery using 3D printing’, *Pharmaceutics*, 12(2). doi: 10.3390/pharmaceutics12020105.

Strasberg, S. M., Linehan, D. C. and Hawkins, W. G. (2007) ‘Radical Antegrade Modular Pancreatosplenectomy Procedure for Adenocarcinoma of the Body and Tail of the Pancreas: Ability to Obtain Negative Tangential Margins’, *Journal of the American College of Surgeons*. No longer published by Elsevier, 204(2), pp. 244–249. doi: 10.1016/J.JAMCOLLSURG.2006.11.002.

Strobel, O. *et al.* (2013) ‘Re-resection for isolated local recurrence of pancreatic cancer is feasible, safe, and associated with encouraging survival’, *Annals of Surgical Oncology*, 20(3), pp. 964–972. doi: 10.1245/s10434-012-2762-z.

Strobel, O. *et al.* (2017) ‘Pancreatic Cancer Surgery’, *Annals of Surgery*, 265(3), pp. 565–573. doi: 10.1097/SLA.0000000000001731.

Sultana, A. *et al.* (2007) ‘Meta-analyses of chemotherapy for locally advanced and metastatic pancreatic cancer’, *Journal of Clinical Oncology*, 25(18), pp. 2607–2615. doi: 10.1200/JCO.2006.09.2551.

Sun, M. *et al.* (2018) ‘The relation between the rheological properties of gels and the mechanical properties of their corresponding aerogels’, *Gels*, 4(2), pp. 2–11. doi: 10.3390/gels4020033.

Sung, H. W. *et al.* (1999) ‘Mechanical properties of a porcine aortic valve fixed with a naturally occurring crosslinking agent’, *Biomaterials*, 20(19), pp. 1759–1772. doi: 10.1016/S0142-9612(99)00069-1.

Tabatabei, S. A. and Hashemi, S. M. (2015a) ‘Pancreatic anastomosis leakage management following pancreaticoduodenectomy how could be manage the anastomosis leakage after pancreaticoduodenectomy?’, *Journal of Research in Medical Sciences*, 20(2), pp. 161–164.

Tabatabei, S. A. and Hashemi, S. M. (2015b) ‘Pancreatic anastomosis leakage management following pancreaticoduodenectomy how could be manage the anastomosis leakage after pancreaticoduodenectomy?’, *Journal of Research in Medical Sciences : The Official Journal of Isfahan University of Medical Sciences*. Wolters Kluwer -- Medknow Publications, 20(2), p. 161. Available at: /pmc/articles/PMC4400711/ (Accessed: 3 April 2023).

Tabernero, A. *et al.* (2020) ‘Role of rheological properties on physical chitosan aerogels obtained by supercritical drying’, *Carbohydrate Polymers*. Elsevier, 233(January), p. 115850. doi: 10.1016/j.carbpol.2020.115850.

Tabriz, A. G. *et al.* (2021) ‘Investigation on hot melt extrusion and prediction on 3D printability of pharmaceutical grade polymers’, *International Journal of Pharmaceutics*. Elsevier B.V., 604(April), p. 120755. doi: 10.1016/j.ijpharm.2021.120755.

Tahara, J., Shimizu, K. and Shiratori, K. (2008) ‘Engulfment of necrotic acinar cells by pancreatic stellate cells inhibits pancreatic fibrogenesis’, *Pancreas*, 37(1), pp. 69–74. doi: 10.1097/MPA.0B013E318160A5CB.

Takikawa, T. *et al.* (2022) ‘Clinical features and prognostic impact of asymptomatic pancreatic cancer’, *Scientific Reports*. Nature Publishing Group UK, 12(1), pp. 1–11. doi: 10.1038/s41598-022-08083-6.

Taleuzzaman, M., Ahmed, M. M. and Chattopadhyay, M. (2016) 'Particle size role, Importance and Strategy of HPLC Analysis - An update', *International Archives of BioMedical and Clinical Research*. Marwah Infotech, 2(2), pp. 5–11. doi: 10.21276/IABCR.2016.2.2.2.

Tamargo, R. J. *et al.* (1989) 'Brain biocompatibility of a biodegradable, controlled-release polymer in rats', *Journal of biomedical materials research*. J Biomed Mater Res, 23(2), pp. 253–266. doi: 10.1002/JBM.820230209.

Tan, W. H. K. *et al.* (2003) 'Computer simulation of the delivery of etanidazole to brain tumor from PLGA wafers: Comparison between linear and double burst release systems', *Biotechnology and Bioengineering*, 82(3), pp. 278–288. doi: 10.1002/bit.10571.

Tempero, M. A. *et al.* (2017) 'Pancreatic adenocarcinoma, version 2.2017: Clinical practice guidelines in Oncology', *JNCCN Journal of the National Comprehensive Cancer Network*, 15(8), pp. 1028–1061. doi: 10.6004/jnccn.2017.0131.

Teodora Tihan, G. *et al.* (2015) 'Chloramphenicol collagen sponges for local drug delivery in dentistry', *Comptes Rendus Chimie*, 18(9), pp. 986–992. doi: 10.1016/j.crci.2015.06.004.

Thomas, D. and Radhakrishnan, P. (2019) 'Tumor-stromal crosstalk in pancreatic cancer and tissue fibrosis', *Molecular Cancer*. Molecular Cancer, 18(1), pp. 1–15. doi: 10.1186/s12943-018-0927-5.

Tian, P. *et al.* (2019) 'Applications of excipients in the field of 3D printed pharmaceuticals', *Drug Development and Industrial Pharmacy*. Taylor & Francis, 45(6), pp. 905–913. doi: 10.1080/03639045.2019.1576723.

Toh, H. W. *et al.* (2021) 'Polymer blends and polymer composites for cardiovascular implants', *European Polymer Journal*. Elsevier Ltd, 146(December 2020), p. 110249. doi: 10.1016/j.eurpolymj.2020.110249.

Tomlinson, J. S. *et al.* (2007) 'Accuracy of staging node-negative pancreas cancer: a potential quality measure', *Archives of surgery (Chicago, Ill. : 1960)*. Arch Surg, 142(8), pp. 767–773. doi: 10.1001/ARCHSURG.142.8.767.

Torrejon, V. M. *et al.* (2022) 'Gelatin-based cellular solids: Fabrication, structure and properties', *Journal of Cellular Plastics*, 58(5), pp. 797–858. doi: 10.1177/0021955X221087602.

Touri, M. *et al.* (2019) 'Additive Manufacturing of Biomaterials − The Evolution of Rapid Prototyping', *Advanced Engineering Materials*. John Wiley & Sons, Ltd, 21(2), p. 1800511. doi: 10.1002/ADEM.201800511.

Trede, M., Richter, A. and Wendl, K. (2001) 'Personal observations, opinions, and approaches to cancer of the pancreas and the periampullary area', *The Surgical clinics of North America*. Surg Clin North Am, 81(3), pp. 595–610. doi: 10.1016/S0039-6109(05)70146-8.

Treves, N. (1952) 'Prophylaxis of postmammectomy lymphedema by the use of gelfoam laminated rolls; a preliminary report, with a review of the theories on the etiology of elephantiasis chirurgica and a summary of previous operations for its control', *Cancer*. Cancer, 5(1), pp. 73–84. doi: 10.1002/1097-0142(195201)5:1.

Udroiu, R. and Nedelcu, A. (2011) 'Optimization of Additive Manufacturing Processes Focused on 3D Printing', *Rapid Prototyping Technology - Principles and Functional*

Requirements. doi: 10.5772/21433.

Ukhrowiyah, N. *et al.* (2017) 'Synthesis and characterization of breast-phantom-based gelatine-glutaraldehyde-TiO2 as a test material for the application of breast cancer diagnosis', *Journal of Physics: Conference Series*, 853(1). doi: 10.1088/1742-6596/853/1/012028.

Ulker, Z. and Erkey, C. (2014) 'An emerging platform for drug delivery: Aerogel based systems', *Journal of Controlled Release*. Elsevier B.V., pp. 51–63. doi: 10.1016/j.jconrel.2013.12.033.

Ulubayram, K. *et al.* (2001) 'EGF containing gelatin-based wound dressings', *Biomaterials*. Biomaterials, 22(11), pp. 1345–1356. doi: 10.1016/S0142-9612(00)00287-8.

Ulubayram, K. *et al.* (2002) 'Cytotoxicity evaluation of gelatin sponges prepared with different cross-linking agents', *Journal of Biomaterials Science, Polymer Edition*, 13(11), pp. 1203–1219. doi: 10.1163/156856202320892966.

Vary, A. *et al.* (2021) 'FOLFIRINOX relative dose intensity and disease control in advanced pancreatic adenocarcinoma', *Therapeutic Advances in Medical Oncology*, 13, pp. 1–12. doi: 10.1177/17588359211029825.

Veillette, G. *et al.* (2008) 'Implications and management of pancreatic fistulas following pancreaticoduodenectomy: The Massachusetts General Hospital experience', *Archives of Surgery*, 143(5), pp. 476–481. doi: 10.1001/archsurg.143.5.476.

Verbeke, C. S. (2013) 'Resection Margins in Pancreatic Cancer', *Surgical Clinics of North America*, pp. 647–662. doi: 10.1016/j.suc.2013.02.008.

Verbeke, C. S. and Gladhaug, I. P. (2012) 'Resection margin involvement and tumour origin in pancreatic head cancer'. doi: 10.1002/bjs.8734.

Verbeke, C. S. and Menon, K. V. (2009) 'Redefining resection margin status in pancreatic cancer', *HPB : The Official Journal of the International Hepato Pancreato Biliary Association*. Elsevier, 11(4), p. 282. doi: 10.1111/J.1477-2574.2009.00055.X.

Veres, P. *et al.* (2015) 'Hybrid aerogel preparations as drug delivery matrices for low water-solubility drugs', *International journal of pharmaceutics*. Int J Pharm, 496(2), pp. 360–370. doi: 10.1016/J.IJPHARM.2015.10.045.

Vidushi, Y., Meenakshi, B. and Bharkatiya, M. B. (2017) 'A REVIEW ON HPLC METHOD DEVELOPMENT AND VALIDATION'. doi: 10.26479/2017.0206.12.

Van Vlierberghe, S. *et al.* (2007) 'Porous gelatin hydrogels: 1. Cryogenic formation and structure analysis', *Biomacromolecules*, 8(2), pp. 331–337. doi: 10.1021/bm060684o.

Vonlaufen, A. *et al.* (2008) 'Pancreatic stellate cells: Partners in crime with pancreatic cancer cells', *Cancer Research*, 68(7), pp. 2085–2093. doi: 10.1158/0008-5472.CAN-07-2477.

Vordemvenne, T. *et al.* (2020) 'Bone Regeneration: A Novel Osteoinductive Function of Spongostan by the Interplay between Its Nano- and Microtopography', *Cells*, 9(3). doi: 10.3390/cells9030654.

Vyas, K. S. and Saha, S. P. (2013) 'Comparison of hemostatic agents used in vascular surgery', *http://dx.doi.org/10.1517/14712598.2013.848193*. Taylor & Francis, 13(12), pp. 1663–1672. doi: 10.1517/14712598.2013.848193.

Wagner, M. *et al.* (2004) 'Curative resection is the single most important factor determining

outcome in patients with pancreatic adenocarcinoma', *The British journal of surgery*. Br J Surg, 91(5), pp. 586–594. doi: 10.1002/BJS.4484.

Wallis, M. *et al.* (2020) '3D printing for enhanced drug delivery: current state-of-the-art and challenges', *Drug Development and Industrial Pharmacy*. Taylor & Francis, 46(9), pp. 1385–1401. doi: 10.1080/03639045.2020.1801714.

Wanebo, H. J. and Vezeridis, M. P. (1995) 'Pancreatic cancer: An overview', *Seminars in Surgical Oncology*, 11(2), pp. 168–180. doi: 10.1002/ssu.2980110214.

Wang, A. Z., Langer, R. and Farokhzad, O. C. (2012) 'Nanoparticle delivery of cancer drugs', *Annual Review of Medicine*, 63, pp. 185–198. doi: 10.1146/annurev-med-040210-162544.

Wang, B. *et al.* (2022) 'Efficacy and safety of 3D printing coplanar template-assisted iodine-125 seed implantation as palliative treatment for inoperable pancreatic cancer', *Journal of Contemporary Brachytherapy*, 14(2), pp. 140–147. doi: 10.5114/jcb.2022.114990.

Wang, W. *et al.* (2015) 'Physical crosslinkings of edible collagen casing', *International Journal of Biological Macromolecules*. Elsevier B.V., 81, pp. 920–925. doi: 10.1016/j.ijbiomac.2015.09.032.

Wang, X. *et al.* (2016) 'The mechanism of a chitosan-collagen composite film used as biomaterial support for MC3T3-E1 cell differentiation', *Scientific Reports*. Nature Publishing Group, 6. doi: 10.1038/SREP39322.

Wang, Y. *et al.* (2020) '3D printed biodegradable implants as an individualized drug delivery system for local chemotherapy of osteosarcoma', *Materials and Design*. Elsevier Ltd, 186, p. 108336. doi: 10.1016/j.matdes.2019.108336.

Wang, Y. *et al.* (2020) 'Overview of 3D additive manufacturing (AM) and corresponding AM composites', *Composites Part A: Applied Science and Manufacturing*. Elsevier, 139(July), p. 106114. doi: 10.1016/j.compositesa.2020.106114.

Weadock, K. S. *et al.* (1995) 'Physical crosslinking of collagen fibers: comparison of ultraviolet irradiation and dehydrothermal treatment', *Journal of biomedical materials research*. J Biomed Mater Res, 29(11), pp. 1373–1379. doi: 10.1002/JBM.820291108.

Wee, J. H. *et al.* (2012) 'Comparison between Gelfoam packing and no packing after endoscopic sinus surgery in the same patients', *European Archives of Oto-Rhino-Laryngology*, 269(3), pp. 897–903. doi: 10.1007/s00405-011-1768-7.

Wex, C. *et al.* (2015) 'Experimental analysis of the mechanical behavior of the viscoelastic porcine pancreas and preliminary case study on the human pancreas', *Journal of the Mechanical Behavior of Biomedical Materials*, 41, pp. 199–207. doi: 10.1016/j.jmbbm.2014.10.013.

Whang, K. *et al.* (1995) 'A novel method to fabricate bioabsorbable scaffolds', *Polymer*, 36(4), pp. 837–842. doi: 10.1016/0032-3861(95)93115-3.

Whipple, A. O., Parsons, W. B. and Mullins, C. R. (1935) 'TREATMENT OF CARCINOMA OF THE AMPULLA OF VATER', *Annals of Surgery*. Lippincott, Williams, and Wilkins, 102(4), p. 763. doi: 10.1097/00000658-193510000-00023.

Wilson, J. S., Pirola, R. C. and Apte, M. V. (2014) 'Stars and stripes in pancreatic cancer: Role of stellate cells and stroma in cancer progression', *Frontiers in Physiology*, 5

FEB(February), pp. 1–11. doi: 10.3389/fphys.2014.00052.

Wolinsky, J. B., Colson, Y. L. and Grinstaff, M. W. (2012) 'Local drug delivery strategies for cancer treatment: Gels, nanoparticles, polymeric films, rods, and wafers', *Journal of Controlled Release*. Elsevier B.V., 159(1), pp. 14–26. doi: 10.1016/j.jconrel.2011.11.031.

Wolkers, W. and Oldenhof, H. (2021) 'Cryopreservation and Freeze-Drying', *Methods in Molecular Biology*, 4, pp. 1–731. Available at: http://www.springer.com/series/7651.

Wong, P. *et al.* (2013) 'Performance of Biopsy Needle With Therapeutic Injection System to Prevent Bleeding Complications', *Journal of Medical Devices, Transactions of the ASME*. American Society of Mechanical Engineers Digital Collection, 7(1). doi: 10.1115/1.4023274/376533.

Wynn, T. A. (2007) 'Common and unique mechanisms regulate fibrosis in various fibroproliferative diseases', *Journal of Clinical Investigation*, 117(3), pp. 524–529. doi: 10.1172/JCI31487.

Xing, Q. *et al.* (2010) 'Porous biocompatible three-dimensional scaffolds of cellulose microfiber/gelatin composites for cell culture', *Acta biomaterialia*. Acta Biomater, 6(6), pp. 2132–2139. doi: 10.1016/J.ACTBIO.2009.12.036.

Xu, L., Wang, Y. and Li, W. (2021) 'A case report of fatal hepatic portal venous gas after transcatheter arterial chemoembolization in a patient with hepatocellular carcinoma', *Translational Cancer Research*, 10(12), pp. 5437–5442. doi: 10.21037/tcr-21-1721.

Yamamoto, J. *et al.* (2020) 'A universal gelfoam 3-D histoculture method to establish patient-derived cancer cells (3D-PDCC) without fibroblasts from patient-derived xenografts', *Anticancer Research*, 40(12), pp. 6765–6768. doi: 10.21873/anticanres.14699.

Yamamoto, T. *et al.* (2015) 'Long-term survival after resection of pancreatic cancer: A single-center retrospective analysis', *World Journal of Gastroenterology : WJG*. Baishideng Publishing Group Inc, 21(1), p. 262. doi: 10.3748/WJG.V21.I1.262.

Yan, Q. *et al.* (2018) 'A Review of 3D Printing Technology for Medical Applications', *Engineering*. Chinese Academy of Engineering, 4(5), pp. 729–742. doi: 10.1016/j.eng.2018.07.021.

Yang, G. *et al.* (2018) 'Assessment of the characteristics and biocompatibility of gelatin sponge scaffolds prepared by various crosslinking methods', *Scientific Reports*, 8(1). doi: 10.1038/s41598-018-20006-y.

Yang, X. L. *et al.* (2016) 'Core-Shell Chitosan Microcapsules for Programmed Sequential Drug Release', *ACS Applied Materials and Interfaces*, 8(16), pp. 10524–10534. doi: 10.1021/acsami.6b01277.

Yang, Y. Y. *et al.* (2019) 'A novel biopolymer device fabricated by 3D printing for simplifying procedures of pancreaticojejunostomy', *Materials Science and Engineering C*. Elsevier, 103(29), p. 109786. doi: 10.1016/j.msec.2019.109786.

Yano, S. *et al.* (2015) 'Cancer cells mimic in vivo spatial-temporal cell-cycle phase distribution and chemosensitivity in 3-dimensional gelfoam histoculture but not 2-dimensional culture as visualized with real-time fucci imaging', *Cell Cycle*, 14(6), pp. 808–819. doi: 10.1080/15384101.2014.1000685.

Yao, Z. A. *et al.* (2018) 'Efficacy of chitosan and sodium alginate scaffolds for repair of

spinal cord injury in rats', *Neural Regeneration Research*. Wolters Kluwer Medknow Publications, 13(3), pp. 502–509. doi: 10.4103/1673-5374.228756.

Ye, S. *et al.* (2019) 'Development of gelatin/bacterial cellulose composite sponges as potential natural wound dressings', *International Journal of Biological Macromolecules*. Elsevier B.V., 133, pp. 148–155. doi: 10.1016/j.ijbiomac.2019.04.095.

Yi, H. G. *et al.* (2016) 'A 3D-printed local drug delivery patch for pancreatic cancer growth suppression', *Journal of Controlled Release*. Elsevier, 238, pp. 231–241. doi: 10.1016/J.JCONREL.2016.06.015.

Ying, H. *et al.* (2016) 'Genetics and biology of pancreatic ductal adenocarcinoma', *Genes and Development*, 30(4), pp. 355–385. doi: 10.1101/gad.275776.115.

Yu, L., Dean, K. and Li, L. (2006) 'Polymer blends and composites from renewable resources', *Progress in Polymer Science (Oxford)*, 31(6), pp. 576–602. doi: 10.1016/j.progpolymsci.2006.03.002.

Zakeri-Milani, P. *et al.* (2005) 'Simultaneous determination of naproxen, ketoprofen and phenol red in samples from rat intestinal permeability studies: HPLC method development and validation', *Journal of Pharmaceutical and Biomedical Analysis*, 39(3–4), pp. 624–630. doi: 10.1016/j.jpba.2005.04.008.

Zhan, H. X. *et al.* (2017) 'Neoadjuvant therapy in pancreatic cancer: a systematic review and meta-analysis of prospective studies', *Cancer Medicine*, 6(6), pp. 1201–1219. doi: 10.1002/cam4.1071.

Zhan, Q. *et al.* (2013) 'Drug-eluting scaffold to deliver chemotherapeutic medication for management of pancreatic cancer after surgery', *International Journal of Nanomedicine*, 8, pp. 2465–2472. doi: 10.2147/ijn.s47666.

Zhang, H. *et al.* (2021) 'Sponge particulates for biomedical applications: Biofunctionalization, multi-drug shielding, and theranostic applications', *Biomaterials*. Elsevier Ltd, 273(April), p. 120824. doi: 10.1016/j.biomaterials.2021.120824.

Zhang, Q. *et al.* (2016) 'Comparison of collagen and gelatin extracted from the skins of Nile tilapia (Oreochromis niloticus) and channel catfish (Ictalurus punctatus)', *Food Bioscience*. Elsevier Ltd, C(13), pp. 41–48. doi: 10.1016/J.FBIO.2015.12.005.

Zhang, Q. *et al.* (2016) 'Pancreatic Cancer Epidemiology, Detection, and Management', *Gastroenterology Research and Practice*. Hindawi Publishing Corporation, 2016. doi: 10.1155/2016/8962321.

Zhang, Z. *et al.* (2018) 'Sandwich-Like Fibers/Sponge Composite Combining Chemotherapy and Hemostasis for Efficient Postoperative Prevention of Tumor Recurrence and Metastasis', *Advanced Materials*, 30(49), pp. 1–9. doi: 10.1002/adma.201803217.

Zhao, Z. Y. and Liu, W. (2020) 'Pancreatic Cancer: A Review of Risk Factors, Diagnosis, and Treatment', *Technology in Cancer Research and Treatment*, 19, pp. 1–13. doi: 10.1177/1533033820962117.

Zou, Y. *et al.* (2020) 'Protein-reduced gold nanoparticles mixed with gentamicin sulfate and loaded into konjac/gelatin sponge heal wounds and kill drug-resistant bacteria', *International journal of biological macromolecules*. Int J Biol Macromol, 148, pp. 921–931. doi: 10.1016/J.IJBIOMAC.2020.01.190.

Zuo, L. *et al.* (2015) 'Polymer/Carbon-Based Hybrid Aerogels: Preparation, Properties and Applications', *Materials*. MDPI AG, pp. 6806–6848. doi: 10.3390/ma8105343.

Zur, G. *et al.* (2011) 'Chondroprotective effects of a polycarbonate-urethane meniscal implant: Histopathological results in a sheep model', *Knee Surgery, Sports Traumatology, Arthroscopy*, 19(2), pp. 255–263. doi: 10.1007/s00167-010-1210-5.